University of Alberta

Reservoir and Geomechanical Coupled Simulation of CO_2 Sequestration and Enhanced Coalbed Methane Recovery

by

Fagang Gu

A thesis submitted to the Faculty of Graduate Studies and Research
in partial fulfillment of the requirements for the degree of

Doctor of Philosophy

in

Geotechnical Eengineering

Civil and Environmental Engineering

Fall 2009

Edmonton, Alberta

EXAMINING COMMITTEE

Dr. Rick Chalaturnyk, Supervisor, Civil and Environmental Engineering

Dr. Dave H. Chan, Civil and Environmental Engineering

Dr. Alireza Nouri, Civil and Environmental Engineering

Dr. Mauricio D. Sacchi, Physics

Dr. Zhenghe Xu, Chemical and Materials Engineering

Dr. Antonin (Tony) Settari, External Examiner, Chemical & Petroleum Engineering, University of Calgary

DEDICATION

To

My wife, Xiaoyan Pu

My sons, Xiangzhi Gu

Richard Xiangcan Gu

My parents, Caiquan Gu

Dalun He

My sisters

ABSTRACT

Coalbeds are an extremely complicated porous medium with characteristics of heterogeneity, dual porosity and stress sensitivity. In the past decades great achievements have been made to the simulation models of pressure depletion coalbed methane (CBM) recovery process and CO_2 sequestration and enhanced coalbed methane (ECBM) recovery process. However, some important mechanisms are still not or not properly included. Among them, the influence of geomechanics is probably the most important one. Because of its influence coalbed permeability, the key parameter for the success of methane recovery processes, changes drastically with alterations of in situ stresses and strains during these processes. In present reservoir simulators, the change of coalbed permeability is estimated with analytical models. Due to the assumptions and over simplifications analytical models have limitations or problems in application.

In this research in order to properly estimate the changes of permeability and porosity in the simulation of CO_2 sequestration and ECBM recovery process, comprehensive permeability and porosity models have been developed with minimum assumptions and corresponding simulation methods established. Firstly, a set of continuum medium porosity and permeability coupling models is built up and a corresponding simulation procedure to apply these models in reservoir and geomechanical coupled simulations is proposed. Using the models and simulation procedure a sensitivity study, mainly on the parameters related to coalbed permeability change and deformation, has been made for the CBM recovery

process. Then based on the understanding, a set of discontinuum medium porosity and permeability coupling models is developed and a corresponding procedure to apply these models in reservoir and geomechanical coupled simulations is presented. The new models are more comprehensive and adaptable, and can accommodate a wide range of coalbeds and in situ conditions. The proposed equivalent continuum deformation model for coal mass is validated by simulating a set of lab tests including a uniaxial compression test in vacuum and a CO_2 swelling test under axial constraint in the longitudinal (vertical) direction. At last the discontinuum medium porosity and permeability coupling models and the simulation procedure are successfully applied to simulate part of a series of micro-pilot tests of ECBM and CO_2 sequestration at Fenn Big Valley of Alberta, Canada.

ACKNOWLEDGEMENT

I wish to express my deepest appreciation and gratitude to my supervisor, Dr. Rick Chalaturnyk, for his helps and supports in these years. The guidance and encouragements provided by Dr. Chalaturnyk, both professionally and personally, are externally acknowledged.

The sacrifice and time required to complete a Ph.D. program were not endured entirely by myself. The loves, helps and supports provided by my wife, Xiaoyan Pu, and our sons, Xiangzhi Gu and Richard Xiangcan Gu, are lovingly acknowledged.

Special thanks to my father, Caiquan Gu, and my mother, Dalun He, for their selfless loves and helps in my life, especially when I was writing the thesis while my little son, Richard, needed special cares.

I would like to make a grateful acknowledgement to The University of Alberta and Alberta Ingenuity Fund for their sponsorships to my study and thesis research. The supports give me great opportunities to explore the area I have been interested in and to develop necessary technical skills for my long term professional career.

I am extremely grateful to Dr. Jerzy Gustkiewicz in the Polish Academy of Science for kindly and generously sending me his research papers that are very important references to my research.

I especially appreciate the generous helps and supports provided by other professors in the Geotechnical Engineering Group, including Dr. Dave H. Chan, Dr. C. Derek Martin, Dr. David C. Sego, Dr. Kevin W. Biggar and Dr. David M. Cruden, and by the professors in the School of Mining and Petroleum, including Dr. Ergun Kuru, Dr. Clayton V. Deutsch, Dr. Luciane B. Cunha and Dr. Marcel Polikar.

I like to sincerely thank the graduates in the Geotechnical Engineering Group and in the School of Mining and Petroleum who gave me tremendous helps during my study.

I am also grateful for the supports and assistances provided by the staff in the Faculty of Graduate Studies and Research, the department of Civil and Environmental Engineering and the University of Alberta’s libraries.

TABLE OF CONTENTS

LIST OF TABLES

LIST OF FIGURES

LIST OF SYMBOLS

a = width of coal matrix block

a_1 = new width of coal matrix block

A = a material parameter in Equation (5.5a)

A_i = empirical parameter (i = 1, 2, 3…)

b = aperture of fracture (cleat) (ignoring the difference between mechanical apertures and hydraulic apertures)

b_m = mechanical aperture of fracture (cleat)

$<b_m>$ = statistical average of mechanical apertures

b_h = hydraulic aperture of fracture (cleat)

$(b_m)^{max}$ = maximum mechanical aperture of fracture under zero stress

b^r = residual aperture of fracture (cleat) at high effective stress

b' = reciprocal of Langmuir pressure

b_ε = reciprocal of p_ε, the pressure at a half of ε_∞ in Langmuir-type curve match of volumetric strain change

B_i = empirical parameter (i = 1, 2, 3…)

c' = a coefficient related to Young's modulus and Poisson's ratio

c_m = coefficient of volumetric matrix swelling/shrinkage due to gas adsorption/desorption in terms of gas mass

c'_m = matrix shrinkage compressibility due to gas desorption

c_p = pore compressibility

$\bar{C}_p$ = average pore compressibility between two stress states

c_s = grain compressibility

c_x = shrinkage coefficient in Equation (2.3-11)

C_f = hydraulic conductivity of fracture (under effective stress σ')

C_m = hydraulic conductivity of matrix (under effective stress σ')

CBM = (pressure depletion) coalbed methane

CD_f = dimensionless fracture conductivity, $CD_f=W_fk_f/(\pi kL_f)$

cos = cosine (trigonometric function)

d = differential

dp/dx = pressure gradient in direction x (flow direction)

e = base of natural logarithm

exp = exponent

E = Young's modulus of matrix

E_F = analog of Young's Modulus for fracture

E^* = equivalent Young's modulus of matrix and fracture

ECBM = enhanced coalbed methane

f = a fraction between 0 to 1 in Equation (2.3-17a)

g = gravity acceleration

G = shear modulus of matrix, $G=E/[2(1+\nu)]$

G^* = equivalent shear modulus of matrix and fracture

h = fracture asperity height

h_{rms} = root mean square of fracture asperity height distribution

JCS = joint wall compression strength

JRC = joint roughness coefficient

JRC^m = mobilized joint roughness coefficient

JRC^p = original (peak) joint roughness coefficient

k, k_f = permeability of fracture (cleat)

$\langle k \rangle$ = mean permeability of fractures (cleats)

$k_{average}$ = average permeability of fractures (cleats)

k_{butt} = permeability of cleat in the direction of butt cleats

k_{face} = permeability of cleat in the direction of face cleats

K = bulk modulus of coal, $K=E/[3(1-2\nu)]$

K_{frac} = bulk modulus of fracture porous medium

K_n = normal stiffness of fracture (cleat)

K_n^0 = initial normal stiffness of fracture (cleat) corresponding to initial normal stress, σ_n^0

K_S = shear stiffness of fracture (cleat)

K_S^{max} = maximum shear stiffness when the normal stress reaches the magnitude of uniaxial compressive strength (UCS)

K_{solid} = bulk modulus of solid grains

l_m^* = dimension change of per unit coal matrix block in horizontal direction under per unit pressure change

ln = natural logarithm

log = common logarithm

L_f = length of propped hydraulic fracture

mD = milli-darcy

min = minimum

M = constrained axial modulus of coal, $M=E*(1-\nu)/[(1+\nu)*(1-2\nu)]$

MPa = mega Pascal

n(h) = distribution function of fracture asperity height (h)

nm = nano-meter

p_L = Langmuir pressure of adsorption (defined as the pressure that gives gas adsorption equal to one-half of the monolayer capacity)

p = (pore) pressure

p_ε = pressure at a half of ε_∞ in Langmuir-type curve to match the change of volumetric strain

p_s = adsorption pressure

Q = volumetric flow rate

r_n = mole fraction of gas component n (n = i, j, k…)

s = fracture (cleat) spacing

<s> = mean fracture (cleat) spacing

scf = standard cubic feet

sin = sine (trigonometric function)

tan = tangent

t = a material parameter

T = temperature

u_n = normal displacement (closure) of fracture (cleat)

u_n^{max} = maximum normal displacement (closure) of fracture (cleat)

u_s = shear displacement of fracture (cleat)

u_s^k = shear displacement of fracture (cleat) in time step k

u_s^p = peak shear displacement of fracture (cleat)

u_s^r = residual shear displacement of fracture (cleat)

U = sliding potential

V, V_D = volume of adsorbed gas per unit weight of coal

V_m = Langmuir volume of adsorption (the maximum monolayer volumetric capacity per unit weight of coal)

w = width of a unit containing one matrix block and one adjacent cleat

W = width of a fracture (along the longer side of rectangular cross section of a fracture)

x = direction x in Cartesian coordinate system

y = direction y in Cartesian coordinate system

z = direction z in Cartesian coordinate system

Greek symbol

α = Biot coefficient

$\propto$ = proportional

β_D = coefficient of volumetric matrix shrinkage/swelling due to desorption/adsorption of gas

β_{LD} = coefficient of linear matrix shrinkage/swelling due to desorption/adsorption of gas

β_{LT} = coefficient of linear thermal expansion

β_T = coefficient of volumetric thermal expansion

γ = shear strain

Δ = change of a parameter, defined as the new value minus the old value

Δa = change of width of a matrix block

Δb_h = change of fracture (cleat) hydraulic aperture

Δb_m = change of mechanical aperture of fracture (cleat) (due to change of normal stress)

Δb^{max} = maximum change (deformation) of fracture aperture

$(\Delta b_m)_n$ = change of fracture (cleat) mechanical aperture due to change of normal stress

$(\Delta b_m)_S$ = change of fracture (cleat) mechanical aperture due to shear displacement

ΔC = change in gas concentration

ΔC_{max} = maximum change in gas concentration

Δd = standard deviation of mechanical aperture

Δm = change of adsorbed mass of gas

Δp = change of pore pressure

Δp_{max} = maximum change of pore pressure

ΔS = change of adsorbed methane mass

ΔT = change of temperature

Δu = change of displacement of fracture (cleat)

Δu_n = change of normal displacement of fracture (cleat)

Δu_s = change of shear displacement of fracture (cleat)

Δu_s^k = change in shear displacement of fracture (cleat) in time step k

ΔV_D = change of adsorbed gas volume per unit weight of coal

ΔV_{Di} = change of adsorbed volume of gas component i per unit weight of coal

Δw = change of the width of a unit containing one matrix block and one adjacent fracture

$\Delta \gamma$ = change of shear strain

$\Delta \gamma_f$ = change of shear strain of fracture (cleat) defined by Equations (5.26) or (6.17b)

$\Delta \varepsilon$ = change of normal strain

$\Delta \varepsilon_f$ = change of normal strain of fracture (cleat) defined by Equations (5.20) or (6.17a)

$\Delta \varepsilon_L$ = change of linear normal strain of coal matrix

$\Delta \varepsilon_L^t$ = total change of linear normal strain of a unit including one matrix block and one adjacent fracture (cleat)

$\Delta \varepsilon_{LE}$ = change of linear normal strain due to change of total stress

$\Delta \varepsilon_{LD}$ = change of linear normal strain due to desorption/adsorption of gases

$\Delta \varepsilon_{LP}$ = change of linear normal strain due to pressure change

$\Delta \varepsilon_{LS}$ = change of linear normal strain due to change of effective stress

$\Delta \varepsilon_{LT}$ = change of linear normal strain due to temperature change

$\Delta \varepsilon_{VD}$ = change of volumetric strain due to desorption/adsorption of gas

$\Delta\varepsilon_{VT}$ = change of volumetric strain due to temperature change

$\Delta\sigma$ = change of total normal stress

$\Delta\sigma_S$ = change of normal stress due to shear displacement

$\Delta\sigma_T$ = change of normal stress due to thermal effect

$\Delta\sigma'$ = change of effective (normal) stress

$\Delta\sigma'_x$ = change of effective stress in direction x (horizontal direction)

$\Delta\tau$ = change of shear or tangential stress

ε = normal strain, defined positive for extension

ε_L = linear normal strain

ε_L^h = linear normal strain in horizontal direction due to gas adsorption under no constraint condition

ε_L^v = linear normal strain in vertical direction due to gas adsorption under no constraint condition

ε_L^{vc} = linear normal strain in vertical direction due to gas adsorption under vertical constraint

$\varepsilon_{L\infty}$ = linear normal strain corresponding to maximum volumetric strain at infinite pressure in Langmuir-type curve match to volumetric strain change, if isotropic $\varepsilon_{L\infty}=\varepsilon_\infty/3$

ε_V = volumetric strain

ε_∞ = Maximum volumetric strain at infinite pressure in Langmuir-type curve match to volumetric strain change

θ = friction angle

θ^m = mobilized friction angle

θ^r = residual friction angle

μ = fluid viscosity

ν = Poisson's ratio of matrix in a discontinuum medium, or Poisson's ratio of coal mass in a continuum medium

ν^* = equivalent Poisson's ratio of coal mass (including matrix and fracture)

ν_{ij} = factor (Poisson's ratio) to determine normal strain in direction j when a stress is added in direction i (i and j are orthogonal directions)

π = ratio of circumference of a circle, π=3.1415926…

ρ_L = density of fluid

Σ = summation symbol

σ = total normal stress

σ' = effective normal stress

σ_3 = confining stress

σ_c = unconfined compressive strength (UCS) of coal matrix (or rock) adjacent to joint wall

σ_h = hydrostatic stress

σ_m = mean stress

σ_v = vertical (overburden) stress

τ = shear stress

ϕ, ϕ_f = porosity of fracture (cleat)

ψ = dilation angle

ψ^{eff} = effective dilation angle

ψ^m = mobilized dilation angle

ψ^p = peak dilation angle

Other symbols

$\int$ = integral symbol

∂ = partial differential symbol

Superscripts

0 = initial state, or original state, or reference state

eff = effective

k = time step k

k-1 = time step k-1

m = mobilized

max = maximum

n = exponent related to the relation between permeability ratio and mechanical aperture of cleat

p = peak

r = residual

t = total

Subscripts

0 = initial condition, or value under effective stress σ_0'

c = compressive

E = due to change of total stress

D = due to change of gas desorption or adsorption

The conventions of index notation that are generally adopted in geomechanics are not applied in this thesis.

f = fracture (cleat)

i = direction i, or index i, or gas component i

j = direction j, or component j

k = direction k

L = linear

m = mobilized

max = maximum

min = minimum

n = normal direction

p = pore

P = due to change of pressure

r = residual

s = shear direction

t = tangential direction

T = temperature, or due to change of temperature

x = direction x, or cleat set intersecting axis x

y = direction y, or cleat set intersecting axis y

yx = plane y-x

z = direction z

zx = plane z-x

zy = plane z-y

1 INTRODUCTION

1.1 BACKGROUND

The greenhouse effect is a scientifically proven main factor causing the global warming. The relative contributions of greenhouse gases to the greenhouse effect are: 63.6% from carbon dioxide (CO_2), 19.2% from methane (CH_4), 5.7% from nitrous oxide (N_2O) and chlorofluorocarbons (CFCs), and 11.5% from other sources (Mavor et al, 2002). According to their contributions the reduction of CO_2 emission into the atmosphere can significantly decrease the greenhouse effect. However CO_2 produced by human activities is not expected to significantly decrease because most CO_2 comes from the combustion of fossil fuels, including electricity generation, transportation, house warming, oil refinery and gas process etc., and fossil fuels will remain as a dominant component of the world's energy supply for at least this century due to their inherent advantages such as availability, competitive cost, easy transportation and storage, and large resources (Bachu and Shaw, 2003).

Although CO_2 produced by human activities will not decrease in this century there are several approaches that can be used to reduce CO_2 emission into the atmosphere. The approaches include improving the efficiency of energy utilization and conversion systems, switching to the fuels that are less carbon-intensity (such as from coal to natural gas), expanding as much as possible the power generation with nuclear and renewable energy (e.g. wind, solar, geothermal, tidal and hydroelectric energy), and CO_2 capture and sequestration in geological formations, i.e. geological sequestration (White et al, 2003). Among these options geological sequestration is increasingly seen as a cost-effective strategy to achieve deep reduction of CO_2 emission (Beecy et al, 2001). Geological sinks that can be used for CO_2 sequestration are depleted oil and gas reservoirs, deep unmineable coal seams and deep saline reservoirs. Two commercial-scale sequestration projects (one injected CO_2 into a deep unmineable coal seam with simultaneous recovery of CH_4 and another injected CO_2 into a deep saline aquifer as a part of natural gas production) along with more than 30 years of commercial EOR applications of CO_2 in depleted petroleum reservoirs make a compelling argument that the sequestration of CO_2 in geological formations represents a safe, practical, and viable approach to

stabilize the atmospheric concentration of CO_2 while still using fossil fuels and allowing economy to continue to grow (White et al, 2003). Depleted oil and gas reservoirs and deep unmineable coal seams are the most attractive geological formations for CO_2 sequestration due to their "value-added" merit. The study of Stevens et al (2001) indicates that the "value-added" sequestration offers at least 1070 Gt (gigaton) of a low-cost and secure CO_2 sequestration capacity. This is equivalent to over 150 years of emission from fossil fuel-burned power plants worldwide.

The advantages of deep unmineable coal seams for CO_2 sequestration include the huge coal resources around the world and the fact that the sorption capacity of coal to CO_2 is 1.8 to 10 times of that to methane (Mavor et al, 2002). CO_2 injection into coal seams would not only be a sequestration process but also an enhanced coalbed methane (ECBM) recovery process. As a result CO_2 sequestration may be operated at a low cost or even net profit depending on the revenue from produced methane. In addition since coalbed methane is a clean-burning fuel, considered more environmentally friendly than coal, oil even conventional natural gas, using captured coalbed methane to replace coal or oil for electricity generation, vehicle burning and house heating etc. can further reduce tremendous greenhouse gas emissions.

1.2 STATEMENT OF PROBLEMS

Numerical simulation is a necessary tool for designing and evaluating CO_2 sequestration and ECBM recovery projects. In the past decades a lot of efforts have been devoted to developing simulation models for pressure depletion coalbed methane (CBM) recovery process and great achievements have been made (King and Ertekin, 1991; King and Ertekin, 1995). However, available simulators based on these models still need to improve in order to correctly simulate the complicated mechanisms involved in CO_2 sequestration and ECBM recovery process (Law et al, 2002). The main reason is that some mechanisms are not considered or not properly considered in these simulators due to the limitations of understanding, simulation models and simulation techniques. From a comprehensive literature review we found that the influence of geomechanics is a paramount mechanism that is not properly considered in the present simulators. Due to the influence of geomechanics (i.e. the changes of in situ stresses and strains), the permeability of coalbeds, which is a key parameter

for the success of CBM recovery process and CO_2 sequestration and ECBM recovery process, is not a constant but varies drastically during these processes.

To improve the reliability of simulation results the change of coalbed permeability must be properly considered in numerical simulations. At present the method to include the influences of permeability changes is based on analytical models, such as the models of Sawyer and Paul (1990), Levine (1996), Palmer and Mansoori (1998), Shi and Durucan (2003), and Chikatamarla et al (2004). With these models, a monotonic relationship between the change of permeability and the alternation of pressures can be calculated and applied in numerical simulations. The advantage of analytical models is their easy application in present simulators with minor code modifications. However, analytical models have limitations or problems due to their assumptions and over simplifications made in the formulation. The following summarizes the major problems.

(1) The permeability of coalbeds was assumed to be isotropic throughout the life of production processes.

This assumption implies initial permeability and the change of permeability are all isotropic. Nevertheless, due to the significant difference between butt cleats and face cleats, initial permeability is usually not isotropic in coalbeds. Based on the results of field well tests, Koenig and Stubbs (1986) reported the anisotropy ratio of permeability in the bedding plane was as high as 17:1 in the Rock Creek coalbeds of the Warrior Basin in the USA. In addition, it will be shown in Chapter 5 of this thesis that during production the change of in situ stresses is not isotropic in most areas of a coalbed even if initial permeability is assumed to be isotropic, illustrating that the change of permeability is not isotropic as well.

(2) Coal mass was regarded as a continuum isotropic medium undergoing linear elasticity due to the changes of stress and/or strain.

In analytical models coal mass was regarded as a continuum isotropic medium and the theory of linear elasticity for continuum isotropic media was applied to estimate the deformation of coal mass, i.e. the relationship between stress and strain was described with a constant Young's modulus and a constant Poisson's ratio. Actually coal mass is a discontinuum anisotropic medium

containing matrix and cleats (fractures). The results of the triaxial tests by Hobbs (1964) and the uniaxial tests by Czaplinski and Gustkiewicz (1990) indicate that a typical curve of strain versus stress consists of a concave part under lower stresses and a linear part under higher stresses, as shown in Figure 1.1. The concave part is mainly due to the deformation of cleats while the linear part is due to the deformation of coal matrix. It will be illustrated later in this thesis that it is easy to model the linear part (the deformation of coal matrix) using the theory of linear elasticity but difficult to simulate the concave part (the deformation of cleats). In addition, coal mass is not an isotropic medium. Beside the well known anisotropy of cleats, coal matrix is also anisotropic. The test results of Szwilski (1984) showed that the ratio of elastic moduli in the directions perpendicular to cleats over the modulus in the direction perpendicular to bedding was as much as 2.6.

(3) The application of the principle of superposition was problematic.

In the formulation of analytical models, the changes of either stresses or strains were superposed in order to obtain the total change of stress or strain. To do so, it was assumed that the change of stress or strain caused by the alternation of fluid pressures was independent of the change of stress or strain by the shrinkage/swelling strain due to gas desorption/absorption. In estimating the change due to gas desorption/absorption, the shrinkage/swelling strains measured under no constraint condition were applied in analytical models. In reality, the changes of stress or strain from these two sources are interdependent. The shrinkage/swelling strains under in situ stress conditions are much smaller than that under no constraint condition. This means that the change of stress or strain due to gas desorption/absorption was overestimated in analytical models. The application of shrinkage/swelling strains measured under in situ stresses can improve the estimation. Nevertheless, in situ stresses are not static but dynamic during production. Experimental measurements of shrinkage/swelling strains under dynamic in situ conditions would be very challenging and costly. A similar problem also happened in estimating the change of stress or strain due to the alternation of fluid pressures.

In addition, for the models of superposing stresses, uniaxial or vertical deformation was assumed throughout coalbeds, i.e. horizontal strains were assumed to be zero. However this assumption does not really hold. Because the

change of fluid pressures and the change of shrinkage/swelling strains are not uniform throughout coalbeds during production, horizontal strains would not keep being zero but change non-uniformly. For the models of superposing strains, the volumetric strains due to gas desorption/absorption and due to pressure changes were all converted to the change of cleat porosity. Actually, the change of strain in the direction normal to the bedding plane (usually vertical direction) would mainly cause the displacement of overburdens rather than contribute the change of cleat porosity and permeability since few cleats develop along the bedding plane.

(4) Cleats were assumed to be smooth plate channels.

This assumption ignored the influences of tortuosity, surface roughness, and contact areas of cleats on fluid flow. In other word the mechanical aperture of a cleat was assumed to be identical to the hydraulic aperture of that cleat. However, the results of Barton et al (1985) indicated that a mechanical aperture and a hydraulic aperture are not equivalent. Their relationship can be described by an empirical equation:

$$b_h = \min\left\{b_m, \frac{{b_m}^2}{JRC^{2.5}}\right\} \quad \text{.....(1-1)}$$

From the above analyses, it is clear that due to the improper assumptions or over simplifications made in the formulation, analytical permeability models cannot correctly describe the in situ changes of permeability during CBM process and CO_2 sequestration and ECBM process.

1.3 SCOPE, OBJECTIVE AND METHODOLOGY

The objective of this research is to develop comprehensive models and corresponding simulation procedure to properly estimate the changes of permeability and porosity in the simulations of CO_2 sequestration and ECBM recovery process. Specifically, mathematical models will be established to quantify the changes of permeability and porosity during the process by considering the influences of geomechanics, i.e. the influences of the changes of stress and strain. The simulation procedure will be developed and the application will be demonstrated in this research. To achieve the goal, the scope of thesis research includes:

(1) To analyze the factors influencing the changes of permeability and porosity.

(2) With minimum assumptions and simplifications and considering most factors influencing permeability, to develop reliable models to quantify the changes of permeability and porosity during the process.

(3) To make a sensitivity study on the parameters causing the changes of permeability and porosity and/or significantly influencing well performances and methane recovery.

(4) To establish a simulation procedure with which the developed models can be applied in the simulation of the process.

(5) To demonstrate the applicability of the proposed models and simulation procedure in the simulation of the process.

In this research the explicitly sequential reservoir and geomechanical coupled simulation is applied to study the change of permeability and porosity and to simulate CBM recovery process and CO_2 sequestration and ECBM recovery process. GEM© (CMG, 2004), a three dimensional, isothermal equation-of-state (EOS) compositional simulator, is used to model the multiphase fluid flow in coalbeds. FLAC (Itasca, 2002a) and FLAC3D (Itasca, 2002b), thermohydromechanical simulators, serve to simulate the deformation of coalbeds. The experimental results of Czaplinski and Gustkiewicz (1990) and Szwilski (1984) are utilized to validate the proposed deformation model of coal mass. The field results of micro-pilot tests of ECBM and CO_2 sequestration made at Fenn Big Valley of Alberta, Canada, are used to demonstrate the applicability of the models and method established in this research.

1.4 ORGANIZATION OF THE THESIS

Chapter 1 introduces the relative contributions of green house gases to the green house effect, the methods to mitigate the green house effect and the merits of CO_2 sequestration and ECBM recovery process as one solution to decrease the emission of the major green house gas, CO_2. It also presents the problems with present simulators used to model CO_2 sequestration and ECBM recovery process and states the objective, scope and methodology of this research.

Chapter 2 is a comprehensive review of the state-of-the-art research results related to CBM recovery process and CO_2 sequestration and ECBM recovery process. The reviewed areas include the characteristics of coalbeds, the

mechanisms of coalbed methane recovery, available analytical models to predict the changes of permeability and porosity during coalbed methane recovery processes, the deformation and permeability models of fractured rocks, and the thermo-hydro-mechanical coupled simulation.

Chapters 3-6 are a style of "collection of papers" thus there are some duplications. In Chapter 3 the continuum media porosity and permeability coupling models are developed. The calculation procedure and application case to use these models in reservoir and geomechanical coupled simulation are presented. In addition, the mechanisms of coalbed methane production and the influences of geomechanics on methane recovery processes are also discussed in this chapter.

Chapter 4 contains a sensitivity study to examine how significant the influences of reservoir parameters on CBM recovery would be. The study focuses on the parameters that are related to the changes of in situ stress and strain in coalbeds and the parameters that significantly affect CBM production identified from previous studies.

Chapter 5 present the discontinuum medium porosity and permeability coupling models. In the formulation of these models discontinuous coal mass (containing cleats and matrix) is regarded as an equivalent continuum elastic medium. The anisotropies of coal in permeability, the coefficients of shrinkage/swelling due to gas desorption/absorption, the mechanics parameters of cleats and matrix, and the coefficients of thermal expansion due to temperature changes, are considered. The simulation procedure and application case to apply these models in coupled simulation is demonstrated. The important issues and limitations of the proposed models are also discussed.

Chapter 6 focuses on the verification of the deformation model for coal mass, i.e. the equivalent continuum elastic model, by matching the results of uniaxial lab tests made on one specimen by other researchers. The simulated tests include a uniaxial compression test in vacuum and a CO_2 swelling test under an axial constraint in the longitudinal (vertical) direction. The contrasts are made to the changes of porosity and permeability estimated with different models (analytical and numerical models) during CBM recovery process. In addition, a brief review to analytical permeability and porosity models is included in this chapter.

Chapter 7 demonstrates the applicability of the discontinuum medium porosity and permeability coupling models and corresponding calculation

procedure in reservoir and geomechanical coupled simulation of field scale cases. The methodology is applied to simulate part of the micro-pilot tests of ECBM and CO_2 sequestration in Alberta, Canada. The well background and history are introduced. The input data and simulation (match) results are presented. The difficulties and problems met in the coupled simulation are discussed.

Chapter 8 summarizes the main results and findings of this research and gives recommendations to future studies.

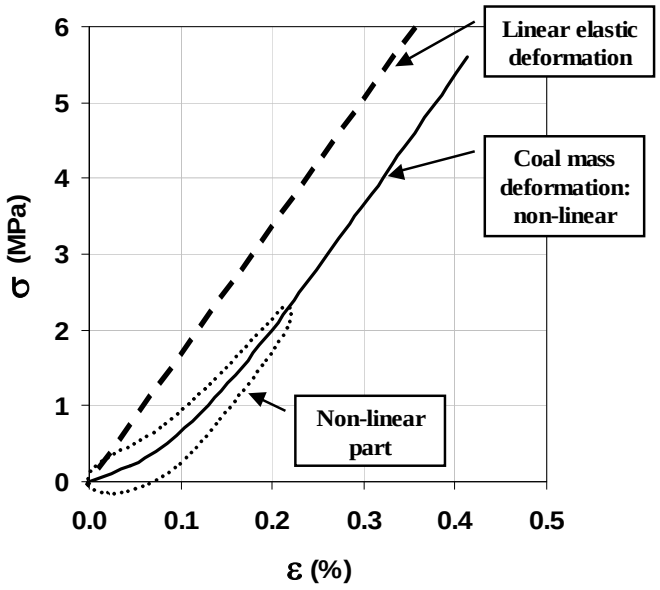

Figure 1.1: Comparison between Linear Elastic Deformation and Coal Mass Deformation

2 LITERATURE REVIEW

2.1 CHARACTERISTICS OF COALBED

2.1.1 Pore Structure

Coalbeds or coal seams are well known for their dual porosity characteristics. They contain both micropores and macropores. The plan view of an ideal pore structure model of coalbeds is shown in Figure 2.1. Micropores exist in coal matrix and macropores are almost uniformly spaced natural fractures, called cleats. Cleats include face cleats and butt cleats. Butt cleats are about 90^o to face cleats and commonly terminate at face cleats. Both types of cleats develop along bedding planes and are essentially perpendicular or near-perpendicular to bedding planes.

2.1.2 Gas Storage Mechanism and Adsorption Isotherm

Physical adsorption is the primary gas storage mechanism of coalbeds. It typically accounts for about 98% of the gas in a coalbed, depending on the pressure at which gas is adsorbed (Gray, 1987). Gases adsorb on the walls of micropores which have a diameter of 0.5 to 1.0 nm and are inaccessible to formation water (brine). Besides, gases are also stored in cleats either as free gas or solution gas.

For a given temperature, the relationships between the gas storage capacity of coal and pressure are called adsorption isotherms. Figure 2.2 (Arri et al, 1992) shows the typical adsorption isotherms of methane, nitrogen and carbon dioxide. It indicates that carbon dioxide has much higher affinity with coal than nitrogen and methane.

2.1.2.1 Adsorption/Desorption of Methane

The adsorption capacity of coal to methane has been widely studied and most adsorption isotherms can be described approximately with the Langmuir equation:

$$V = V_m \frac{p}{p_L + p} \quad \text{……...……..…...(2.1-1)}$$

where V_m and p_L are Langmuir volume and Langmuir pressure of adsorption. p is pressure and V is absorption volume at p.

Yang and Saunders (1985) reported the adsorption isotherms of methane on coals in a temperature range of 22 ~ 300°C and a pressure range of 0 ~ 6.9 MPa. Their data were well fitted with the Langmuir equation. Patching and Mikhail (1986) presented their methane isotherms of Canadian coals. They pointed out that gas adsorption isotherms were dependent on temperature, moisture content, the gas type involved and the type of coal, and could be expressed approximately with the Langmuir or the Freumdlich equations. Mavor et al (1990) studied the adsorption isotherms of methane to a variety of American coals. Their study showed that the Langmuir equation was applicable to all the adsorption isotherm data they collected.

However, some early adsorption isotherms indicated that the adsorption capacity of coal to methane was not proportional to the ambient pressure applied thus the Langmuir equation was incapable to describe them. For example, Moffat and Weale (1955) studied the adsorption of methane on a number of British coals under 25°C and high pressures (up to 1000 atm). Their results showed that the adsorption isotherms usually rose to the maxima in a pressure range of 100 to 200 atm and decreased at higher pressures, but apparently to limiting values.

2.1.2.2 Adsorption/Desorption of Gas Mixtures

Many researchers have studied the adsorption of gas mixtures to coal and the results showed that the extended Langmuir isotherm and the ideal adsorbed solution (IAS) theory could provide acceptable predictions of adsorption isotherms of gas mixtures.

Stevenson et al (1991) measured the adsorption isotherms for binary and ternary mixtures of CH_4, CO_2 and N_2 on coal at 30°C and pressures up to 5.2 MPa. Their results showed that equilibrium gas and adsorbate phase compositions differed considerably and that the total amount of gas mixture adsorbed was strongly dependent on the composition and the system pressure. They concluded that IAS theory, which assumes the ideality of adsorbed phase, provides acceptable predictions for adsorption of mixtures on coal over a wide range of pressure and composition in many coalbed gas applications.

Arri et al (1992) investigated the adsorption of methane-nitrogen and methane-carbon dioxide mixtures at a temperature of 46.11°C (115°F) and pressures of 3.45, 6.89 and 10.34 MPa (i.e. 500, 1000 and 1500 psi respectively). The results showed that each gas did not adsorb independently, instead two gases competed for the same sorption sites. The results indicated that the extended

Langmuir isotherm, in which the Langmuir constants for pure gas sorption only were used and no binary sorption constants were needed, provided a reasonable fit to the experimental data. The extended Langmuir isotherms of gas mixtures were expressed as:

$$V_i = (V_m)_i \frac{p \frac{r_i}{(P_L)_i}}{1 + p \sum_j \frac{r_j}{(P_L)_j}} \quad \text{.....(2.1-2)}$$

Pariti and Harpalani (1993) established the adsorption isotherms of a multicomponent (methane and carbon dioxide) gas mixture. Their studies showed that during desorption, the concentration of methane decreased as the pressure decreased while carbon dioxide concentration increased. The experimental results of the adsorption of the gas mixture and the variation in gas compositions were compared well with the isotherms numerically obtained from IAS theory applying the isotherms of pure methane and pure carbon dioxide. They concluded that the extended Langmuir isotherm provided better results and recommended it for theoretical prediction.

Hall et al (1994) measured the adsorption of pure methane, nitrogen and carbon dioxide, and their binary mixtures on wet Fruitland coal at 115°F (46.11°C). They used the results to test predictive methods for describing the adsorption behavior of the pure and gas mixtures. The models included various two-dimensional equations of state, as well as more traditional methods, such as the Langmuir model and IAS model. They concluded that overall, the two-dimensional equation-of-state and IAS models performed comparably, and they were more accurate than Langmuir model.

Huddleston et al (1995) studied the adsorption of methane under a temperature of 51.8°C (125°F) and pressures up to 15.17 MPa (2200 psi). Their results indicated that the particle size of samples affected the sorption capacity of coal. For relatively lager particles gas sorption capacity increased with the decrease of the particle size or the increase of surface areas. But as the particle size of the continued to decrease, the gas sorption capacity began to decrease. The Langmuir model could fit the isotherm results at low pressure and a third-order polynomial could fit the whole isotherm. They thought the deviation from the Langmuir model at near 6.21 MPa (900 psi) resulted from the pressure dependent factors such as permeability, condensation, and gas compositions.

Chaback et al (1996) studied the adsorption/desorption irreversibility of gas mixtures for ECBM recovery process. They reported that no adsorption

/desorption irreversibility was observed to methane and carbon dioxide or methane and nitrogen binary mixtures adsorbed on coal. For binary mixtures not containing oxygen, desorption gases arising from pressure depletion became richer in the more strongly absorbed species and using the extended Langmuir isotherm the adsorption/desorption behaviour could be described. However, for oxygen-bearing sorption gases, irreversible chemi-sorption occurred and could not be described with the Langmuir isotherm.

2.1.3 Swelling/Shrinkage Strains of Coal Matrix due to Adsorption /Desorption of Gases

In sorptive gas, coal matrix swells or expands due to the adsorption of sorptive gas with pressures increasing and shrinks or contracts due to the desorption of sorptive gas with pressures decreasing. This is another characteristic of coal. In contrast, coal matrix in non-adsorptive gas contracts with pressure increasing and expands with pressure decreasing.

2.1.3.1 Swelling/Shrinkage under No Constraint Condition

A lot of investigations have been made to the swelling/shrinkage strains of coal due to the adsorption/desorption of sorptive gases under conditions without constraints. A summary of the test conditions and measured swelling/shrinkage strains of coal in sorptive gases such as methane (CH_4), carbon dioxide (CO_2) and nitrogen (N_2) is shown in Table 2.1 and the details are described in the following section. For comparison the contraction strains of coal with pressure increase and expansion strains with pressure decreasing in non-adsorptive gas, helium (He), are also listed in the table if they were measured for the same coal. It should be noted that in the table swelling strains are defined positive and shrinkage strains are negative.

Using a number of British coal blocks Moffat and Weale (1955) investigated the shrinkage and swelling due to the desorption and adsorption of methane. Their results showed that Cannock Wood coal had the largest swelling and shrinkage strains. The maximum volumetric swelling strain was 1.75% during the adsorption of methane from 0 to 70 MPa (700 atm) and the maximum volumetric shrinkage strain was 1.49% during the desorption of methane from 70 to 0 MPa. Their results also indicated that coal shrinkage in desorption did not follow the path of expansion in adsorption. The shrinkage strain was smaller than the

swelling strain and left 0.27% residual volumetric strain for Cannock Wood coal after the pressure reached zero.

Reucroft and Patal (1986) studied coal swelling due to the adsorption of N_2 and CO_2 under 0.1379 MPa (20 psi) and 298 K with three Kentucky coals of bituminous, sub-bituminous and lignite ranks. They found the volumetric swelling strains ranged from 0.36% to 1.07% due to the adsorption of CO_2 and coal with a lower carbon content showed a higher degree of swelling. For the adsorption of N_2 and He, small contractions were observed.

Reucroft and Sethuraman (1987) also tested coal swelling due to CO_2 adsorption under 0.5, 1.0 and 1.5 MPa (5, 10 and 15 atm) and 298 K with three Kentucky coals in bituminous, sub-bituminous and lignite ranks. Their results indicated that the volume of coal increased by as little as 0.75% under 0.5 MPa (5 atm) and as much as 4.18% under 1.5 MPa (15 atm).

With a micro-dilatometer Walker et al (1988) measured the expansion of eighteen coals of various ranks during CO_2 adsorption under 298 K. Vitrinite content of coals varied from 53 vol.% to 98 vol.% and vitrinite content of the macerals exceeded 96 vol.%. The results showed that the expansion of coals, when exposed to an elevated pressure of CO_2, was not reversible, i.e. when pressures were reduced back to the atmospheric pressure the expansion would not become zero. The expansion increased with pressures increasing. For different coal ranks, the expansion varied from 0.59% to 1.03% at 0.68 MPa and from 1.57% to 3.79% at 4.8 MPa. At higher CO_2 pressures, there was a trend of expansion increase with coal ranks decreasing.

Using coal specimens from the Piceance Basin and the Black Warrior Basin, Harpalani and Schraufnagel (1990a and 1990b) studied the swelling and shrinkage of coal due to adsorption and desorption of CH_4. They found that the coal volume increased linearly up to 0.48% in adsorption when pressures were increased from 0 to 6.2 MPa (900 psi). When the pressure reduced, the decrease in the matrix volume was not linear. The bulk shrinkage in desorption was smaller than expansion in adsorption and remained 0.1% residual expansion at atmospheric pressure. If considered the contraction of coal due to compression of hydrostatic pressure, the volumetric expansion due to adsorption of methane was 0.57%.

Ceglarska-Stefanska and Czaplinski (1993) measured the coal expansion in CO_2 at 298 K used a gas-flame coal, a gas-coking coal and an anthracite. The samples were 15mm×15mm×15mm cubes cut from coal lumps. The measured

linear expansion in the direction parallel to the bedding was 0.44% ~ 0.65% and in the direction perpendicular to the bedding was 0.50% ~ 0.92% at 4.7 MPa to 4.8 MPa.

Ceglarska-Stefanska (1994) experimentally obtained coal expansion in CH_4 under pressures of 0.4 MPa to 4 MPa and a temperature of 298K. The samples were also 15mm×15mm×15mm cubes cut from coal lumps. It was found that the rate of gas adsorption exceeded the rate of expansion and similarly the gas desorption was faster than the coal contraction. During the initial period (about 30 minutes) of the contact of sorbate molecules with coal main adsorption occurred. Up to 60% of the total amount of the gas was adsorbed at this stage and no change in sample dimensions was observed. Under a gas pressure of 0.32 MPa swelling expansion was 0.02% in the directions parallel to and perpendicular to the bedding. Under a gas pressure of 3.04 MPa swelling expansion was 0.134% in the direction parallel to the bedding and 0.175% in the direction perpendicular to the bedding. The shrinkage due to gas desorption was usually smaller than the expansion and left some residual stains.

Harpalani and Chen (1995) tested the shrinkage of coal in CH_4. The samples were from the San Juan Basin and the desorption pressures from 10.3 MPa to 0 MPa. They obtained a shrinkage (volumetric strains) of 0.21% after subtracted the matrix compression due to pressure changes. They also found that matrix shrinkage (volumetric strain) was almost proportional to the adsorbed gas volume.

Using a high-volatile bituminous coal from Illinois, Levine (1996) observed that the swelling and shrinkage (volumetric) strains were around 0.53% due to CH_4 adsorption and desorption at 5.17 MPa and about 1.26% due to CO_2 adsorption and desorption at 3.09 MPa.

Using cubic samples (15mm×15mm×15mm) Ceglarska-Stefanska and Brzoska (1998) studied the expansion and contraction of “dry” coal and “pre-wetted” coal (water vapour pre-adsorbed) during adsorption and desorption. The strains were measured in the direction perpendicular to lamination and illustrated in Figure 2.3. The results showed that during adsorption the “dry” coal underwent a lower extensional strain course than the “pre-wetted” coal. During desorption both “dry” and “pre-wetted” coals experienced an increase then decrease strain course.

George and Barakat (2001) measured the volumetric shrinkage of coal due to gas desorption using a coal sample from the Ohai coal mine in the South Island of New Zealand. They fully saturated the sample in gas under 4 MPa for 500

minutes and the tested volumetric expansion due to adsorption was 2.16% with CO_2, 0.38% with CH_4 and 0.17% with N_2. Under the same condition, the volumetric compression of coal is 0.08% with He. The volumetric shrinkage due to desorption with pressure decrease was 2.07% for CO_2, 0.429% for CH_4 and 0.126% for N_2. The changes of effective volumetric strain with the desorption pressures are illustrated in Figure 2.4.

Using the coal B (the 'Brzeszcze' mine coal) and coal M (the 'Moszczenica' mine coal) in Poland, Ceglarska-Stefanska and Zarebska (2002a) studied the expansion of coal during the adsorption of CH_4 and the mixture of 41.5% CO2 + 58.5% CH4 under different gas pressure. The samples were 15mm×15mm×15mm cubes cut from coal lumps. The coal expansion in the direction perpendicular to stratification was 0.008% with CH_4 under gas pressure of 0.34 MPa and 0.249% with the gas mixture under a gas pressure of 3.70 MPa. Using the same size samples and the same coals, Ceglarska-Stefanska and Zarebska (2002b) obtained the contraction of coal due to the desorption of CH_4 and CO_2 after the samples were pre-adsorbed CO_2 and then adsorbed CH_4 under pressures of 0.53 ~ 2.83 MPa. The contraction measured in the direction perpendicular to the bedding was 0.026% ~ 0.157%.

Using subbituminous to medium volatile rank coals from the Western Canadian Sedimentary Basin (WCSB), Chikatamarla et al (2004) found the swelling strains of coal under a gas pressure of 0.6 MPa and obtained volumetric strains were 1.402% ~ 9.327% with H_2S, 0.261% ~ 0.656% with CO_2, 0.091% ~ 0.297% with CH_4 and 0.004% ~ 0.026% with N_2.

Zutshi and Harpalani (2004) tested the swelling strain of coal during the adsorption of CO_2 and CH_4 under a temperature of 45°C with samples from a coal mine in the USA. The effective strains (subtracted the compression in pressures) due to adsorption of gas obtained were 1.35% with CO_2 under 5.86 MPa and 0.7% with CH_4 under 7.45 MPa. With non-adsorptive gas (He) the compression of coal was 0.26% under 10.34 MPa.

Robertson and Christiansen (2005) measured the swelling strains of the longitudinal direction of coal samples from Utah of the USA under a temperature of 26.7 °C (80 °F) and a variety of pressures. With coal samples from Anderson mine the linear swelling strains were 2.13% with CO_2 under 5.6 MPa, 0.48% with CH_4 under 6.9 MPa and 0.14% with N_2 under 6.9 MPa. With coal samples from Gilson mine the tested linear swelling strains were 0.93% with CO_2 under 5.4 MPa, 0.39% with CH_4 under 6.9 MPa and 0.11% with N_2 under 6.3 MPa.

2.1.3.2 Swelling/Shrinkage under Constraint

There are a few of studies on the swelling/shrinkage of coal due to the adsorption/desorption of gas under constraint conditions. Czaplinski and Gustkiewicz (1986) studied the changes of stresses and strains under constraint conditions using coal from the 'Brzeszcze' mine in Poland. In the test an initial longitudinal (axial) stress was applied on a cylindrical sample or a cuboid sample with a square base and the changes of longitudinal stress and the changes of longitudinal and transversal strains were measured during the adsorption and desorption of CO_2. They got the longitudinal stress and longitudinal and transversal strains all increased during adsorption. For example, under an initial longitudinal stress of 9.8 MPa and a gas pressure of 2 MPa, the longitudinal stress increased by 4 MPa and the changes of strain were 0.125% in longitudinal direction and 0.39% in transversal direction due to adsorption of CO_2. Using coal from the 'Brzeszcze' mine in Poland, Czaplinski and Gustkiewicz (1990), and Gustkiewicz and Orengo (1998) presented similar study results of stress changes induced by the adsorption of CO_2. They found positive swelling stresses and strains due to adsorption. For instance, they obtained the longitudinal stress increased by 11.5 MPa under an initial longitudinal stress of 4.8 MPa and a gas pressure of 3.0 MPa due to the adsorption of CO_2.

2.1.3.3 Relationship between Strains and Adsorbed Gas Volume

Several studies showed that the swelling strains of coal due to the adsorption of adsorptive gases were positively correlated to the adsorbed volume of gas. The results of Harpalani and Chen (1995) with coal from the San Juan Basin of the USA indicated that the volumetric strain of coal matrix due to the adsorption of methane has approximately a linear relation with the adsorbed gas volume. The proportional coefficient, called the coefficient of matrix swelling due to gas adsorption (or the coefficient of matrix shrinkage due to gas desorption) was 2×10^{-4} g/ml when the adsorbed gas volume was in ml/g. Using a coal from the Colorado portion of the San Juan Basin, Seidle and Huitt (1995) tested the coefficient of matrix swelling of coal was $1.87\times10^{-5} \sim 4.7\times10^{-5}$ g/ml ($0.53\times10^{-6} \sim 1.33\times10^{-6}$ ton/scf) with CH_4 and $0.24\times10^{-5} \sim 3.92\times10^{-5}$ g/ml ($0.068\times10^{-6} \sim 1.11\times10^{-6}$ ton/scf) with CO_2. They also confirmed that matrix shrinkage was proportional to the adsorbed gas volume. Using the coals in ranks of subbituminous to medium volatile coals from the Western Canadian Sedimentary

Basin (WCSB), Chikatamarla et al (2004) also investigated the relationship between the swelling strains of coal and the adsorption of gases (H_2S, CO_2, CH_4 and N_2). Their results showed that the volumetric swelling/shrinkage of coal was strongly and positively correlated with gas concentration in all coals and for all gases.

Some researchers related swelling strains due to the adsorption of gas to adsorption pressures with the Langmuir type equation as:

$$\varepsilon_v = \frac{\varepsilon_\infty}{1 + \frac{p_\varepsilon}{p}} \quad \text{.....(2.1-3)}$$

These researchers include Levine (1996), Chikatamarla et al (2004) and Robertson and Christiansen (2005).

2.1.4 Permeability of Coalbeds

2.1.4.1 Anisotropy

The anisotropic characteristic of the pore structure of coal suggests that the permeability of coalbeds would be anisotropic and the greatest permeability in the direction of face cleats. With 50.8 mm (2 in) cubes of Cwmtillery Garw coal, Promery and Robinson (1967) found that the flow rates of water (corresponding to permeability) were significantly different when the confining pressures were perpendicular to main cleats (face cleats), cross cleats (butt cleats) or bedding planes. Permeability anisotropy of coal was confirmed by the experiment results of Gash et al (1993). Using coal samples from La Plata mine in the San Juan Basin and under a confining stress of 6.9 MPa (1000 psi) they found that the permeability parallel to bedding planes was 0.6 ~ 1.7 mD in the direction of face cleat and 0.3 ~ 1.0 mD in the direction of butt cleat, but 0.007 mD in the direction vertical to bedding planes.

From field well tests, Koenig and Stubbs (1986) reported the anisotropy ratio of permeability in the plane of bedding was as high as 17:1 in the Rock Creek coalbeds of the Warrior Basin of the USA.

2.1.4.2 Stress Dependency

Cleats in coalbeds are naturally fractures and are the main flow path of fluid flow. The permeability of coalbeds is of stress sensitive characteristic as those in

conventional fractured reservoirs. Like heat expansion and contraction of material due to temperature changes, coal expands and contracts due to the change of effective stresses occurring from the alterations of total stresses and/or pressures. Thus cleats open and close resulting in permeability changes.

Stress sensitivity of coalbed permeability has been studied for decades. In most studies, isotropic confining pressures (stresses) were applied to simulate in situ overburden stresses. Using N_2 and CO_2 as permeant, Patching (1965) studied the deformation and associated permeability changes of coal. He found that the permeability of coal drastically reduced with increasing confined pressures, the permeability decreasing approximately four orders while the confining stress increasing from 0.07 to 20.68 MPa (10 to 3000 psi). The effects of mean gas pressures and gas sorption on permeability were found much less comparing with the effect of confining stresses.

Promery and Robinson's results (1967) showed that the flow rate of water (corresponding to permeability) increased with the increase of injecting pressure (pore pressure) and decreased with the increase of confining pressure.

The study by Dabbous et al (1974) indicated that the permeability of coal to both air and water was greatly reduced due to the increase of overburden pressures.

Somerton et al (1975) investigated the permeability of fractured coal to methane under simulated subsurface stress conditions and found that the permeability of coal was strongly stress dependent, decreasing by more than two orders of magnitude in a stress range of 0.34 ~ 13.79 MPa (50 ~ 2000 psi). The types of stress applied, i.e. hydrostatic or triaxial, appeared to have little effect on the permeability reduction. The mean effective stress level was found to be the controlling factor in the permeability reduction.

Reznik et al (1978) tested the permeability of coal to nitrogen under confining pressures using the samples of Pricetown bituminous, Hanna and Gillette sub-bituminous and Texas lignite coals of the USA. The results showed that with confining pressures increasing from 0.689 to 4.83 MPa (100 to 700 psi) the permeability of coal decreased approximately two orders of magnitude.

The results of Rose and Foh (1984) indicated that the permeability of coal to water decreased as much as two orders of magnitude over a pressure range of simulating normal dewatering and production cycles in fields.

Harpalani and McPherson (1985) showed that in semi-log plot coal permeability decreased linearly with the increase of confining stress. Based on

their results they presented an empirical equation to predict the change of permeability with confining stresses:

$$k = A_1 e^{B_1 \cdot \sigma} \quad \text{.....(2.1-4)}$$

where the confining stress, σ, is in MPa and permeability, k, is in m^2.

Using whole core samples of coal from Fruitland Formation in the Northern San Juan Basin, Puri and Seidle (1991) measured permeability reduction during the depletion of reservoir pressures under uniaxial strain conditions. Their results were fitted with the following equation:

$$\frac{k}{k_0} = e^{[1.690(p/p_0 - 1)]} \quad \text{.....(2.1-5)}$$

where p is the pore pressure in psi and k is permeability in mD.

Enever and Hening (1997) analyzed and compared the changes of coal permeability with minimum effective stress based on experiments and field well tests of three Australian basins, i.e. the Sydney Basin, the North Bowen Basin and the South Bowen Basin. Their results showed that the logarithm of coal permeability linearly decreased with the increase of effective stresses and obtained a relationship as:

$$\frac{k}{k_0} = e^{-3 \cdot C_p \cdot \Delta\sigma'} \quad \text{.....(2.1-6)}$$

Al-hawaree (1999) also tested the change of coal permeability to carbon dioxide and methane with the change of effective stresses using coal samples from Coal Valley Luscar and Cardinal River open pit mines in Alberta of Canada. The results indicated that under the same pore pressure permeability to carbon dioxide reduced by 51% to 90% when effective stresses increased from 6 to 16 MPa and permeability to methane also decreased significantly when effective stresses increased.

In addition to the absolute permeability, some researchers also studied the influences of stresses on relative permeability. The study of Reznik et al (1974) showed that the relative permeability changed as overburden pressures were increased but the shape of relative permeability curves was similar. The results of Gash et al (1993) showed that with increasing confining pressures from 3.10 MPa (450 psi) to 6.89 MPa (1000 psi) the ratio of gas relative permeability to water relative permeability increased.

2.1.4.3 Gas Desorption/Adsorption Dependency

The shrinkage of coal matrix due to gas desorption causes the increase of cleat width thus permeability increases. In reverse the swelling of coal matrix due to gas adsorption results in the decrease of cleat width thus the decrease of permeability.

Early researchers did not realize the shrinkage/swelling of coal matrix due to the desorption/adsorption of gas and their effects on permeability. Patching (1965) found the permeability tested by carbon dioxide was somewhat less than the permeability by air or nitrogen. Based on further measurements using nitrogen, argon, helium and carbon dioxide in sequence he concluded that the permeability of coal was not noticeably affected by gas adsorption, but depended on the size of gas molecule. Somerton et al (1975) also found the permeability to methane was substantially lower than to nitrogen and on average the decrease was 20% for Pittsburgh coal and 40% for Greewich coal. They thought the reductions would appear too large to be explained on the basis of molecular diameters alone (proposed by Patching, 1965) and the sorption of methane on coal could not be ruled out as a possible cause of permeability reduction.

Later people studied and found the influence of shrinkage/swelling of coal matrix on permeability. Harpalani and Zhao (1989) investigated the effect of gas desorption on the permeability of coal using the specimens obtained from underground coal mines in the Piceance Basin and the Black Warrior Basin of the USA. The measurements were carried out with cylindrical specimens under triaxial stresses to simulate the in situ conditions and the changes of gas pressures ranged from 0.345 to 6.895 MPa (50 to 1000 psi). The results showed that above the desorption pressure the permeability of coal decreased with the decrease of gas pressure (pore pressure) (i.e. with the increase of effective stress). However, below the desorption pressure, the permeability of coal to methane increased dramatically with the decrease of gas pressure. In contrast, the permeability of coal to helium, which is almost non-adsorptive, decreased continuously with the decrease of gas pressure. Harpalani and Schraufnagel (1990a and 1990b) studied the relationships between gas pressures and permeability and the relationships between gas pressures and volumetric strains with specimens from a gassy coal seam in the Piceance Basin of Colorado in the USA. The experiments were operated under triaxial stresses to simulate the in situ stress condition. The results indicated that permeability of coal to methane increased with the decrease of gas

pressure (pore pressure) in spite of the increase of effective stress, and that the volume of coal matrix shrank by 0.4% when the gas pressure fell from 6.9 MPa to the atmospheric pressure. The shrinkage of coal matrix due to methane desorption caused gas flow paths wider and permeability increasing. Al-hawaree (1999) tested the change of permeability of coal to carbon dioxide and methane with pore pressures using the coal samples from Coal Valley Luscar and Cardinal River open pit mines in Alberta of Canada. The results indicated that under the same effective stress the permeability to carbon dioxide reduced about 55% ~ 84% when the pore pressure was increased from 3.5 MPa to 12 MPa and the permeability to methane reduced about 20% ~ 50% when the pore pressure was increased from 3.5 MPa to 10 MPa. In contrast, the permeability to carbon dioxide decreased more with the increase of pore pressure than the permeability to methane. With ground coal from the Power River Basin, Lin et al (2008) measured the permeability change due to the sorption of pure N_2, CH_4, CO_2 and the mixtures of N_2 and CO_2 under a constant effective stress of 2.76 MPa (400 psi). Their results indicated that the permeability of coal decreased with the increase of sorption pressures (corresponding to the increase of gas sorption). For the sorption of pure gases, CO_2 caused the highest permeability decrease followed by CH_4 and N_2. For the sorption of the mixtures, the permeability decreased with the increase of CO_2 component.

Field well test data supported that the permeability of coalbed increased due to desorption of methane. Mavor and Vaughn (1998) reported the permeability of three CBM wells in the San Juan Basin increased based on the well test results. The permeability of well VC 29-4 increased 4.09 times (from 16.6 to 67.9 mD) and the permeability of well VC 32-1 rose 2.72 times (from 17.1 to 46.7 mD) after produced 3 years. The permeability of well VC 32-4 increased 7.07 times (from 19.5 to 137.9 mD) after produced 3 years and 4 months. According to the results of build up well tests, Zahner (1997) showed a relationship between the permeability ratio (k/k_0) and the decline of reservoir pressures, illustrated Figure 2.5. The results indicated that permeability increased with the decrease of coalbed pressures. .

Field observations also indicated that the permeability of coalbed decreased due to the injection (desorption) of carbon dioxide in ECBM pilot tests. Reeves (2001) showed the field observations of the first field scale pilot of ECBM with carbon dioxide in the Allison Unit of the San Juan Basin in the USA. At the beginning the injection rate of CO_2 in four pilot wells was 5 MMcf/day but later

reduced to about 3 MMcf/day because of the loss of injectivity. This implies that the permeability around the wellbores decreased due to the injection (adsorption) of CO_2. Van der Meer and Fokker (2003) showed that in order to match the history of a cyclic CO_2 injection test the permeability of the coalbed had to be artificially decreased during the injection process. The simulated pressures and the changes of permeability are illustrated in Figure 2.6 and 2.7 respectively. Mavor et al (2004) also analyzed the field CO_2 sequestration and ECBM pilot tests in Alberta of Canada and found that in well FBV 4A the absolute permeability decreased from 3.65 mD to 0.985 mD due to the injection of CO_2.

2.1.4.4 Stress History Dependency

Coal permeability depends not only on the applied stresses but also on stress history. Patching (1965) tested the change of permeability with a cyclic loading and unloading confining history. His results indicated that the permeability of coal was higher in stress loading than in unloading and that with the increase of the number of loading and unloading cycle the permeability of coal decreased.

Dabbous et al (1974) studied the effects of cyclic overburden pressures on permeability with samples of Pittsburgh and Pocahontas coals. The results showed that as the number of loading cycles increased, the permeability of coal decreased, and in general a loading stress path had higher permeability than an unloading stress path.

Under triaxial loading conditions Somerton et al (1975) tested the change of permeability to nitrogen with a loading and unloading history using samples of Pittsburgh and Greenwich coal. Their results showed that the permeability of fractured coal was very much stress-history dependent, permeability decreasing with each loading cycle, except the cases where the applied stress caused new fractures. Under the same stress the permeability in loading was higher than the permeability in unloading.

Harpalani and McPherson (1985) studied the influence of axial stresses on coal permeability under cyclic loading. Their results indicated that the permeability of coal was lower under an unloading stress path than the permeability of coal under a loading stress path, and that a part of strains was irreversible at the end of each loading-unloading cycle.

2.2 MECHANISMS OF COALBED METHANE RECOVERY

2.2.1 Pressure Depletion Coalbed Methane Recovery

The pressure depletion coalbed methane (CBM) recovery method is simple and effective but become less efficient with decreasing seam pressures because of the loss of drive energy within coalbeds. The ultimate methane recovery by pressure depletion is generally not expected to be greater than 50% of the gas-in-place, even after several decades of production (Puri and Yee, 1990).

Coalbeds can be classed as saturated, undersaturated, and oversaturated coalbeds. For coalbeds containing pure methane, these classes are marked as points A, B, and C, respectively, in the adsorption isotherm diagram shown in Figure 2.2. The production mechanisms of each coalbed class are different. For a saturated coalbed (point A), once the pressure is reduced, methane is immediately released. Due to the pressure decrease, coal becomes less capable of retaining methane in an adsorbed state, thus gas molecules start detaching themselves from the surfaces of micropores and cleats, initiating the desorption process. The desorbed methane diffuses through solid matrix to cleats then flows to the wellbore. With methane producing the coalbed reaches a new saturated state on the isotherm under the lower pressure.

For an undersaturated coalbed (point B), the initial pressure reduction causes mobile water in cleats to flow to the production well. With water producing and reservoir pressures continuously declining, following a path as illustrated by the arrow pointing from B to the adsorption isotherm in Figure 2.2, the coalbed reaches a state of saturation. Then the production from this state follows the same mechanism as a saturated coalbed.

For an oversaturated coalbed (point C), the decreasing reservoir pressure results in mobile water and free gas in cleats to flow simultaneously towards the producing well. Once the coalbed, following a path as shown by the arrow pointing from C to the adsorption isotherm in Figure 2.2, reaches a state of saturation, the methane production follows the same mechanism as a saturated coalbed as well.

2.2.2 Enhanced Coalbed Methane Recovery

For ECBM recovery, in the regions where injection gases have not reached the mechanism of methane recovery is the same as the abovementioned CBM

recovery and pressure differences provide the drive energy for fluid movements from the coalbed towards the production wellbore. However, in the regions where injection gases have reached, the production mechanism depends on the type of injection gas. For simplicity, the following discussions are restrained to the situations of pure N_2 or pure CO_2 as injection gases.

When N_2 is applied in ECBM recovery, it releases methane by both sorption displacement and partial pressure reduction without necessarily depleting the total reservoir pressure (Puri and Yee, 1990). The injected N_2 flushes gaseous methane from cleats, creating a near 100% N_2 saturation and 'zero' partial pressure of methane in the cleats. This creates a disequilibrium condition in the system containing both methane and nitrogen. As a result, methane desorbs and is drawn (or 'pulled') into the gaseous phase to achieve a partial-pressure equilibrium (Mavor et al, 2002).

When CO_2 is used in ECBM recovery, compared to methane it preferentially adsorbs onto coal such that injected CO_2 is quickly adsorbed into the coal matrix to achieve sorbed equilibrium, displacing sorbed CH_4 (Mavor et al, 2002). Methane is "pushed" from the coal matrix by the highly adsorptive CO_2.

These different mechanisms result in different responses in field ECBM pilots of N_2 and CO_2 injection. Field and simulation results suggest that methane production rates increase faster and injected gas breakthroughs occur more rapidly for N_2 injection than for CO_2 injection (Reeves, 2001; Mavor et al, 2002).

2.3 MODELS TO PREDICT CHANGES OF PERMEABILITY AND POROSITY

The available models used to predict the change of permeability and porosity are analytical models and can be divided into empirical models and theoretical models.

2.3.1 Empirical Models for CBM Recovery

Based upon measured permeability data of fractured coal to methane under simulated subsurface stress conditions, Somerton et al (1975) obtained an empirical equation to predict the permeability due to stress changes as:

$$k = k_0[e^{-3\times10^{-3}\sigma_m \cdot k_0^{-0.10}} + 2\times10^{-4}\sigma_m^{1/3}k_0^{1/3}] \quad \text{.....(2.3-1)}$$

where k and k_0 are the permeability under present mean stress and zero stress respectively. The permeability is in mD and stresses are in psi.

Based on test results Harpalani and McPherson (1985) presented an empirical equation to compute the change of permeability with the change of confining stresses:

$$k = A_2 \cdot e^{B_2 \cdot \sigma_3} \quad \text{.....(2.3-2)}$$

where the confining stress is in MPa and the permeability is in m^2.

According to experimental data Gray (1987) also obtained an empirical equation to calculate the change of permeability as:

$$k = 1.013 \times 10^{-0.31 \cdot \sigma'} \quad \text{.....(2.3-3)}$$

where the permeability is in mD and the effective stress is in MPa.

By fitting the test data which simulated the reservoir pressure depletion under uniaxial strain conditions, Puri and Seidle (1991) also presented an empirical equation as:

$$\frac{k}{k_0} = e^{[1.690(p/p_0 - 1)]} \quad \text{.....(2.3-4)}$$

where pore pressures are in psi and permeability is in mD.

Durucan et al (1993) studied the failure of intact coal under triaxial compression conditions and measured the consequence changes in volumetric strain and corresponding permeability. They obtained a relationship between confining pressures (stresses) and the post-failure permeability of coal seams in the yield and stress relief zones of long wall faces as:

$$k = A_3 + B_3 \ln \sigma_3 \quad \text{.....(2.3-5)}$$

2.3.2 Theoretical Models for CBM Recovery

2.3.2.1 Basic Relationship between Permeability and Porosity

There are two basic relations between permeability and porosity that were widely used in formulating the analytical models of permeability and porosity of coalbeds. According to Mckee and Hanson (1975), the relationship between permeability and porosity of a medium containing a homogenous fracture (cleat) set can be described as:

$$k \propto \frac{\phi^3}{(1-\phi^2)} \quad \text{.....(2.3-6a)}$$

If porosity is of the order of 1%, Equation (2.3-6a) can be simplified to the following equation:

$$\frac{k}{k_0} = \left(\frac{\phi}{\phi_0}\right)^3 \quad \text{……..…….……(2.3-6b)}$$

Assuming coalbeds to be a matchstick fracture system (as illustrated in Figure 2.8) and cleats or fractures to be homogeneous and smooth plate channels, porosity and permeability can be expressed as (Van Golf-Racht, 1982d):

$$\phi = \frac{2b}{a} \quad \text{……..…..(2.3-7a)}$$

$$k = \frac{1}{24} b^2 \phi = \frac{b^3}{12a} \quad \text{…….…….(2.3-7b)}$$

where the difference between hydraulic and mechanical apertures is ignored.

2.3.2.2 Models Considering Pressure Changes

In the early models, the only influence considered was the change of pore pressures on porosity and permeability. Neglected the compressibility of solid grains, Mckee et al (1987 and 1988) conducted relationships to predict the change of porosity and permeability of coal with the change of in situ effective stresses as:

$$\frac{\phi}{\phi_0} = \frac{e^{-\bar{c}_p \cdot \Delta\sigma'}}{1 - \phi_0 (1 - e^{-\bar{c}_p \cdot \Delta\sigma'})} \quad \text{……...……...…(2.3-8a)}$$

$$\frac{k}{k_0} = \frac{e^{-3\bar{c}_p \cdot \Delta\sigma'}}{1 - \phi_0 (1 - e^{-\bar{c}_p \cdot \Delta\sigma'})} \quad \text{…….……...……..…(2.3-8b)}$$

For most deeply buried media, porosity is on an order of 1%, and Equation (2.3-8b) is simplified to:

$$\frac{k}{k_0} = e^{-3\bar{c}_p \cdot \Delta\sigma'} \quad \text{…….…….……...……(2.3-8c)}$$

The permeability predicted with this model fitted closely with the data measured by Rose and Foh (1984).

Seidle et al (1992) developed a relationship between permeability and the change of hydrostatic stresses by considering coal cleats as a matchstick fracture system (Figure 2.8):

$$\frac{k_2}{k_1} = e^{-3\bar{c}_p \cdot [(\sigma_h)_2 - (\sigma_h)_1]} \quad \text{……..……..(2.3-9)}$$

This model is just a little different from Equation (2.3-8c) in that the change of effective stresses in Equation (2.3-8c) was replaced by the change of

hydrostatic stresses under experimental conditions in Equation (2.3-9). The following equation was applied to convert vertical overburden stresses under in situ uniaxial strain conditions to hydrostatic stresses under experimental conditions:

$$\sigma_h = \frac{1}{3}\left(\frac{1+\nu}{1-\nu}\right)\sigma_V \quad \text{……(2.3-10a)}$$

The change of pressures during depleting was also related with the change of hydrostatic stresses under experimental conditions with:

$$(\sigma_h)_2 - (\sigma_h)_1 = \frac{1}{3}\left(\frac{1+\nu}{1-\nu}\right)(p_2 - p_1) \quad \text{……(2.3-10b)}$$

2.3.2.3 Models Considering Shrinkage/Swelling

For this type of model, the change of porosity and permeability was attributed to the influence of shrinkage/swelling of coal due to the desorption/adsorption of gases.

Seidle et al (1992) presented a model to calculate the change of permeability due to the shrinkage of coal matrix from gas desorption as:

$$\frac{k}{k_0} = \frac{(1 + 2 \cdot c_x \cdot \Delta p / \phi_0)^3}{1 - c_x \cdot \Delta p} \quad \text{……(2.3-11)}$$

where c_x is in psi^{-1}.

Based on the matchstick fracture (cleat) system shown in Figure 2.8, Seidle and Huitt (1995) presented an equation to predict the change of porosity due to the influence of shrinkage/swelling as:

$$\frac{\phi}{\phi_0} = 1 + \left(1 + \frac{2}{\phi_0}\right)\beta_D V_m \left(\frac{b' p_0}{1 + b' p_0} - \frac{b' p}{1 + b' p}\right) \quad \text{……(2.3-12)}$$

Then the change of permeability was computed with Equation (2.3-6b).

Harpalani and Chen (1995 and 1997) also presented models to predict the changes of permeability and porosity due to desorption based on the fracture system in Figure 2.8. The model of porosity is:

$$\frac{\phi}{\phi_0} = \frac{1 + 2 \cdot l_m^* \cdot \Delta p / \phi_0}{1 - l_m^* \cdot \Delta p} \quad \text{……(2.3-13a)}$$

And the model of permeability is:

$$\frac{k}{k_0} = \frac{(1 + 2 \cdot l_m^* \cdot \Delta p / \phi_0)^3}{1 - l_m^* \cdot \Delta p} \quad \text{……..…..…..……(2.3-13b)}$$

Lin et al (2008) used three assumed models of gas molecule shape to calculate the gas adsorption volume ($V_{adsorption}$) under adsorption temperature and pressure. Then they estimated new pore volumes (V_p) by subtracting gas adsorption volumes from original pore volumes (V_p^0) to calculate porosity ratio, $\phi/\phi_0=V_p/V_p^0=$ (V_p^0-$V_{adsorption}$)/V_p^0. They found the curves of the relationship between their measured permeability ratio, k/k_0, and their calculated porosity ratio, ϕ/ϕ_0, fell below the curve of the cubic law, i.e. Equation (2.3-6b).

2.3.2.4 Models Considering Both Pressure Changes and Shrinkage/Swelling

In formulating this type of analytical models, the principle of superposition was applied to strains or stresses in order to estimate the influences of both pressure changes and the shrinkage/swelling of coal matrix due to gas desorption/adsorption during production. The interaction between stresses and strains was ignored. The models can be further divided into two groups: the models of superposing strain and the models of superposing stress.

2.3.2.4.1 Models of Superposing Strains

Sawyer et al (1990) presented a model to calculate the change of porosity as:

$$\phi = \phi_0[1 + c_p \Delta p] - c_m^{'}(1 - \phi_0)(\frac{\Delta p_{\max}}{\Delta C_{\max}}) \cdot \Delta C \quad \text{……...……..(2.3-14)}$$

Then the change of permeability was calculated with Equation (2.3-6b).

Levine (1996) calculated the width of a deformed fracture with:

$$b = b_0 + \Delta\varepsilon_{LP} \cdot s + \Delta\varepsilon_{LD} \cdot s \quad \text{……...…..……...…..……(2.3-15)}$$

The change of permeability was calculated with Equation (2.3-7b).

Palmer and Mansoori (1996 and 1998) presented a model to estimate the change of porosity as a function of pore pressures as:

$$\frac{\phi}{\phi_0} = 1 + \frac{c_m^{''}}{\phi_0}\Delta p + \frac{\varepsilon_\infty}{\phi_0}(\frac{K}{M} - 1)(\frac{b_\varepsilon p}{1 + b_\varepsilon p} - \frac{b_\varepsilon p_0}{1 + b_\varepsilon p_0}) \quad \text{……..……..…..……(2.3-16)}$$

where $c^{''}_m$ is defined as:

$$c_m^{''} = \frac{1}{M} - [\frac{K}{M} + f - 1]c_s \quad \text{……..……(2.3-17)}$$

Then the change of permeability was estimated with Equation (2.3-6b).

Ignoring matrix compressibility, i.e. assuming $c_m^{"} = 1/M$, Mavor and Vaughn (1997 and 1998) simplified Equation (2.3-16). The change of permeability was still calculated with Equation (2.3-6b).

Chkatamarla et al (2004) presented the following model to predict the change of cleat porosity:

$$\phi - \phi_0 = \tfrac{1}{M}(p - p_0) + \left(\tfrac{K}{M} - 1\right)\left[\beta_D (V_D - V_{D0})\right] \quad \text{.....(2.3-18)}$$

This model is the same as the model of Mavor and Vaughn (1997 and 1998) except the way to express the swelling/shrinkage of coal. The change of permeability was also computed with Equation (2.3-6b).

2.3.2.4.2 Models of Superposing Stresses

In formulating this type of model, it was additionally assumed that coalbeds are subject to constant overburdens and undergo uniaxial (vertical) deformations, i.e. horizontal strains were assumed to be zero.

Gilman and Bechie (2000) conducted an equation to calculate the change of permeability during methane production as:

$$\frac{k}{k_0} = e^{-3\Delta\sigma_x^{'}/E_F} \quad \text{.....(2.3-19)}$$

Using the Terzaghi's effective stress formula (Terzaghi, 1943), the change of horizontal effective stresses due to the changes of pressures and the changes of gas desorption was estimated with:

$$\Delta\sigma_x^{'} = -\tfrac{\upsilon}{1-\upsilon}\Delta p + \tfrac{E}{1-\upsilon} c_m \cdot \Delta m \quad \text{.....(2.3-20)}$$

Shi and Durucan (2003) presented a model to estimate the change of effective horizontal stresses during pressure depletion as:

$$\Delta\sigma_x^{'} = -\frac{\nu}{1-\nu}(p - p_0) + \frac{E}{3(1-\nu)}\varepsilon_{L\infty}\left(\frac{p}{p + p_\varepsilon} - \frac{p_0}{p_0 + p_\varepsilon}\right) \quad \text{.....(2.3-21)}$$

In their model the change of permeability was calculated by Equation (2.3-8c).

2.3.3 Models for ECBM Recovery and CO_2 Sequestration

2.3.3.1 Models by Superposing Strains

The following analytical models were developed through applying the principal of superposition to strains. Using these models the change of porosity

during ECBM recovery and CO_2 sequestration process can be calculated. Then the change of permeability was estimated with Equation (2.3-6b).

Chikatamarla et al (2004) presented a model to predict the change of porosity considering the influence of multiple absorptive gases:

$$\phi - \phi_0 = \tfrac{1}{M}\Delta p + (\tfrac{K}{M} - 1)\left\{\sum_{i=1}^{i=n}(\beta_D)_i[(V_D)_i - (V_{D0})_i]\right\} \quad \text{.....(2.3-22)}$$

Mavor and Gunter (2004) modified the Mavor and Vaughn's model (Mavor and Vaughn, 1998) to calculate the change of porosity during ECBM recovery and CO_2 sequestration process. The two major modifications include: (1) it can be applied in both ECBM and CBM processes; (2) it uses the atmospheric pressure as a reference state. The model to estimate the change of porosity is:

$$\frac{\phi}{\phi_0} = 1 + c_p\Delta p + \frac{1}{\phi_0}\left(1 - \frac{K}{M}\right)\sum_{j=1}^{j=n}\frac{(\varepsilon_\infty)_j}{(p_\varepsilon)_j}\left(\frac{r_{j,0}p_0}{1 + p_0\sum_{k=1}^{k=n}\frac{r_{k,0}}{(p_\varepsilon)_k}} - \frac{r_j p}{1 + p\sum_{k=1}^{k=n}\frac{r_k}{(p_\varepsilon)_k}}\right) \quad \text{.....(2.3-23)}$$

If the number of gas components is one and the initial reservoir pressure is used as the reference state, Equation (2.3-23) becomes the Mavor and Vaughn's model.

The Palmer-CMG model (CMG, 2005) was also modified from the Mavor and Vaughn's model (Mavor and Vaughn, 1998) for ECBM recovery and CO_2 sequestration process. It is the same as the Mavor and Gunter's mode except the reference state. This model uses the initial in situ state rather than the atmospheric pressure as a reference state.

2.3.3.2 Models by Superposing Stresses

Shi and Durucan (2005) presented a model to predict the change of horizontal effective stress during CBM and ECBM processes as:

$$\Delta\sigma_x^{'} = -\frac{\upsilon}{1-\upsilon}\Delta p + \frac{E}{3(1-\upsilon)}\sum_{j=1}^{n}(\beta_D)_i[(V_D)_i - (V_{D0})_i] \quad \text{.....(2.3-24)}$$

Then the change of permeability was again computed with Equation (2.3-8c).

2.4 PERMEABILITY AND DEFORMATION MODELS FOR FRACTURED ROCK

2.4.1 Definition of Fracture Permeability, Conductivity and Aperture

Traditionally fluid flow through a single fracture or joint was assumed analogous to laminar flow between two perfectly smooth parallel plates. This led to the so-called "cubic law":

$$Q = -W\frac{b^3}{12\mu}\frac{dp}{dx} \quad \text{……..……..…….(2.4-1)}$$

Comparing Equation (2.4-1) with Darcy's Law the intrinsic permeability of a parallel plate fracture is obtained:

$$k = \frac{b^2}{12} \quad \text{…….……..……...……..(2.4-2a)}$$

Then

$$\frac{k}{k_0} = \left(\frac{b}{b_0}\right)^2 \quad \text{……..……..……...….(2.4-2b)}$$

Hydraulic conductivity of a fracture is defined as:

$$C_f = \frac{\rho_L \cdot g}{\mu}k = \frac{\rho_L \cdot g}{\mu}\cdot\frac{b^2}{12} \quad \text{……...…..……..….(2.4-3a)}$$

Then

$$\frac{C_f}{(C_f)_0} = \frac{\rho_L\mu_0}{\rho_{L0}\mu}\left(\frac{b}{b_0}\right)^2 \quad \text{……..……...……..….(2.4-3b)}$$

If assuming the density and viscosity of fluid to be constant, k/k_0 equals to C/C_0.

In above equations, the fracture aperture is hydraulic aperture. However, in the early time the difference between hydraulic aperture and mechanical aperture was ignored. For convenience the definition of fracture permeability, i.e. Equation (2.4-2a), is widely used in applications, such as in petroleum engineering (Van Golf-Racht, 1982) and geotechnical engineering (Itasca, 2000).

Fracture apertures may be determined either from direct or indirect measurements. The variation of the aperture along a fracture is generally expected. The apertures from direct measurements are called mechanical apertures while the apertures from indirect measurements, i.e. the fracture aperture back calculated with Equation (2.4-1) from the measured volumetric

flow rate, the flow width of the fracture, pressure gradient and fluid viscosity under steady flow conditions, are called hydraulic apertures or effective aperture of fractures. Owing to the influences of wall roughness, tortuosity and contact area etc. mechanical apertures are generally greater than the corresponding hydraulic apertures.

2.4.2 Influences of Fracture Geometry on Permeability

2.4.2.1 Influences of Tortuosity

Tsang (1984) studied the influences of fracture tortuosity on fluid flow rates through a single fracture. The results showed that the more the small apertures in the aperture distribution, the larger the influence of tortuosity on fluid flow. When the fraction of contact area between fracture surfaces rose above 30%, the aperture distributions were invariably large at small apertures, and the effect of fracture roughness and flow path tortuosity depressed the flow rate by three or more orders of magnitude from the value predicted with the parallel plate channel representing the fracture.

However, the results of Gavrilenko and Gueguen (1989) indicated that under a pressure change the permeability change was due mainly to the variation of crack apertures and the influences of tortuosity modification was negligible.

2.4.2.2 Influences of Roughness

According to the experimental results of many investigators, fractures, unlike that described with Equation (2.4-1), are spatially not smooth and parallel. Brown (1987) studied the influence of surface roughness on fluid flow through a single fracture. The rock surfaces were generated using fractal models and laminar flow between rough surfaces was numerically simulated with the Reynolds equation (a particular form of the Navier-Stokes equations approximating flow between rough surfaces). The surface height (roughness) was Gaussian distribution with a standard deviation. The results suggested that the flow rate predictions with the cubic law, i.e. Equation (2.4-1), worsened as the surface of a rough-walled fracture brought closer together. When the surfaces were separated by one standard deviation of surface height, the actual flow rate was 40-60% of that predicted with the use of mean aperture in the cubic law. Brown also pointed out the use of arithmetic mean aperture gave better results than other more

complicated averages, and that better results could be obtained if the cubic law was modified to account for the tortuosity or for the real area of surface contacts.

The results of Renshaw (1995) indicated that in many cases fracture apertures nearly followed lognormal distribution and the relationship between mechanical and hydraulic apertures depended on a nondimensional roughness parameter, $<b_m>/\Delta d$ (the ratio between arithmetic mean of mechanical aperture and standard deviation of fracture apertures). For a low roughness parameter value ($<b_m>/\Delta d<1$), the mechanical aperture might be significantly greater than the hydraulic aperture. However, at some critical value of roughness, the hydraulic aperture became approximately constant and equal to the residual aperture but the mechanical aperture might continue to decrease. The value of the critical roughness below which the hydraulic aperture was constant was different for various types of fractures, yet appeared to generally decrease as the roughness of the fracture increase.

Brown (1995) presented a surface roughness model to describe undeformed rough-walled single fractures. This model required only three main parameters: fractal dimension (a measure of surface texture, describing the proportion of high-frequency to low-frequency roughness), the rms (root-mean-square) roughness at a reference length scale, and a length scale (describing the degree of mismatch between two fracture surfaces). The profiles of many natural fractures were analyzed to determine the range of these parameters in nature and the results showed that the fracture surface data fitted the model reasonably well.

2.4.2.3 Influences of Contact Area

Zimmerman et al (1992) investigated the effect of contact areas on the fracture permeability. In order to isolate the effect of contact areas, fracture apertures were assumed to be constant. For the fractures with circular obstacles in the plane of fractures, the effective permeability can be estimated with the equation derived by Walsh (1981) using the Maxwell effective medium approximation for contact areas up to at least 25%:

$$\frac{k}{k_0} = \frac{1-c}{1+c} \qquad \text{.....(2.4-4)}$$

where k and k_0 are the permeability of fractures with and without obstacles respectively and c is the fractional contact area of a fracture.

For the fractures with randomly oriented elliptical obstacles the expression of the effective permeability was extended from Equation (2.4-4) as:

$$\frac{k}{k_0} = \frac{1-\beta \cdot c}{1+\beta \cdot c} \quad \text{.....(2.4-5)}$$

where $\beta=(1+R)^2/4R$ and R is the aspect ratio, defined as the ratio of the minor to the major axis of elliptical obstacles.

The fractures with irregular contact areas were found having lower permeability (by as much as 30%) than that predicted with Equation (2.4-4) but could be fitted fairly well with the effective medium approach, i.e. Equation (2.4-5), if an equivalent aspect ratio is used.

2.4.2.4 Effects of Fracture Shape

Bogdanov et al (2003) investigated the influences of fracture shapes on effective permeability of fractured media by considering networks of square, rectangle, icosagonal (twentysided) and hexagonal fractures. The results showed that for a constant number of fractures, the permeability of icosagons is larger than that of hexagons in both percolating and nonpercolating networks and that under the same conditions the permeability of squares and rectangles is smaller than that of hexagons.

2.4.3 Permeability, Conductivity and Aperture due to Stress Change

A lot of experimental and theoretical studies have been made to find the relationship between the change of stresses and the changes of fracture permeability, or conductivity, or aperture. The review herein mainly focuses on the theoretical and empirical model studies.

2.4.3.1 Gangi's Model

Using a "bed of nails" model to represent the asperities on fracture faces and a power-law distribution function for asperity heights, Gangi (1978) developed a model to determine the variation of permeability with effective normal stresses:

$$k = k_0[1-(\sigma'/Y)^m]^3 \quad \text{.....(2.4-6)}$$

where k and k_0 are permeability at effective stress σ' and at zero effective stress respectively, and

$Y=E\cdot Ar/A$

where E is the Young's modulus of intact rock and Ar/A is the fraction of the fracture face covered with the "nails". m=1/n and n is related to fracture asperities ($1 \le n \le \infty$).

Gangi claimed the model could fit the experimental data of fractured carbonate rock very well.

2.4.3.2 Walsh's Model

Based on elastic deformation and the analogy between heat flow in a sheet and fluid flow in a planar joint, Walsh (1981) deducted a relationship between hydraulic conductivity of joints and effective normal stresses as:

$$\frac{C_f}{(C_f)_0} = \left[1 - \sqrt{2}\frac{h_{rms}}{(b_m)_0/2}\ln\left(\frac{\sigma'}{\sigma_0'}\right)\right]^3 \left[\frac{1 - c'(\sigma' - \sigma_0')}{1 + c'(\sigma' - \sigma_0')}\right] \quad \text{.....(2.4-7)}$$

Walsh pointed out that except at very high pressures, Equation (2.4-7) could be simplified as:

$$\frac{C_f}{(C_f)_0} == \left[(1 - \sqrt{2}\frac{h_{rms}}{(b_m)_0/2}\ln\left(\frac{\sigma'}{\sigma'_0}\right)\right]^3 \quad \text{.....(2.4-8)}$$

The predictions with Equation (2.4-8) were verified by the experimental results of many researchers.

2.4.3.3 Tsang and Witherspoon's Model

In Tsang and Witherspoon's model (1981) a single fracture was represented with a collection of voids between contacting apertures and the closure of the fracture due to the deformation of voids. After the roughness characteristics of fractures had been determined, a statistical average of mechanical apertures, $<b_m>$, was calculated as a function of fracture deformation and effective normal stresses by:

$$\left[< b_m(\Delta u_n, \sigma') >\right]^3 = \frac{\int_0^{(b_m)^{\max} - \Delta u_n} [(b_m)^{\max} - \Delta u_n - h]^3 n(h) dh}{\int_0^{(b_m)^{\max}} n(h) dh} \quad \text{.....(2.4-9)}$$

Fluid flow still followed an equivalent "cubic" law in which the fracture aperture was replaced by the statistical average of mechanical apertures. In other word hydraulic aperture was equal to the statistical average mechanical aperture.

2.4.3.4 Swan's Model

Swan (1983) presented a model to describe joint hydraulic conductivity as a function of normal stresses and roughness properties as:

$$\sqrt{\frac{C_f}{(C\ )_0}} = \left(1 - \frac{a_b}{(b_m)_0}\right) - \frac{\Delta d}{(b_m)_0}\ln(\sigma') \quad \text{.....(2.4-10)}$$

where a_b is a constant.

2.4.3.5 Barton et al's Model

After analyzed the experimental results of many investigators Barton et al (1985) proposed an empirical model to describe the relationship between mechanical apertures and hydraulic apertures as:

$$b_h = \min\left\{b_m, \frac{b_m{}^2}{JRC^{2.5}}\right\} \quad \text{.....(2.4-11)}$$

where b_h and b_m are all in microns. JRC can be roughly estimated by comparing the fracture profile of specimens with the typical profiles provided by Barton and Choubey (1977). A more accurate estimation of JRC can be made with the method of Barton and Choubey (1977) or the improved method of Tse and Cruden (1979) or the more contemporary method of Yang et al (2001).

The mechanical aperture was calculated by:

$$b_m = (b_m)_0 + \Delta b_m \quad \text{.....(2.4-12)}$$

where Δb_m is the change of mechanical apertures with normal stresses and $(b_m)_0$ is the initial mechanical aperture which can be calculated by:

$$(b_m)_0 \approx \frac{JRC}{5}\left(0.2\sigma_c / JCS - 0.1\right) \quad \text{.....(2.4-13)}$$

where $(b_m)_0$ is in millimeters. By implication, when a joint is unaltered or unweathered, i.e. JCS=σ_c, the initial aperture may be a function only of surface roughness. An alternative method to estimate initial apertures is to implement well test. Hydraulic aperture can be back calculated from the interpreted fracture permeability with the relation of Equation (2.4-2a).

2.4.3.6 Elsworth's Model

Elsworth (1989) presented a model to describe the permeability enhancement due to the change of temperature and pore pressure. The joint aperture was expressed as:

$$b = b^r - \Delta u_n \quad \text{……..…….……..…….(2.4-14)}$$

The normal displacement of the joint was estimated with:

$$\Delta u_n = \left[\frac{E}{s\cdot(1-2\nu)} + K_n\right]^{-1}(\Delta\sigma_T - \Delta p) \quad \text{……...…...……(2.4-15)}$$

Elsworth and Xiang (1989) extended the work of Elsworth (1989) by considering the influence of shearing. The displacement of the joint was estimated by:

$$\Delta u_n = \left[\frac{E}{s\cdot(1-2\nu)} + K_n\right]^{-1}(\Delta\sigma_T - \Delta p + \Delta\sigma_S) \quad \text{……..…….……(2.4-16)}$$

The permeability and conductivity of the joint can be calculated by substituting Equation (2.4-14) into Equation (2.4-2a) and Equation (2.4-3a).

2.4.3.7 Bai and Elsworth's Model

Bai and Elsworth (1994) proposed models to estimate the change of hydraulic conductivity due to the change of stress as:

$$C_m = (C_m)_0\{1 \mp \tfrac{1}{2}[\tfrac{9(1-\nu^2)}{2}(\tfrac{\pi\cdot\Delta\sigma}{E})^2]^{1/3}\}^2 \quad \text{(for rock matrix)} \quad \text{……..(2.4-17a)}$$

$$C_f = (C_f)_0[1 + \Delta\varepsilon(\tfrac{K_n\cdot b}{E} + \tfrac{b}{s})^{-1} + \Delta\gamma(s + \tfrac{G}{K_S})(\tan\Psi)]^3 \quad \text{(for fracture)}$$

$$\text{……...……..(2.4-17b)}$$

where $\Delta\varepsilon$ and $\Delta\gamma$ are the changes of normal strain and shear strain due to change of stresses respectively. In Equation (2.4-17a) a negative sign refers to compressive loading and a positive sign corresponds to dilatational loading. In the conduction of Equation (2.4-17b) the fractured porous media was approximated as an equivalent fracture networks in which a single fracture was idealized as a planar opening having a constant equivalent thickness or aperture.

2.4.3.8 Renshaw's Model

According to the analysis of experimental results of many other investigators Renshaw (1995) pointed out that in many cases fracture apertures followed a

lognormal distribution. This distribution also supported by the data of fractures under different loads. For lognormally distributed apertures, the relation between the arithmetic mean of mechanical apertures, $<b_m>$, and hydraulic apertures, b_h, was:

$$\frac{b_h}{< b_m >} = \exp\left(-\frac{(\Delta d)^2}{2} \right) \quad \text{.....(2.4-18)}$$

2.4.3.9 Selvadurai and Nyuyen's Model

Experiments had shown that the rate of increase in permeability decreased as shearing proceeds to a very late stage. The behaviour was attributed to the gouge production. The Selvadurai and Nyuyen's model (Ohnishi et al, 1996) was developed to consider this effect. In the model the relationship between hydraulic and mechanical apertures was expressed as following:

$$b_h = (b_h)_0 + f' \cdot \Delta b_m' \quad \text{.....(2.4-19)}$$

where $\Delta b_m'$ is the change of mechanical apertures due to the combined effects of compression and shearing. f' is a proportionality factor.

The effect of gouge production on joint permeability was assumed to be related to the total plastic work due to shear. If the exponential law for surface damage was adopted, f' might be related to the plastic work, W^p, produced by shear forces as following:

$$f' = f_0' e^{-c_g \cdot W^P} \quad \text{.....(2.4-20)}$$

where c_g is a gouge production factor. Parameters f'_0 and c_g are empirically related to JRC, JCS and σ. A detailed experimental program is needed in order to arrive at a specific correlation.

2.4.3.10 Willis-Richards et al's Model

Willis-Richards et al (1996) proposed a model to predict the aperture of a sheared fracture with unabraded asperities in contact as:

$$b_m = \frac{(b_m)^0}{1 + 9\sigma'/\sigma'_{ref}} + (\Delta b_m)_S + b^r \quad \text{.....(2.4-21)}$$

where σ'_{ref} is the effective normal stress applied to cause 90% reduction in the compliant aperture. $(\Delta b_m)_S$ was calculated by:

$$(\Delta b_m)_S = u_s \tan\psi^{eff} \quad \text{……(2.4-22)}$$

where ψ^{eff} is effective shear dilation angle and estimated by:

$$\psi^{eff} = \frac{\psi^0}{1 + 9\sigma_n' / \sigma_{ref}'} \quad \text{……(2.4-23)}$$

where ψ^0 is the shear dilation angle measured in laboratory at zero stress or at least very low effective stresses.

Then the length weighted average of the cube of fracture apertures, $<b_m>^3$, was estimated based on Equation (2.4-21) and used to calculate mean permeability, <k> , by:

$$< k >= \frac{< b_m >^3}{12 \cdot < s >} \quad \text{……(2.4-24)}$$

2.4.3.11 Chen and Bai's Model

Chen and Bai (1998) conducted a stress-dependent permeability tensor, k_{ij}, for a single set of parallel fractures oriented in arbitrary directions:

$$k_{ij} = \frac{[(b_h)^0 + (\Delta u_n)^t]^3}{12 \cdot s} \begin{bmatrix} (n_2)^2 + (n_3)^2 & -n_1 n_2 & -n_3 n_1 \\ -n_1 n_2 & (n_3)^2 + (n_1)^2 & -n_2 n_3 \\ -n_3 n_1 & -n_2 n_3 & (n_1)^2 + (n_2)^2 \end{bmatrix}$$

……(2.4-25)

where n_1, n_2 and n_3 are the components of a unit normal vector perpendicular to the fracture plane. $(\Delta u_n)^t$ is the total change of normal displacement of fractures and estimated by:

$$(\Delta u_n)^t = (\Delta u_n)^f + (\Delta u_n)^S \quad \text{……(2.4-26)}$$

where $(\Delta u_n)^f$ is the change of normal displacement of fracture and $(\Delta u_n)^s$ is the change of normal displacement of solid matrix.

2.4.3.12 Liu et al's Model

Liu et al (1999) developed the relations to determine the changes of effective porosity and hydraulic conductivity resulting from the redistribution of stresses and strains in disturbed rock masses. In each instance, the changes of porosity and directional conductivities were determined from pre-disturbance porosities and conductivities, the number of joint sets, and the indices of Rock Quality

Designation (RQD) and Rock Mass Rating (RMR). The study indicated that the hydraulic conductivity field of the equivalent continuous medium for a rock mass with only one set of fractures is highly anisotropic, and that the hydraulic conductivity field of the equivalent continuous medium for a rock mass with two orthogonal sets of identical fractures is isotropic. Therefore, the rock mass with two orthogonal sets of identical fractures can be substituted by an equivalent continuous medium.

2.4.3.13 Matsuki et al's Model

Based on the aperture distributions of aperture local minima and their radii, Matsuki et al (2001) derived a formula for the relationship between constant normal stresses and the time-dependent closure of a fracture as a function of time. The time-dependent closure of a fracture with rough surfaces subjected to stepwise normal stresses was theoretically considered by viscoelastic modeling of rock.

Experiments and a Monte Carlo simulation on elastic and time-dependent closure were conducted for a hydraulic fracture created in granite to provide theory verification and to understand the mechanism of the independence of time-dependent closure of a Goodman's fracture (i.e. in the fracture the elastic closure is linear with the logarithm of normal stresses) under the normal stress. The experiments showed that the time-dependent closure of a Goodman's fracture was almost independent of normal stresses. A Monte Carlo simulation on time-dependent closure approximately reproduced the experimental results, and showed that the time-dependent closure of a Goodman's fracture did not depend on normal stresses because during time-dependent closure of a fracture contact areas increase as normal stresses increase.

2.4.3.14 Min et al's Model

Based on a discrete fracture network, Min et al (2004) investigated the stress-dependent permeability in fractured rock masses considering the effects of nonlinear normal deformation and shear dilation of fractures using a two-dimensional distinct element method program, UDEC. They adopted Snow's model (1969) to calculate the permeability of fractures from normal opening, $k_{opening}$, as:

$$(k_{opening})_j = f_j'' \frac{b_j^3}{12} \quad \text{……..……...……..…….(2.4-27a)}$$

where f" is fracture frequency and j represents directions x and y. Similarly, the permeability of fractures due to shear dilation, $k_{dilation}$, was expressed as:

$$(k_{dilation})_j = (f_d)_j \frac{(b_d)_j^3}{12} \quad \text{…….……...…….…….(2.4-27b)}$$

where f_d is the equivalent frequency of dilating fractures. b_d is the equivalent aperture of a dilating fracture and estimated by:

$$(b_d)_j = \begin{cases} 0 & \text{for } R' < R_c' \\ (b_d^{\max})_j[1 - e^{-\gamma_j'(R' - R_c')}] & \text{for } R' \geq R_c' \end{cases} \quad \text{……...……...….(2.4-28)}$$

where R' is stress ratio and R'c is the critical stress ratio that can cause the failure of fractures. b_d^{max} is the maximum aperture of a fracture due to dilation and can be obtained from laboratory experiments. γ' is stress coefficient for the equivalent aperture of dilating fractures. The values for critical stress ratio and the critical orientation of fractures for failure can be calculated with the Coulomb failure criterion.

They used the relation between fracture apertures and stresses proposed by Rutqvist et al (2003):

$$b_j = b^r + \Delta b^{\max} e^{-[(\alpha_x)_j \sigma_x + (\alpha_y)_j \sigma_y]} \quad \text{……..…….……..….(2.4-29)}$$

where α_x and α_y are the coefficients for fracture closure in direction j under the normal stresses, σ_x and σ_y. From this equation, the initial aperture at zero stress level, b_i, is given by the summation of b^{res} and Δb^{max}.

Equivalent permeability can then be calculated by superimposing the permeability contributions from normal opening and shear dilations as:

$$k_j = (k_{opening})_j + (k_{dilation})_j = f_j'' \frac{b_j^3}{12} + (f_d)_j \frac{(b_d)_j^3}{12} \quad \text{……...…….(2.4-30a)}$$

or in explicit form

$$k_j = \frac{f_j''}{12}\{b_r + \Delta b^{\max} e^{-[(\alpha_x)_j \sigma_x + (\alpha_y)_j \sigma_y]}\}^3 + \frac{(f_d)_j}{12}\{(b_d^{\max})_j[1 - e^{-\gamma_j(R' - R_c')}]\}$$

……..(2.4-30b)

2.4.4 Constitutive Models of Rock Fractures

The constitutive models of rock fractures are formulated with two basic approaches: empirical and theoretical approaches. In an empirical approach, constitutive models are obtained by the curve fitting of experimental results. In a theoretical approach, constitutive models are established based on theories, such as solid mechanics, theory of plasticity and the contact theory of elasticity.

2.4.4.1 Goodman's Empirical Model

Goodman (1976) first presented an empirical constitutive model for rock fractures. In this model the normal displacement and normal stress were related with a hyperbolic equation:

$$\frac{\sigma-\xi}{\xi}=A'\left(\frac{u_n}{u_n^{\max}-u_n}\right)^{t'} \quad \text{……(2.4-31)}$$

where ξ is the "seating pressure". A' and t' are the coefficients obtained from joint compression experiments. The normal stiffness of a joint was written as:

$$K_n=\frac{\partial\sigma}{\partial u_n}=\frac{t'}{u_n^{\max}-u_n}(\sigma-\xi) \quad \text{……(2.4-32)}$$

The relation between shear displacements and shear stresses and the relation describing the normal displacement increment caused by shear dilatancy were obtained by experiments.

2.4.4.2 Barton et al's Empirical Model

Based on numerous experimental results of rock joints Barton et al (1985) proposed an empirical constitutive model, generally called BB model. In their model normal stresses and normal displacements were related by:

$$\sigma'=K_n^0\left(\frac{u_n}{1-u_n/u_n^{\max}}\right) \quad \text{……(2.4-33)}$$

Then the change of mechanical apertures due to normal displacements was:

$$(\Delta b_m)_n=\Delta u_n \quad \text{……(2.4-34)}$$

The change of mechanical apertures due to shear dilation was calculated by:

$$(\Delta b_m)_S=\Delta u_S\tan\psi^m \quad \text{……(2.4-35)}$$

Dilation began when roughness was mobilized and reduced as the roughness decreased. The peak and mobilized shear dilation angle were estimated by:

$$\psi^m = \frac{1}{2} JRC^m \log\left(JCS/\sigma'\right) \quad \text{……...……...…...…….....….(2.4-36a)}$$

$$\psi^p = \frac{1}{2} JRC^p \log\left(JCS/\sigma'\right) \quad \text{……...…...…….....…...….(2.4-36b)}$$

During shearing, shear displacement behaviour was defined with a relation between the ratio of shear displacement to peak shear displacement, u_s/u_s^p, and the ratio of mobilized joint roughness coefficient to peak joint roughness coefficient, JRC^m/JRC^p, shown in Figure 2.13 (in the figure δ is shear displacement).

Friction was mobilized when shearing began. The mobilized drained friction angle was given by:

$$\theta^m = JRC^m \log\left(JCS/\sigma'\right) + \theta^r \quad \text{……...…...…….…….…….…(2.4-37)}$$

The mobilized shear strength at given shear displacement was:

$$\tau = \sigma' \tan\theta^m \quad \text{……..……..……..……....…...….(2.4-38)}$$

Thus the total change of mechanical apertures was:

$$\Delta b_m = (\Delta b_m)_n + (\Delta b_m)_s \quad \text{……...…….……..……(2.4-39)}$$

Then the new mechanical aperture was:

$$b_m = (b_m)_0 + \Delta b_m \quad \text{……..……(2.4-40)}$$

The hydraulic aperture was then calculated from the corresponding mechanical aperture with Equation (2.4-11).

2.4.4.3 Improved Barton et al's Empirical Model

Because BB model (Barton et al, 1985) was not satisfactory in predicting the hydraulic aperture of post-peak shear phase it was improved by Olsson and Barton (2001). They divided shear process into two phases, pre-peak/peak and post peak. Hydraulic apertures were determined by different equations:

For $u_s \leq 0.75 u_s^p$, Equation (2.4-11) was used;

For $u_s \geq u_s^p$,

$$b_h = \sqrt{b_m} JRC^m \quad \text{……...……..……..…….…….…(2.4-41)}$$

Considering the influences of destruction of joint walls the equation to estimate mobilized shear dilation angle, Equation (2.4-36a), was modified as:

$$\psi^m = \frac{1}{M'} JRC^m \log\left(JCS/\sigma'\right) \quad \text{.....(2.4-42)}$$

where M' is a damage coefficient, given values of 1 and 2 for shearing under low or high normal stresses respectively. Other equations are the same as the Barton et al's empirical model.

2.4.4.4 Amadei-Saeb's Theoretical Model

Amadei and Saeb (Ohnishi and Kobayashi, 1996) developed a 2D constitutive model for rock joints. The incremental equations are expressed as:

$$\begin{Bmatrix} \Delta\sigma_n \\ \Delta\sigma_t \end{Bmatrix} = \begin{bmatrix} K_{nn} & K_{nt} \\ K_{tn} & K_{tt} \end{bmatrix} \begin{Bmatrix} \Delta u_n \\ \Delta u_t \end{Bmatrix} \quad \text{.....(2.4-43)}$$

where n and t represent normal and tangential directions respectively; $[K_{i,j}]$ (i,j=n,t) denotes the stiffness tensor of the joint. The stiffnesses are determined with corresponding relations related to uniaxial compressive strength, initial dilatancy angle, friction angle when sliding along the asperities, cohesion and internal friction angel of intact rock matrix, shear strength of the intact rock matrix and material constants etc.

Amadei-Saeb's model has two distinct advantages: (1) the model can predict different deformability in normal direction of joints for both mated and unmated joints; (2) the constraint due to the deformability of surrounding rock to joints can be considered. The major shortcoming is that dilatancy due to asperities is reversible.

2.4.4.5 Plesha's Theoretical Model

Plesha (Ohnishi et al, 1996) also developed a 2D constitutive model for rock joints considering surface damage and the capacity of cyclic shear paths. The joint surface was assumed to be macroscopically planar. The model was based on the theory of plasticity and the assumption of uniform tooth-shaped asperities with the stress transformation given by:

$$\begin{cases} \sigma_t^c = \eta(\sigma_t \cos\alpha_k + \sigma_n \sin\alpha_k) \\ \sigma_n^c = \eta(-\sigma_t \sin\alpha_k + \sigma_n \cos\alpha_k) \end{cases} \quad \text{.....(2.4-44)}$$

where n and t represent normal and tangential directions respectively and the superscript, c, denotes the converted stresses. η is a constant representing the aerial ratio of active asperity surface over the base surface of the representative asperity. α_k is the current active asperity angle.

The total displacement increment was:

$$du_i = du_i^e + du_i^p \quad \text{……...…….……...….(2.4-45)}$$

where du_i^e is a reversible displacement part which is related to the elastic response through stiffness tensor, K_{ij}, by:

$$d\sigma_i = K_{ij} du_i^e \quad \text{…….……...…..(2.4-46a)}$$

In Equation (2.4-45) du_i^p was an irreversible displacement part that was described by a sliding rule by:

$$du_i^p = \begin{cases} 0 & F < 0 \\ \lambda \frac{\partial U}{\partial \sigma_i} & F \geq 0 \end{cases} \quad \text{…….……...……..…...….(2.4-46b)}$$

where F and U are the slip function and sliding potential respectively, defined for the joints, similar to the yield function and flow potential in the theory of plasticity. λ is a positive scalar quantity.

The final constitutive model was:

$$d\sigma_i = \left(K_{ij} - \frac{K_{ir} \frac{\partial U}{\partial \sigma_r} \frac{\partial F}{\partial \sigma_p} K_{pj}}{\frac{\partial F}{\partial \sigma_r} K_{rp} \frac{\partial U}{\partial \sigma_p} + m\sigma_r \frac{\partial U}{\partial \sigma_r}} \right) du_i \quad \text{…….……..……...….(2.4-47)}$$

where $d\sigma_i$ and du_i are increments of stress and displacements respectively; the range of i,j,r,p=n and t representing normal and tangential directions respectively; and m is a modulus related to the strength of joint surface. However, Plesha's model did not consider the post-peak shear stress behaviour and the shear stiffness of the interface was taken as constant.

2.4.4.6 Jing et al's Theoretical Model

Based on Plesha's original model and considering post-peak shear-weakening and the changes of normal and shear stiffnesses over shear process, Jing et al (1993) developed a 2D constitutive model. In this model slip function F and sliding potential U were given by:

$$F = \left| \sigma_t \cos\alpha_k + \sigma_n \sin\alpha_k \right| + \tan\theta_r (-\sigma_t \sin\alpha_k + \sigma_n \cos\alpha_k) - C_J$$

……..(2.4-48a)

$$U = \left|\sigma_t \cos\alpha_k + \sigma_n \sin\alpha_k\right| \quad \text{……..(2.4-48b)}$$

where n and t represent normal and tangential directions respectively. α_k is the current active asperity angle and C_J is the cohesion of rock joints.

In this model, to replace m in Equation (2.4-47) m=H for the case of shear-strengthening and m=S for the case of shear-weakening. H and S were given by empirical equations as:

$$H = \frac{(u_s^p - u_s)}{(u_s^p - u_s^0)} K_S \quad \text{……..(2.4-49a)}$$

$$S = -s_c \frac{(u_s^r - u_s)(u_s - u_s^p)}{(u_s^r - u_s^p)^2} \frac{K_S}{U} \sin^2\alpha_k \quad \text{……..(2.4-49b)}$$

where s_c is a material constant. For the unloading and reverse shear stages, m=0 was maintained.

The normal stiffness was related to the normal displacement with the model derived by Bandis et al (1983):

$$K_n = \begin{cases} \dfrac{K_n^0}{(1 - u_n / u_n^{\max})^2} & \text{(for closure)} \\ 0 & \text{(for opening)} \end{cases} \quad \text{……..(2.4-50)}$$

The change of shear stiffness with normal stress was described with an empirical model:

$$K_S = \begin{cases} \dfrac{[-\sigma']}{\sigma_c}\left(A - \dfrac{[-\sigma']}{\sigma_c}\right) K_S{}^{\max} & (0 \le [-\sigma'] \le \sigma_c) \\ 0 & ([-\sigma'] > \sigma_c) \end{cases} \quad \text{……..(2.4-51)}$$

where the maximum shear stiffness was experimentally obtained when the normal stress reaches the magnitude of uniaxial compressive strength (UCS) of the material.

The substitution of Equations (2.4-48), (2.4-49), (2.4-50) and (2.4-51) into Equation (2.4-47) leaded to the incremental constitutive model for rough joints as following:

$$d\sigma_t = \left(K_S - \frac{a_1 K_S^2}{a_1 K_S + a_2 K_n + mU}\right) du_s - \frac{a_3 K_S K_n}{a_1 K_S + a_2 K_n + mU} du_n$$

……..(2.4-52a)

$$d\sigma_n = -\frac{a_4 K_S K_n}{a_1 K_S + a_2 K_n + mU} du_s + \left(K_n - \frac{a_2 K_n^2}{a_1 K_S + a_2 K_n + mU} \right) du_n$$

……..…(2.4-52b)

where

$$a_1 = \cos^2 \alpha_k - \tan \theta_r \, \mathrm{sgn}(\sigma_t^c) \sin \alpha_k \cos \alpha_k$$ ……..……...…….(2.4-53a)

$$a_2 = \sin^2 \alpha_k - \tan \theta_r \, \mathrm{sgn}(\sigma_t^c) \sin \alpha_k \cos \alpha_k$$ ……..……..…….(2.4-53b)

$$a_3 = \sin \alpha_k \cos \alpha_k + \tan \theta_r \, \mathrm{sgn}(\sigma_t^c) \cos^2 \alpha_k$$ ……..……..…….(2.4-53c)

$$a_4 = \sin \alpha_k \cos \alpha_k + \tan \theta_r \, \mathrm{sgn}(\sigma_t^c) \sin^2 \alpha_k$$ ……..……...……...…….(2.4-53d)

where σ_t^c is defined by Equation (2.4-44) and $\mathrm{sgn}(\sigma_t^c)$ is the sign of σ_t^c.

2.4.5 Equivalent Continuum Models for Deformation of Fractured Rocks

Abovementioned constitutive models can be used to describe the deformation of rock masses with fractures or joints. However, in many situations the number of fractures or joints is so large that dealing with each joint individually is nearly impossible. In this situation, the analysis of fractured or jointed rock mass needs to conduct with an equivalent continuum model.

2.4.5.1 Model for Media with One or Two Orthogonal Thin Joints

Singh (1973a) presented a method of continuum characterization for jointed rock masses. Singh used an equivalent anisotropic continuum model to represent the behaviour of jointed rock mass. Rock matrix was assumed to have Young's modulus (E), shear modulus (G) and Poisson's ratio (ν). The joint set normal to axis i was noted as joint set i with normal stiffness, $K_{n\,i}$, shear stiffness, $K_{S\,i}$ and joint spacing, s_i. The thickness of joints was neglected. The expressions to estimate the elastic moduli of the equivalent continuum anisotropic rock mass were as following.

(1) Single joint set normal to axis 2

$$E_1 = E$$ ……..……...……...…….(2.4-54a)

$$\frac{1}{E_2} = \frac{1}{E} + \frac{1}{s_2 K_{n2}}$$ ……..……..……...……...…….(2.4-54b)

$$\frac{1}{G_{12}} = \frac{1}{G} + \frac{1}{s_2 K_{S2}}$$ ……..……..……...……...…….(2.4-54c)

(2) Orthogonal joint sets normal to axes 1 and 2

$$\frac{1}{E_1} = \frac{1}{E} + \frac{1}{s_1 K_{n1}} \quad \text{.....(2.4-55a)}$$

$$\frac{1}{E_2} = \frac{1}{E} + \frac{1}{s_2 K_{n2}} \quad \text{.....(2.4-55b)}$$

$$\frac{1}{G_{12}} = \frac{1}{G} + \frac{1}{s_1 K_{S1}} + \frac{1}{s_2 K_{S2}} \quad \text{.....(2.4-55c)}$$

(3) Orthogonal joint sets with staggered cross joints normal to axis 1

$$\frac{1}{E_1} = \frac{1}{E} + \frac{B_{N1}}{s_1 K_{n1}} \quad \text{.....(2.4-56a)}$$

$$\frac{1}{E_2} = \frac{1}{E} + \frac{1}{s_2 K_{n2}} \quad \text{.....(2.4-56b)}$$

$$\frac{1}{G_{12}} = \frac{1}{G} + \frac{B_{T1}}{s_1 K_{S1}} + \frac{1}{s_2 K_{S2}} \quad \text{.....(2.4-56c)}$$

where B_{N1} and B_{T1} are the stress concentration factors for normal and shear stresses respectively and expressed as:

$$B_{N1} = \left[1 + \frac{K_{S2} \cdot s'}{K_{n1} \cdot s_2}\left(1 - \frac{s'}{s_1}\right)\right]^{-1} \quad \text{.....(2.4-57a)}$$

$$B_{T1} = \left[1 + \frac{K_{n2} \cdot s'}{K_{S1} \cdot s_2}\left(1 - \frac{s'}{s_1}\right)\right]^{-1} \quad \text{.....(2.4-57b)}$$

where s' is the joint offset of staggered joint set 1.

Hooke's law requires the stress-strain matrix to be symmetric, so that:

$$\frac{\nu_1}{E_1} = \frac{\nu_2}{E_2} = \frac{\nu}{E} \quad \text{.....(2.4-58)}$$

The analyses (Singh, 1973b) showed that the displacement field predicted with the proposed equivalent continuum anisotropic model was quite close to that of a jointed rock mass simulated with a finite element joint model, except in the region of high stress gradients near the loaded area. In the special case where the rock mass consisted of a single joint set of very low shear stiffness, this model broke down due to excessive bending of rock layers. Nevertheless, the proposed model could be safely used in predicting overall displacements and stresses for design purposes.

2.4.5.2 Model for Media with Three Orthogonal Thin Joints

Amadei and Goodman (1981) presented an equivalent continuum anisotropic model to describe the non-linear behaviour of a discontinuous, homogeneous and anisotropic body of rock containing up to three orthogonal joint sets. Intact rock had following anisotropic properties: Young's moduli, E_i (i = n, s and t), shear moduli, G_{st}, G_{nt} and G_{ns} in the planes st, nt and ns, and Poisson's ratios, ν_{sn}, ν_{tn}

and ν_{ts}. Poisson's ratio ν_{ij} (i,j = two orthogonal directions rotating in n, s and t) determined the normal strain in the symmetry direction j when a stress was added in direction i. Poisson's ratio ν_{ij} and ν_{ji} were related by:

$$\frac{\nu_{ij}}{E_i} = \frac{\nu_{ji}}{E_j} \quad \text{.....(2.4-59)}$$

Three orthogonal joint sets intersecting directions n, s and t had spacings, normal stiffnesses and shear stiffnesses: s_1, K_{n1} and K_{S1} for joint set 1; s_2, K_{n2} and K_{S2} for joint set 2; s_3, K_{n3} and K_{S3} for joint set 3. The thickness of the joints was neglected. Then the equivalent moduli in direction i (i=n, s and t for the intact rock or i=1, 2 and 3 for the joint sets) were derived as:

$$\frac{1}{E_i^*} = \frac{1}{E_i} + \frac{1}{s_i \cdot K_{ni}} \quad \text{.....(2.4-60a)}$$

$$\frac{1}{G_{ij}^*} = \frac{1}{G_{ij}} + \frac{1}{s_i \cdot K_{S_i}} + \frac{1}{s_j \cdot K_{S_j}} \quad \text{.....(2.4-60b)}$$

Base on the principle of energy conservation, Huang et at (1995) proposed an equivalent continuum model for rock mass with three intersecting joint sets and derived the elastic moduli. The first two joint sets had the same normal and shear stiffnesses and spacing, and the angle between the joint sets was θ. The third joint set had different stiffnesses and spacing. The matrix of the rock mass was assumed isotropic. Bagheri and Settari (2006 and 2008) extended the model to saturated rock mass and corrected the elastic moduli. They also applied their model in the reservoir and geomechanical coupled simulation of naturally fractured reservoirs.

2.4.5.3 Model for Media with Multiple Thick Joints

Based on an equivalent homogenous orthorhombic medium, Gerrard (1982) formulated three sets of models to describe the moduli of rock masses having one, two or three joint sets. The joints were considered as a material having own thickness and modulus. The joints in each set were assumed to be planar and equally spaced. When more than one set of joint were present, they were assumed to be mutually perpendicular to each other.

2.4.5.4 Model for Media with Random Thin Joints

Fossum (1985) developed a set of relations to estimate the effective elastic properties for rock masses with random joints. In the model the joints had normal stiffness and shear stiffness, and intact rock was isotropic. The expressions to

calculate effective elastic properties such as effective Young's modulus, Poisson's ratio, Lame's constant and bulk modulus were conducted.

2.4.5.5 Chen's Model

Chen (1986) has presented a two-dimensional continuum approximation based on average discontinuous displacements across jointing planes within a representative elementary volume. The constitutive model was based on the continuum assumption of strain-partitioning among the elastic rock matrix and joint sets with nonlinear normal and shear responses. Chen (1989) developed the numerical implements of the two-dimensional continuum model.

2.4.5.6 Model for Media with Planar Tunnel Cracks

Hu and Huang (1993) presented the estimations of effective moduli by modeling discontinuities as planar tunnel cracks, i.e. long cracks in rock masses. The interaction between the cracks was taken into account with the self-consistent scheme. Three kinds of crack orientations, i.e. randomly, parallel and perpendicular, were considered. The uncracked material was assumed isotropic, while the cracked solid behaved as an orthotropic material. The damaged elastic moduli, in-plane and out-of-plane, were presented in terms of a defined planar crack density.

The study showed that for all three cases, the out-of-plane moduli decayed much slower than the in-plane moduli as the crack density increases. The results also indicated the effective moduli were scale-dependent and when the sample size was so large that all of the crack density information was sampled, the moduli achieved stable values.

2.4.5.7 Model Based on Statistics

Based on the statistical analysis of a large amount of experimental data, Sitharam et al (2001) presented the empirical relations for the strength and stiffness of rock masses as:

$$\sigma_{cr} = \frac{\sigma_{cj}}{\sigma_{ci}} = f_1(J_f) \quad \text{.....(2.4-61)}$$

$$E_r = \frac{E_j}{E_i} = f_2(J_f) \quad \text{.....(2.4-62)}$$

where σ_{cr} and E_r are the ratio of strength and ratio of tangent modulus respectively. σ_{cj} and σ_{ci} are the strength of jointed rock mass and the strength of intact rock respectively. E_j and E_i are the tangent modulus of jointed rock mass and the tangent modulus of intact rock respectively. f_1 and f_2 are two functions. The effect of joints in rock mass was taken into account by a joint factor defined as:

$$J_f = \frac{J_n}{n \cdot r} \quad \text{.....(2.4-63)}$$

where J_n is the number of joints per meter depth; n is inclination parameter depending on the orientation of the joint and r is the roughness or joint strength parameters depending on the joint condition.

The equivalent continuum model, in which the moduli of joints were described with aforementioned properties, was applied to analyze the underground cavern of the Shiobara power station in Japan. Sitharam and Latha (2002) also applied the equivalent continuum model to the Nathpa-Jhakri hydropower project in the state of Hinachal Pradesh in India and the Kiirunavaara mine in Sweden. The results indicated that the numerical analysis estimated the field behaviour very well.

2.4.5.8 Model Based on Micromechanics Continuum

Yoshida and Horii (2004) presented a micromechanics-based continuum model (MBC) for rock mass. In the modeling, problems involving microscopic elements were stated as equivalent continuum problems. Microstructure behaviour is modeled and the constitutive equation of an equivalent continuum is derived from the relationship between average stresses and average strains over a representative volume element (RVE) containing a large number of microstructures. The relationship was assumed to be satisfied at each point in the equivalent continuum body. To derive the overall constitutive relationship, the behaviour of each microstructure was estimated and the solution of each microscopic element was derived using an averaging scheme. It was emphasized that the evolution of inelastic behaviour of the microstructures is dominant in most cases. Therefore, considering the overall modulus only is not sufficient, since changes in microstructure need to be treated in the derivation of the constitutive equation.

The time history of relative displacement near the cavern wall and the distribution of displacement along each measurement line at the completion of the

entire excavation obtained by the proposed method were in good agreement with measured data.

2.4.5.9 Equivalent Elastic Properties Determined by Numerical Simulation

Min and Jing (2003) established a methodology to determine the equivalent elastic properties of fractured rock masses by explicit representations of stochastic fracture systems. Fractured rock masses were regarded as equivalent elastic continua and the general theory of anisotropic elasticity was used to describe the macroscopic mechanical behaviour. The results demonstrated the existence of representative elementary volume (REV) for fractured rock masses with given fracture data. The results also implied that fractured rock masses of equivalent statistical homogeneity of fracture systems can be represented as a homogeneous continuum above a certain scale. In order to evaluate the two criteria for the appropriateness of equivalent continuum approach, two measures has been suggested: 'coefficient of variation' used to evaluate the variation from the multiple realization of stochastic DFNs and 'mean prediction error' used to evaluate the error involved in the prediction of compliance tensor in rotated axes.

2.5 THERMO-HYDRO-MECHANICAL COUPLED SIMULATION

2.5.1 Methods of Coupled Simulation

According to Settari and Walters (2001), Rutqvist et al (2002) and Tran et al (2002) the coupled simulation methods of fluid flow and solid deformation (geomechanics) could be classified into full coupled, sequential coupled and decoupled simulation methods. Sequential coupled simulation is also called partial or loose coupled simulation (Longuemare et al, 2002 and Minkoff et al, 2003). In full coupled simulation, flow variables (such as pressure and maybe temperature etc.) and geomechanical variables (such as stress and displacement) are simultaneously calculated by solving a system of equations governed by and established on the three basic principals: mass, momentum and energy conservations.

In sequential coupled simulation, flow variables and geomechanical variables are sequentially solved from a reservoir simulator and a geomechanical simulator and the coupling parameters are iterated between two simulators. If the coupling

parameters are iterated within each time step the simulation is called implicitly sequential coupled simulation (Rutqvist et al, 2002) or iterative coupled simulation (Tran et al, 2002). If the coupling parameters are assumed to be constant during each time step and they are evaluated and iterated at the end of each time step, the simulation is called explicitly sequential coupled simulation.

Decoupled simulation is also called uncoupled simulation or one way coupled simulation. Namely, changes in fluid pressure fields influence stresses and strains but changes in the stresses or strains fields are assumed not to affect fluid pressures (Wang, 2000). Thus the fluid flow equations can be solved independently and the resulting pore pressure field inserted into the geomechanical simulation.

The solution techniques for full coupled simulation include finite different method (FDM) such as the codes of FLAC and FLAC3D (Itasca Consulting Group Inc., 2002), finite element method (FEM) such as the codes of FRACON (Nguyen, 1996), THAMES (Ohnishi and Kobayashi, 1996), ROCMAS (Noorishad and Tsang, 1996), CORES (Gutierrez et al, 2001) and LAGAMINE (Charlier et al, 2002), and distinct element method (DEM) such as the code of UDEC (Itasca Consulting Group Inc, 2000). In sequential coupled simulation both fluid flow and rock deformation can be solved with FDM (Rutqvist et al, 2002) or FEM (Longuemare et al, 2002 and Minkoff et al, 2003). Decoupled simulation can be implemented with FDM (Gong, 2002) or FEM (Minkoff et al, 1999).

2.5.2 Coupled Simulation of CBM Recovery

There are few models of CBM recovery simulation where coupled simulation method is applied. Durucan et al (1993) developed a finite element model to simulate the in situ stress changes near wellbores and couple with fluid flow to characterize the dynamic change of permeability. But their study on the influence of stresses was limited to areas around wellbores.

Zhao et al (2004) presented a coupled simulation model to simulate CBM production. In their model fluid was single phase and single component gas, i.e. methane. The flows and deformations in matrix and cleats were considered separately. The permeability changes of matrix and cleats with in situ stresses were described with different models. The simulation model was solved with finite element method.

2.5.3 Coupled Simulation of Fractured Rock

There are several coupled simulation models that can be used to simulate flow and rock deformation in fractured media. Elsworth (1989) presented a model to describe permeability enhancement within the competent blocky rock masses subjected to temperature and pressure changes. The permeability model is presented in Equations (2.4-14) and (2.4-15). The model accommodated a ubiquitously jointed and initially stressed mass into which fluid with different temperature was injected. The transient behavior of fluid flow in the coupled system was described with a 1-D or radial model. Elsworth and Xiang (1989) extended the work of Elsworth (1989) by considering the influence of shearing. The displacement of joints was presented in Equation (2.4-16). The local assumption of full lateral restraint that was coupled with analytical representation of thermal strains rendered a nonlinear initial-value problem which was fully defined in terms of the two dependent variables (fluid pressure and temperature) only. Finite element method was used for the coupled simulations.

Elsworth and Bai (1992) presented a constitutive model for the coupled flow-deformation response of single-phase fluid in dual-porosity media. The constitutive model was represented in finite element format and can be applied to a dual-porosity system with general boundary conditions. The model was extended to multi-porosity/multi-permeability media by Bai et al (1993).

Bai and Roegiers (1994) presented analytical solutions based on a porothermomechanical formulation for single-phase fluid flow in double-porosity media. For convenience the decoupled simulation of heat flow was implemented to obtain a analytical solution sequentially. Comparing with their previous models the new model was more realistic in charactering the change of reservoir storage.

Bai and Elsworth (1994) investigated the changes of deformation and stress dependant hydraulic conductivity that occurred in the underground mining of intact and fractured porous media. Coupling models between strain and hydraulic conductivity were illustrated in Equations (2.4-17a) and (2.4-17b). The model was based on the theory of coupled steady-state poroelasticity. The displacement and fluid pressure fields were simulated with finite element method for single phase fluid flow.

Bai et al (1995) presented an analytical model based on a poromechanical formulation for dual-porosity media. The solution was developed for the radial flow of single phase fluid in a reservoir subject to the conditions of constant

bottom hole pressure or constant flow rate using Hankel transforms. The study showed that poromechanical effect is significant in the well vicinity where the change of pressures and stresses are substantial, and that dual-porosity behavior is most obvious only when the poromechanical properties fall within a certain range.

Ghafouri and Lewis (1996) presented a coupled simulation model for single-phase fluid flow through a deformable fractured porous media. The model was based on the double porosity theory and solved with finite element method. The results predicted with this model were found more meaningful and realistic comparing with those with the model based on a conventional single average porosity.

Chen and Teufel (1997) presented a fluid-flow and geomechanics coupled model for single-phase flow in a naturally fractured reservoir. The fluid flow was simulated within dual-porosity (or overlapping-continuum) media while geomechanics was modeled following Biot's isothermal, linear poroelastic theory.

Indraratna et al (1999) implemented a coupled simulation study of water flow through a network of joints. Universal Distinct Element Code (UDEC) was used to quantify the influences of joint orientations and external stresses acting on idealized joints in tunnel excavation. The study showed that the cubic law could only accurately estimate the flow rates under low surrounding stresses. For each joint, the conductivity of water was governed by a residual aperture. Once a critical load was exceeded, the change of permeability was negligible. It was found that flow rates into an excavation depended on the ratio of boundary block size to excavation size. The inflow became excessive if the ratio was less than 4 while very small if the ratio exceeded 8.

Masters et al (2000) extended the double porosity deformable model developed by Ghafouri and Lewis (1996) to include the influences of temperatures. The model assumed that a single-energy continuum was sufficient to quantify the state of material with temperature dependency. This postulate implied that the quantity of energy flux carried by the fluid mass in the matrix and fissure network was the same. Throughout the formulation, displacements, pore pressures and temperatures were considered as primary unknowns and the final equations were fully coupled and solved with finite element method. The authors presented a first attempt in understanding the more complicated process of non-isothermal transport in a deformable porous media.

Rutqvist el (2002) linked and jointly executed two computer codes, TOUGH2 and FLAC3D, for coupled thermal-hydrologic-mechanical (THM) analysis of

multiphase fluid flow, heat transfer, and deformation in fractured and porous rock. In the study, the codes were sequentially executed and linked through external coupled modules: one that dictated the change of effective stresses as a function of multi-phase pore pressures and thermal expansion, and another corrected porosity, permeability, and capillary pressures due to the change of stresses. The capability of a linked TOUGH-FLAC simulator were demonstrated with two complex coupled problems related to the injection and storage of carbon dioxide in aquifers and the disposal of nuclear waste in unsaturated fractured porous media.

2.5.4 Coupled Simulation of Complex Systems

As Jing and Hudson (2002) pointed out, over the last three decades the advances in the use of computational methods in rock mechanics have been impressive, especially in specific numerical methods, based on both continuum and discrete approaches, for representation of fracture systems, for comprehensive constitutive models of fractures and interfaces, and in the development of coupled THM models. Despite all the advances, our computer methods and codes can still be inadequate when facing the challenge of some practical problems, and especially when adequate representation of rock fracture systems and fracture behaviour are a pre-condition for successful modelling. Today's numerical modelling capability can handle very large scale and complex system, but the quantitative representation of physics of fractured rocks remains generally questionable, although much progress has been made in this direction.

For the complex fluid-flow system and very large scale in the petroleum industry, all the factors as multiphase (oil, gas and water), phase change (from liquid to gas and verse vice), and maybe multi-components (methane, ethane etc.) and multimedia (pore and fracture) are important and must be considered in the simulation. In order to save time and cost and make reservoir simulation practical, the systems are usually solved by finite difference method. In the developed industrial simulators the influences of rock deformation due to in situ stress changes are generally neglected (CMG, 2003a). The influences of geomechanics are considered in some simulators (CMG, 2003b) but when fractures exist in the system a lot of improvements are still needed. On the other hand, geomechanical codes are traditionally developed to simulate mainly soil or rock deformation with less emphasis on fluid flow, i.e. usually considering single-phase fluid flow or simple two-phase (water and air) flow, such as in FLAC or FLAC 3D (Itasca,

2002a and Itasca, 2002b). There are only a few models that currently treat multiphase flow and much development effort is still needed to bring the flow-model capabilities of fully coupled simulation on par with existing commercial reservoir simulators (Settari and Walters, 2001).

Therefore, at present using either reservoir simulators or geomechanical simulators separately can not satisfactorily solve our multiphase, multicomponent and fracture flow systems with the consideration of rock deformation. Sequential coupled simulation with equivalent continuum approach for fracture rock mass is a practical solution for our studying system because both reservoir and geomechanical simulators are available, well developed and widely applied in the industry.

2.6 SUMMARY

The review of the chapter is summarized as following:

(1) Coalbeds are dual porosity media containing micropores which exist in coal matrix and macropores called cleats or fractures. Micropores provide the main site of gas storage. Gas absorbs on the walls of micropores and the gas absorption capacity of coal is described with adsorption isotherms. Coal matrix swells due to gas adsorption and shrinks due to gas desorption. Cleats are the major conduit of fluid flow in coalbeds and have permeability with the characteristics of anisotropy, stress dependency, gas adsorption/desorption dependency, and stress history dependency.

(2) The methods of coalbed methane recovery include pressure depletion coalbed methane (CBM) recovery and enhanced coalbed methane recovery (ECBM). The ultimate methane recovery with CBM method is generally not greater than 50% of the gas-in-place. CO_2, N_2 even flue gas can be applied in ECBM process. However the techniques of ECBM are under development and field experiences are limited.

(3) The available analytical models used to predict the change of permeability and porosity can be classed into empirical and theoretical models. The former was established based on experiment results made with the specimens of specific coalbeds and cannot be extended to other coalbeds. The later includes the models considering the influences of pressure changes only, the influences of shrinkage/swelling of matrix only, and the influences of both. According to the application, the models can also be divided into the models applied in CBM or ECBM.

(4) For fractured rock, the tortuosity, roughness and contact area of fractures would influence fracture permeability. Many analytical models have been developed to predict the change of permeability or conductivity of a single fracture due to the changes of in situ stresses. They include the models of Barton et al, Walsh, Bai and Elsworth, and Willis-Richards et al, etc. There are several constitutive models available to describe the deformation of fractures, such as the Goodman's empirical model, Barton et al's empirical model and Jing et al's theoretical model. For fractured rocks with massive fractures, equivalent continuum models are the best to simulate their deformations since constitutive models need too high computing resources to be affordable or available.

(5) Based on the degree of coupling, the coupled simulations can be classed into full coupled, sequential coupled and decoupled simulations. There are few models developed to simulate coalbed methane production in a small scale with full coupled simulation method. The coupled simulations of fractured rocks have been studied for almost 20 years and applications can be found in single phase situation such as hydrogeology, geotechnical engineering and radiation waste storage. For multiphase, multicomponent and large scale fractured reservoirs in petroleum industry, sequential coupled simulation with equivalent continuum approach for fractured rock mass is a practical solution at present.

Table 2.1: Swelling/Shrinkage Strains of Coal due to Adsorption/Desorption of Gases

Reference	Coal Source	Test Conditions: Specimen Shape | Gas | Temperature(°C) | Pressure (MPa) | Constraint (MPa)	Gas Pressure Applied	Measure Direction to Bedding	Maximum Strain (%): Linear | Vol.
Moffat and Weale, 1955	Bear Park and Vitrain, British	block | CH_4 | 25 | 0~67, 73 | (no)	increase	⊥	0.2~0.3 |
		block | CH_4 | 25 | 0~67, 73 | (no)	increase	//	0.1 |
		block | CH_4 | 25 | 67, 73~0 | (no)	decrease	⊥	-0.4 |
	Cannock Wood, British	block | CH_4 | 25 | 0~70/ | (no)	increase	// and ⊥	| 1.75
		block | CH_4 | 25 | 70~0 | (no)	decrease	// and ⊥	| -1.49
		block | He | 25 | 0~30 | no	increase	// and ⊥	| -0.35
	S. Wales Anthracite, British	block | CH_4 | 25 | 0~39 | (no)	increase	(isotropic)	| -0.1
		block | CH_4 | 25 | 39~0 | (no)	decrease	(isotropic)	| -0.73
Reucroft and Patal, 1986	Webster, USA	cylinder | CO_2 | 25 | 0.14 | (no)	constant	⊥	| 0.36
	Hopkins, USA	cylinder | CO_2 | 25 | 0.14 | (no)	constant	⊥	| 0.60
	Carlisle, USA	cylinder | CO_2 | 25 | 0.14 | (no)	constant	⊥	| 1.07
Reucroft and Sethuraman, 1987	Webster, USA	cylinder | CO_2 | 25 | 0.5 | (no)	constant	⊥	| 0.75
	Webster, USA	cylinder | CO_2 | 25 | 1.0 | (no)	constant	⊥	| 0.85
	Webster, USA	cylinder | CO_2 | 25 | 1.5 | (no)	constant	⊥	| 1.33
	Hopkins, USA	cylinder | CO_2 | 25 | 0.5 | (no)	constant	⊥	| 1.24
	Hopkins, USA	cylinder | CO_2 | 25 | 1.0 | (no)	constant	⊥	| 2.23
	Hopkins, USA	cylinder | CO_2 | 25 | 1.5 | (no)	constant	⊥	| 3.11

	Carlisle, USA	cylinder | CO_2 | 25 | 0.5 | (no)	constant	⊥	| 2.16
	Carlisle, USA	cylinder | CO_2 | 25 | 1.0 | (no)	constant	⊥	| 3.00
	Carlisle, USA	cylinder | CO_2 | 25 | 1.5 | (no)	constant	⊥	| 4.18
Walker et al, 1988	(one coal, unknown source), USA	block | CO_2 | 25 | 0.1,3.4 | 0.001	increase	(unknown)	| 0.44~1.27
	(eleven coals, unknown source) , USA	powder | CO_2 | 25 | 0.1 | 0.001	constant	(isotropic)	| 0.028~0.139
	(six coals, unknown source) , USA	powder | CO_2 | 25 | 0.68~4.8 | 0.001	increase	(isotropic)	| 0.59~3.79
Harpalani and Schraufnagel, 1990a & 1990b	Piceance Basin, USA	cylinder | He | (unknown) | 0~6.9 | (no)	increase	(unknown)	| -0.1
	Piceance Basin, USA	cylinder | He | (unknown) | 6.9~0 | (no)	decrease	(unknown)	| 0.07
	Piceance Basin, USA	cylinder | CH_4 | (unknown) | 0~6.2 | (no)	increase	(unknown)	| 0.48
	Piceance Basin, USA	cylinder | CH_4 | (unknown) | 6.2~0 | (no)	decrease	(unknown)	| -0.38
Ceglarska-Stefanska and Czaplinski, 1993	(gas-flame coal, unknown source), Poland	cube | CO_2 | 25 | 0~4.7 | (no)	increase	//	0.65 |
				⊥	0.92 |
	(gas-coking coal, unknown source), Poland	cube | CO_2 | 25 | 0~4.8 | (no)	increase	//	0.44 |
				⊥	0.52 |
	(anthracite, unknown source), Poland	cube | CO_2 | 25 | 0~4.8 | (no)	increase	//	0.58 |
				⊥	0.50 |
	(unknown source),	cube | CH_4 | 25 | 3.04 | (no)	increase	//	0.134 |

Ceglarska-Stefanska, 1994	Poland			⊥	0.175 |
			decrease	//	-0.126 |
				⊥	-0.142 |
	(unknown source), Poland	cube | CH_4 | 25 | 0.32 | (no)	increase	//	0.02 |
				⊥	0.02 |
			decrease	//	-0.012 |
				⊥	-0.012 |
	(unknown source), Poland	cube | CH_4 | 25 | 2.82 | (no)	increase	//	0.135 |
				⊥	0.123 |
			decrease	//	-0.085 |
				⊥	-0.073 |
Harpalani and Chen, 1995	San Juan Basin, USA	cylinder | He | (unknown) | 10.3~0 | (no)	decrease	// and ⊥	| 0.05
		cylinder | CH_4 | (unknown) | 10.3~0 | (yes)	decrease	// and ⊥	| -0.16
Levine, 1996	Illinois, USA	block | CH_4 | (unknown) | 0~5.19 | (unknown)	increase	// and ⊥	0.16~18 | 0.48~0.53
		block | CO_2 | (unknown) | 0~3.09 | (unknown)		// and ⊥	0.4~0.5 | 1.26
Ceglarska-Stefanska and Brzoska, 1998	(dry coal, unknown source), Poland	cube | CH_4 | 25 | 0~4.8 | (no)	increase	⊥	0.111 |
		cube | CH_4 | 25 | 4.0~0 | (no)	decrease	⊥	-0.093 |
	(wet coal, unknown source), Poland	cube | CH_4 | 25 | 0~4.0 | (no)	increase	⊥	0.133 |
		cube | CH_4 | 25 | 4.0~0 | (no)	decrease	⊥	-0.04 |
	Ohai, New Zealand.	cylinder | CO_2 | (unknown) | 4.0 | (no)	constant	// and ⊥	| 2.16

George and Barakat , 2001		cylinder|CO_2|(unknown)|4.0~0|(no)	decrease	// and ⊥	|-2.07
		cylinder| CH_4|(unknown)|4.0|(no)	constant	// and ⊥	|0.38
		cylinder| CH_4|(unknown)|4.0~0|(no)	decrease	// and ⊥	|-0.429
		cylinder| N_2|(unknown)|4.0|(no)	constant	// and ⊥	|0.17
		cylinder| N_2|(unknown)|4.0~0|(no)	decrease	// and ⊥	|-0.126
		cylinder| He |(unknown)|4.0|(no)	constant	// and ⊥	|-0.08
		cylinder| He |(unknown)|4.0~0|(no)	decrease	// and ⊥	|0.047
Ceglarska-Stefanska and Zarebska, 2002a	Brzeszcze, Poland	cube|CH_4|25|0.34~3.88|(no)	constant	⊥	0.008~0.242|
	Brzeszcze, Poland	cube|CO_2+CH_4|25|0.20~3.61|(no)	constant	// and ⊥	|0.066~0.463
	Moszczenica, Poland	cube|CO_2+CH_4|25|0.17~3.70|(no)	constant	⊥	0.017~0.249|
Ceglarska-Stefanska and Zarebska, 2002b	Brzeszcze, Poland	cube|CO_2+CH_4|25|0.70~2.83|(no)	decrease	⊥	-0.044~-0.157|
	Moszczenica, Poland	cube|CO_2+CH_4|25|0.53~2.46|(no)	decrease	⊥	-0.026~-0.05|
Chikatamarla et al, 2004	Wolf (Mountain, Quinsam, Illinois, Ardley), Canada	cylinder |H_2S|25|0.6|(no)	constant	// and ⊥	|1.402~9.327
		cylinder |CO_2|25|0.6|(no)	constant	// and ⊥	|0.261~0.656
		cylinder |CH_4|25|0.6|(no)	constant	// and ⊥	|0.091~0.297
		cylinder |N_2|25|0.6|(no)	constant	// and ⊥	|0.004~0.026
Zutshi and Harpalani, 2004	(unknown source), USA	rectangular|He|45|0~10.34|(no)	increase	// and ⊥	|0~-0.26
		rectangular|CO2|45|0~5.86|(no)	increase	// and ⊥	|1.35
		rectangular|CH_4|45|0~7.45|(no)	increase	// and ⊥	|0.70

Robertson and Christiansen, 2005	Utah(Anderson), USA	rectangular | CO_2 | 26.7 | 0~5.6 | (no)	increase	(unknown)	2.13 |
	Utah(Anderson), USA	rectangular | CH_4 | 26.7 | 0~6.9 | (no)	increase	(unknown)	0.48 |
	Utah(Anderson), USA	rectangular | N_2 | 26.7 | 0~6.9 | (no)	increase	(unknown)	0.14 |
	Utah (Gilson), USA	rectangular | CO_2 | 26.7 | 0~5.4 | (no)	increase	(unknown)	0.93 |
	Utah (Gilson), USA	rectangular | CH_4 | 26.7 | 0~6.9 | (no)	increase	(unknown)	0.39 |
	Utah (Gilson), USA	rectangular | N_2 | 26.7 | 0~6.3 | (no)	increase	(unknown)	0.11 |

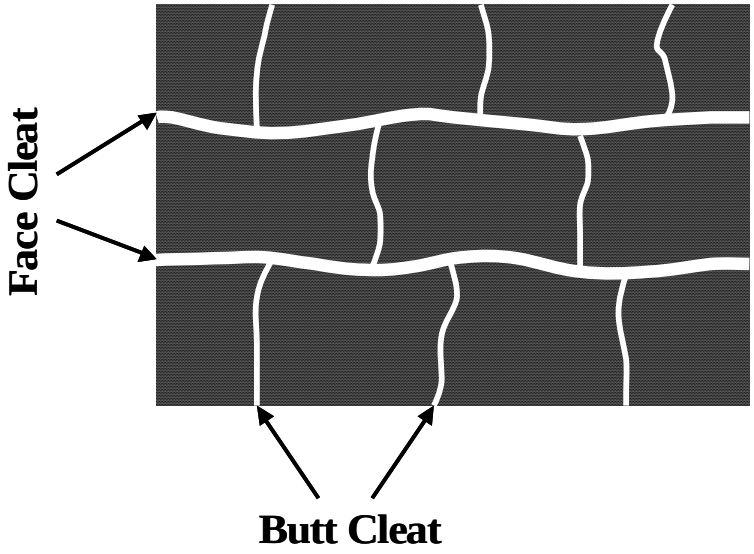

Figure 2.1: Ideal Pore Structure Model of Coal (modified from Davidson et al, 1995)

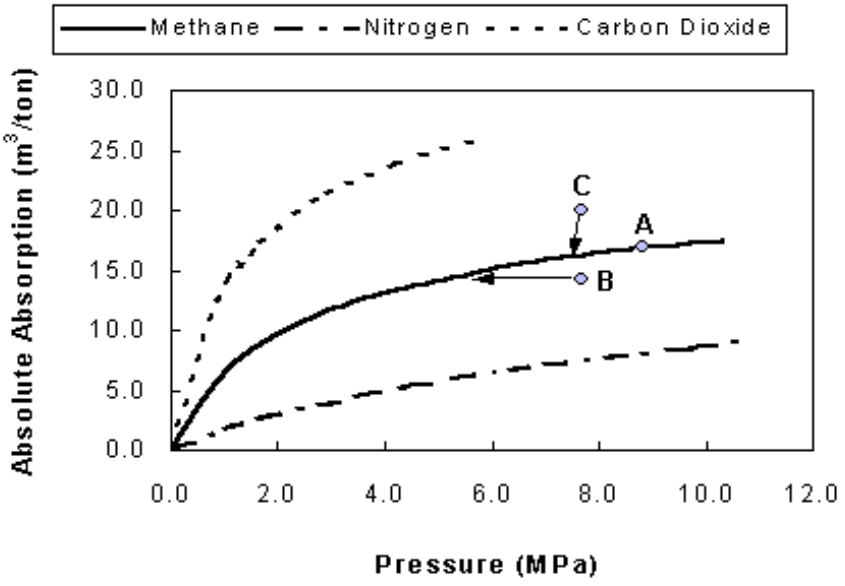

Figure 2.2: Adsorption Isotherms of Gases to Coal (modified from Arri et al, 1992)

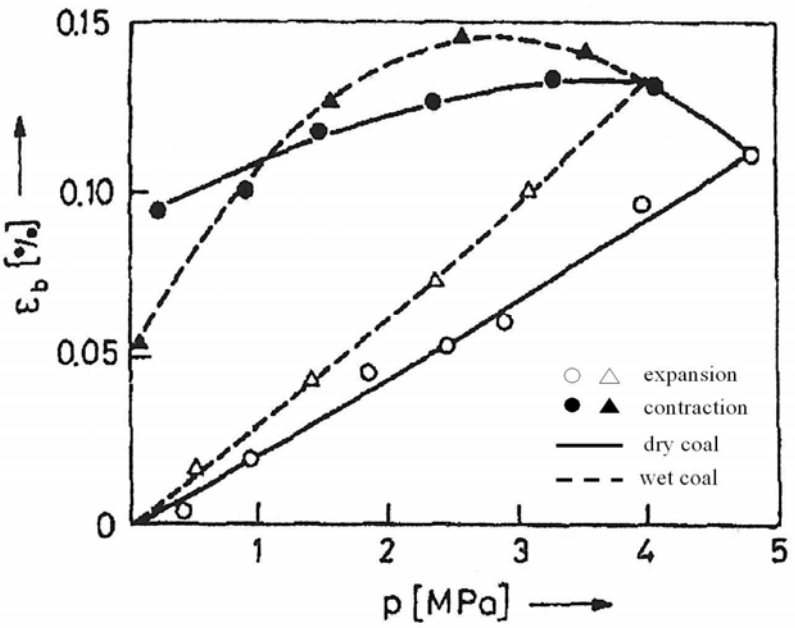

Figure 2.3: Expansion and Contraction of Coal during Adsorption and Desorption of Methane (Ceglarska-Stefanska and Brzoska , 1998)

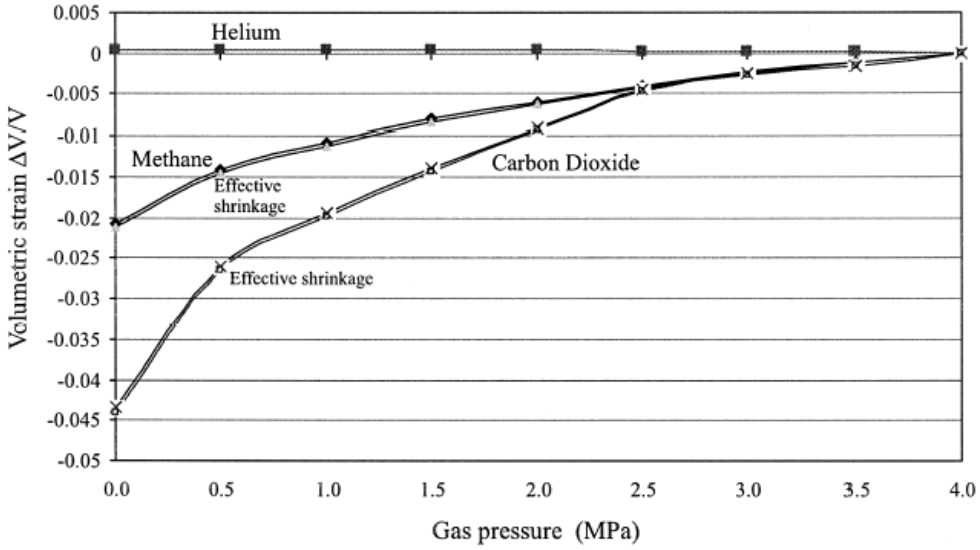

Figure 2.4: Volumetric Strain of Coal Matrix with Decreasing Gas Pressure (George and Barakat, 2001)

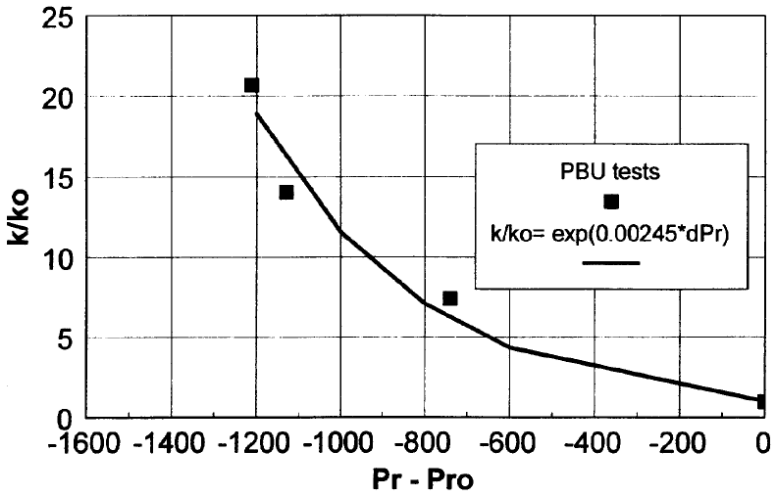

Figure 2.5: Change of Permeability with Pressure (in psi) Decline (Zahner, 1997)

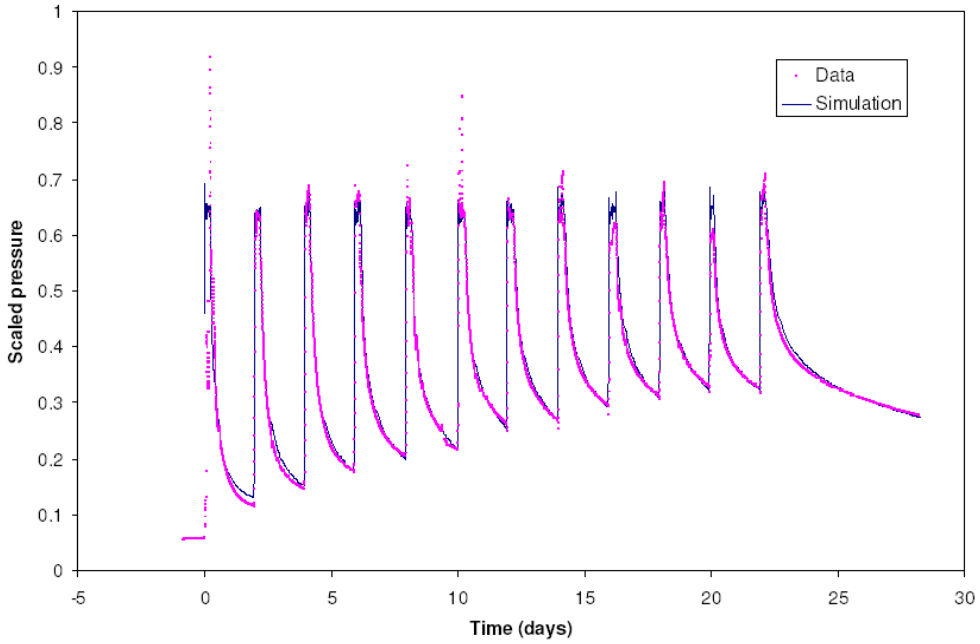

Figure 2.6: Simulation of Pressures during A Cyclic CO_2 Injection Test (van der Meer and Fokker, 2003)

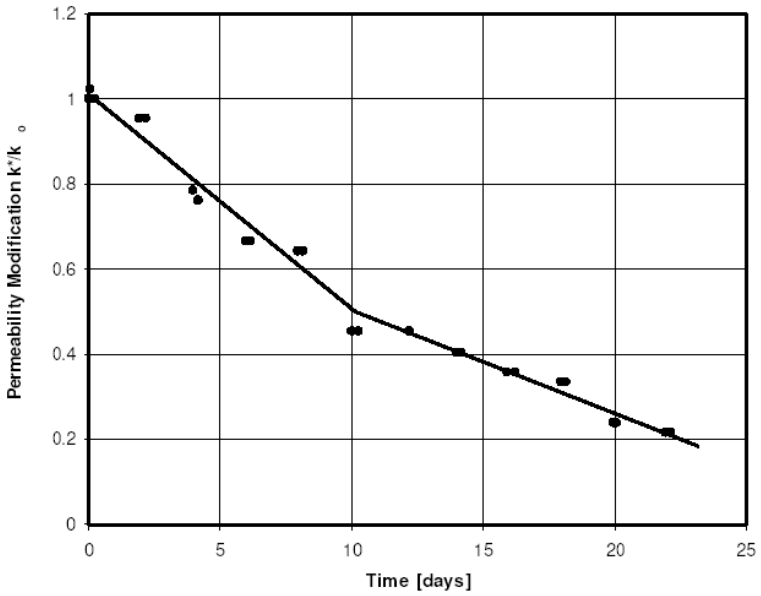

Figure 2.7: Change of Permeability during A Cyclic CO_2 Injection Test (van der Meer and Fokker, 2003)

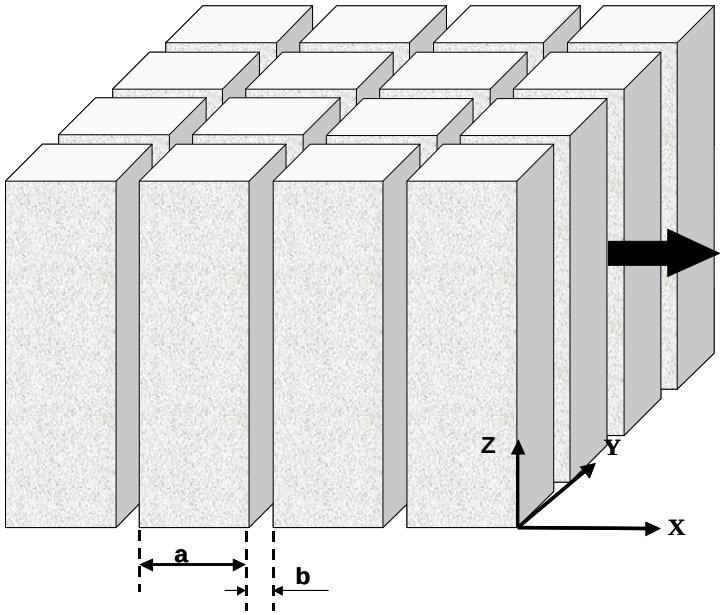

Figure 2.8: Fracture System with Matchstick Matrix Blocks (Seidle et al, 1992)

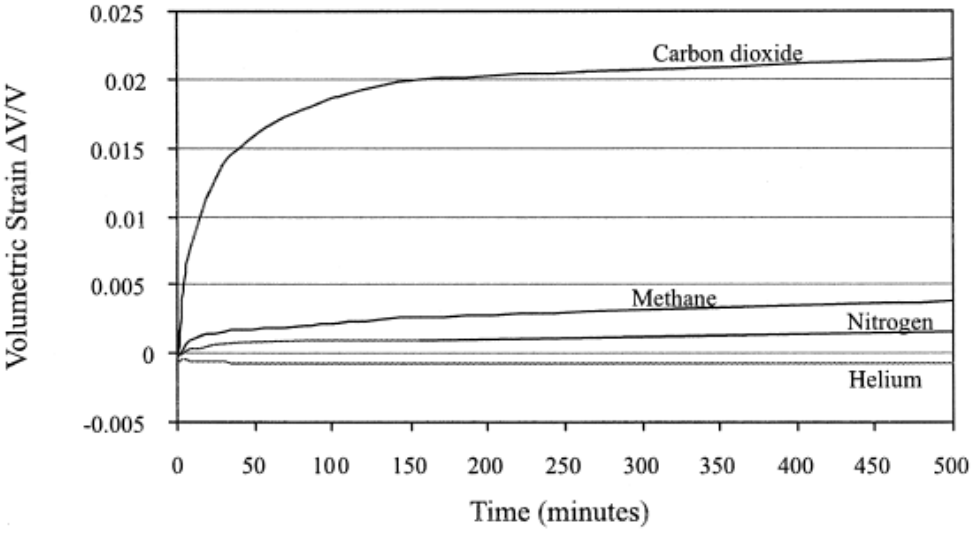

Figure 2.9: Volumetric Strain Associated with Adsorption at 4 MPa for Different Gases

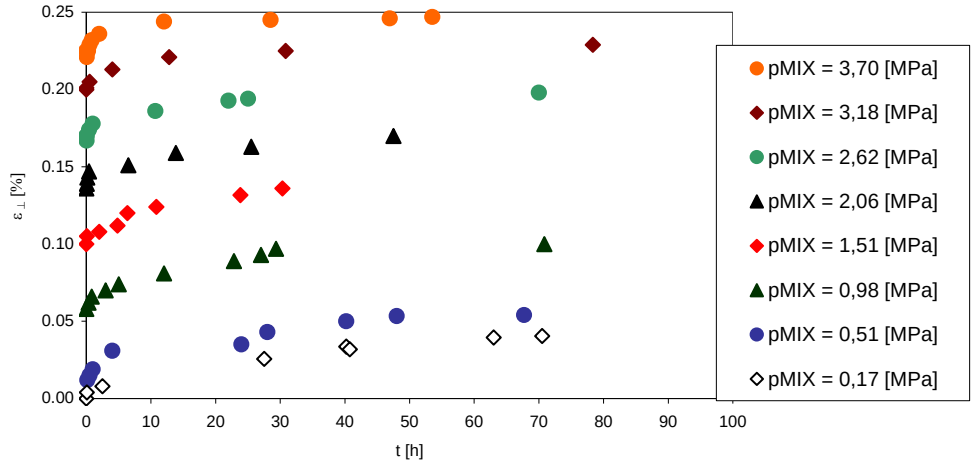

Figure 2.10: Swelling of Coal M due to Adsorption of Gas Mixtures of 51.8% CO_2 + 48.2 % CH_4

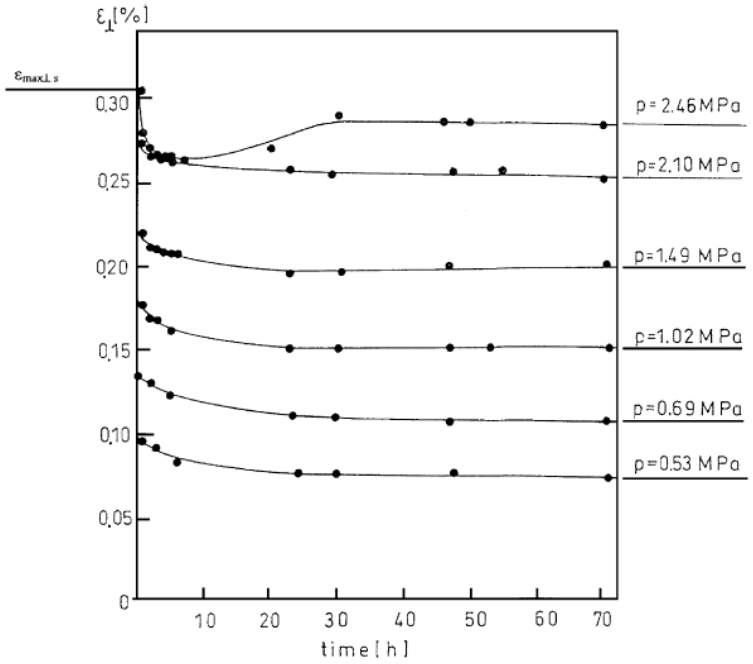

Figure 2.11: Shrinkage of Coal M due to Desorption of CH_4 and CO_2, after CO_2 Pre-sorption and CH_4 Sorption

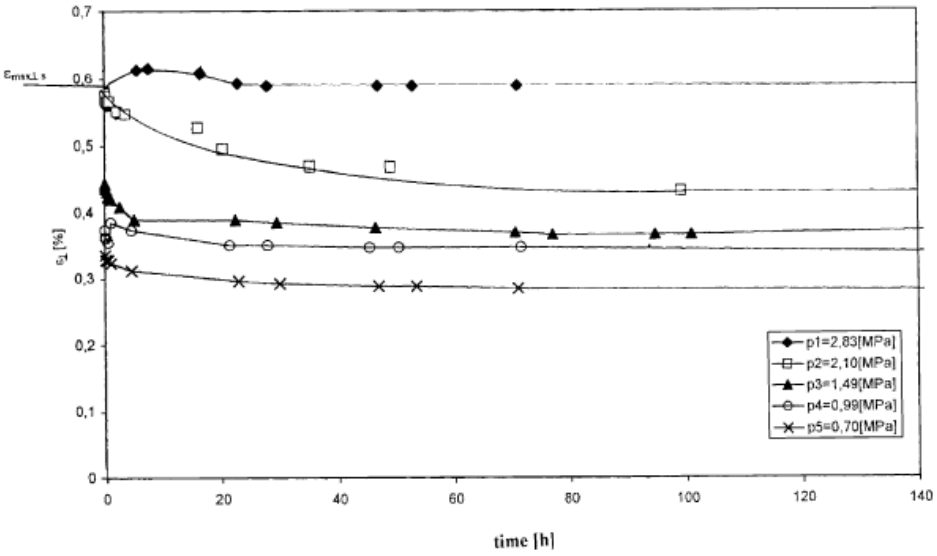

Figure 2.12: Shrinkage of Coal B due to Desorption of CH_4 and CO_2, after CO_2 Pre-sorption and CH_4 Sorption

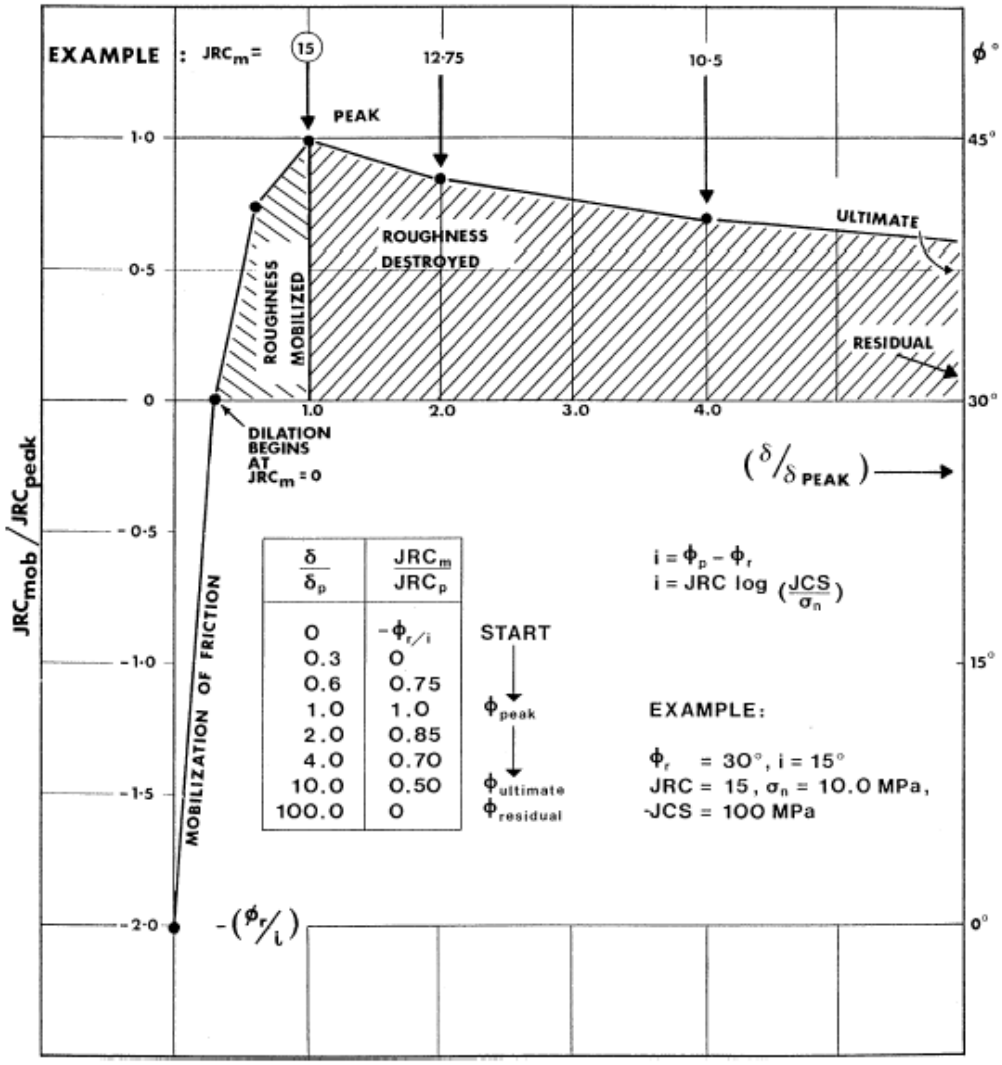

JRC= joint roughness coefficient; JCS= joint wall compression strength

ϕ=frication angle; δ=shear displacement

Subscripts: m=mobilized; n=normal; p=peak; r=residual

Figure 2.13: Recommended Dimensionless Model for Generating Realistic Shear Stress versus Shear Displacement Plots for Joints (Barton et al, 1985)

3 CONTINUUM MEDIUM POROSITY AND PERMEABILITY COUPLING MODELS

3.1 INTRODUCTION

Worldwide coalbed methane reserves have been estimated at 2980~9260 trillion ft^3 (84 ~ 262 trillion m^3) (Davidson et al, 1995). The majority of these reserves are located in Russia (17 ~ 113 trillion m^3), Canada (6 ~ 76 trillion m^3), China (30 ~ 35 trillion m^3), Australia (8 ~ 14 trillion m^3), and the USA (11 trillion m^3). In the United States, coalbed methane accounted for 10% of dry gas reserves and 8% of dry gas production in 2003 (EIA, 2004). In other countries, such as China, Canada, and Australia, coalbed methane projects are attracting more and more attention of petroleum companies.

The production methods of coalbed methane include conventional pressure depletion production (CBM) and enhanced coalbed methane recovery (ECBM). At present, coalbed methane is mainly recovered by the former method. In ECBM, gases such as N_2, CO_2, or flue gas are injected to displace methane and maintain coalbed pressures. This recovery method is still in its infancy with only two field-scale ECBM projects (one injected N_2 and the other injected CO_2) (Reeves, 2001), and one single-well pilot project (Law et al, 2002) worldwide.

The evaluation and prediction of productivity are important steps in the development of coalbeds or coal seams. Because gas storage mechanisms in coal seams (where gas mainly adsorbs on the walls of pores) are different from that in conventional gas reservoirs (where gas is compressed in pores), conventional reservoir simulators generally do a poor job in predicting coalbed methane production. Over the past decades, many models have been developed to characterize coalbed methane production processes (King and Ertekin, 1991 and 1995; Manik et al, 2002) and two types of commercial simulators developed to simulate coalbed methane production, i.e. modified conventional black oil simulators and modified compositional simulators. With the recognition of the stress dependency of coalbed permeability and porosity and the shrinkage/swelling of coal matrix due to gas desorption/adsorption, some simulators have been modified to accommodate these characteristics (Reeves, 2001; CMG, 2005). However, in these simulators the influence of in situ stresses

---

A version of this chapter has been published. Gu, F. and Chalaturnyk, R.J., 2005. Journal of Canadian Petroleum Technology. 44(10):33-42.

is simplified with analytical models or monotonic relations between permeability ratios and pressure changes. Durucan et al (1995) developed a finite element model to simulate the changes of in situ stresses near wellbores. They coupled the stress changes with fluid flow simulation by characterizing dynamic changes in permeability. But the investigation on the influence of stresses was limited to the areas around wellbores and the influence of shrinkage/swelling due to methane desorption/adsorption was not properly simulated.

The chapter is to develop permeability and porosity coupling models by assuming coalbeds as a continuum medium and to establish a method for reservoir and geomechanical coupled simulation based on industrial developed simulators to improve the numerical evaluations of CBM and ECBM. Following the descriptions of coalbed characteristics and production mechanisms, the influences of geomechanics on coalbed methane production are discussed. Then the models used to predict the changes of cleat permeability and porosity during production are established. A simulation procedure for the explicitly sequential reservoir and geomechanical coupled simulation is presented and the capability of the models is demonstrated by simulating a CBM recovery case.

3.2 COALBED CHARACTERISTICS

Coalbeds or coal seams are well known for their dual porosity characteristics. They contain both micropores and macropores. The plan view of an ideal pore structure model of coalbeds is shown in Figure 3.1 (Davidson et al, 1995). Micropores exist in coal matrix and macropores are almost uniformly spaced natural fractures, called cleats. Cleats include face cleats and butt cleats. Butt cleats are about 90^o to face cleats and commonly terminate at face cleats. Both types of cleats develop along bedding planes and are essentially perpendicular or near-perpendicular to bedding planes.

The anisotropic characteristic of coal pore structure suggests that the permeability of coalbeds would be anisotropic with the greatest permeability in the direction of face cleats. This was confirmed by the experimental results of Gash et al (1993). Using the coal from the La Plata mine in the San Juan Basin and under 6.895 MPa (1000 psi), they found that parallel to the bedding plane, the permeability was 0.6 ~ 1.7 mD in the direction of face cleats and 0.3 ~ 1.0 mD in the direction of butt cleats, but the permeability in the direction normal to the bedding plane was just 0.007 mD!

Physical adsorption is the primary mechanism of gas storage in coalbeds. Gas adsorbs on the walls of micropores, which have the diameter of 0.5 to 1.0 nm and are inaccessible to reservoir water or brine. For a given temperature, the relationships between pressures and gas storage capacity of coal are called adsorption isotherms. Typical adsorption isotherms of methane, nitrogen, and carbon dioxide are shown in Figure 3.2.

3.3 PRODUCTION MECHANISMS

3.3.1 Pressure Depletion Coalbed Methane Production

The pressure depletion method for coalbed methane recovery, called CBM, is simple and effective but become less efficient with decreasing seam pressures because of loss of drive energy within seams. The ultimate methane recovery by depletion method is generally not expected to be greater than 50% of gas-in-place, even after several decades of production (Puri and Yee, 1990).

Coal seams are classed as saturated, undersaturated, and oversaturated seams. For coal seams containing pure methane, these classes are marked as points A, B, and C, respectively, in the adsorption isotherm diagram shown in Figure 3.2. The production mechanisms of each seam class are different. For a saturated seam (point A), once the pressure is reduced, methane is immediately released. Due to pressure decreases, coal becomes less capable of retaining methane in an adsorbed state, thus gas molecules start detaching themselves from the surfaces of micropores and cleats, initiating the desorption process. The desorbed methane diffuses through solid matrix to cleats and flows to wellbores. With the production of methane the coal seam reaches a new saturated state on the isotherm under a lower pressure.

For an undersaturated seam (point B), an initial pressure reduction causes mobile water in cleats to flow to production wells. With water production and reservoir pressure decline, as illustrated by the arrow pointing from B to the adsorption isotherm in Figure 3.2, the coal seam reaches a state of saturation. Then the production from this forward follows the same mechanism as a saturated seam.

For an oversaturated seam (point C), the decrease of reservoir pressures results in mobile water and free gas in cleats to flow simultaneously towards production wells. Once the coal seam reaches a state of saturation, following the

path shown by the arrow pointing from C to the adsorption isotherm in Figure 3.2, the production follows the same mechanism as a saturated seam.

3.3.2 Enhanced Coalbed Methane Recovery

For ECBM recovery, in the regions where injection gases have not reached the mechanism of methane recovery is the same as the above mentioned pressure depletion method of coalbed methane recovery and pressure differences provide the drive energy for fluid movements from coalbeds towards production wellbores. However, in the regions where injection gases have reached, the production mechanism depends on the type of injection gas. For simplicity, the following discussions are restrained to the situations of pure N_2 or pure CO_2 as injection gases.

When N_2 is applied in ECBM, it releases methane by both sorption displacement and partial pressure reduction without necessarily depleting the total reservoir pressure (Puri and Yee, 1990). The injected N_2 flushes gaseous methane from cleats, creating near 100% N_2 saturation and 'zero' partial pressure of methane in the cleats. This creates a disequilibrium condition in the system containing both methane and nitrogen. As a result, methane desorbs and is drawn (or 'pulled') into the gaseous phase to achieve partial-pressure equilibrium (Mavor et al, 2002).

When CO_2 is used in ECBM, compared to methane it preferentially adsorbs onto coal such that injected CO_2 is quickly adsorbed into coal matrix to achieve sorbed equilibrium, displacing sorbed CH_4 (Mavor et al, 2002). Methane is "pushed" from coal matrix by highly adsorptive CO_2.

These different mechanisms result in different responses in field ECBM pilots of N_2 and CO_2 injection. Field and simulation results suggest that methane production rates increase faster and injected gas breakthroughs occur more rapidly for N_2 injection than for CO_2 injection (Reeves, 2001; Mavor et al, 2002).

3.4 INFLUENCE OF GEOMECHANICS

Once the gas content of a coal seam is deemed significant in a coalbed methane project, coalbed permeability likely remains the most important factor impacting the success of the project. Since intact coal has extremely low permeability, cleats are the main pathways for the flow of methane from a coal seam to wellbores. During the production life of a coalbed, its permeability does

not keep constant. It changes as methane production progresses, or more precisely, it changes with the variations of in situ stresses, fluid pressures and gas content etc. The change of coalbed permeability mainly results from: (a) the deformation of coal rock due to the effective stress changes caused by pore pressure variations; (b) the shrinkage and swelling of coal matrix due to the desorption/absorption of gases; (c) the opening and closing of cleats. In the following sections we will discuss how these factors influence the changes of coalbed permeability.

3.4.1 Distribution of Pressure and In Situ Stress

The characteristics of the changes of reservoir pressures and effective stresses during conventional CBM and ECBM production have been investigated in this research using the Computer Modelling Group's simulator, GEM©. The coalbed has permeability of 3.65 mD and an initial pore pressure of 7.65 MPa. The simulation area is ¼ of 250 acres. The permeability of the studied coalbed is assumed to be homogeneous and kept constant during production. The minimum bottom hole pressure of production is 275 kPa and the maximum bottom hole pressure of injection is 15 MPa. Effective stresses are roughly estimated by subtracting pore pressures from the initial total stress. In this ECBM process, pure CO_2 is injected and a five-spot well pattern is assumed. The production and injection rates and bottom hole pressures are shown in Figure 3.3.

The typical distributions of pressures and effective stresses during CBM recovery are shown in Figure 3.4(a). These results indicate that pressures around the producer decrease (as expected) thus the corresponding effective stresses increase. The typical distributions of pressures and effective stresses during ECBM recovery are illustrated in Figure 3.4(b). The changes of pressures and effective stresses around the producer are similar to that in CBM recovery. But around the injector, the injection results in the increases of pressures thus the decreases of the corresponding effective stresses.

The distributions of pressures and effective stresses vary with time. As shown in Figure 3.4(c), during CBM recovery the pressures around the injector continuously decrease thus the corresponding effective stresses continuously increase until an economical pressure limit is reached. As indicated in Figure 3.4(d), in the early stage of ECBM process the pressures around the producer continuously decrease while the corresponding effective stresses continuously increase, similar to those in CBM recovery. But the pressures around the injector

continuously increase and the corresponding effective stresses continuously decrease. When injection and production rates are relative stable, or after the communication between the injector and the producer has been established, the pressures and effective stresses tend to stabilize.

3.4.2 Influence of Stress Changes

It is well known that the permeability of fractured reservoirs is stress sensitive. Cleats in coalbeds, which are natural fractures, have stress sensitive permeability as well. Like heat expansion and contraction of materials due to the change of temperature, the change of effective stresses causes the deformation (expansion and contraction) of coal matrix and the opening and closing of cleats that result in the increase and decrease of coal permeability.

Stress sensitivity of coal permeability has been studied for decades. Using N_2 and CO_2 as flow fluid, the deformation and associated changes in permeability have been found to be time dependent and the permeability decreased as the average gas pressure increased (Patching, 1965). The results of Promeroy and Robinson (1967) showed that water flow rates (corresponding to permeability) increased with increasing injection pressure (pore pressures) and decreased with increasing confining pressure. The study by Dabbous et al (1974) indicated that both air and water permeability was greatly reduced with the increases of overburden pressures. Somerton et al (1975) found that the permeability of coal was strongly stress dependent, decreasing by more than two orders of magnitude with the stress increasing from 1.72 MPa (50 psi) to 13.8 MPa (2000 psi). The results of Rose and Foh (1984) illustrated that the permeability ratio (k/k_0) of liquid decreased roughly along a straight line with net stresses in a log-log diagram.

3.4.3 Influence of Coal Shrinkage and Swelling

The shrinkage of coal matrix due to gas desorption and swelling due to gas adsorption are the special characteristics of coalbeds. While gases desorb from micropores, coal matrix tends to shrink. In reverse, while gases adsorb onto micropores, coal matrix swells. If assume the total geometry of coal to be unchanged, the width of cleats will increase due to matrix shrinking and decrease due to matrix swelling. This leads to coal permeability, which is strongly dominated by cleat permeability, to increase due to desorption and decrease due to adsorption.

The shrinkage and swelling of coal was not well understood in early studies, although investigators found the differences of permeability tested with gases such as He, N_2, and CO_2 (Patching, 1965; Somerton et al, 1975). Harpalani and Schraufnagel (1990a) tested coal samples from the Piceance Basin and found that the effective volumetric shrinkage was 0.6% with the pressure changing from 6.2 MPa to 0 MPa. For coal specimens from the San Juan Basin, the fluid pressure change from 10 MPa to 0 MP produced a volumetric strain of 0.16% (Harpalani and Chen, 1995). Using high-volatile bituminous coal from Illinois, Levine (1996) experimentally measured volumetric swelling strains of 0.52% at 5.17 MPa due to CH_4 adsorption and 1.25% at 3.10 MPa due to CO_2 adsorption.

Later studies indicated the volumetric strain due to gas absorption or desorption is more correlated to absorbed gas volume rather than gas pressure. Harpalani and Chen (1995) found that the magnitude of volumetric strain was almost proportional to the absorbed gas volume. Seidle and Huitt (1995) also obtained that matrix shrinkage was correlated to gas content (corresponding to partial pressures) rather than pressures.

The influence of volumetric strain due to gas absorption or desorption on coalbed permeability is significant. Based on laboratory test data, Harpalani and Chen (1995) predicted that with a volumetric strain of 0.16%, the cleat porosity and permeability would increase as much as 80% and 480% for an initial cleat porosity of 0.2% and as much as 18% and 40% for an initial cleat porosity of 1% respectively. Levine's study (1996) showed that coal permeability would increase from 1 mD to 250 mD for the upper case (with a maximum volumetric strain of 0.6647%) and increase from 1 mD to 25 mD for the lower case (with a maximum volumetric strain of 0.1995%) due to methane desorption from 8.9 MPa to 0.69 MPa.

3.4.4 Combined Influence of Stress and Shrinkage/Swelling

Around a producer in production, the permeability due to methane desorption only will increase while the decrease of pore pressures (or increase of in situ stresses) will cause cleats to be compressed and permeability to decrease. Both effects will partly offset. Palmer and Mansoori's study showed that the permeability increase due to desorption may completely offset the permeability loss due to the in situ stress increase resulting from the reduction of fluid pressures (Palmer and Mansoori, 1998). Consequently, in CBM recovery, the

permeability around a producer might increase above its original permeability after it had first decreased below its original value.

In contrast, the permeability around an injector in ECBM recovery would decrease due to swelling (causing matrix expansion) if a more sorptive gas (such as CO_2) than methane is injected. But this decrease may also be counteracted by the increase of cleat width due to the increase of pore pressures (or the decrease of effective stresses).

3.4.5 Influence of Stress History

Coalbed permeability has also been shown to be stress history dependent. Dabbous et al's results (1974) showed that as the number of loading cycles increased the permeability of coal decreased, and that in general a loading stress path had higher permeability than an unloading stress path. Somerton et al (1975) confirmed coal permeability decreased with increasing loading cycles. The study of Harpalani and McPherson (1985) also indicated that coal permeability was lower in an unloading stress path than the permeability in a loading stress path and that there was a small residual volumetric strain remaining at the end of loading/unloading cycles.

3.4.6 Influence of Stress Path

A stress path describes the ratio of the change in minimum effective stress to the change in maximum effective stress from the initial state. Although the influence of stress paths to coalbed permeability has not been reported, its influences on the permeability and volumetric strain of weakly cemented sandstone and on the failure of rock are significant. It has been found that stress paths have strong influences on the deformation and permeability of poorly consolidated or weakly-cemented sandstone (Krishnan et al, 1996; Ruistuen et al, 1999; Hettema et al, 2000). The studies by Ruistuen et al (1999) on weakly cemented sandstone reservoirs indicated that the influence of stress paths on volumetric strains was very pronounced, as illustrated in Figure 3.5. Stress paths also play an important role in the failure of rocks. As shown in Figure 3.6, point A is the original stress state of a reservoir with maximum effective principal stress, σ'_{10} and minimum effective principal stress, σ'_{30} and a pore pressure, p. Figure 3.6 shows four stress paths corresponding to pore pressure decreasing, i.e., K= 0, 0.25, 0.5, 1.0. It is clear that for the stress path of K= 0, the rock mass may reach failure with about half the pressure drop compared to the stress path of K=0.25.

The influences of stress paths on coal deformation and permeability changes are unknown. However, because coal is a brittle, naturally fractured, and anisotropic medium, it would be anticipated that stress paths would have significant influences on coalbed permeability. Further research is needed to quantify the influences.

3.5 DEVELOPMENT OF COUPLED SIMULATION METHODOLOGY

3.5.1 Porosity and Permeability Coupling Models

The models to predict the changes of porosity and permeability with the alterations of in situ conditions are the fundamental component of reservoir and geomechanical coupled simulations. Many analytic models have been developed to calculate porosity and permeability changes due to stress changes and/or coal matrix shrinkage for CBM recovery (Harpalani and Chen, 1995; Seidle and Huitt, 1995; Levine, 1996; Palmer and Mansoori, 1998; Gray, 1987; Mckee et al, 1988; Seidle et al, 1992; Mavor and Vaughn, 1998). The main limitation of these analytic models is due to the unreliable estimation to the changes of in situ stresses and strains. Applying the porosity and permeability coupling models developed in the section to reservoir and geomechanical coupled simulations can overcome the limitation.

3.5.1.1 Sign Conventions

In the following model development, the signs of extensional stresses and strains are defined as positive while the signs of compressional stresses and strains as negative. Fluid pore pressures are positive in compression and negative pore pressures indicate fluid in tension. Although these sign conventions are reverse with that used in geotechnical engineering, they are consistent with the sign conventions in FLAC and in petroleum engineering thus it is convenient to apply the proposed models in FLAC© or similar simulators for coupled simulations of the CBM recovery.

3.5.1.2 Cleat Porosity and Permeability

Coalbeds are generally considered as natural fractured reservoirs, where the coal matrix is ideally represented with a collection of matchsticks as shown in

Figure 3.7 (Seidle et al, 1992). For this fracture system initial fracture porosity is expressed as (Van Golf-Racht, T.D., 1982c):

$$(\phi_f)_0 = \frac{2b}{a} \quad \text{.....(3.1)}$$

Initial fracture permeability as:

$$(k_f)_0 = \frac{b^2}{24}(\phi_f)_0 = \frac{b^3}{12a} \quad \text{..... (3.2)}$$

Assume the width of a unit containing a coal matrix block and an adjacent cleat is unchanged. Namely after a period of time, the change of the coal matrix block, Δa ($\Delta a = a_1 - a$), is equal to the opposite change of the cleat width. In other words, a becomes a_1 ($a_1 = a + \Delta a$) and b becomes $b - \Delta a$. Thus after deformation, new fracture porosity is:

$$\phi_f = \frac{2(b-\Delta a)}{(a+\Delta a)} = \frac{2(\frac{b}{a} - \frac{\Delta a}{a})}{(\frac{a}{a} + \frac{\Delta a}{a})} = \frac{(\phi_f)_o - 2\Delta\varepsilon_L}{1+\Delta\varepsilon_L} \quad \text{..... (3.3)}$$

where $\Delta\varepsilon_L = \Delta a/a$. Note that extensive strains are defined as positive here. And new fracture permeability is:

$$k_f = \frac{(b-\Delta a)^3}{12(a+\Delta a)} \quad \text{.....(3.4)}$$

After Equation (3.4) is divided by Equation (3.2), the ratio of permeability is obtained:

$$\frac{k_f}{(k_f)_0} = \frac{(1-\frac{\Delta a}{b})^3}{1+\frac{\Delta a}{a}} = \frac{(1-\frac{a}{b}\Delta\varepsilon_L)^3}{(1+\Delta\varepsilon_L)} \quad \text{.....(3.5)}$$

If the initial strain is set to be zero in simulations, i.e., $\varepsilon_{L0} = 0$, we obtain $\Delta\varepsilon_L = \varepsilon_L - \varepsilon_{L0} = \varepsilon_L$ for Equations (3.3) and (3.5). Further if the deformation is small, i.e., $\varepsilon_L \to 0$ or $1+\varepsilon_L \to 1$, Equations (3.3) and (3.5) can be simplified as:

$$\phi_f = (\phi_f)_0 - 2\varepsilon_L \quad \text{.....(3.6)}$$

$$\frac{k_f}{(k_f)_0} = (1-\frac{a}{b}\varepsilon_L)^3 \quad \text{.....(3.7)}$$

In order to predict porosity and permeability at a certain time, the change of linear strain, $\Delta\varepsilon_L$, in Equations (3.3) and (3.5) or the linear strain, ε_L, in Equations (3.6) and (3.7), must be determined first.

3.5.1.3 Changes of Linear Strains of Matrix

Considering the mechanical deformation due to stress and pressure changes, matrix shrinkage/swelling due to desorption/absorption and heat contract/expansion due to temperature changes (a possible case in ECBM recovery when flue gas is injected), the change of linear strains can be expressed as:

$$\Delta\varepsilon_{Li} = \Delta\varepsilon_{LEi} + \Delta\varepsilon_{LPi} + \Delta\varepsilon_{LDi} + \Delta\varepsilon_{LTi} \quad \text{……...……..(3.8)}$$

where subscript i represents direction x or y in Figure 3.7 and strain terms will be defined in the following.

The change of the linear strain due to the change of total stresses is:

$$\Delta\varepsilon_{LEi} = \frac{1}{E}\left[\Delta\sigma_i - \nu\left(\Delta\sigma_j + \Delta\sigma_k\right)\right] \quad \text{……..……..……(3.9)}$$

where i, j and k are mutually orthogonal and alternate in directions x, y and z. For example, when i represents direction x, j and k must only be directions y and z.

The change of the linear strain due to the change of pressures is:

$$\Delta\varepsilon_{LP} = \frac{-\alpha\cdot\Delta p}{3K} \quad \text{……..…….(3.10)}$$

Assuming the shrinkage/swelling of coal matrix is isotropic, the linear strain due to gas desorption/absorption can be expressed as:

$$\Delta\varepsilon_{LD} = \tfrac{1}{3}\Delta\varepsilon_{VD} \quad \text{…….……...(3.11a)}$$

The studies by Harpalani and Chen (1995) and Seidle and Huitt (1995) indicated that the volumetric strain of coal matrix has an approximately linear relation with the volume of adsorbed methane per unit weight of coal, that is:

$$\Delta\varepsilon_{VD} = \beta_D\Delta V_D \quad \text{…… ……(3.11b)}$$

The matrix shrinkage/swelling coefficient of coal due to methane desorption/adsorption, β_D, depends on coal and gas types and can be determined experimentally.

We assume that similar relations are valid for each gas component in CBM and ECBM recovery processes and that the total volumetric strain due to the desorption/swelling of multiple gases is equal to their arithmetical addition. Then a general expression of the volumetric strain change due to the desorption/absorption of multiple gases could be expressed as:

$$\Delta\varepsilon_{VD} = \sum_i \beta_{Di}\Delta V_{Di} \quad \text{.....(3.11c)}$$

The extended Langmuir isotherm (Arri et al, 1992) or IAS (ideal adsorbed solution) (Hall et al, 1994) can provide a reasonable estimation of the desorption/absorption of multiple gases on coal.

If the deformation due to temperature changes is also isotropic the change of the linear strain due to the change of temperatures is:

$$\Delta\varepsilon_{LT} = \tfrac{1}{3}\Delta\varepsilon_{VT} \quad \text{.....(3.12a)}$$

where

$$\Delta\varepsilon_{VT} = \beta_T \Delta T \quad \text{.....(3.12b)}$$

3.5.1.4 Matrix Porosity and Permeability

As discussed previously, in CBM production gases diffuse through matrix to cleats. Matrix is not a path for Darcy flow but provides the storage space for gases by adsorbing on the walls of micropores. Thus the changes of matrix porosity and permeability will not influence fluid flow thus they are treated as constant in coupled simulations.

3.5.2 Methods of Coupled Simulations

The methods of coupling between fluid flow and solid deformation can be classified into decoupled simulation, sequential coupled simulations and full coupled simulation (Settari and Walters, 2001; Rutqvist et al, 2002). In full coupled simulation, reservoir flow variables (such as pressures and temperatures) and geomechanical variables (such as stresses and displacements) are simultaneously calculated by solving a system of equations. In sequential coupled simulation, reservoir flow variables and geomechanical variables are solved in sequence from a reservoir simulator and a geomechanical simulator and coupling parameters (such as permeability and porosity) are iterated between two

simulators. If coupling parameters are iterated within each time step it is called implicit-sequential coupled simulation. If coupling parameters are assumed to be constant during each time step and are evaluated at the end of a time step, it is called explicitly sequential coupled simulation. Decoupled simulation is also called uncoupled simulation. It is "one way coupled simulation", namely, the changes of fluid pressures cause the changes of stresses and strains, but the changes of stresses and strains are assumed not to affect fluid pressures (Wang, 2000). Thus fluid flow equations can be solved independently and resulting pore pressures are inserted into geomechanical simulation.

In petroleum industry, fluid flow equations are traditionally solved with the finite difference method because of the complexity of flow systems, such as multiphase, phase change, and/or multi-components. Geomechanical programs, on the other hand, are developed with the finite element method to simulate mainly soil or rock deformation with less emphasis on fluid flow, usually adopting a single-phase fluid flow only or simple two-phase (air and water) flow approach. Using either simulator separately would not satisfactorily solve the multi-phase, multi-component flow systems with rock deformation in petroleum engineering. However, there are a few of models for fully coupled simulation that currently treat multiphase flow, but large development efforts are needed to bring their flow-model capabilities on par with existing commercial reservoir simulators (Settari and Walters, 2001). Therefore, at present, sequential coupled simulation is advantageous because both reservoir and geomechanical simulators are available, well developed, and widely applied in the industry.

3.5.3 Calculation Procedure of Coupled Simulation

A CBM recovery case is explored with the explicitly sequential coupled simulation method. The commercial software GEM© (CMG, 2003a), FLAC© (Itasca, 2002a) and AutoMate©, and self-programmed codes are used in the coupled simulation. GEM© is a multidimensional, multiphase, isothermal and compositional simulator. This well-established reservoir simulator has the capability of coalbed methane simulations. FLAC© is a widely used geomechanical code that is designed for rock and soil mechanics analyses. It can simulate thermo-mechanical, hydro-mechanical and thermo-hydro-mechanical interactions. GEM© is used to simulate fluid flow and FLAC© is used to calculate coalbed deformation. Self-programmed codes function to prepare and calculate data for the two simulators. AutoMate© is utilized to manage the whole coupled

simulation process and make it automatically execute. The procedure is schematically illustrated in Figure 3.8. The calculations of an arbitrary time step (time step i) are indicated in the diamond dash box in Figure 3.8 and described as follows:

(1) Calculate pressures (P), adsorbed gas volumes (V_D), water saturation (S_W), and well production rates of gas and water (Q_g, Q_W) etc. using GEM©.

(2) Deal with the results of step (1) and prepare the pressures (P) and adsorbed gas volumes (V_D) in the format that can be used by FLAC© with a self-programmed code.

(3) Calculate stresses (σ) and linear strains (ε_l) with the new pressures and adsorbed gas volumes from step (2) with FLAC©.

(4) Calculate cleat permeability (k_f) with Equation (3.5) based on the linear strains (ε_l) of step (3) and prepare the permeability data in the format that can be used by GEM© with a self-programmed code.

Compared with the volume of coal matrix, the volume of cleats is very small and its influence on methane storage is negligible. Consequently, the change of cleat porosity is not coupled here.

The change of temperatures is also ignored in this coupled simulation since generally CBM recovery can be treated as an isothermal process and GEM© is an isothermal reservoir simulator. On the other hand even though FLAC© has the capacity to simulate thermal stresses and strains due to the change of temperatures, it cannot directly simulate the shrinkage/swelling stresses and stains due to the change of adsorbed gas volumes. Since the recovery process is isothermal, the thermal function in FLAC© will not be used in this study. In order to calculate the shrinkage/swelling stresses and strains with FLAC©, a simple method is devised whereby the shrinkage/swelling stresses and strains are simulated using the thermal function in FLAC©. This analogy can be understood by comparing the similarities between Equations (3.11a) and (3.12a) and between Equations (3.11b) and (3.12b). With this method the adsorbed gas volumes are input as if they were temperatures and the linear matrix shrinkage coefficient of coal matrix ($\beta_D/3$) is analogous to the linear thermal expansion coefficient, i.e. letting the strain from Equation (3.11b) be exactly equal to the strain from Equation (3.12b).

3.6 APPLICATION OF COUPLED SIMULATION

An example of CBM recovery under isothermal condition is investigated in this study. The objective is to demonstrate the procedure of sequential coupled simulation and to compare coupled simulation with conventional non-coupled simulation. The basic parameters of the coal seam are tabulated in Table 3.1 and the rock mechanics data in Table 3.2. The production constraints are listed in Table 3.3. These data are idealized and from multiple sources, but the Fruitland formation in the San Juan Basin (Mavor and Vaughn, 1998) serves as the main reference. The relative permeability curves of cleats for methane and water are borrowed from the San Juan Basin (Gash et al, 1993) and shown in Figure 3.9.

The coupled simulation models are shown in Figure 3.10. In both simulations, the radial grids are exactly the same. The radial grid sizes are variable, i.e. smaller near the wellbore and larger near the boundary with a size ratio of 1.2:1 for adjacent grids. For the fluid flow simulation, the grids are 30(radial)× 9(perimeter)×1(vertical) and the grid sizes are the same in the perimeter direction. For the geomechanical simulation, the grids are 30(radial)×20(vertical), of which one grid is attributed to the coal seam in the vertical direction and the grid size is the same as the vertical grid size in fluid flow simulation, and the grid sizes in the overburden are also variable, i.e. smaller near the coalbed and larger near the upper boundary with a size ratio of 1.1:1 for adjacent grids.

The results of coupled simulations are illustrated in Figures 3.11 to 3.14. In the simulations, three types of linear strains, i.e. one third of volumetric strain, the average of horizontal strains and directional strains (for calculating anisotropic permeability), are applied to the permeability coupling model developed in this chapter, i.e. Equation (3.5). For comparison, the results from conventional simulation (constant permeability or no coupling) and from the simulations with two analytical permeability models, i.e. the simplified Palmer and Mansoori's model (Mavor and Vaughn, 1998) and the Shi and Durucan's model (2003), are shown in the plots.

The results indicate that the rates and cumulative production of gas and water from the coupled simulations using the permeability coupling model are higher than that from conventional simulation. Relatively, the results of the coupled simulations using the average of horizontal strains and using the directional strains to the permeability coupling model are close but lower than the results of

the coupled simulation using one third of volumetric strain to the permeability coupling model. This means the effect of matrix shrinkage due to gas desorption on permeability increase is exaggerated in the last situation. However, the simulation results with analytical permeability models show different trends. The rates and cumulative production of gas and water from the simulation using the simplified Palmer and Mansoori's model are smaller than the results from conventional simulation while the results from the simulation using the Shi and Durucan's model are larger than the results from conventional simulation.

For the coupled simulation with the average of horizontal strains in Equation (3.5), the changes of permeability in the coal seam during production are shown in Figure 3.15 and the changes of mean effective stress in Figure 3.16. These results show that in the areas close to the producer, coal matrix shrinkage due to methane desorption dominates the permeability change since the permeability increases even though the mean effective stresses increases, which lead to permeability reduction. The permeability and mean effective stresses continue to increase with the production progress. The magnitude of the changes in permeability and mean effective stress is larger in the regions close to the producer than the regions close to the boundary. In addition, the permeability increase mainly happens in the area close to the producer while the mean stress increase occurs in the whole drainage area.

3.7 DISCUSSION

Using the coupled permeability model, Equations (3.5) or (3.7), the permeability anisotropy of coal seams can be simulated in coupled simulation. As noted in Figure 3.7, when calculating the cleat permeability in direction x, the width of coal matrix blocks, the aperture of cleats and the linear strain in direction y (corresponding to the deformation of the cleat set intersecting y axis) should be used. The same is true for calculating the cleat permeability in direction y.

Following these simulations, a comprehensive sensitive study over a wide range of coal seam parameters will be presented in the following chapter.

3.8 SUMMARY

The study of this chapter can be summarized as following:

(1) The influences of geomechanics are important for CBM recovery and ignoring the influences may lead to errors in the evaluation of coalbed methane production.

(2) On the basis of geomechanics and considering the changes of in situ total stresses, pore pressures, adsorbed gas and heat expansion, the models to predict the changes of cleat permeability and porosity have been developed for reservoir and geomechanical coupled simulation. Permeability anisotropy of coal seams can also be considered using the developed model.

(3) The explicitly sequential coupled simulation method and simulation procedure have been established to simulate CBM recovery using recognized, developed and well-supported industrial simulators.

(4) The simulation results of the study case show that the matrix shrinkage due to methane desorption will result in the increase of cleat permeability in most seam areas close to a producer even though the mean effective stresses increase during CBM recovery. The methane production rates and cumulative production from explicitly sequential coupled simulations using the permeability coupling model (developed in this chapter) are higher than that from conventional simulation (constant permeability).

Table 3.1: Parameters of Coal Seam

Depth of coal seam top (m)	1000
Drainage area (m^3)	1000000
Seam thickness (m)	10
Well radius (m)	0.1
Seam temperature (^oC)	38
Seam pressure (kPa)	8500
Gas-in-place (m^3(gas)/ton(rock))	24.73
Cleat porosity (decimal)	0.001
Cleat permeability (mD)	4
Cleat spacing (mm)	10
Water saturation in cleat (decimal)	1
Matrix porosity (decimal)	0.005
Matrix permeability (mD)	0.001
Water viscosity (cp)	0.644
Water density (kg/m^3)	990
Rock compressibility (1/kPa)	1.45E-07
Reference pressure of rock compressibility (kPa)	8500
Water compressibility (1/kPa)	5.80E-07
Reference pressure of water compressibility (kPa)	101.325
Maximum methane adsorbed capacity of coal (m^3(gas)/ton(rock))	32
Reciprocal of Langmuir pressure (1/kPa)	4.0E-04
Gas diffusion time through matrix (days)	100
Matrix shrinkage coefficient (g/ml)	3.0E-04

Table 3.2: Mechanics Parameters

Parameters	Overburden	Coal seam
Dry bulk modulus (kPa)	1.10E+05	2.064E+06
Shear modulus (kPa)	6.50E+04	1.484E+06
Density (kg/m^3)	2305.871	1542

Table 3.3: Production Constraints

Water production constraint	
Time (day)	0~12
Maximum water rate (m^3/day)	6
Minimum BHP (kPa)	100
Methane production constraint	
Time (day)	13~3650
Minimum BHP (kPa)	275

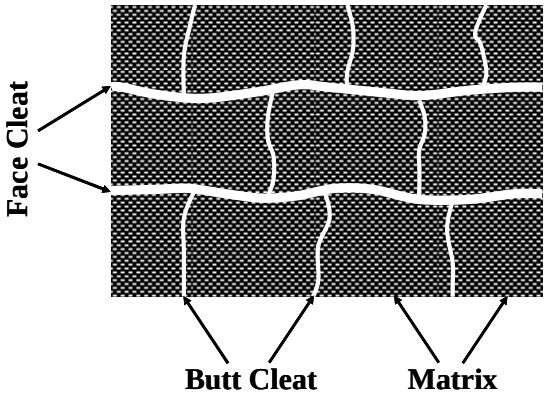

Figure 3.1: Ideal Pore Structure Model of Coalbeds (modified from Davidson et al, 1995)

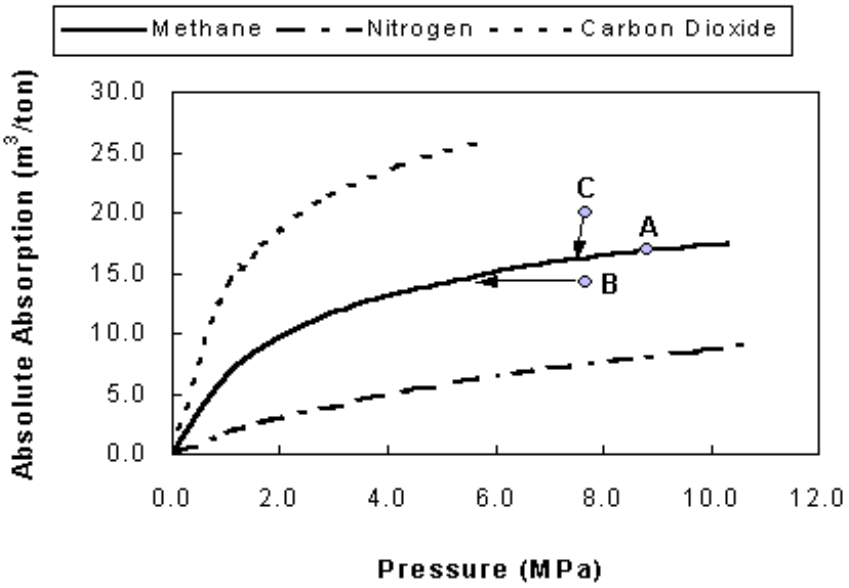

Figure 3.2: Adsorption Isotherms of Gases to Coal (Reproduced from Arri et al, 1992)

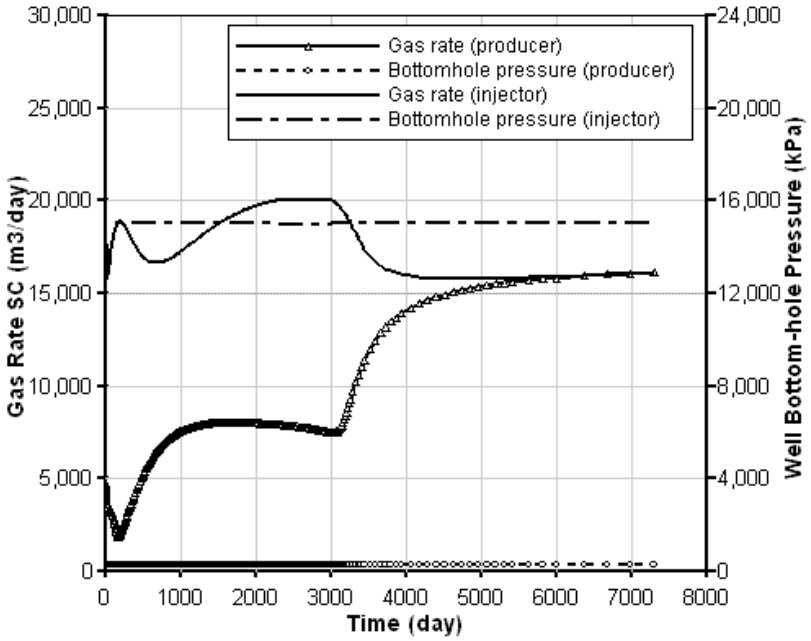

Figure 3.3: Rates and Bottom Hole Pressures in ECBM

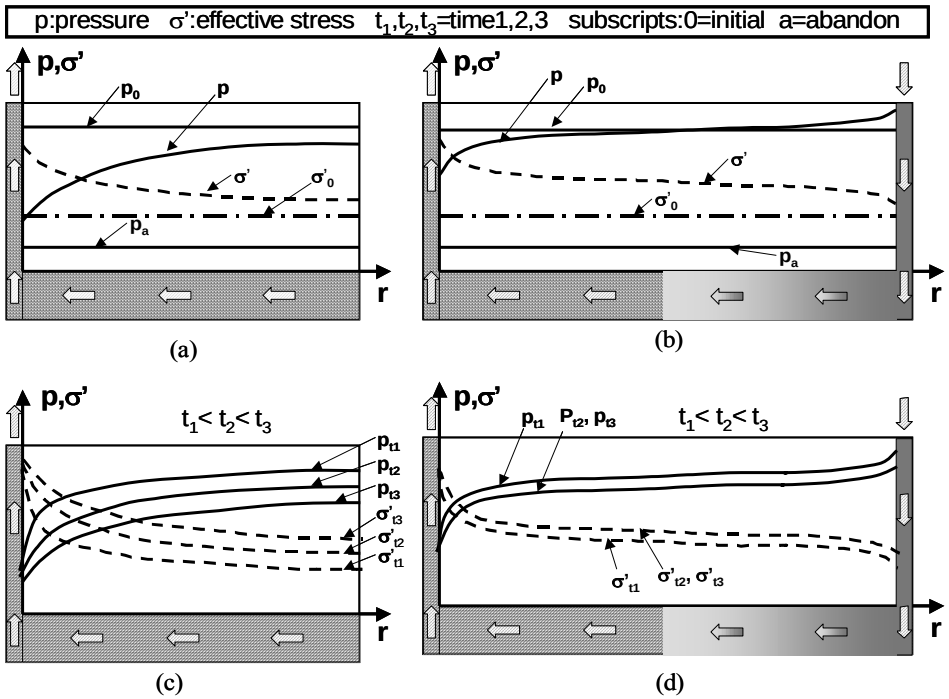

(a) Pressures & effective stresses during CBM recovery

(b) Pressure & effective stresses during ECBM recovery

(c) Changes of pressures & effective stresses during CBM recovery

(d) Changes of pressures & effective stresses during ECBM recovery

Figure 3.4: Pressure and Effective Stress Distributions in Coalbeds

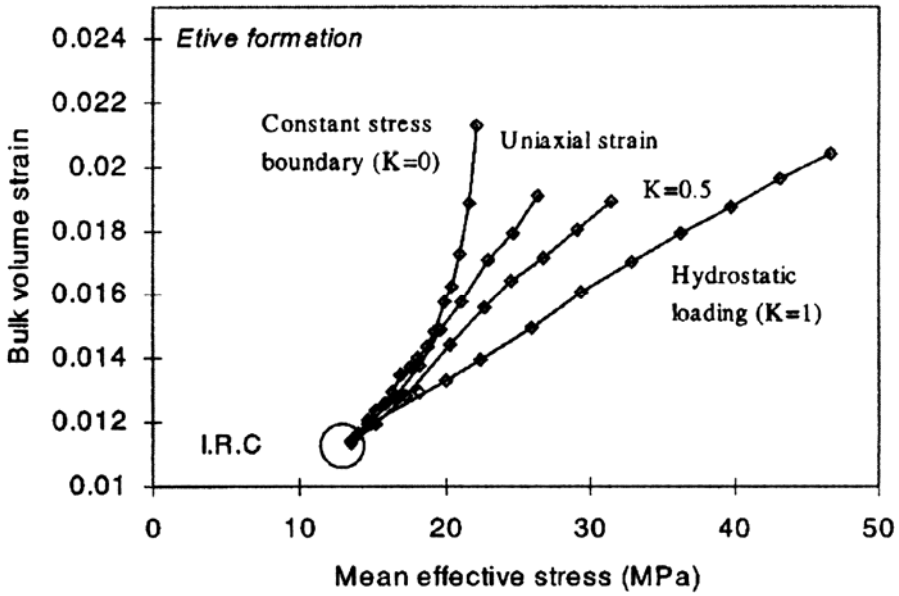

Figure 3.5: Influence of Stress Paths on Volumetric Strain (Ruistuen et al, 1999)

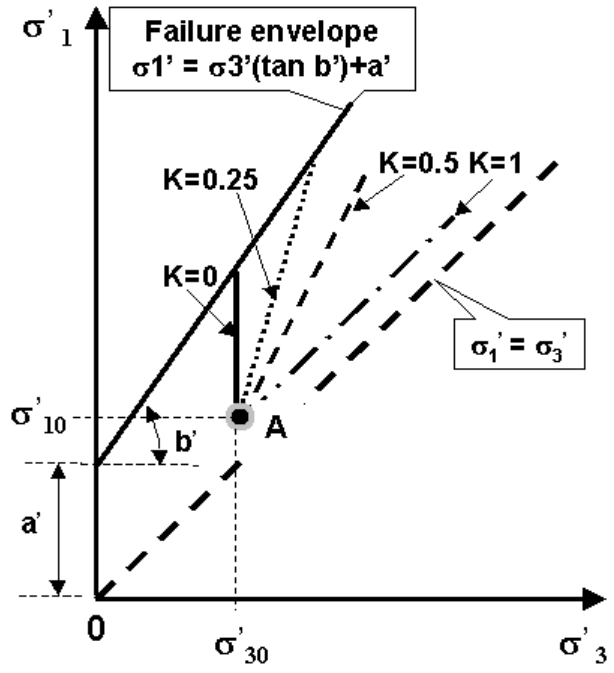

Figure 3.6: Influence of Stress Path on Rock Failure

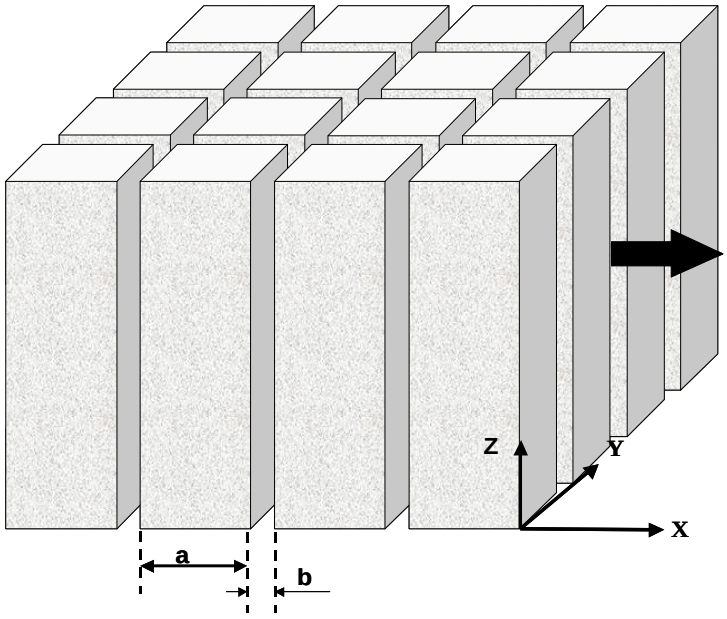

Figure 3.7: Fracture System with Matchstick Matrix Blocks (Seidle et al, 1992)

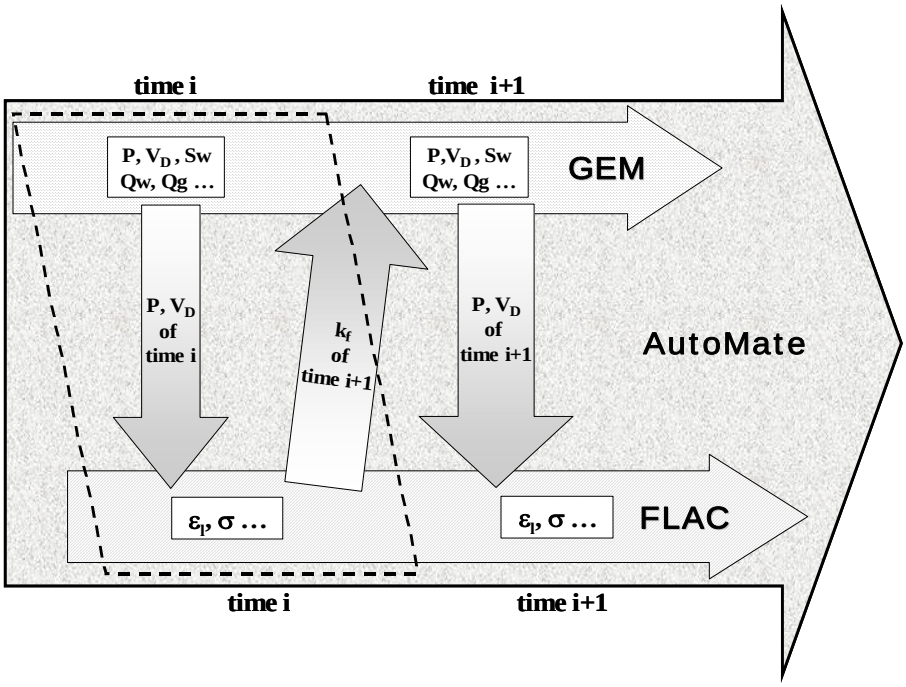

Figure 3.8: Procedure of Reservoir and Geomechanical Coupled Simulation

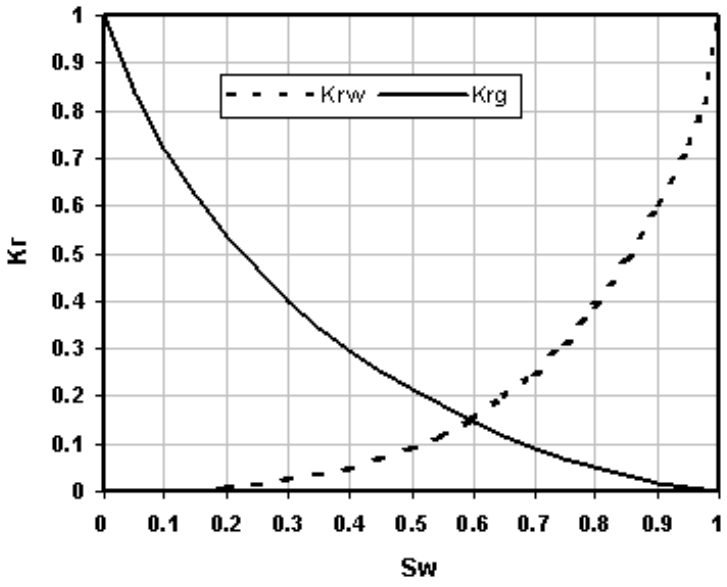

Figure 3.9: Curve of Relative Permeability of Coalbed (Gash et al, 1993)

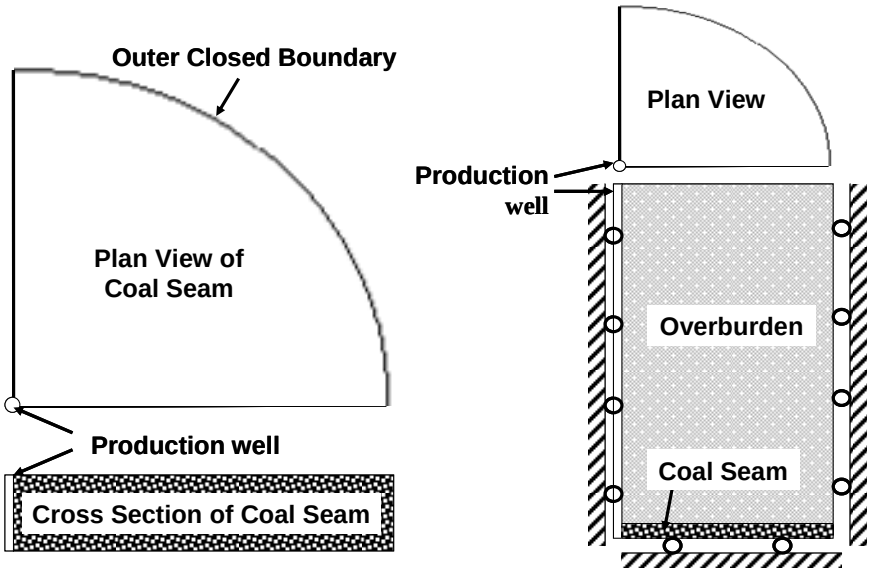

(a) Fluid Flow Model **(b) Geomechanical Model**

Figure 3.10: Fluid Flow and Geomechanical Simulation Models

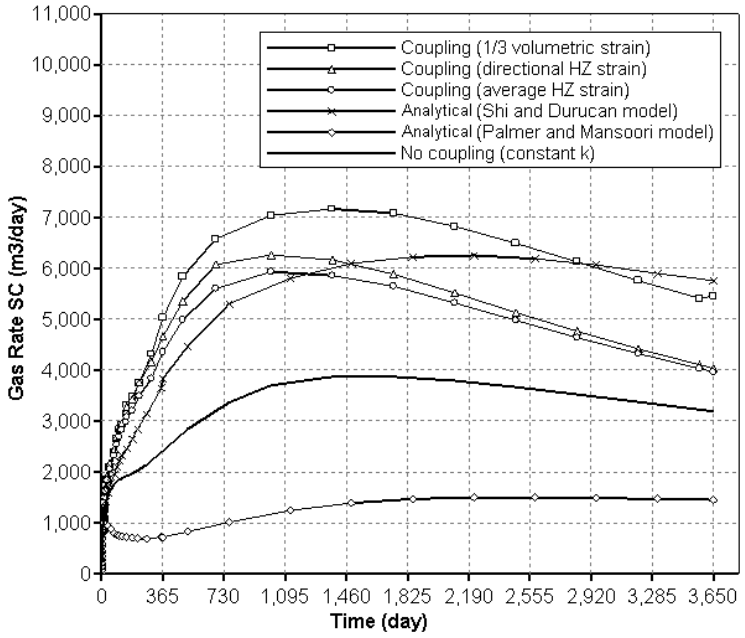

Figure 3.11: Influences of Coupling on Gas Production Rates

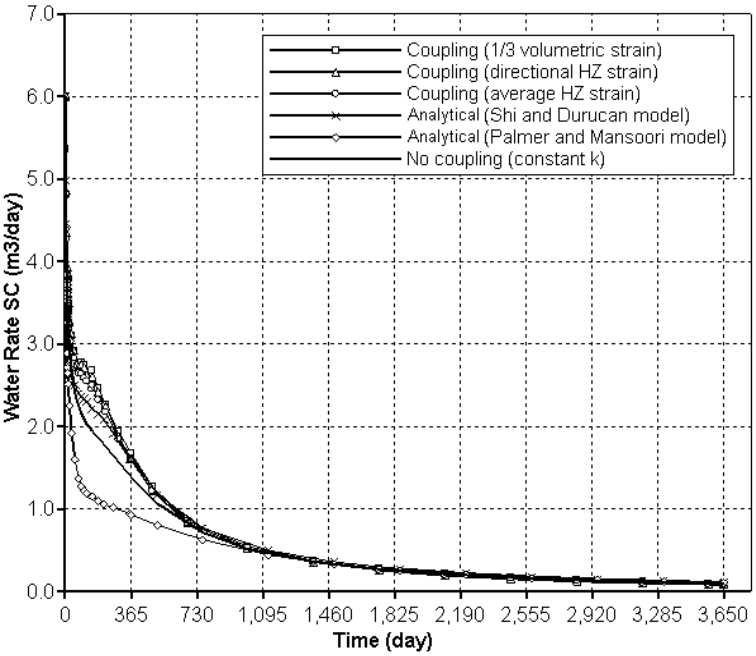

Figure 3.12: Influences of Coupling on Water Production Rates

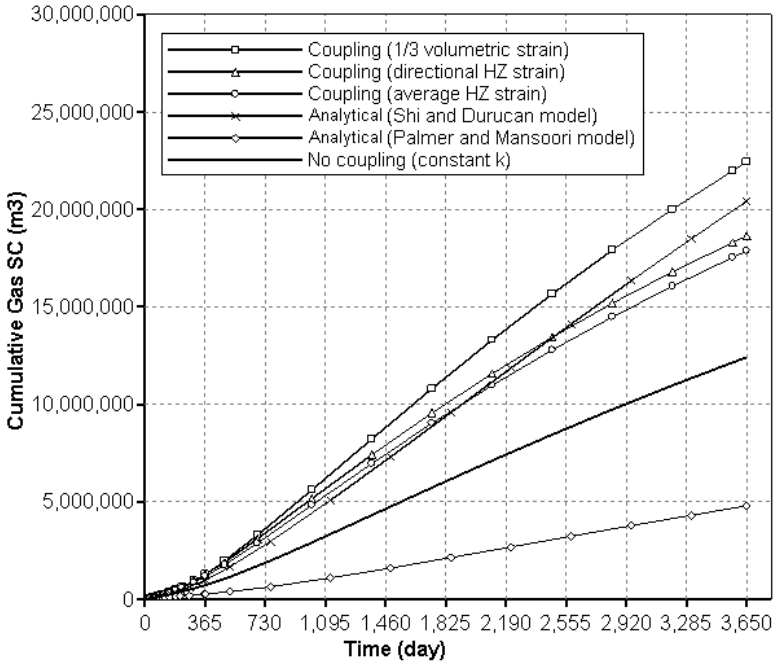

Figure 3.13: Influences of Coupling on Cumulative Gas Production

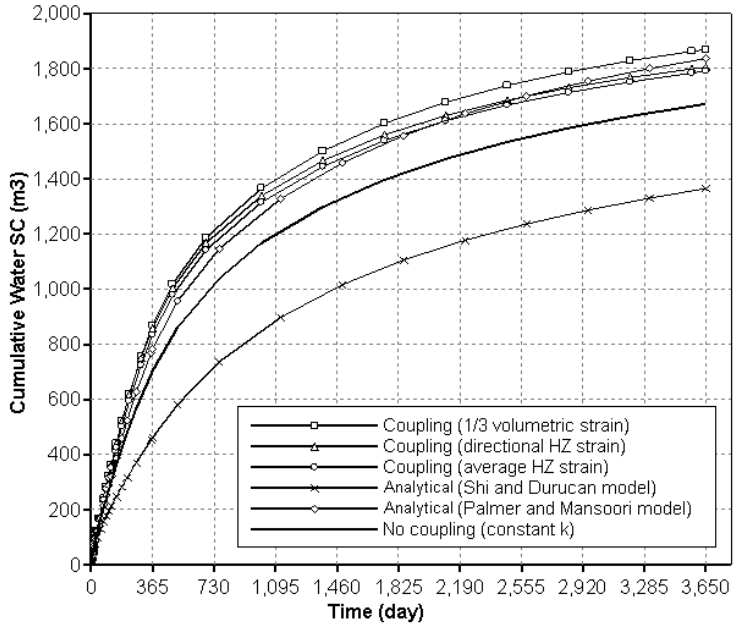

Figure 3.14: Influences of Coupling on Cumulative Water Production

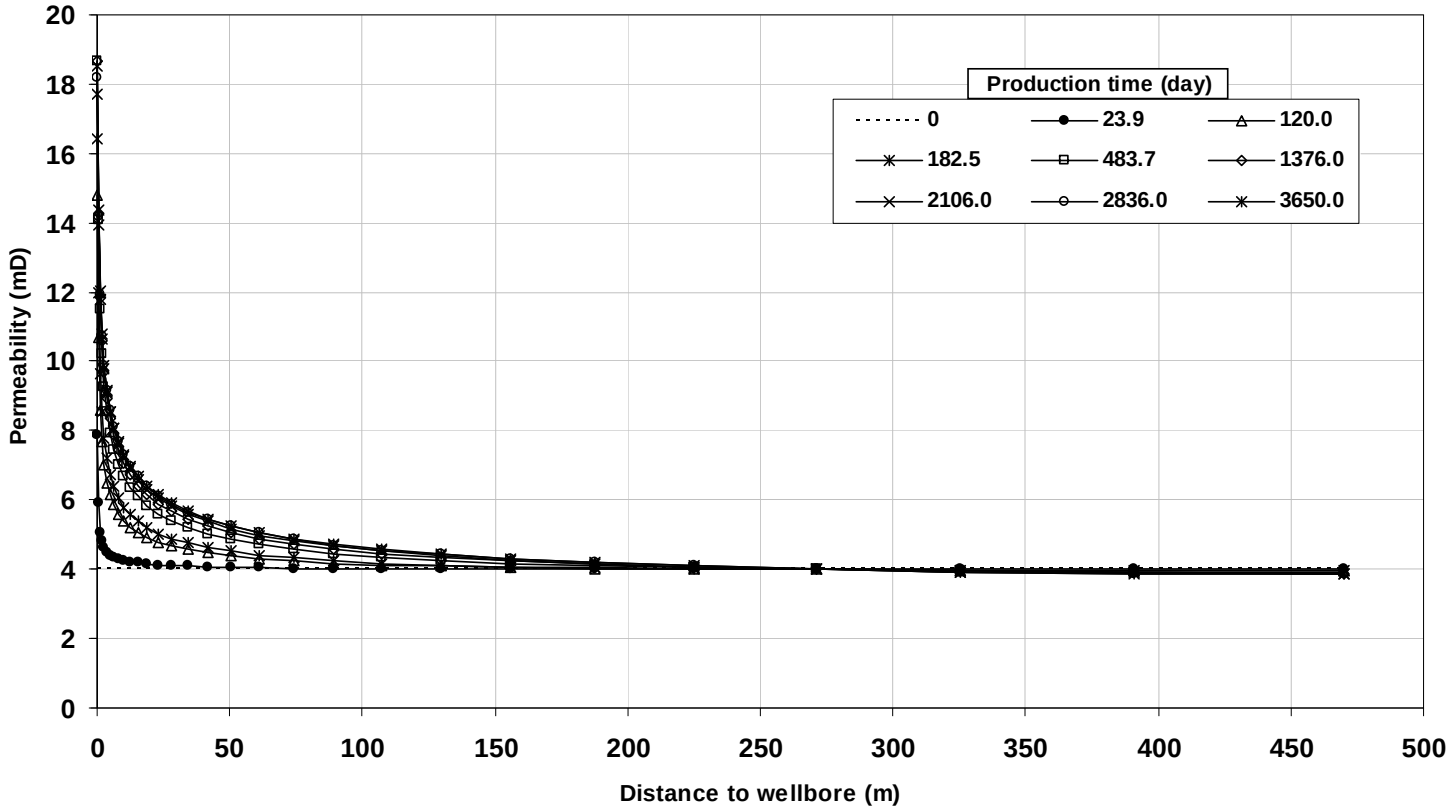

Figure 3.15: Changes of Permeability in Coalbed during Production

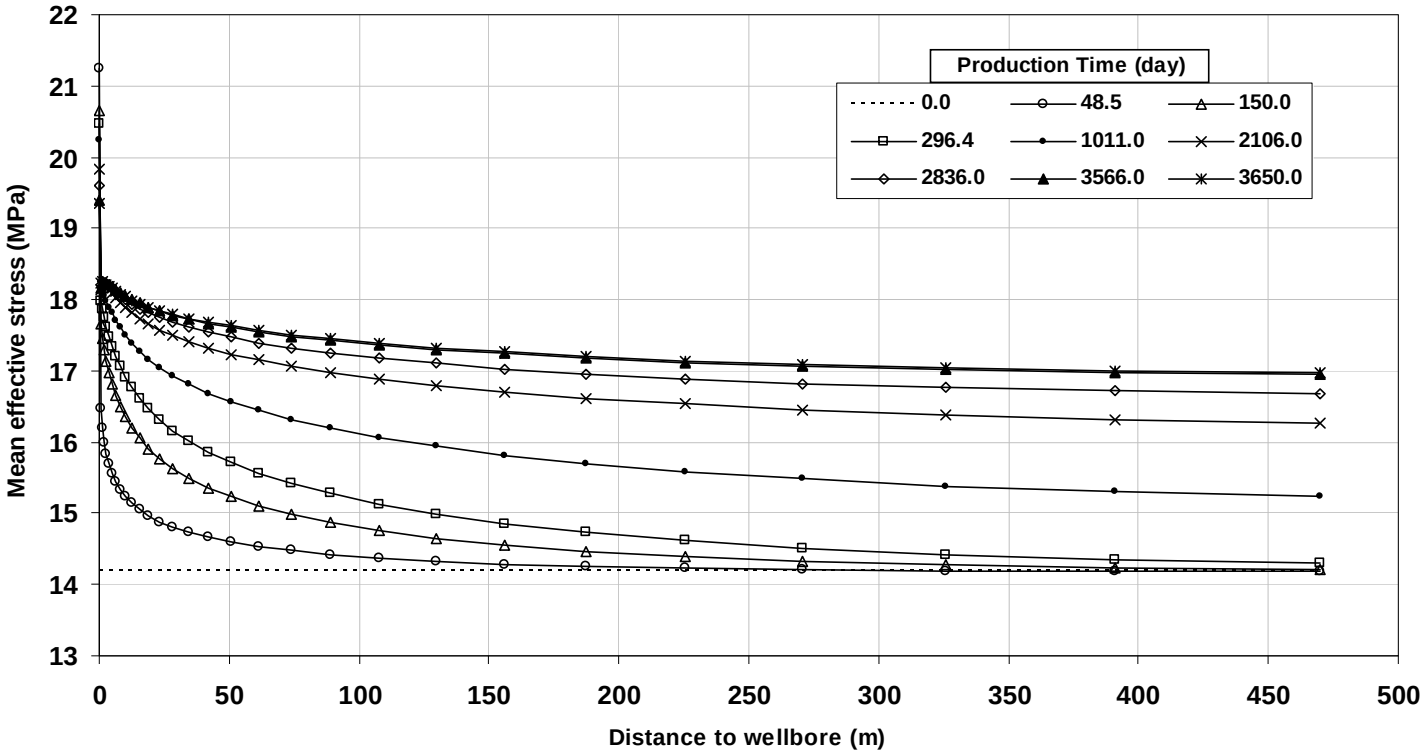

Figure 3.16: Changes of Mean Effective Stress in Coalbed during Production

4 SENSITIVITY STUDY OF CBM RECOVERY

4.1 INTRODUCTION

The success of coalbed methane development depends on many factors, but the reservoir properties of a coal seam remain the fundamental controlling factor. Many people have investigated the effect of reservoir properties on coalbed methane recovery. The studies of Sawyer et al (1987) indicated that cleat (fracture) permeability and relative permeability, not gas diffusion, controlled long-term productivity, and that optimum well spacing also depended on cleat permeability. Reid et al's results (1992) showed that permeability, initial desorption pressure and drainage area were the most important reservoir parameters for coalbed methane recovery. Young et al (1992) pointed out that permeability, well spacing and the degree of coal saturation had the greatest influence on the long-term performance of coalbed methane wells. A completed parametric study by Roadifer et al (2003) illustrated that for coal-only reservoirs (without adjacent sand layers), the five parameters having the most impact on the peak gas rate were, in the order of highest to lowest, permeability, free gas saturation, the degree of coal saturation, damage skin factor and thickness.

The results of the above-mentioned studies clearly indicate that cleat permeability is likely the most important factor for coalbed methane production. However, in all these investigations permeability was considered as a constant. Actually, it is not only a variable but also changes drastically during coalbed methane production due to the alteration of in situ conditions, such as pressure changes and the production of methane.

The decrease of pore fluid pressures during CBM recovery results in the increase of in situ effective stresses and causes cleats to be compressed or cleat apertures to decrease thus permeability decreases. The strong stress dependency of coal permeability has been recognized for a long time. Using N_2 and CO_2, Patching (1965) found that coal permeability decreased approximately by four orders of magnitude with the confining stress increased from 0.07 to 20.68 MPa (10 to 3000 psi). The investigation of Somerton et al (1975) showed that the permeability of fractured coal to methane decreased by more than two orders in

---

A version of this chapter has been published. Gu, F. and Chalaturnyk, R.J., 2005. Journal of Canadian Petroleum Technology. 44(10):23-32.

the stress range of 0.34 to 13.79 MPa (50 to 2000 psi). Reznik et al (1978) measured coal permeability to nitrogen and found it decreased approximately two orders when the confining pressure increased from 0.689 to 4.83 MPa (100 to 700 psi). The results of Rose and Foh (1984) indicated that coal permeability to water also decreased as much as two orders of magnitude over a pressure range of field normal dewatering and production cycles. Enever and Hening (1997) illustrated that the logarithm of coal permeability linearly decreases with the increase of effective stresses. Seidle et al (1992) theoretically deduced the logarithm of permeability ratio (k/k_0) linearly decreases with the increase of horizontal stresses. The results of Schwerer and Pavone (1984) indicated that the pressure-dependant permeability phenomenon significantly reduced the production of water and gas compared with that expected on the basis of a constant permeability equal to the value at initial coal seam conditions.

Another important change of in situ conditions during CBM recovery is the extraction of methane. Coal matrix shrinks due to the desorption of methane. This shrinkage produces a relaxation of in situ stresses resulting in the increase of cleat apertures and permeability. Harpalani and Zhao's studies showed that under pressures higher than the desorption pressure of methane (without methane desorption) coal permeability decreased with decreasing gas pressures. However under pressures lower than the desorption pressure (with methane desorption) coal permeability to methane drastically increased with decreasing gas pressures (Harpalani and Zhao, 1989). In contrast, the permeability to helium (almost non-adsorptive gas) decreases continuously with decreasing gas pressure. This clearly showed that the shrinkage of coal due to methane desorption caused the increase of coal permeability. Harpalani and Schraufnagel's results also indicated that coal permeability to methane increased with decreasing gas pressures, in spite of the increase of effective stresses (Harpalani and Schraufnagel, 1990a). Based on the shrinkage coefficient measured with San Juan coal, Seidle and Huitt (1995) estimated that if the coalbed fluid pressure was decreased from 10.342 MPa to 0.689 MPa (1500 to 100 psi) the porosity would increase by 20% and the permeability increase by 70% due to the shrinkage of coal. From field well tests of three wells, Mavor and Vaughn illustrated that the absolute permeability increased as much as 2.7 to 7 times comparing with their original values after produced 3-4 years (Mavor and Vaughn, 1998).

Therefore, coal permeability decreases due to pressure decline while increases due to matrix shrinkage during CBM recovery. These opposing effects

will partially offset each other. However, the degree to which each factor influences the magnitude of permeability change varies with production time and locations within a coal seam. Consequently, a proper treatment of both mechanisms is necessary to improve the simulation reliability of coalbed methane production.

In simulations there are two types of methods that can be used to include the dynamic change of permeability during production. One is to use analytical models to calculate coalbed permeability as a function of fluid pressure and directly apply their relation in reservoir simulations. Many analytical models have been developed and a review of these models is presented in section 2.3 of Chapter 2. In general, the models established by Sawyer and Paul (1990), Palmer and Mansoori (1998) and Shi and Durucan (2003) are the most suitable and popular analytical models since they capture both the decline of pore pressure and the shrinkage of coal matrix due to gas desorption. In these models, a monotonic relation between in situ stresses and pore pressures was obtained based on their assumptions. Our study in the following chapters will show that during CBM recovery the changes of in situ stresses depend not only on fluid pressures but also on spatial positions within a coal seam. Using 3D simulations, it is found that no unique (monotonic) relationship exists between permeability and pore pressures (Chapter 6). This result suggests caution is required in applying these analytical models in the simulations of coalbed methane production.

The second method to model the dynamic change of permeability is to utilize the reservoir and geomechanical coupled simulation, in which deformation and stress changes are solved with a geomechanical simulator while multiphase flow is calculated with a reservoir simulator, as illustrated in Chapter 3.

The following sections of this chapter will conduct a sensitivity study with the coupled simulation established in Chapter 3 in order to examine the influences of reservoir parameters that relate to in situ stresses and matrix shrinkage on coalbed methane production. A complete sensitivity study, such as the one made by Roadifer et al (2003), is not our goal here. However the factors that were identified from previous studies as the most significances affecting coalbed methane production will also be investigated in this study.

4.2 DESCRIPTION OF COUPLED SIMULATION

Coal seams are idealized as a matchstick fracture system (Seidle et al, 1992), as shown in Figure 4.1. Coal blocks are intersected by two orthogonal and

homogenous fracture or cleat sets representing face cleats and butt cleats. The initial apertures of two cleat sets are assumed to be equal (i.e. permeability is initially isotropic) in this study though the permeability coupling model presented in Chapter 3 can handle the anisotropy of permeability.

The models for multiphase fluid flow and geomechanical coupled simulation are illustrated in Figure 4.2. In both simulations, their radial grids are exactly the same. The radial grid sizes are variable, i.e. smaller near the wellbore and larger near the boundary with a size ratio of 1.2:1 for adjacent grids. In fluid flow simulation, the grids are 30(radial)×9(perimeter)×1(vertical) and the grid sizes are equal in the perimeter direction. In geomechanical simulation, the grids are 30(radial)×20(vertical), of which one grid is distributed to the coal seam in the vertical direction and its size is the same as the vertical grid in the model of fluid flow simulation, and the grid sizes in the overburden are also variable, i.e. smaller near the coalbed and larger near the upper boundary with a size ratio of 1.1:1 for adjacent grids.

In the explicitly sequential coupled simulation, fluid flow is calculated with GEM© (CMG, 2003a) and geomechanical deformation is calculated with FLAC© (Itasca, 2002a). The former is a multidimensional, multiphase, isothermal, compositional simulator and has the capability of coalbed methane simulation. The latter is a widely used geomechanical code that is designed for rock and soil mechanics analyses. It can simulate thermo-mechanical, hydro-mechanical, and thermo-hydro-mechanical interactions. Self-programmed codes are used to prepare and calculate data for the two simulators. The whole coupled simulation job is managed by AutoMate© and can execute automatically. The procedure of the coupled simulation is shown in Figure 4.3. The calculations of an arbitrary time step (e.g. time step i) are indicated in the diamond dash box. The sub-calculation steps in one time step include:

(1) Calculate pressures (P), adsorbed gas volumes (V_D), water saturation (S_W), and well production rates of gas and water (Q_g, Q_W) etc. using GEM©.

(2) Deal with the results of step (1) and prepare the pressures (P) and adsorbed gas volumes (V_D) in the format that can be used by FLAC© with a self-programmed code.

(3) Calculate stresses (σ) and linear strains (ε_L) with the new pressures and adsorbed gas volumes from step (2) with FLAC©.

(4) Calculate cleat permeability (k_f) with Equation (4.1) based on the linear strains (ε_L) of step (3) and prepare permeability data in the format that can be used by GEM© with a self-programmed code.

In the coupled simulation, the change of cleat permeability during production is predicted with Equation (3.5) developed in Chapter 3 as:

$$\frac{k_f}{(k_f)_0} = \frac{(1-\frac{a}{b}\Delta\varepsilon_L)^3}{(1+\Delta\varepsilon_L)} \quad \text{.....(4.1)}$$

Note that the sign of extensional strain is positive and the sign of compressional strain is negative. Thus the strain of coal matrix shrinkage due to gas desorption is negative and causes the permeability increase. Besides, in this model the width of a unit containing one coal matrix block plus one adjacent cleat in the bedding plane is assumed to be unchanged during production.

The change of linear strains is calculated by FLAC© and shown in Equation (3.8) in Chapter 3 as:

$$\Delta\varepsilon_L = \Delta\varepsilon_{LE} + \Delta\varepsilon_{LP} + \Delta\varepsilon_{LD} + \Delta\varepsilon_{LT} \quad \text{.....(4.2)}$$

In this study, the production of methane is considered as an isothermal process thus the change of thermal strains, $\Delta\varepsilon_T$, is zero. Because the volume of cleats is much smaller compared to the volume of matrix, the influence of cleat volume on methane production is negligible thus cleat porosity is assumed to be constant in this study.

4.3 EFFECT OF COAL DEFORMATION

Prior to sensitivity study, it is instructive to investigate how the deformation or strain change of coal influences methane production with the reservoir and geomechanical simulation. The coalbed to be studied is assumed to have isotropic geomechanical properties. The coalbed and production well data are shown in Tables 4.1, 4.2 and 4.3, the "base value" column of Table 4.4, and Figure 4.4. In coupled simulation, three types of linear strains, i.e. one third of volumetric strain, the average of horizontal strains (the linear strains in the bedding plane or plane x-y in Figure 4.1) and directional strains (for calculating anisotropic permeability), are applied to calculate the permeability change with Equation (4.1).

The effects of different strains applied in the permeability coupling model on coalbed methane production are shown Figures 4.5 and 4.6. For comparison, the simulation results applied zero linear strain, i.e. using constant permeability, are also plotted in the figures. The results indicate that the gas rates and cumulative gas recovery from the coupled simulations (considering the deformation of coal) are higher than that from the conventional simulation (not considering the deformation of coal or using constant permeability). This occurs because during production the shrinkage of coal matrix due to methane desorption dominates the deformation and leads to the increase of cleat permeability. Figures 4.4 and 4.5 also show that the gas rates and cumulative gas recovery from the simulation applied one third of the volumetric strain are much higher than that from the simulations applied the average of horizontal linear strains and applied directional strains. The reason is that although coal is assumed to have isotropic mechanical properties, the change of strains is anisotropic and the change of vertical strain, which mainly causes the movement of overburdens rather than contribute to the changes of horizontal permeability, is larger than the change of strains in the horizontal plane. The results also indicate that the results applied the average of horizontal linear strains are close the results applied directional strains. In the following sensitivity study, the average of horizontal linear strains is utilized in all simulations.

4.4 SENSITIVITY STUDY

This study focuses on the factors related to the change of in situ stresses and matrix shrinkage of coal due to methane desorption with the explicitly sequential coupled simulation. Those factors having been recognized from previous studies as the significances that influence coalbed methane production will also be investigated here. The coalbed related data are tabulated in Tables 4.1 and 4.2 and Figure 4.4. The operation constraints of the production well are shown in Table 4.3. The parameters and their values for sensitivity study are listed in Table 4.4. The ranges of these parameters are from several sources, but mainly from the studies of Levine (1996), Mavor et al (1990) and Roadifer et al (2003). The base values in Table 4.4 are used in all coupled simulations except for the parameter that is investigated, i.e. the study is a single-parameter sensitivity study.

4.4.1 Cleat Permeability

The changes of cleat permeability and corresponding cleat width and porosity are shown in Table 4.4. It should be noted that with the fixed cleat spacing, i.e. 0.02 m, the lower and upper values of porosity are calculated with Equation (3.1) in Chapter 3 as:

$$\phi_f = \frac{2b}{a} \quad \text{.....(4.3)}$$

The effects of cleat permeability on CBM production are shown in Figures 4.7 and 4.8. As expected, cleat permeability has a significant influence on CBM production. The higher the initial cleat permeability is, the higher the maximum rate and cumulative recovery are.

The results from conventional simulations (no coupling or constant permeability) are shown in Figure 4.9. Comparing these results with those shown in Figures 4.7 and 4.8 indicates that for the same initial cleat permeability the maximum gas rates and final gas recovery from the coupled simulations are higher than those from the conventional simulations with constant permeability. In comparison, the differences of final gas recovery from different simulation methods are not pronounced.

4.4.2 Cleat Spacing

In the study of the influence of cleat spacing on CBM production, the cleat aperture must be corrected in order to keep cleat permeability equal to the base value. Then porosity was adjusted based on Equation (4.3). The simulation results are plotted in Figures 4.10 and 4.11. The results show that with the increase of cleat spacing, the maximum gas rates and final gas recovery increase significantly but the time to reach the maximum gas rate decreases. The primary reason for this effect is that as the cleat spacing becomes larger, for the same change of linear strains the permeability increase is higher according to Equation (4.1).

Comparing the results of coupled simulations with that of conventional simulations plotted in Figure 4.12, it shows that the maximum gas rates and final gas recovery from coupled simulations are much higher than that from conventional simulation. This illustrates again that the influence of coal matrix shrinkage due to methane desorption on CBM production is significant.

4.4.3 Coefficient of Matrix Shrinkage

According to the assumption that the volumetric strain of coal due to methane desorption is linearly related to the volume of adsorbed methane per unit weight of coal, i.e. Equation (3.11b) of Chapter 3, the coefficient of coal matrix shrinkage is defined as:

$$\beta_D = \frac{\Delta \varepsilon_{VD}}{\Delta V_D} \quad \text{.....(4.4)}$$

The results of the sensitivity of CBM production to the coefficient of coal matrix shrinkage are shown in Figures 4.13 and 4.14. These results suggest that for a coal seam with a higher coefficient of matrix shrinkage, its maximum rate and final gas recovery are higher comparing with a seam with a lower coefficient of matrix shrinkage. This is expected since a higher coefficient of matrix shrinkage will cause a larger shrinkage strain or compressive strain, thus a larger increase of permeability according to Equation (4.1).

4.4.4 Well Control Area

The effects of well control area on CBM production are indicated in Figures 4.15 and 4.16. The results illustrate that the influence of well control area on the maximum gas rate is not significant. However, for a well with a larger control area, the time to achieve the maximum rate is longer since it needs longer time to produce the water in cleats. In addition, the decline of the gas rate is slower and the final cumulative gas production is higher due to more initial gas in place comparing with a well with a smaller control area.

The simulation results from conventional simulations (no coupling) are shown in Figure 17. The comparison between the results from coupled simulations and those from conventional simulations shows that for the wells with smaller control areas (i.e. the cases with well control radii of 253.8m and 474.8m) the gas rate and final cumulative gas production from coupled simulations are higher than those from conventional simulations. But these trends are reverse for the case with well control radius of 621.6m. This happens due to that for the well with a too larger control area the permeability change is dominated by pressure decrease, which cause in situ stress increase thus permeability decreases, rather than the shrinkage of coal matrix due to gas desorption.

4.4.5 Pressure Gradient

The pressure gradient of a reservoir is defined as the quotient of the initial reservoir pressure divided by the reservoir depth. The corresponding reservoir pressures shown in Table 4.4 are obtained by multiplying the pressure gradients with the fixed reservoir depth, i.e. 900m.

The coupled simulation results to examine the sensitivity of CBM production on pressure gradients are shown in Figures 4.18 and 4.19. The results imply that the maximum gas rate and final cumulative gas production of a well with a higher pressure gradient are larger and its time to achieve the maximum rate is shorter comparing with a well with a lower pressure gradient.

A similar conclusion is also obtained for the results of conventional simulations shown in Figure 4.20. Comparing Figure 4.20 with Figures 4.18 and 4.19 clearly shows that the maximum rates and final cumulative gas production from coupled simulations are higher than that from conventional simulations.

4.4.6 Seam Depth

In this study, since the pressure gradient is fixed, i.e. 9.727 kPa/m, the initial reservoir pressures are obtained by multiplying this pressure gradient with the depths of reservoirs. Note that the initial in situ total stresses are re-calculated due to the change of depths based on the fixed (average) rock density of overburdens and coal, and on the assumption that the ratio of horizontal stresses to the vertical stress is one.

The influences of seam depths on methane production from coupled simulations are plotted in Figures 4.21 and 4.22. The results indicate that the gas rate and cumulative gas production of deeper wells are much higher than that of shallower wells. This is a misleading conclusion, however, since the sensitivity study has assumed that all other parameters (i.e. cleat permeability, cleat space and pressure gradient) in the simulations maintain baseline values. In reality, this would not be true, especially for cleat permeability, which usually decreases with the increase of seam depths.

4.4.7 Young's Modulus of Coal

The coupled simulation results for the influence of Young's modulus of coal on production are illustrated in Figures 4.23 and 4.24. The results indicate that the maximum gas rate and cumulative gas production of a coal seam with a higher

modulus are larger than that of a coal seam with a smaller modulus but the differences are small. The time to reach the maximum gas rate is almost the same.

4.4.8 Poisson's Ratio of Coal

The influence of Poisson's ratio on CBM production is illustrated in Figures 4.25 and 4.26. The results suggest that the maximum gas rates and cumulative gas production of a coal seam with a higher Poisson's ratio are higher than that of a coal seam with a lower Poisson's ratio. The difference in the time to reach the maximum gas rates is small.

4.4.9 Langmuir Volume

The effects of Langmuir volume on CBM production are shown in Figures 4.27 and 4.28. These results indicate that with the increase of Langmuir volume of a coal seam, the maximum gas rate and final cumulative gas production increase. The time to reach the maximum gas rate also slightly increases. This is because with the increase of Langmuir volume the in situ gas volume increases if the reservoir pressure of a coal seam is unchanged. Thus during production the volume of the desorbed gas is higher and the shrinkage of coal matrix is larger under the same pressure draw-down. As a result the increase of permeability is larger and the production rate is higher.

The comparison of coupled simulation results with conventional simulation results illustrated in Figure 29 shows that the maximum gas rate and final cumulative gas production from the coupled simulations are much higher and the time to achieve the maximum gas rate is also shorter compared with conventional simulations.

4.4.10 Langmuir Pressure

The coupled simulation results to study the influence of Langmuir pressure on CBM production are illustrated in Figures 4.30 and 4.31. These results indicate that with the increase of Langmuir pressure, the maximum gas rate and final gas recovery increase.

For comparison, the results from conventional simulations are shown in Figure 4.32. The results show that the effects of Langmuir pressure reveal a similar trend as seen in the coupled simulations. For the same Langmuir pressure, the gas rate and final cumulative gas production from coupled simulations are

higher than those from conventional simulations. Similarly, the volume of desorbed gas and shrinkage of coal matrix is primarily responsible for this effect.

4.5 SUMMARY

We summarize the results of sensitivity study in this chapter as:

(1) Caution should be exercised in estimating the change of permeability from the change of strains in coupled simulations. If the anisotropic deformation of coal is not treated properly and linear strains are simply computed as one third of the volumetric strain, the simulated CBM production rates and cumulative gas production would be overly optimistic.

(2) Permeability, well control area, seam depth (corresponding to in situ stresses), the Langmuir volume (corresponding to initial gas content) and the Langmuir pressure are the most sensitive parameters that influence CBM production in coupled simulations.

(3) Cleat spacing, coefficient of matrix shrinkage and pressure gradient (related to initial gas content and initial stresses) are the second sensitive parameters that influence CBM production in coupled simulations.

(4) Young's modulus and Poisson's ratio are insensitive parameters influencing CBM production in coupled simulations.

(5) Due to the consideration of matrix shrinkage of coal, the maximum gas rate and final cumulative gas production from coupled simulations are higher than those from conventional simulations (constant permeability) when matrix shrinkage dominates the deformation of the coal, i.e. when pressures decrease matrix shrinkage will result in the increase of permeability although in situ stresses would increase and as a results the compression of cleats would increase.

Table 4.1: Parameters of Coal Seam

Seam thickness (m)	10
Coal density (kg/m^3)	1542
Well radius (m)	0.1
Temperature of surface constant layer (°C)	8
Temperature grad (°C/100m)	2.5
Water saturation in fracture (decimal)	1
Matrix porosity (decimal)	0.005
Matrix permeability (mD)	0.001
Water viscosity (cp)	0.644
Water density (kg/m^3)	990
Rock compressibility (1/kPa)	1.45E-07
Water compressibility (1/kPa)	5.80E-07
Reference pressure of compressibility (kPa)	8500
Gas diffusion time through matrix (days)	100

Table 4.2: Parameters of Overburden

Density (kg/m^3)	2300
Young's modulus (MPa)	1000
Poisson's ratio	0.3

Table 4.3: Well Production Constraints

Water production constraint	
Time (day)	0~18
Maximum water rate (m^3/day)	10
Minimum BHP (kPa)	101.325
Gas production constraint	
Time (day)	19~7300
Minimum BHP (kPa)	275

Table 4.4: Parameters of Sensitivity Study

No	Items		Unit	Lower value	Base value	Upper value
1	Cleat	Permeability	mD	0.2	4	80
		Width	micron	3.36	9.86	26.8
		Porosity	fraction	0.000363	0.001	0.00268
2	Cleat spacing		m	0.005	0.02	0.1
3	Coefficient of Matrix shrinkage		g/ml	1.0×10^{-4}	4.0×10^{-4}	7.0×10^{-4}
4	Well control	Area	acres	50	175	300
		Radius	m	253.8	474.8	621.6
5	Pressure	Gradient	psi/ft	0.33	0.43	0.53
			kPa/m	7.465	9.727	11.989
			KPa	6718.5	8754.3	10790.1
6	Depth		m	300	900	1500
7	Young's modulus of coal		psi	145000	493000	725000
			MPa	999.7	3399.2	4998.7
8	Poisson's ratio of coal			0.22	0.32	0.42
9	Langmuir volume		ft^3/ton	300	800	1300
			m^3/ton	8.495	22.653	36.812
10	Langmuir	Pressure	psi	200	600	1000
			kPa	1379.0	4136.9	6894.8
		Pressure reciprocal	1/kPa	7.252×10^{-4}	2.417×10^{-4}	1.450×10^{-4}

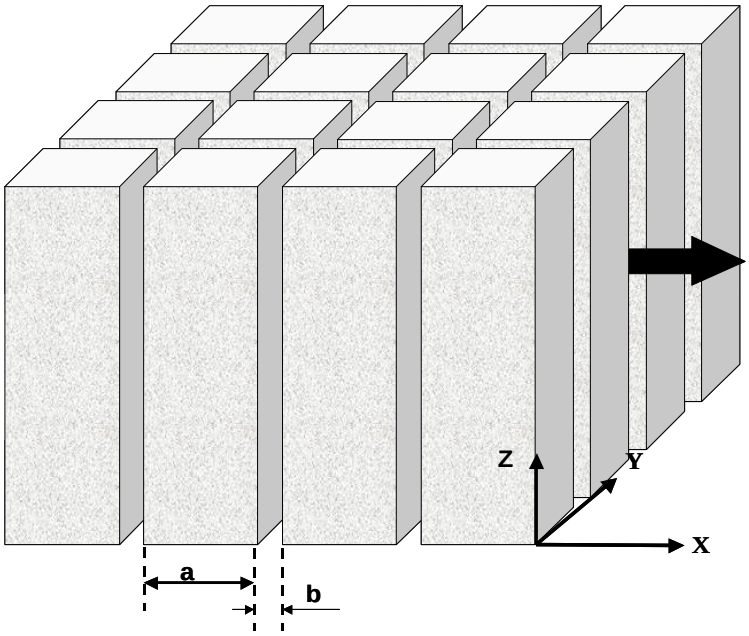

Figure 4.1: Fracture System with Matchstick Matrix Blocks
(Seidle et al, 1992)

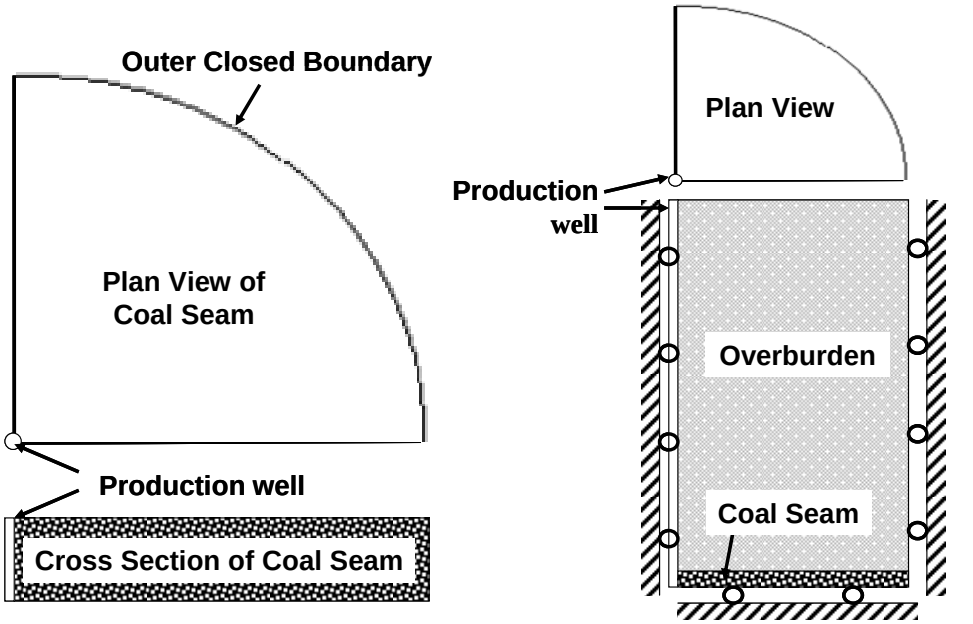

(a) Fluid Flow Model **(b) Geomechanical Model**

Figure 4.2: Fluid Flow and Geomechanical Simulation Models

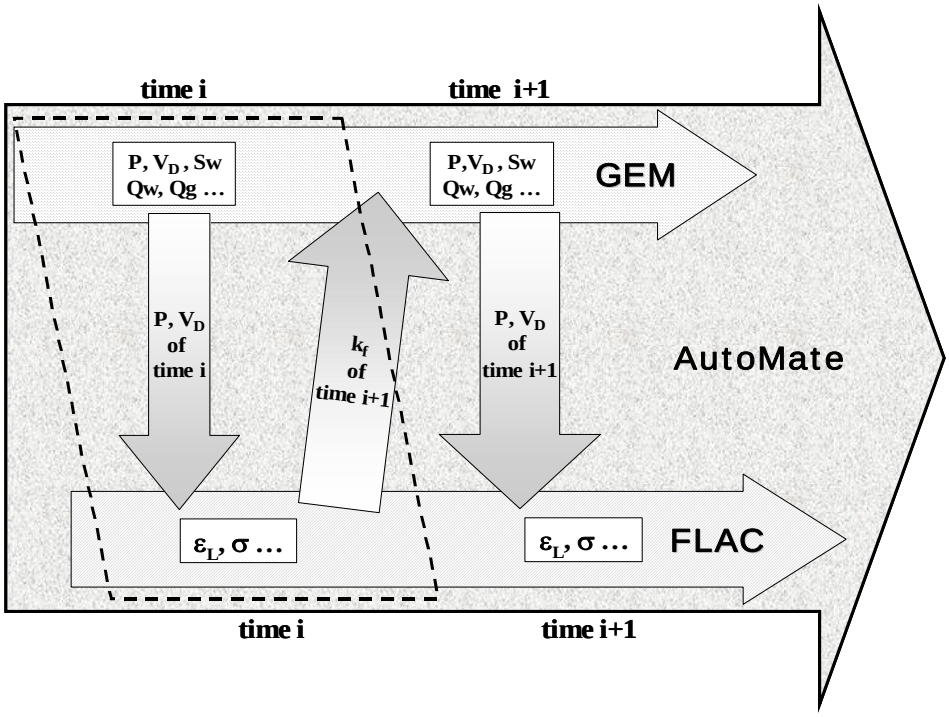

Figure 4.3: Procedure of Reservoir and Geomechanical Coupled Simulation

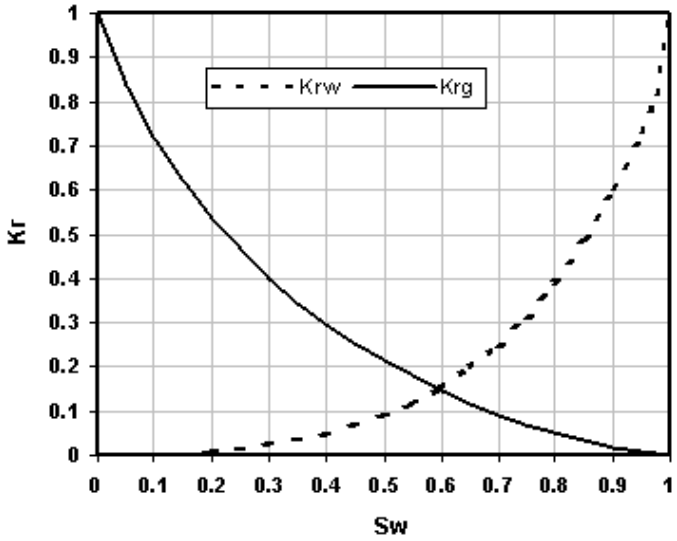

Figure 4.4: Curve of Relative Permeability of Coalbed (Gash et al, 1993)

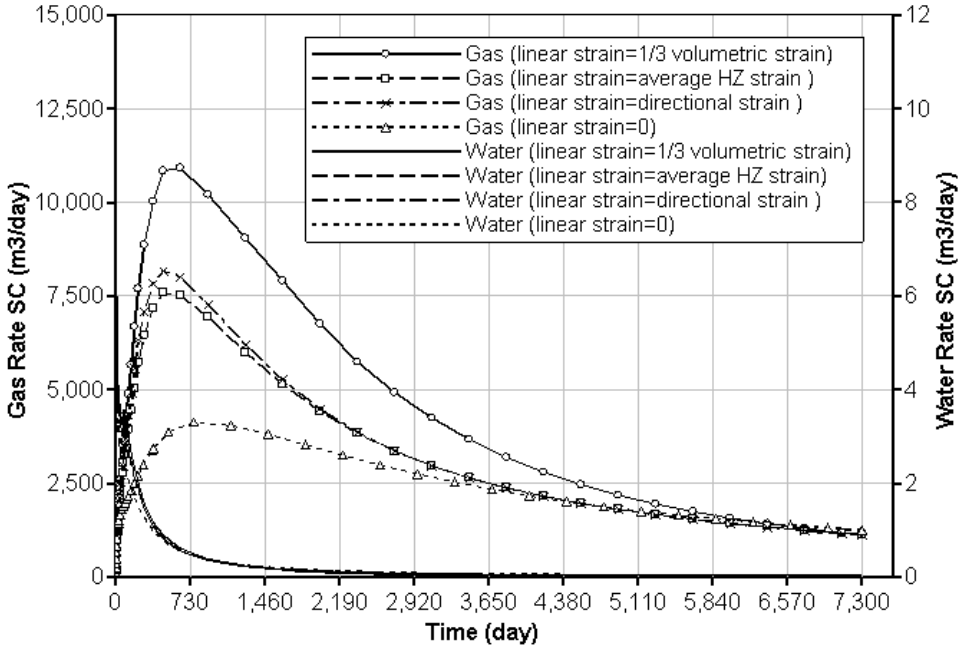

Figure 4.5: Effects of Coal Deformation on Production Rate

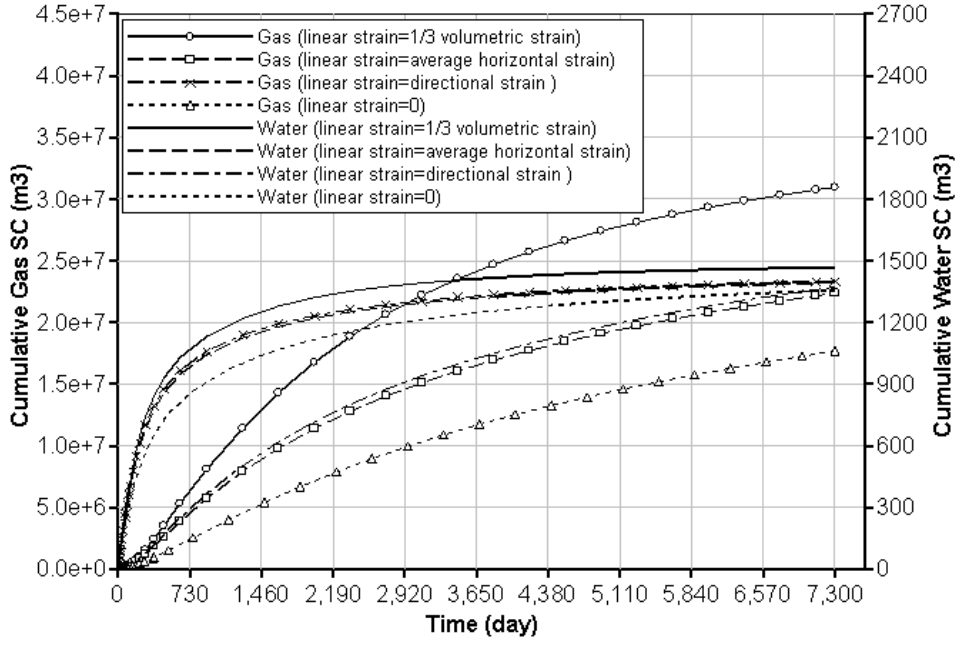

Figure 4.6: Effects of Coal Deformation on Cumulative Production

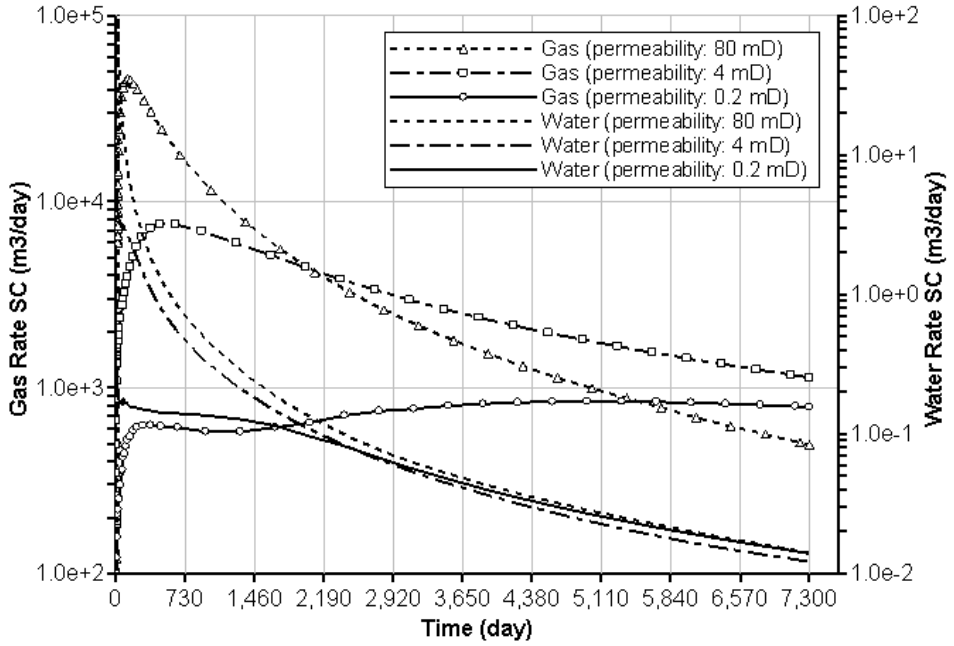

Figure 4.7: Effects of Permeability on Production Rate

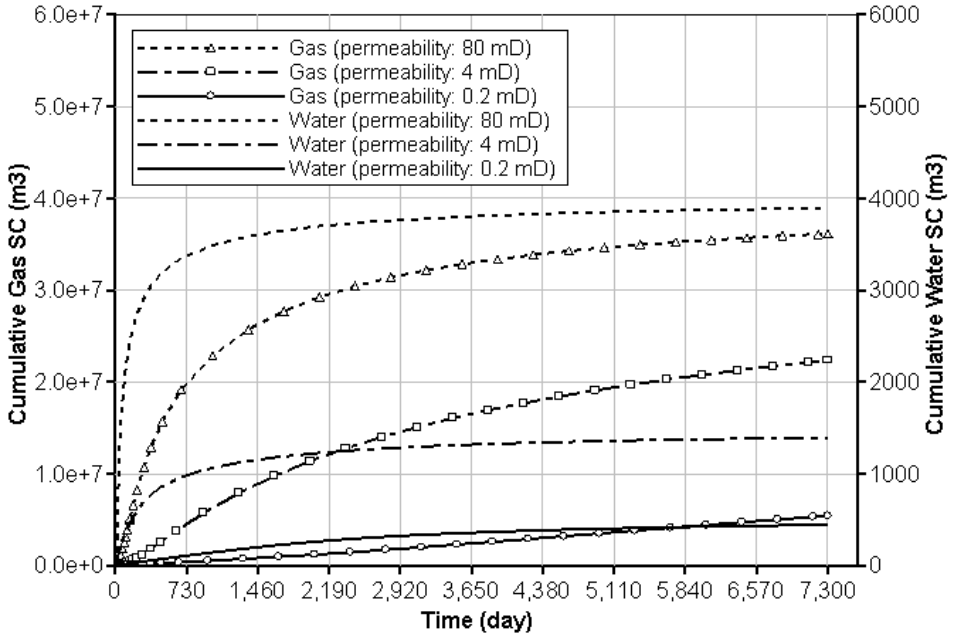

Figure 4.8: Effects of Permeability on Cumulative Production

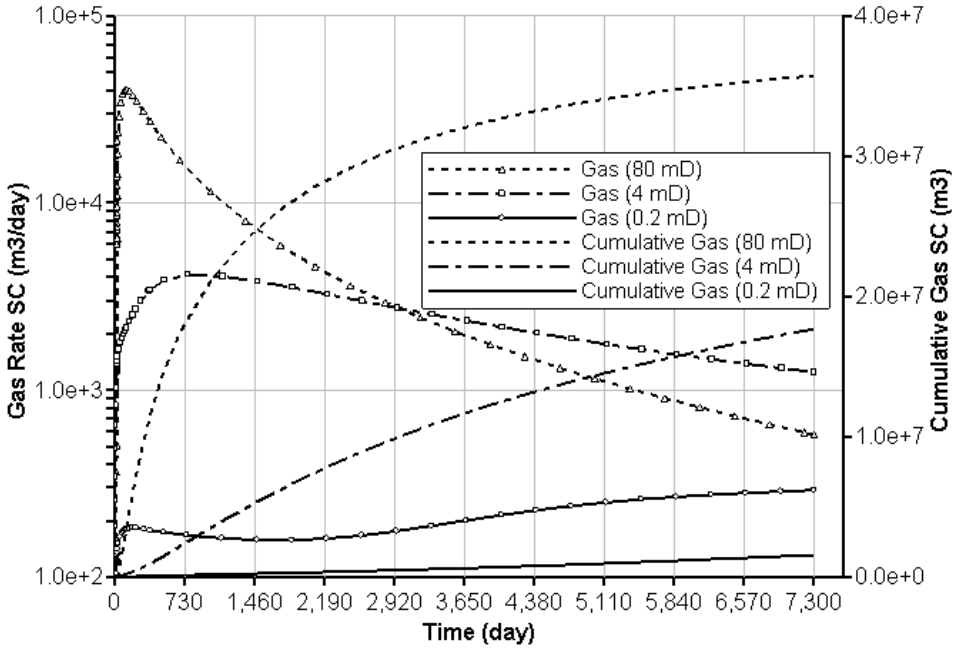

Figure 4.9: Effects of Permeability on Production from Conventional Simulation

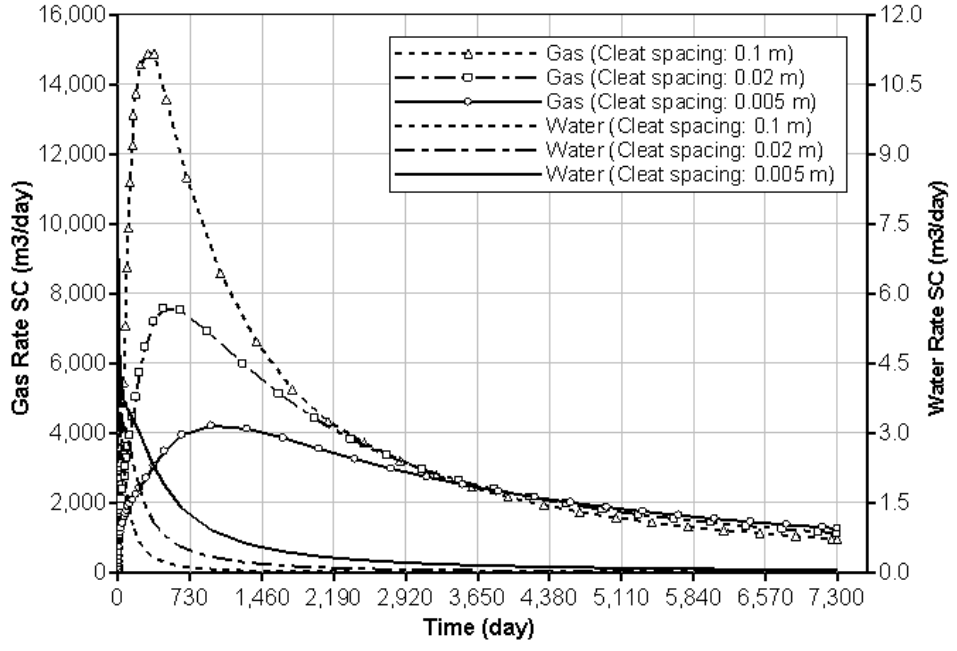

Figure 4.10: Effects of Cleat Spacing on Production Rate

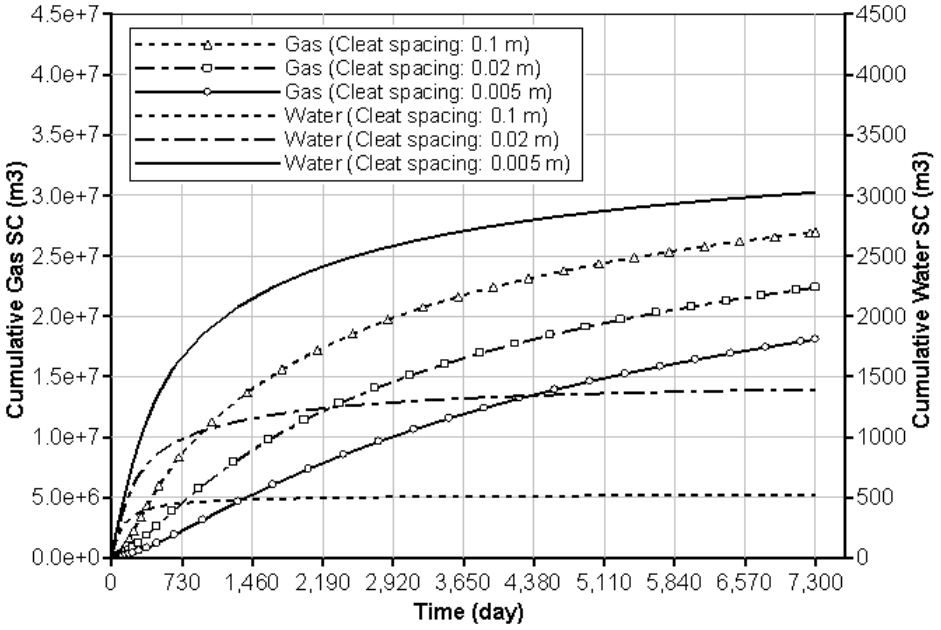

Figure 4.11: Effects of Cleat Spacing on Cumulative Production

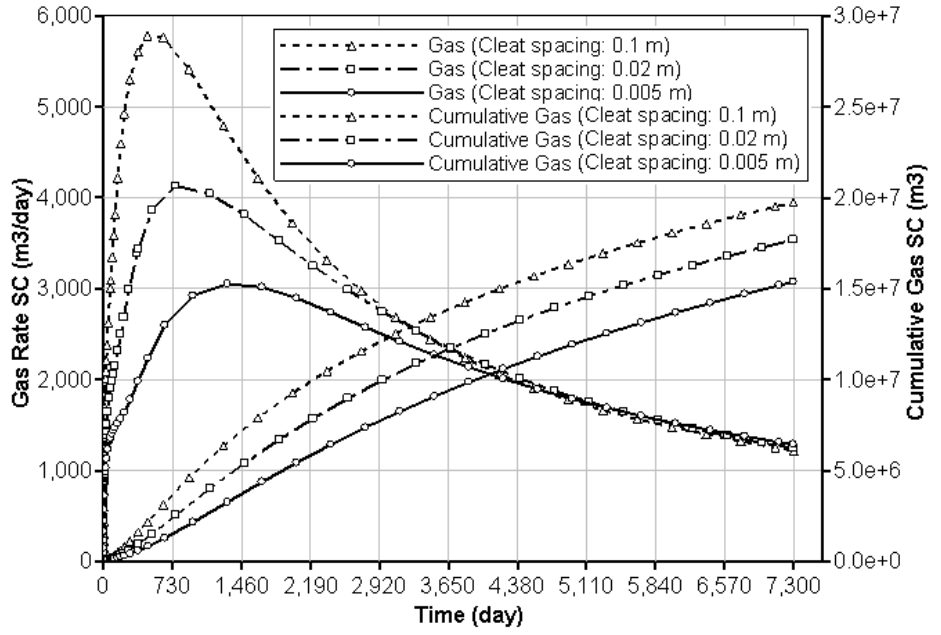

Figure 4.12: Effects of Cleat Spacing on Production from Conventional Simulation

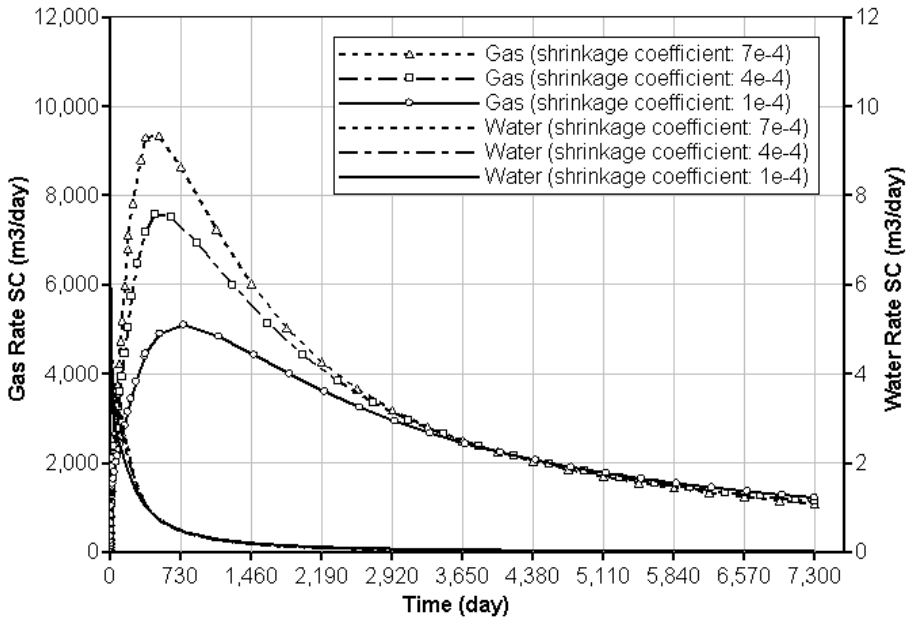

Figure 4.13: Effects of Coefficient of Matrix Shrinkage on Production Rate

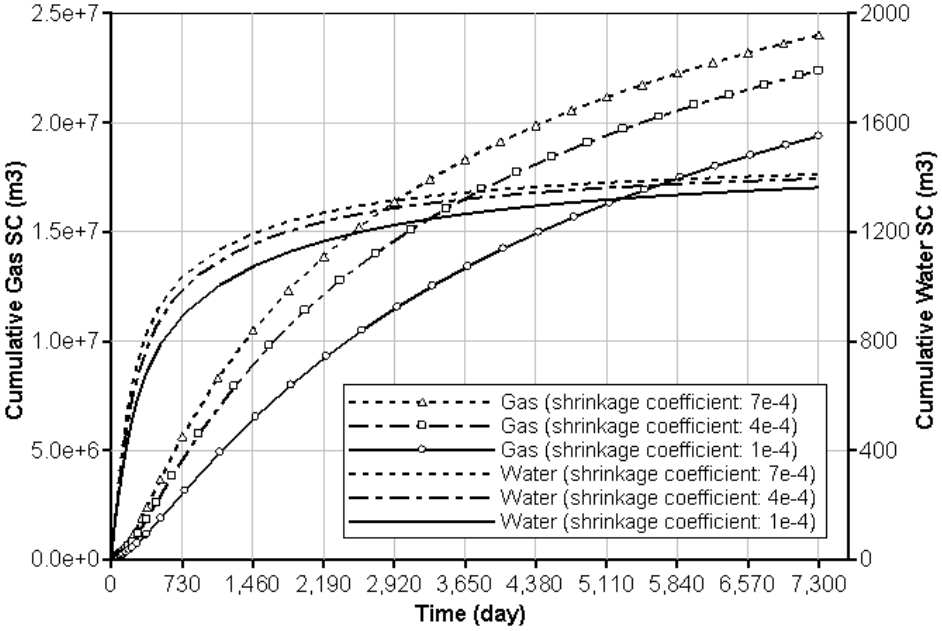

Figure 4.14: Effects of Coefficient of Matrix Shrinkage on Cumulative Production

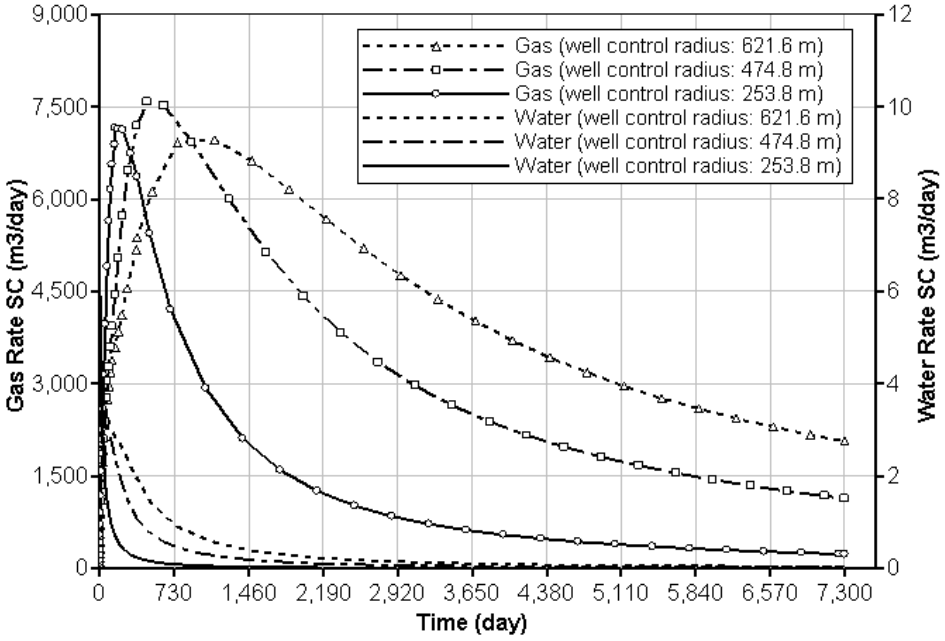

Figure 4.15: Effects of Well Control Area on Production Rate

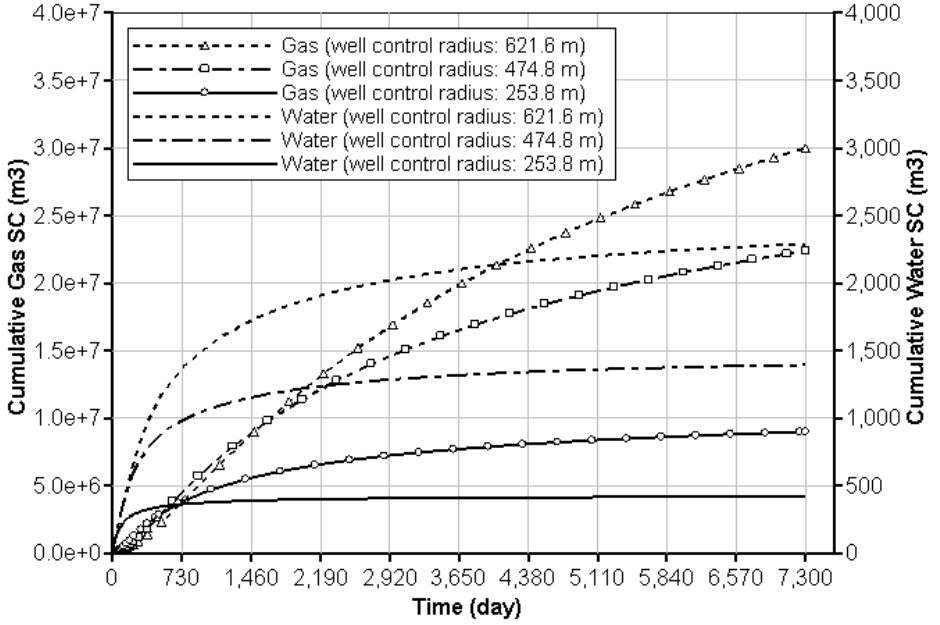

Figure 4.16: Effects of Well Control Area on Cumulative Production

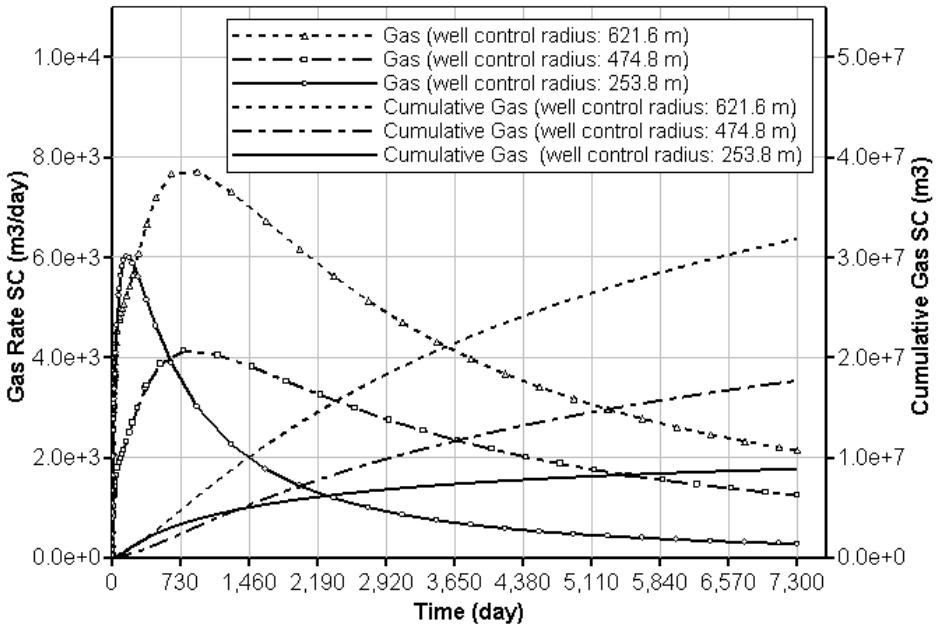

Figure 4.17: Effects of Well Control Area on Production from Conventional Simulation

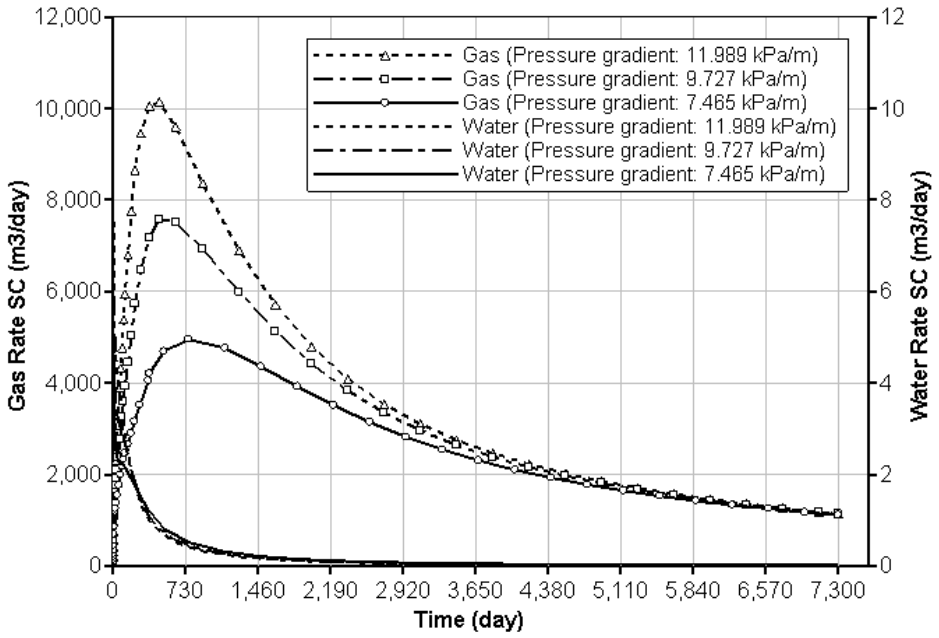

Figure 4.18: Effects of Pressure Gradient on Production Rate

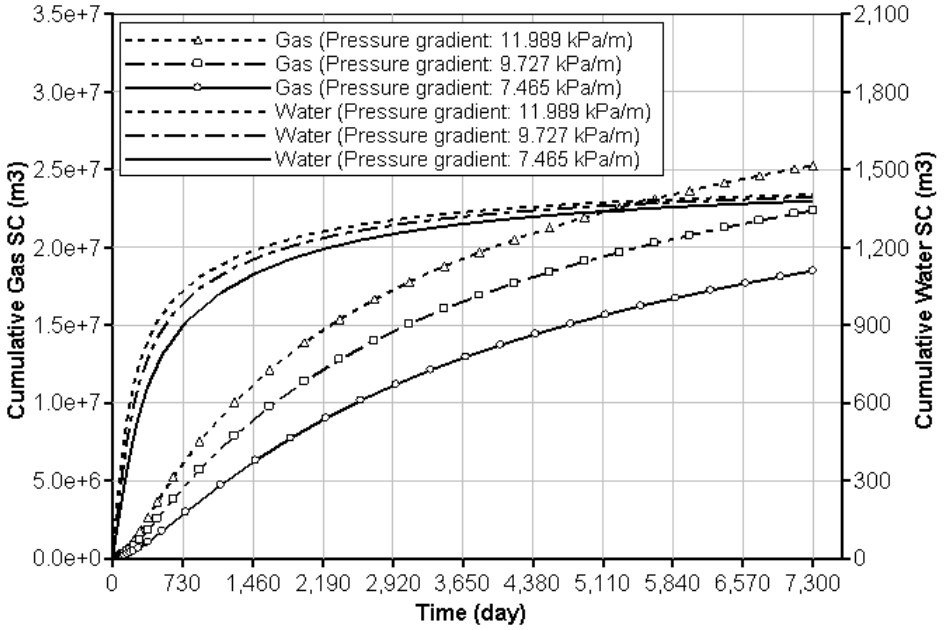

Figure 4.19: Effects of Pressure Gradient on Cumulative Production

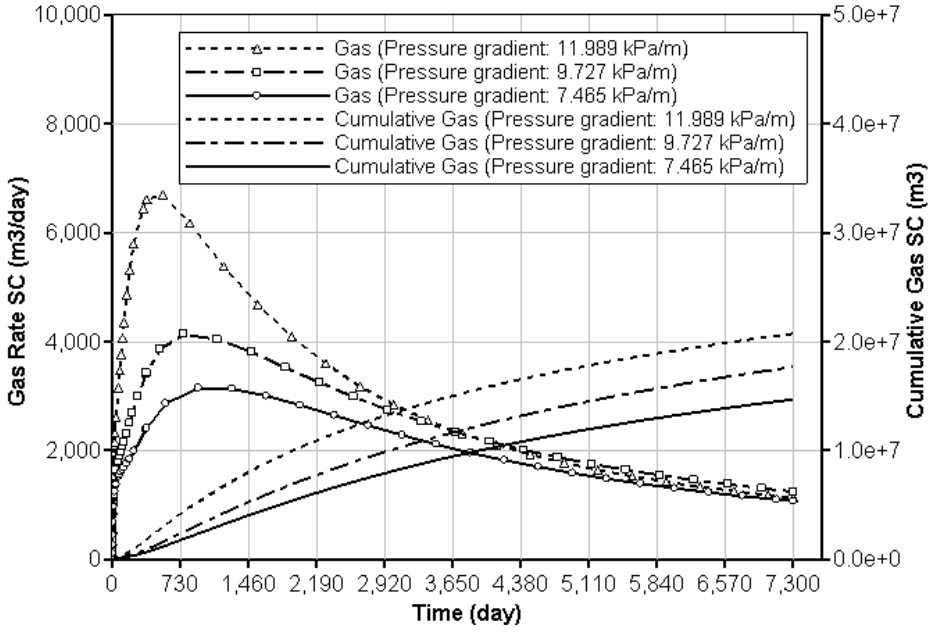

Figure 4.20: Effects of Pressure Gradient on Production from Conventional Simulation

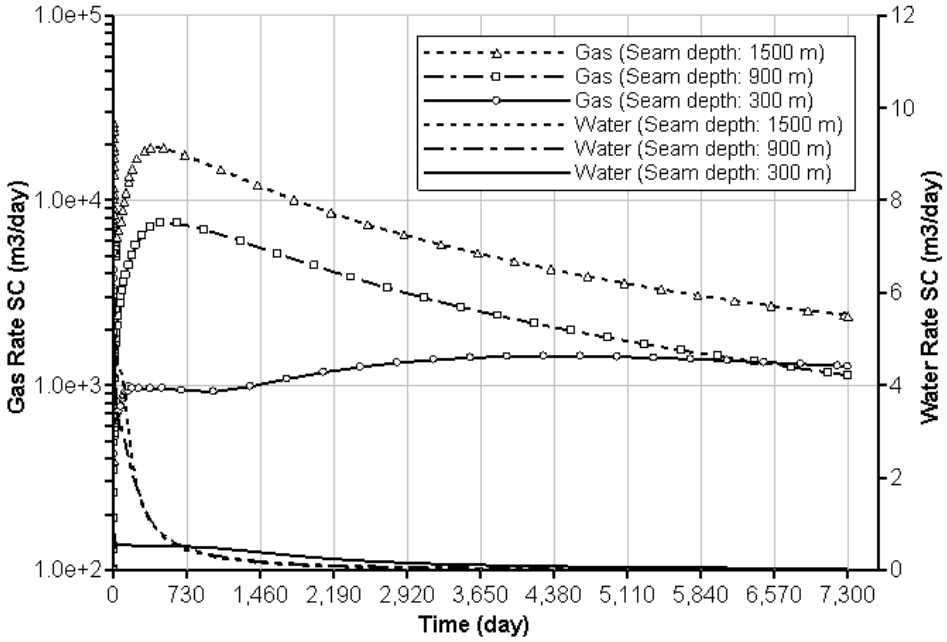

Figure 4.21: Effects of Seam Depth on Production Rate

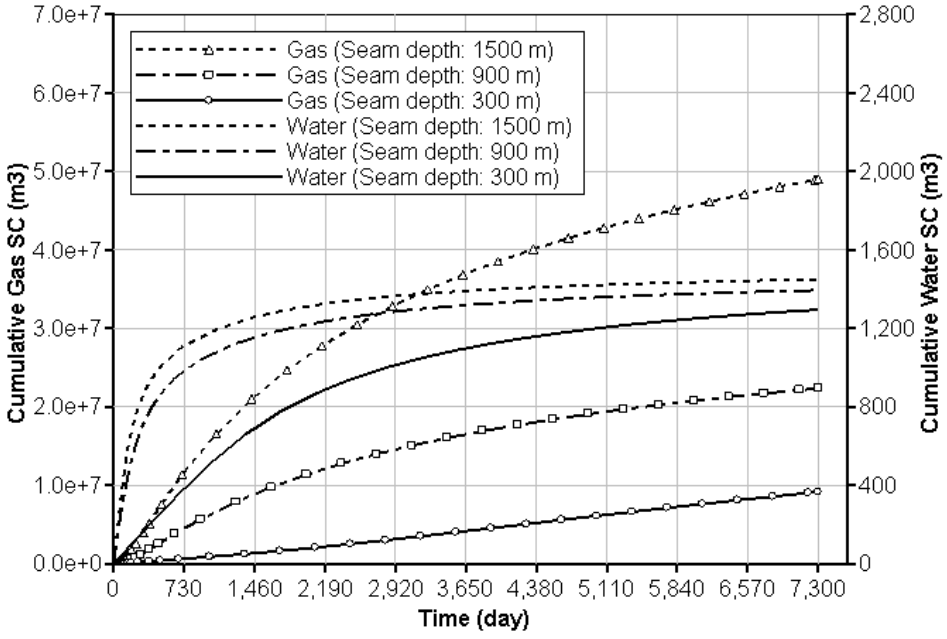

Figure 4.22: Effects of Seam Depth on Cumulative Production

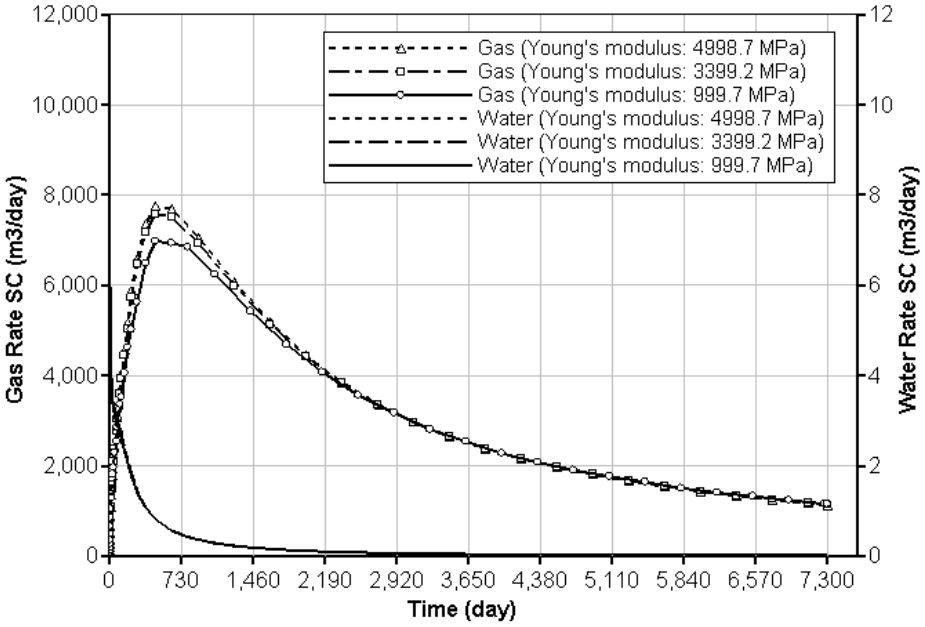

Figure 4.23: Effects of Young's Modulus of Coal on Production Rate

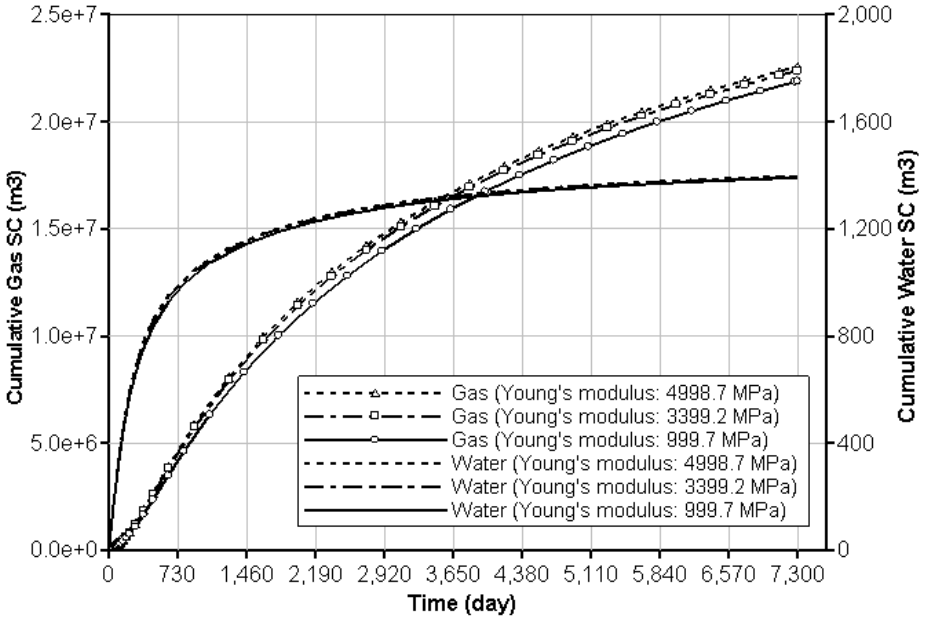

Figure 4.24: Effects of Young's Modulus of Coal on Cumulative Production

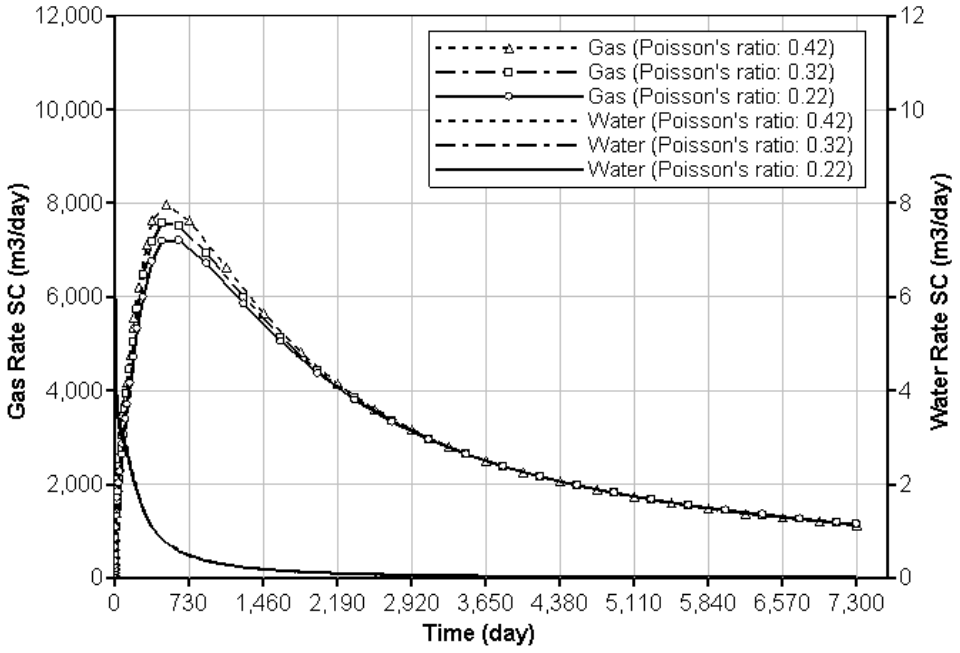

Figure 4.25: Effects of Poisson's Ratio of Coal on Production Rate

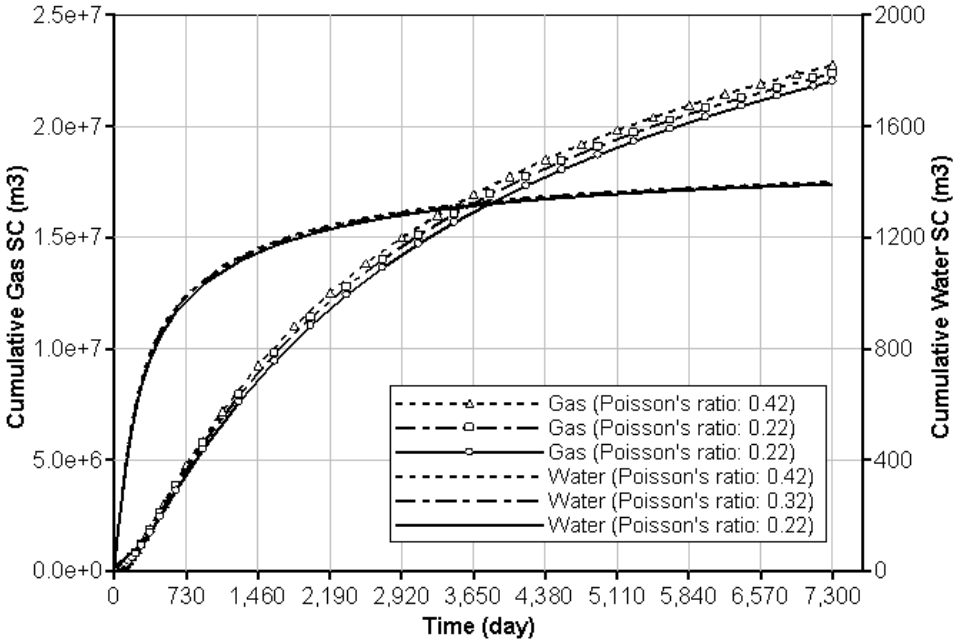

Figure 4.26: Effects of Poisson's Ratio of Coal on Cumulative Production

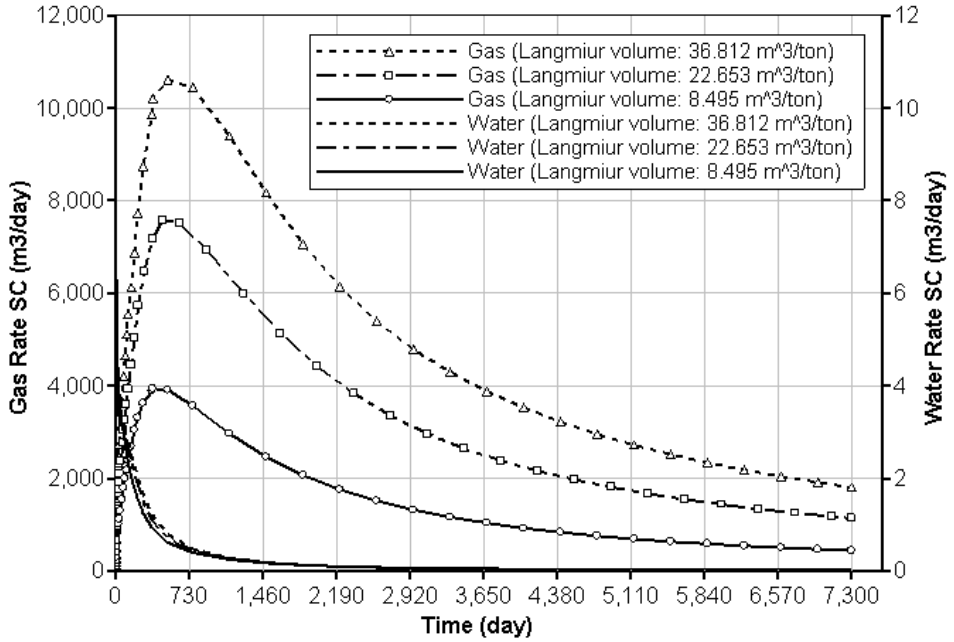

Figure 4.27: Effects of Langmuir Volume on Production Rate

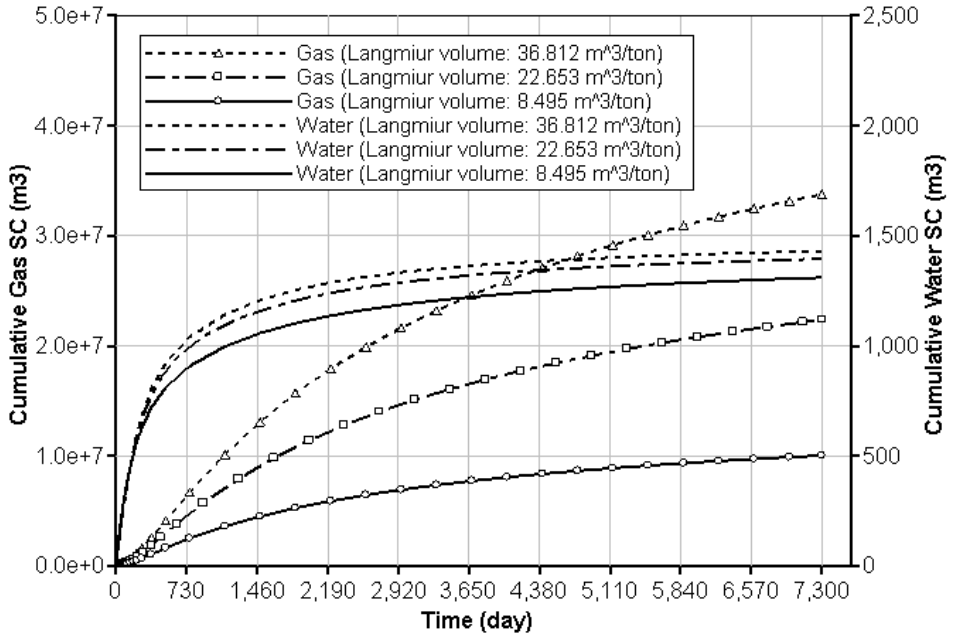

Figure 4.28: Effects of Langmuir Volume on Cumulative Production

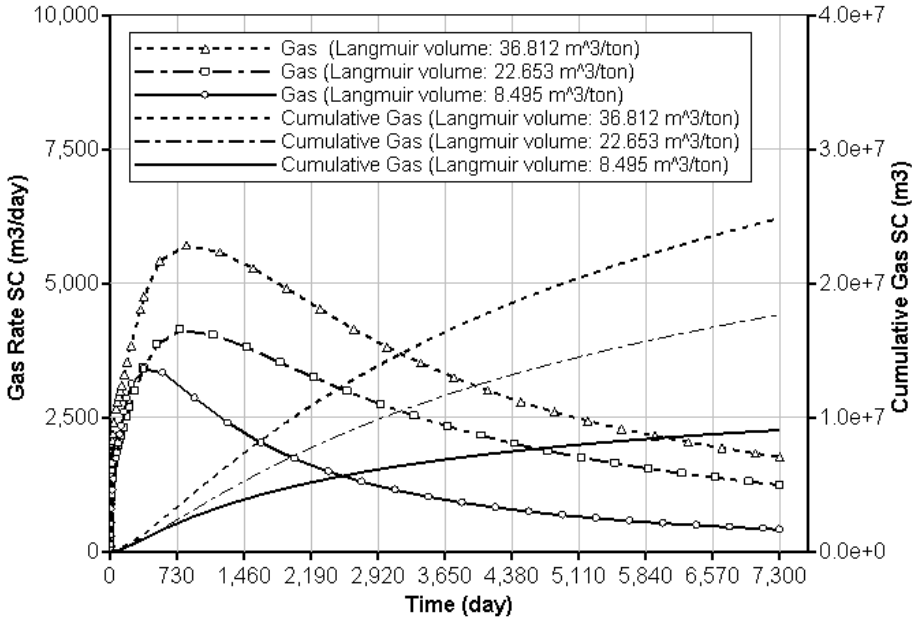

Figure 4.29: Effects of Langmuir Volume on Production from Conventional Simulation

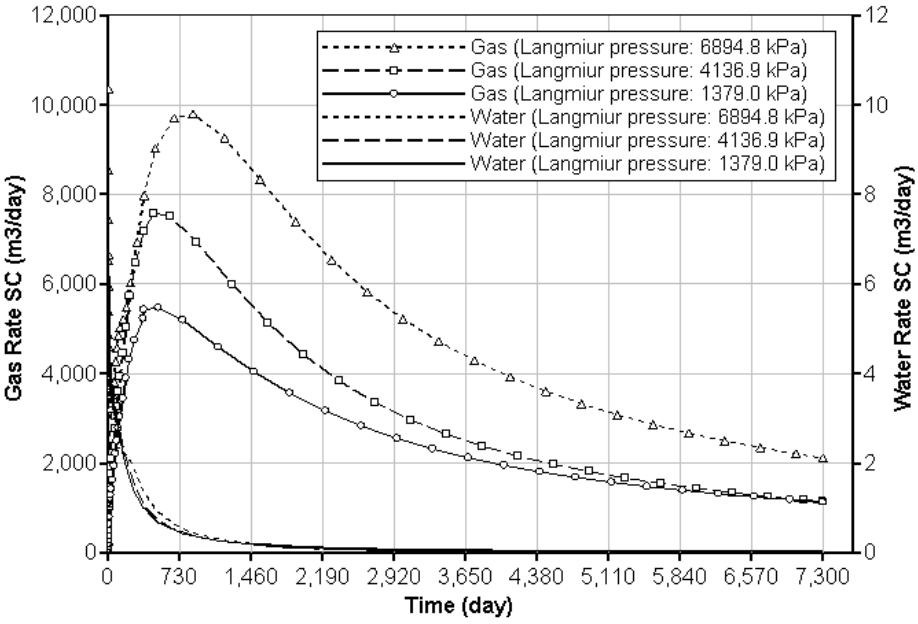

Figure 4.30: Effects of Langmuir Pressure on Production Rate

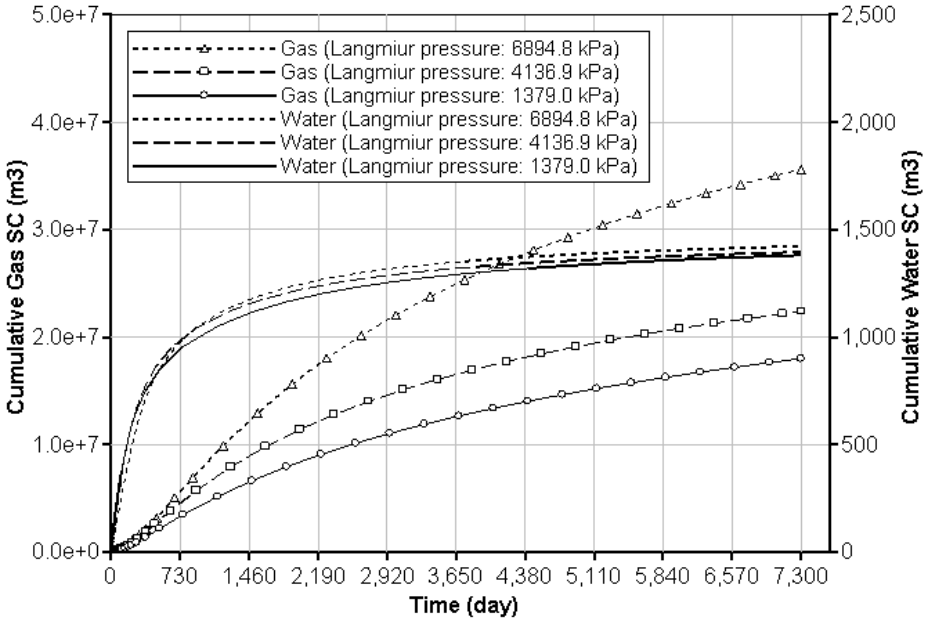

Figure 4.31: Effects of Langmuir Pressure on Cumulative Production

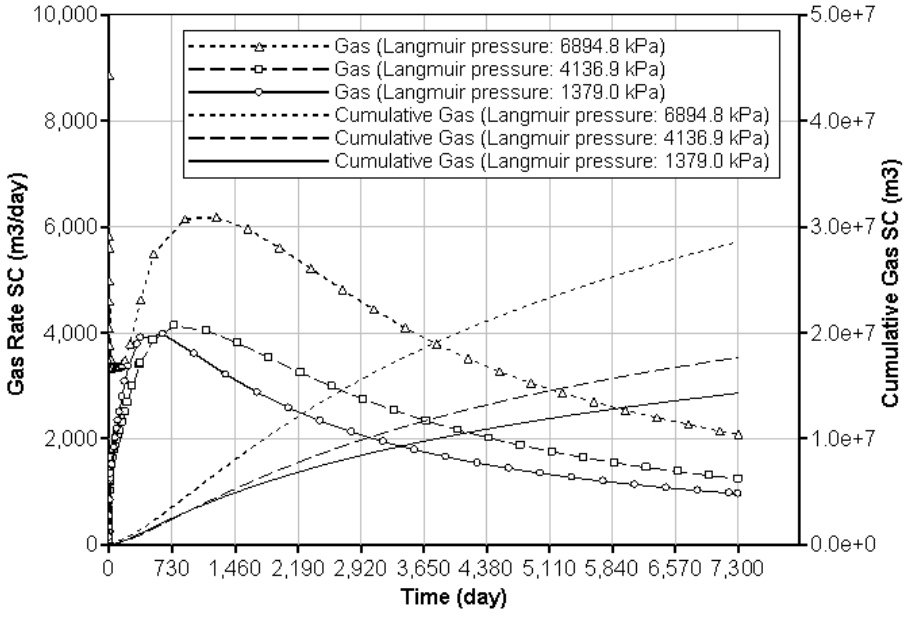

Figure 4.32: Effects of Langmuir Pressure on Production from Conventional Simulation

5 DISCONTINUUM MEDIUM POROSITY AND PERMEABILITY COUPLING MODELS

5.1 INTRODUCTION

Coalbeds or coal seams are well known for the dual porosity characteristic and contain micropores and macropores (Davidson et al, 1995). Macropores, initially taken up by brine, mainly provide the conduit for fluid flow while micropores store most of methane by adsorption. Micropores exist in coal matrix and macropores are almost uniformly spaced natural fractures, called cleats. The studies of Davidson et al (1995) and Laubach et al (1998) showed that cleats or fractures include face cleats and butt cleats, and usually develop perpendicular to bedding planes. Butt cleats are about 90^o to face cleats and commonly terminate at face cleats. A plan view of pore structure of coalbeds is shown in Figure 5.1.

The pore structure of coalbeds determines the permeability of coalbeds is anisotropic and the greatest permeability is in the direction of face cleats. Using 50.8 mm (2 in) cubes of Cwmtillery Garw coal, Promery and Robinson (1967) found the flow rates of water were significantly different when the confining pressures were perpendicular to main cleats (face cleats), cross cleats (butt cleats) and the bedding plane. The anisotropy of permeability was confirmed by the experimental results of Gash et al (1993). Using the coal from the La Plata mine in the San Juan Basin and under 6.895 MPa (1000 psi), they found that the permeability parallel to the bedding plane in the direction of face cleats was 0.6 ~ 1.7 mD and in the direction of butt cleats was 0.3 ~ 1.0 mD, but in the direction perpendicular to the bedding plane was 0.007 mD. From field well tests Koenig and Stubbs (1986) reported the anisotropy ratio of permeability in the bedding plane was as high as 17:1 in the Rock Creek coalbeds of the Warrior Basin in the USA.

Many studies have indicated that of all the parameters that influence the success of coalbed methane (CBM) developments, the permeability of cleats is the paramount one. The results of Sawyer et al (1987) showed that fracture permeability and relative permeability controlled the long-term productivity of

---

A version of this chapter is under review for publishing. Gu, F. and Chalaturnyk, R.J., 2010. Journal of Petroleum Science and Engineering. xx: xxx-xxx.

coalbeds and that the optimum well spacing also depended on the permeability of coalbeds. Reid et al (1992) illustrated that permeability, initial desorption pressures and drainage areas were the most important reservoir parameters for CBM production. Young et al (1992) pointed out that permeability, well spacing and the degree of coal saturation (corresponding to initial gas content) had the greatest impacts on the long-term performances of CBM wells. A complete parametric study by Roadifer et al (2003) showed that for pure coal reservoirs (without adjacent sand layers) the five parameters having the most impacts on peak gas rates, in order of most to least, were permeability, free gas saturation, the degree of coal saturation, damage skin factor and thickness.

However the permeability of coalbeds is not constant during CBM production but varies with the change of in situ conditions. The alternations of in situ conditions cause the changes of stresses and strains thus influence the permeability and porosity of cleats. One of significant changes in situ conditions during CBM production is probably the variation of pore pressures. In pressure depletion CBM production, for instance, the decline of seam pressures results in the increase of effective stresses since total stresses are relatively stable. With effective stresses increasing the apertures of cleats reduce thus permeability decreases. The measurements of Patching (1965) using N_2 and CO_2 showed that the permeability of coal decreased by approximately four orders with the confining stress increasing from 0.07 to 20.68 MPa (10 to 3000 psi). The investigation of Somerton et al (1975) indicated that the permeability of fractured coal to methane dropped by more than two orders under a stress range of 0.34 ~ 13.79 MPa (50 ~ 2000 psi). Reznik et al (1978) found the permeability of coal to nitrogen reduced by approximately two orders with the confining pressure rising from 0.689 to 4.83 MPa (100 to 700 psi). The coal permeability measured by Rose and Foh (1984) with water also decreased as much as two orders of magnitude over a pressure range of normal dewatering and production cycles in the field. With experimental results Enever and Hening (1997) illustrated the logarithm of coal permeability linearly decreased with the increase of effective stresses.

Another pronounced change of in situ conditions during CBM production is the volumetric change of coal matrix due to gas desorption and adsorption. Gas desorption causes the shrinkage of coal matrix while gas absorption results in the swelling of coal matrix. In pressure depletion CBM production, for example, coal matrix shrinks due to gas desorption. The shrinkage of coal matrix leads the

relaxation of coal matrix and the decreases of in situ effective stresses. As a result cleat apertures and permeability increase. Somerton et al (1975) tested the permeability of fractured coal with nitrogen and methane under the same hydrostatic stress and found that the permeability to methane was 20 ~ 40% lower than the permeability to nitrogen. The studies of Harpalani and Zhao (1989) with methane (adsorptive gas) showed that when the pressures were above the desorption pressure of methane (i.e. without methane desorption) the permeability of coal decreased with the decrease of gas pressures but when the pressures were below the desorption pressure (i.e. with methane desorption) the permeability of coal to methane dramatically increased with the decrease of gas pressures. In contrast the permeability to helium (almost non-adsorptive gas) decreased continuously with the drop of pressures. The results of Harpalani and Schraufnagel (1990) also indicated that the permeability of coal to methane increased with the decrease of gas pressures in spite of the increase of effective stresses, and that the volume of coal matrix shrank by 0.4% when the gas pressure fell from 6.9 MPa to the atmospheric pressure. The field well test results of three wells in the San Juan Basin indicated that the permeability of the coalbed increased 2.7 ~ 7 times after produced 3 ~ 4 years (Mavor and Vaughn, 1998).

Although the decrease of permeability due to pressure decrease and the increase of permeability due to methane desorption may partly offset each other, the degrees of their influences are not equal thus the permeability in coal seams varies with location and time during CBM production. Given the above lab and field test results it is expected that permeability would change remarkably during production. Therefore the variation of permeability as a result of the change of pore pressures and absorbed gas volumes must be taken into in estimating and evaluating CBM production. One method to consider the influences of permeability changes in simulations is to calculate the change of permeability with the change of pore pressures using an analytical model. The available analytical models include the models of Seidle and Huitt (1995), Levine (1996), Palmer and Mansoori (1998), Shi and Durucan (2003), and Chikatamarla et al (2004). The main advantage of this method is its easy application in conventional reservoir simulators with minor code modifications. The problems or limitations are mainly owing to the assumptions made in the formulation of these models. One limitation is the permeability of coalbeds was assumed isotropic in the whole production life. This implies initial permeability and the change of permeability are all assumed to be isotropic. Because of the difference between butt cleats and

face cleats, initial isotropic permeability is probably rare for coalbeds. One can see later in this chapter that the change of permeability is also not isotropic even if the initial permeability is assumed to be isotropic. Another limitation comes from the assumption that the total volume of coal matrix plus cleats keeps invariable during production, i.e. the decrease of matrix volume was assumed to equal to the increase of cleat volume and vice versa. However since butt and face cleats are perpendicular to bedding planes, the deformation of coal matrix in the direction normal to the bedding planes, actually, would not contribute to the change of cleat apertures and permeability. Other limitations relate to assuming coal (discontinuous mass containing matrix and cleats) as a continuum isotropic elastic medium and assuming cleats as smooth plate channels etc. Thus research efforts are still required to improve these permeability models.

Another method taking the change of permeability into account in simulation is to use the geomechanical and reservoir coupled simulation. According to the degrees to consider the interaction between solid deformation and fluid flow, coupled simulations can be divided, from lightest degree to full consideration, into decoupled, sequential coupled (including explicitly sequential coupled and implicitly sequential coupled) and full coupled simulations (Settari and Walters, 2001). The application of coupled simulations for CBM production has been attempted by some researchers. Zhao et al (2004) established a fully coupling model for a single phase and single (methane) component CBM production case. Gu and Chalaturnyk (2005a) proposed an explicitly sequential coupled simulation method to simulate pressure depletion CBM production. In the simulation industrial simulators (multiphase and multicomponent fluid flow simulator and geomechanical simulator) and the permeability and porosity coupling models, in which coal mass was considered as a continuum elastic medium and cleats as smooth plate channels, were applied. Gu and Chalaturnyk (2005b) also applied the coupled simulation to the sensitivity study of pressure depletion CBM production.

Because the cleats of most coalbeds are initially saturated with water (brine), two-phase (water and gas) flow usually occurs during production. Besides multicomponents (such as methane, carbon dioxide and nitrogen) may also encounter in some coalbeds and in the enhanced coalbed methane (ECBM) recovery process. The single component and single phase full coupled simulation model proposed by Zhao et al (2004) is not applicable to most coalbeds. In addition an industrial simulator for the full coupled simulation of CBM

production is not available at present. Therefore a sequential coupled simulation method, especially the explicitly sequential coupled simulation method utilized by Gu and Chalaturnyk (2005a, 2005b), is probably a practical and cost affordable solution for field large-scale simulations.

This chapter will present new permeability and porosity models for reservoir and geomechanical coupled simulations of CBM production and to demonstrate their application in the explicitly sequential coupled simulation. The new models are more comprehensive and adaptable to different coalbeds comparing with the early coupling models (Gu and Chalaturnyk, 2005a). The improvements include: (1) coal mass is considered as a discontinuous medium containing matrix and cleats and the equivalent continuum elastic medium model is applied to simulate coal deformation; (2) the difference between hydraulic apertures and mechanical apertures is considered; (3) the anisotropies in permeability, the coefficient of shrinkage/swelling due to desorption/ adsorption and mechanics parameters (such as matrix moduli and cleat stiffness) are considered. The important issues, such as the length of time steps, the relation between permeability and pore pressures or in situ effective stresses, the relation between permeability and porosity, and the influence of initial water saturation, are also discussed in this chapter.

5.2 SIGN CONVENTIONS

The sign of extensional stresses is defined as positive and the sign of compressive stresses as negative. A positive sign of strain indicates an increase in dimensions and a negative sign of strain implies a decrease in dimensions. Although these sign conventions are reverse with that used in geotechnical engineering, they are consistent with the sign conventions in geomechanical simulators (such as FLAC3D©) thus it is convenient to apply the proposed models in the coupled simulations of CBM and ECBM processes.

5.3 DESCRIPTION OF COALBEDS

5.3.1 Physical Model

During production gas diffuses from matrix to cleats then moves along cleats to wellbores. Cleats are the main conduits for water and gas flow. For the purpose of fluid flow, coalbeds can be considered as a fracture system with a collection of impermeable matchsticks (Seidle et al 1992), as shown in Figure 5.2. Directions

x, y and z are the principal symmetric directions in the Cartesian coordinate system. Coal matrix blocks are intersected by two sets of cleats or fractures, i.e. face cleats and butt cleats, in directions x and y. Fluids flow parallel to plane x-y (the bedding plane). The mechanical apertures of cleats and the widths of coal matrix blocks are $(b_m)_x$ and a_x for the cleat set intersecting axis x, and $(b_m)_y$ and a_y for the cleat set intersecting axis y respectively. Corresponding to mechanical apertures, the hydraulic apertures of cleats are $(b_h)_x$ and $(b_h)_y$ respectively.

5.3.2 Cleats

5.3.2.1 Mechanical and Hydraulic Apertures

The apertures (openings) of cleats (fractures) may be determined either from direct or indirect measurements. The apertures from direct measurements are mechanical apertures while apertures from indirect measurements are hydraulic apertures. The latter is back calculated with the cubic law from the permeability that is estimated with Darcy's law based on the measured flow rate, pressure gradient and fluid viscosity etc. Owing to the influences of wall roughness (Brown, 1987), tortuosity (Tsang, 1984), contact area (Zimmerman et al, 1992) and fracture shape (Bogdanov et al, 2003) etc. mechanical apertures, however, are generally greater than the corresponding hydraulic apertures.

The relationship between hydraulic apertures and mechanical apertures can be described with an empirical model presented by Barton et al (1985):

$$b_h = \min\left\{ b_m, \frac{{b_m}^2}{(JRC^p)^{2.5}} \right\} \quad \text{.....(5.1)}$$

where the units of apertures are in microns and JRC^p can be roughly estimated by comparing the fracture profile of specimens with the typical profiles provided by Barton and Choubey (1977). The more accurate estimation of JRC^0 may be made with the methods of Barton and Choubey (1977), Tse and Cruden (1979) and Yang et al (2001).

Olsson and Barton (2001) pointed out that Equation (5.1) could be used from zero shear displacement (u_s) to 75% peak shear displacement (u_{sp}), i.e. $u_s/u_{sp} \leq 0.75$. If shear displacement is greater than this range, the relationship between hydraulic and mechanical apertures may be described with the empirical model presented by Olsson and Barton (2001).

5.3.2.2 Permeability and Porosity

The anisotropic permeability of coalbeds can be expressed as (Van Golf-Racht 1982a):

$$k_i = \frac{(b_h)_j^3}{12a_j} \quad \text{.....(5.2)}$$

where i and j represent direction x or y and are mutually orthogonal. The porosity of cleats can be expressed as (Van Golf-Racht 1982b):

$$\phi = \frac{(b_m)_x}{a_x} + \frac{(b_m)_y}{a_y} = \sum_{i=x,y} \frac{(b_m)_i}{a_i} \quad \text{.....(5.3)}$$

5.3.2.3 Mode of Fractures

The mode of most cleats (fractures) is an opening-mode rather a shearing-mode (Laubach et al, 1998). Positive driving stresses are needed for the formation of opening-mode fractures and could occur under two conditions: the local minimum stress acting on the fracture is tensile or the pore pressure exceeds the minimum stress. Absolute tension may be possible at or near the surface, but for deeper formations, where the minimum stress is compressional, there must be the contribution from pore pressures for the occurrence of positive driving stresses. Compaction takes place during progressive coalification thus fracturing may only be associated with latter stages of coalification when pore pressures are greater than the minimum stress and a positive driving stress reaches. Although moisture and/or volatile matter loss could contribute to coal shrinkage, it is the rearrangement of coal structure that is responsible for most shrinkage which could also contribute to cleat developments.

Because of being an opening-mode, most cleats are probably mated fractures. Unmated fractures also exist in the area where tectonic shearing and folding occurred in history.

5.3.2.4 Stiffnesses

Comparing with the width of a coal matrix block, the aperture of a cleat is physically negligible even though fluid flow is controlled by cleats. Thus in mechanics a cleat may be regarded as a thin layer having normal and shear stiffnesses but without width. The normal and shear stiffnesses are $(K_n)_x$ and $(K_s)_x$

for the cleat set intersecting axis x, and $(K_n)_y$ and $(K_s)_y$ for the cleat set intersecting axis y (referring to Figure 5.2).

The stiffnesses of fractures are not constant but vary with the change of in situ stresses and with fracture types, i.e. mated and unmated fractures. Normal stiffnesses increase with the decrease of normal fracture apertures. Shear stiffnesses increase with the increase of normal stresses. The change of normal stiffnesses can be estimated with the empirical model proposed by Bandis et al (1983):

$$K_n = \frac{K_n^0}{(1 - u_n / u_n^{\max})^2} \quad (\text{mated cleats}) \qquad \text{……(5.4a)}$$

$$K_n = K_n^0 \frac{\sigma'}{\sigma_0'} \quad (\text{unmated cleats}) \qquad \text{……(5.4b)}$$

The change of shear stiffnesses can be approximated with the empirical model presented by Jing et al (1993):

$$K_s = \frac{[-\sigma']}{\sigma_c}\left(A - \frac{[-\sigma']}{\sigma_c}\right)K_s^{\max} \quad (0 \le [-\sigma'] \le \sigma_c) \qquad \text{……(5.5a)}$$

$$K_s = 0 \quad ([-\sigma'] > \sigma_c) \qquad \text{……(5.5b)}$$

where K_S^{max} is experimentally determined when the normal stress reaches the magnitude of uniaxial (or unconfined) compressive strength of coal matrix, σ_c. Note that the sign of σ_c (compression) is adopted positive in Equations (5.5a) and (5.5b) as used in conventional uniaxial tests and different from our sign conventions.

5.3.3 Matrix

5.3.3.1 Mechanics Properties

The orthogonally anisotropic cleat sets (face and butt cleat sets) in coalbeds suggest coalbeds experienced orthogonally anisotropic stresses thus mechanical properties of coal matrix would be orthogonally anisotropic. Szwilski's results (1984) from the load-deformation tests on small cylindrical samples and coal cubes showed that the elastic moduli in the directions perpendicular to butt cleats, face cleats and the bedding plane respectively have a general relation of:

$$E_{\perp butt} > E_{\perp face} > E_{\perp bedding} \qquad \text{……(5.6)}$$

The ratio of elastic moduli in the directions perpendicular to cleats over the modulus in the direction perpendicular to the bedding reached as much as 2.6. But Berkowits (1994) pointed out that the Young's modulus is relatively insensitive to the specimen orientation and rank in the coals with up to 92-93% carbon, and that only among fully developed anthracites does the modulus appear to increase rapidly and depend upon whether it is measured parallel or perpendicular to the bedding plane.

For the sake of generalization coal matrix is considered as an orthogonally anisotropic elastic medium, or simply called an orthotropic medium. For this kind of media Lekhnitskii (1963) showed that elasticity could be described with nine independent parameters. The independent parameters of coal matrix (referring to Figure 5.2) include Young's moduli, E_x, E_y and E_z in directions x, y and z, shear moduli $G_{yx,}$ G_{zx} and G_{zy} corresponding to planes y-x, z-x and z-y and Poisson's ratios ν_{yx}, ν_{zx}, ν_{zy}. Poisson's ratios ν_{ij} are used to determine the normal strain in direction j due to the normal stress applied in direction i. The Poisson's ratios, ν_{ij} and ν_{ji}, are related by the symmetry of the stress-strain relationship (Lekhnitskii, 1963),

$$\frac{\nu_{ij}}{E_i} = \frac{\nu_{ji}}{E_j} \quad \text{.....(5.7)}$$

where i and j are any two mutually orthogonal directions of directions x, y and z.

If coal matrix of a coalbed has layer characteristic, i.e. transversely isotropic within plane x-y (bedding plane), the independent elastic parameters would reduce from nine to five (E_y, E_z, ν_{yx}, ν_{zy} and G_{zy}) since:

$$E_x = E_y \quad \text{.....(5.8a)}$$

$$\nu_{zx} = \nu_{zy} \quad \text{.....(5.8b)}$$

$$G_{zx} = G_{zy} \quad \text{.....(5.8c)}$$

$$G_{yx} = \frac{E_x}{2(1+\nu_{yx})} \quad \text{.....(5.8d)}$$

Further if coal matrix of a coalbed could be treated as an isotropic medium, the independent elastic parameters would reduce to only two, i.e. Young's modulus, E and Poisson's ratio, ν.

5.3.3.2 Coefficients of Thermal Expansion

In ECBM and CO_2 sequestration process, gases with a lower or higher temperature than that of coalbeds may be injected thus the change of temperature would occur in coalbeds. The increase of temperature causes the thermal expansion of coal matrix while the decrease results in the thermal contraction of coal matrix. Nowinski (1978) indicated that for orthotropic media thermal strains due to the change of temperature could be described with three independent linear thermal expansion coefficients corresponding to three orthotropic directions, i.e. $(\beta_{LT})_x$, $(\beta_{LT})_y$ and $(\beta_{LT})_z$. With these three directional coefficients of thermal expansion, orthogonal anisotropy can be considered in coupled simulations.

5.3.3.3 Coefficients of Shrinkage/Swelling

The shrinkage/swelling of coal matrix due to the desorption/adsorption of gases can be analogous to the thermal expansion/contraction of a medium due to the change of temperature, i.e. absorbed gas volume corresponding to temperature and coefficients of linear matrix shrinkage due to the desorption/absorption of gases corresponding to the coefficients of linear thermal expansion. Similarly elastic responses of coal matrix due to the desorption/absorption of gases can be described with three independent coefficients of linear matrix shrinkage/swelling in three orthogonal directions, i.e. $(\beta_{LD})_x$, $(\beta_{LD})_y$ and $(\beta_{LD})_z$. If the shrinkage/swelling of coal matrix is isotropic, the three directional coefficients of linear matrix shrinkage/swelling become identical, i.e. there is only one independent coefficient of linear matrix shrinkage/swelling.

5.4 DEFORMATION OF COALBEDS

5.4.1 Equivalent Continuum Model and Validation

Because coalbeds are fractured reservoirs rather single-pore reservoirs, one difficulty in the coupled simulations of this type of reservoirs is the deformation simulation of fractures (cleats). Although the constitutive models, such as Barton et al's (1985) model and Jing et al's (1993) model etc., are available and can be used to simulate the deformation of fractures, for coalbeds the number of fractures or cleats is extremely large. Thus dealing with each cleat individually is impractical for the memory capacity and calculation speed of present computers.

However, according to Amadei and Goodman (1981) the mechanical properties of an anisotropic discontinuous medium, specifically an orthotropic fractured medium, can be represented with an "equivalent" anisotropic continuum medium. Then the deformation can be estimated with the equivalent continuum medium. Based on the early discussion (Sections 5.1 and 5.3.3.1) coal mass in most coalbeds can be considered as an orthotropic fractured medium thus its deformation can be simulated with an equivalent continuum medium. The equivalent moduli in directions x and y, E^*_x and E^*_y (referring to the coalbed model shown in Figure 5.2) are calculated by:

$$\frac{1}{E_i^*} = \frac{1}{E_i} + \frac{1}{(K_n)_i \cdot a_i} \quad \text{.....(5.9)}$$

where i may be any of directions x and y. The equivalent modulus in direction z, E^*_z, is the same as the modulus of coal matrix in direction z, E_z, since coal mass does not contain cleats in this direction.

The equivalent shear modulus in plane y-x,G^*_{yx}, is estimated by:

$$\frac{1}{G_{yx}^*} = \frac{1}{G_{yx}} + \frac{1}{(K_s)_y \cdot a_y} + \frac{1}{(K_s)_x \cdot a_x} \quad \text{.....(5.10a)}$$

The equivalent shear moduli in plane z-x and plane z-y, G^*_{zx} and G^*_{zy} are:

$$\frac{1}{G_{zi}^*} = \frac{1}{G_{zi}} + \frac{1}{(K_s)_i \cdot a_i} \quad \text{.....(5.10b)}$$

where i may be any of directions x and y.

The equivalent Poisson's ratios, ν^*_{yx}, ν^*_{zx} and ν^*_{xy} are obtained by:

$$\nu_{ij}^* = \frac{E_i^*}{E_i}\nu_{ij} \quad \text{.....(5.11)}$$

where i and j are any two mutually orthogonal directions of directions x, y and z.

Gu and Chalaturnyk (2006b) validated the applicability of the equivalent deformation model to the deformation of coal mass by comparing the numerical simulation results with the experimental results measured by Czaplinski and Gustkiewicz (1990). The lab measurements included a uniaxial compression test and a swelling test in CO_2 under longitudinal constraint condition. The study showed that the deformation behaviour of coal mass cannot be properly simulated with the widely used continuum elastic medium model mainly due to the nonlinear characteristic of cleat deformation. The equivalent continuum elastic

medium model was successfully applied to simulate the measured coal deformations.

5.4.2 Changes of Linear Strains

5.4.2.1 Strain due to Effective Stress

Based on the equivalent continuum model of coal mass the change of linear strains in directions x and y due to the change of effective stresses ($\Delta\sigma^{'}$) is expressed as:

$$\Delta\varepsilon_{LSi} = \frac{\Delta\sigma_i^{'}}{E_i^*} - \nu_{ji}^* \frac{\Delta\sigma_j^{'}}{E_j^*} - \nu_{ki}^* \frac{\Delta\sigma_k^{'}}{E_k^*} \quad \text{.....(5.12)}$$

where i, j and k are mutually orthogonal and alternate in directions x, y and z. For example, when i represents x, j and k must be one of y and z.

The Biot effective stresses of an anisotropic and homogenous medium can be calculated with the model proposed by Cheng (1997):

$$\sigma_i^{'} = \sigma_i + \alpha_i p \quad \text{.....(5.13a)}$$

where i represents any of directions x, y and z and α_i is referred to the directional Biot coefficients of effective stresses. Note that the sign of stresses due to pore pressures is positive according to our sign conventions. For a saturated fractured medium with isotropic matrix, Tuncay and Corapcioglu (1995) presented a model to calculate effective stresses. For the case of coalbeds where the volume of cleats (fractures) is negligible comparing with bulk volume, according to their results the effective stress can be approximated by:

$$\sigma_i^{'} \approx \sigma_i + \left[1 - \frac{(K_{frac})_i}{(K_{solid})_i}\right] p \quad \text{.....(5.13b)}$$

If $K_{frac} << K_{solid}$, Equation (5.13b) becomes the Terzaghi's (1943) effective stress principle.

Although coal mass is an anisotropic medium the implementation of Biot logic in FLAC3D© is unfortunately limited to isotropic porous media. Thus the coupled simulation of this study is made with Terzaghi's (1943) effective stress mode, i.e. the Biot coefficient of effective stresses is assumed to be one.

5.4.2.2 Strain due to Absorbed Gas

The study of Harpalani and Chen (1995) indicated that the volumetric strain of coal matrix due to the desorption/absorption of gases has approximately a linear relation with absorbed gas volume, i.e.

$$\Delta\varepsilon_{VD} = \beta_D \Delta V_D \quad \text{……(5.14a)}$$

The extended Langmuir isotherm (Arri et al, 1992) or ideal adsorbed solution (IAS) (Stevenson et al, 1991) can be used to predict the change of absorbed gases in coal.

If the shrinkage/swelling of coal matrix due to the desorption/adsorption of gases is isotropic, the linear strain in each direction could be estimated from:

$$\Delta\varepsilon_{LD} = \tfrac{1}{3}\Delta\varepsilon_{VD} \quad \text{……(5.14b)}$$

However, the isotropic shrinkage/swelling is not always valid for coalbeds. The measurements of Ceglarska-Stefanska (1994) showed that the linear swelling strain of coal matrix due to methane adsorption was anisotropic and a larger expansion occurred in the direction perpendicular to the bedding plane. Under 0.32 MPa the linear expansion was 0.015% in the direction parallel to the bedding plane and 0.022% in the direction perpendicular to the bedding plane. Under 3.04 MPa the linear expansion was 0.14% in the direction parallel to the bedding plane and 0.18% in the direction perpendicular to the bedding plane. Considering the anisotropy of coal matrix shrinkage/swelling, the change of linear strain is expressed as:

$$\Delta\varepsilon_{LDi} = \beta_{LDi} \Delta V_D \quad \text{……(5.14c)}$$

where i represents any of directions x, y and z.

In some coalbeds or in ECBM process there are more than one adsorptive gas and the coefficients of matrix shrinkage/swelling for each adsorptive gas are usually different thus Equation (5.14c) is not proper to describe this situation. We assume that for each adsorptive gas the relationship between the linear strain of shrinkage/swelling and the absorbed gas volume is linear when multiple adsorptive gases exist in coalbeds and that the total linear strain due to multiple adsorptive gases equals the arithmetical summation of the linear strain of each adsorptive gas. Then a general model of the linear strain due to the shrinkage/swelling of multiple gases can be expressed as:

$$\Delta\varepsilon_{LDi} = \sum_{j}^{n} \beta_{LDi,j} \Delta V_{Dj} \quad \text{……..……..…….……(5.14d)}$$

where i may be any of directions x, y or z and j means gas component j.

5.4.2.3 Strain due to Temperature

If assume the thermal expansion/contraction due to the change of temperature to be anisotropic, a general model of the linear strain due to the change of temperature can be expressed as:

$$\Delta\varepsilon_{LTi} = \beta_{LTi} \Delta T \quad \text{……...…….……..……..(5.15)}$$

where i represents any of directions x, y or z.

5.4.2.4 Total Changes of Linear Strains

Based on the principle of superposition, the total change of linear strain due to the changes of effective stresses, absorbed gases and temperatures can be expressed as:

$$\Delta\varepsilon_{Li}^{t} = \Delta\varepsilon_{LSi} + \Delta\varepsilon_{LDi} + \Delta\varepsilon_{LTi} \quad \text{……...…….……...……(5.16a)}$$

where i could be any of directions x, y or z.

Substituting (12), (14d) and (15) into (16a), the following expression is obtained:

$$\Delta\varepsilon_{Li}^{t} = \frac{\Delta\sigma_{i}^{'}}{E_{i}^{*}} - \nu_{ji}^{*} \frac{\Delta\sigma_{j}^{'}}{E_{j}^{*}} - \nu_{ki}^{*} \frac{\Delta\sigma_{k}^{'}}{E_{k}^{*}} + \sum_{j}^{n} \beta_{LDi,j} \Delta V_{Dj} + \beta_{LTi} \Delta T \quad \text{……...(5.16b)}$$

where i, j and k are mutually orthogonal and alternate in directions x, y and z.

The change of shear strain in plane i-j is:

$$\Delta\gamma_{ij} = \frac{\Delta\tau_{ij}}{G_{ij}^{*}} \quad \text{…….……..……(5.17)}$$

where the subscripts i and j are mutually orthogonal and alternate in directions x, y and z.

It is worth mentioning that FLAC3D© has no direct mode to calculate the changes of stresses and strains due to the shrinkage/swelling from the desorption/absorption of gases. The simulation can be made through a programming code with FISH language inside FLAC3D© as done by Noorany et al (1999) and Rodriguez-Ortiz et al (2003). The changes of total stresses due to

the changes of shrinkage/swelling strains, which are input into FLAC3D©, are calculated with the constitutive equations that are obtained by solving Equation (5.16b) for effective stresses when the change of temperatures are assumed to be zero.

For an isothermal process, e.g. pressure depletion CBM production process, with the nine equivalent continuum mechanics parameters, i.e. E^*, G^* and ν^* each has three values defined by Equations (5.9) to (5.11), and 3×j (three directions and j components of absorbed gases) coefficients of linear matrix shrinkage/swelling due to the desorption/absorption of gases, $\beta_{LDi,j}$, the deformation of a equivalent continuum coal medium due to the changes of pore pressures and absorbed gases can be simulated with FLAC3D©. The total change of normal strains, $\Delta\varepsilon_L^t$, effective normal stresses, $\Delta\sigma'$, and shear stresses $\Delta\tau$, are obtained through the simulation.

5.4.3 Geometric Changes of Coal

The results presented in this section are applicable to both cleat sets intersecting axes x and y.

5.4.3.1 Changes of Cleat Mechanical Apertures

The change of cleat mechanical apertures is composed of two parts. One part is caused by the change of normal stresses and the other by shear displacement. The latter is called shear dilation. The total change of cleat apertures is expressed as:

$$\Delta b_m = (\Delta b_m)_n + (\Delta b_m)_s \quad \text{……..…...…….……...……(5.18)}$$

The change of cleat apertures due to the change of normal stresses is equal to the change of normal displacement and estimated by:

$$(\Delta b_m)_n = \Delta u_n = \frac{\Delta\sigma'}{K_n} \quad \text{…….……...……..…….……(5.19a)}$$

For the convenience of expression the change of cleat apertures is expressed as:

$$(\Delta b_m)_n = a \cdot \Delta\varepsilon_f \quad \text{…….…….……..……(5.19b)}$$

where we define the change of normal strain of cleats as:

$$\Delta\varepsilon_f = \frac{(\Delta b_m)_n}{a} \quad \text{.....(5.20)}$$

Shear dilation results in an increase of cleat apertures and may be significant under some circumstances. For example, Morgenstern and Noonan (1974) measured the shear dilation of a coal joint was as high as 3.48 mm (0.137 in) due to a shear displacement of 4.14 mm (0.163 in) when the sample was moved along the joint plane. The model of shear dilation presented by Barton et al (1985) indicated that the dilation of fractures began when the shear displacement (u_s) between fracture surfaces reached 30% of the peak shear displacement (u_s^p). Using this model the change of apertures due to shear can be estimated:

$$(\Delta b_m)_s = \begin{cases} 0 & (u_s/u_s^p < 0.3) \\ \Delta u_s \tan\psi^m & (u_s/u_s^p \geq 0.3) \end{cases} \quad \text{.....(5.21)}$$

In following Equations (5.22) to (5.25), subscript i represents the cleat set intersecting axis x or y. Subscript j alternates in two directions of x, y and z which are different from i. Subscript n represents direction x or y that is different from i. Directions x and y are orthogonal and parallel to the bedding plane and direction z is perpendicular to the bedding plane (referring to Figure 5.2).

In time step k the change of directional shear displacement of the cleats that intersect axis i along axis j is calculated by:

$$\Delta u_{s\,ij}^k = \frac{\Delta\tau_{ij}}{(K_s)_i} \quad \text{.....(5.22)}$$

The total directional shear displacement at time k is:

$$u_{s\,ij}^k = u_{s\,ij}^{k-1} + \Delta u_{s\,ij}^k \quad \text{.....(5.23)}$$

The total shear displacement of the cleats that intersect axis i at time k is calculated from the total directional shear displacement by:

$$u_{s\,i}^k = \sqrt{(u_{s\,in}^k)^2 + (u_{s\,iz}^k)^2} \quad \text{.....(5.24)}$$

Then the change of shear displacement of the cleats intersecting axis i at time k is estimated by:

$$\Delta u_{s\,i} = u_{s\,i}^k - u_{s\,i}^{k-1} \quad \text{.....(5.25)}$$

Similarly we define the change of shear strains of cleats as:

$$\Delta\gamma_f = \frac{\Delta u_s}{a} \quad \text{.....(5.26)}$$

Applying Equation (5.26) into Equation (5.21) the change in cleat apertures due to shear can be expressed as:

$$(\Delta b_m)_s = \begin{cases} 0 & (u_s/u_s^p < 0.3) \\ a \cdot \Delta\gamma_f \tan\psi^m & (u_s/u_s^p \geq 0.3) \end{cases} \quad \cdots\cdots\cdots\cdots\cdots\cdots\cdots\cdots\cdots\cdots (5.27)$$

Using Equations (5.19b) and (5.27) into Equation (5.18) the total change of cleat apertures is obtained:

$$\Delta b_m = \begin{cases} a\Delta\varepsilon_f & (u_s/u_s^p < 0.3) \\ a(\Delta\varepsilon_f + \Delta\gamma_f \tan\psi^m) & (u_s/u_s^p \geq 0.3) \end{cases} \quad \cdots\cdots\cdots\cdots\cdots\cdots\cdots\cdots\cdots\cdots (5.28)$$

5.4.3.2 Changes of Matrix Blocks

For a unit containing one matrix block and one cleat (referring to Figure 5.2), during a period of time we assume the change of the unit width, Δw, the change of the width of the matrix block, Δa, and the change of the mechanical aperture of the cleat, Δb_m, due to the changes of in situ conditions such as pore pressures and gas desorption/absorption. The changes in directions x and y satisfy:

$$\Delta w = \Delta a + \Delta b_m \quad \cdots\cdots\cdots\cdots\cdots\cdots\cdots\cdots\cdots\cdots\cdots\cdots\cdots\cdots (5.29a)$$

The change of the unit width can also be expressed as:

$$\Delta w = (a + b_m) \cdot \Delta\varepsilon_L^t \quad \cdots\cdots\cdots\cdots\cdots\cdots\cdots\cdots\cdots\cdots\cdots\cdots\cdots\cdots (5.29b)$$

Applying Equations (5.28) and (5.29b) to Equation (5.29a) the change of the matrix block is obtained:

$$\Delta a = \begin{cases} a(\Delta\varepsilon_L^t - \Delta\varepsilon_f) + b_m\Delta\varepsilon_L^t & (u_s/u_s^p < 0.3) \\ a(\Delta\varepsilon_L^t - \Delta\varepsilon_f - \Delta\gamma_f \tan\psi^m) + b_m\Delta\varepsilon_L^t & (u_s/u_s^p \geq 0.3) \end{cases} \quad \cdots\cdots\cdots\cdots (5.30)$$

5.4.3.3 Calculation Procedure for Geometric Changes

From the deformation simulation of FLAC3D© described in Section 4.2, the change of normal strain, $\Delta\varepsilon_L^t$, the change of effective normal stress, $\Delta\sigma'$, and the change of shear stress, $\Delta\tau$, have been obtained. The changes of normal and shear strains of cleats can also be calculated with Equations (5.20) and (5.26) after normal and shear displacements are calculated. At last the changes of cleat apertures, Δb_m, and matrix block, Δa, are estimated with Equations (5.21) an (5.30).

5.5 DEVELOPMENT OF PERMEABILITY AND POROSITY MODELS

In the following conduction, subscripts i and j alternate in directions x and y and are mutually orthogonal. The results presented in this section are also applicable to both cleat sets intersecting axes x and y.

5.5.1 Change of Permeability

As stated in section 4.3.2, during a period of time the mechanical aperture of a cleat changes by Δb_m. Corresponding to this change of the mechanical aperture, we assume the hydraulic aperture of the cleat changes by Δb_h. From Equation (5.1) we have:

$$\frac{b_h + \Delta b_h}{b_h} = 1 + \frac{\Delta b_h}{b_h} = \left(1 + \frac{\Delta b_m}{b_m}\right)^n \quad \text{.....(5.31)}$$

where n equals 2 when $b_m \geq b_h$ and $(b_m+\Delta b_m) \geq (b_h+\Delta b_h)$ and n equals 1 for the other cases.

According to Equation (5.2) the initial permeability of a coalbed is:

$$(k_i)_0 = \frac{(b_h)_j^3}{12 a_j} \quad \text{.....(5.32a)}$$

After deformation, the new permeability of the coalbed becomes:

$$k_i = \frac{[(b_h)_j + (\Delta b_h)_j]^3}{12(a_j + \Delta a_j)} \quad \text{.....(5.32b)}$$

After Equation (5.32b) divided by Equation (5.32a) and using Equation (5.31) the permeability ratio is obtained:

$$\frac{k_i}{(k_i)_0} = \frac{[1 + \frac{(\Delta b_h)_j}{(b_h)_j}]^3}{(1 + \frac{\Delta a_j}{a_j})} = \frac{[1 + \frac{(\Delta b_m)_j}{(b_m)_j}]^{3n_j}}{(1 + \frac{\Delta a_j}{a_j})} \quad \text{.....(5.33)}$$

Applying Equations (5.28) and (5.30) into Equation (5.33) we have:

For $u_s/u_s^p < 0.3$

$$\frac{k_i}{(k_i)_0} = \frac{[1 + \frac{a_j}{(b_m)_j} \Delta \varepsilon_{f\,j}]^{3n_j}}{1 + (\Delta \varepsilon^t_{L\,j} - \Delta \varepsilon_{f\,j}) + \frac{(b_m)_j}{a_j} \Delta \varepsilon^t_{L\,j}} \quad \text{.....(5.34a)}$$

For $u_s/u_s^p \geq 0.3$

$$\frac{k_i}{(k_i)_0}=\frac{\{1+\frac{a_j}{(b_m)_j}[\Delta\varepsilon_{f\,j}+\Delta\gamma_{f\,j}\tan(\psi^m)_j]\}^{3n_j}}{1+[\Delta\varepsilon^t_{L\,j}-\Delta\varepsilon_{f\,j}-\Delta\gamma_{f\,j}\tan(\psi^m)_j]+\frac{(b_m)_j}{a_j}\Delta\varepsilon^t_{L\,j}} \quad \text{…..……...(5.34b)}$$

5.5.2 Change of Porosity

According to Equation (5.3) the new porosity of cleats can be written as:

$$\phi=\sum_{i=x,y}\frac{(b_m)_i+(\Delta b_m)_i}{a_i+\Delta a_i}=\sum_{i=x,y}\frac{(b_m)_i}{a_i}\cdot\frac{[1+\frac{(\Delta b_m)_i}{(b_m)_i}]}{(1+\frac{\Delta a_i}{a_i})} \quad \text{…….……(5.35)}$$

Applying Equations (5.28) and (5.30) into (5.35) we obtain:
For $u_s/u_s^p<0.3$

$$\phi=\sum_{i=x,y}\frac{(b_m)_i}{a_i}\cdot\frac{1+\frac{a_i}{(b_m)_i}\Delta\varepsilon_{f\,i}}{1+(\Delta\varepsilon^t_{L\,i}-\Delta\varepsilon_{f\,i})+\frac{(b_m)_i}{a_i}\Delta\varepsilon^t_{L\,i}} \quad \text{…….……(5.36a)}$$

For $u_s/u_s^p\geq 0.3$

$$\phi=\sum_{i=x,y}\frac{(b_m)_i}{a_i}\cdot\frac{1+\frac{a_i}{(b_m)_i}[\Delta\varepsilon_{f\,i}+\Delta\gamma_{f\,i}\tan(\psi^m)_i]}{1+[\Delta\varepsilon^t_{L\,i}-\Delta\varepsilon_{f\,i}-\Delta\gamma_{f\,i}\tan(\psi^m)_i]+\frac{(b_m)_i}{a_i}\Delta\varepsilon^t_{L\,i}} \quad \text{…….(5.36b)}$$

5.5.3 Model Simplification for Special Cases

With additional assumptions the proposed permeability and porosity models, Equations (5.34) and (5.36), can be simplified. If we neglect the influence of shearing dilation, i.e. the change of shear strains $\Delta\gamma_f$ or the angle of shear dilation is set zero, Equation (5.34b) becomes Equation (5.34a) and Equation (5.36b) becomes Equation (5.36a). Further if we assume the width of a unit containing one matrix block and one cleat keeps unchanged, i.e. assuming $\Delta\varepsilon_L{}^t=0$ or assuming the change of the cleat mechanical aperture equals the opposite change of the matrix block width ($\Delta b_m=-\Delta a$), Equation (5.34a) can be simplified to:

$$\frac{k_i}{(k_i)_0}=\frac{[1+\frac{a_j}{(b_m)_j}\Delta\varepsilon_{f\,j}]^{3n_j}}{1-\Delta\varepsilon_{f\,j}} \quad \text{…….……(5.37)}$$

and Equation (5.36a) simplified to:

$$\phi=\sum_{i=x,y}\frac{\frac{(b_m)_i}{a_i}+\Delta\varepsilon_{f\,i}}{1-\Delta\varepsilon_{f\,i}} \quad \text{…….……(5.38)}$$

Additionally if we ignore the difference between the mechanical aperture and hydraulic aperture of cleats, i.e. let n=1 in Equation (5.37), Equation (5.37) becomes:

$$\frac{k_i}{(k_i)_0} = \frac{[1+\frac{a_j}{(b_m)_j}\Delta\varepsilon_{f\,j}]^3}{1-\Delta\varepsilon_{f\,j}} \quad \text{.....(5.39)}$$

If we suppose that cleats and coal matrix are isotropic, Equation (5.39) becomes:

$$\frac{k}{(k)_0} = \frac{\left(1+\frac{a}{b}\Delta\varepsilon_f\right)^3}{1-\Delta\varepsilon_f} \quad \text{.....(5.40)}$$

And Equation (5.38) becomes:

$$\phi = \frac{2\frac{b}{a}+2\Delta\varepsilon_f}{1-\Delta\varepsilon_f} = \frac{\phi_0+2\Delta\varepsilon_f}{1-\Delta\varepsilon_f} \quad \text{.....(5.41)}$$

Equations (5.40) and (5.41) are the same as Equations (3.5) and (3.3) respectively in Chapter 3. Note that $-\Delta\varepsilon_f$ defined here is equal to $\Delta\varepsilon_L$ defined in Chapter 3 since $\Delta b_m = -\Delta a$.

5.6 CALCULATION PROCEDURE OF COUPLED SIMULATION

The explicitly sequential coupled simulation method is used to demonstrate the application of the proposed models. The multiphase fluid flow is simulated with a multidimensional, isothermal equation-of-state (EOS) compositional simulator, GEM© (CMG, 2003) and the geomechanical deformation is calculated with a thermohydromechanical simulator, FLAC3D© (Itasca, 2002). Additional codes are written in order to prepare data in the formats used by the simulators. The whole coupled simulation is managed by AutoMate© and executes automatically. The procedure of coupled simulation is illustrated in Figure 5.3. The calculation sequences of one time step (step i) are indicated with a dotted diamond in the figure and described as following:

(1) Simulate pressures (P), absorbed gas volumes (V_D), water saturation (S_W), and production rates of gas and water (Q_g, Q_W) etc. using GEM©.

(2) Deal with the results from GEM© and prepare the pressures (P) and absorbed gas volumes (V_D) in the format used by FLAC3D© with a self-programmed code.

(3) Calculate new normal and shear stiffnesses of cleats then calculate equivalent moduli and Poisson's ratios with a self-programmed code.

(4) Simulate the changes of stresses and strains due to the changes of pressures and absorbed gas volumes with FLAC3D©.

(5) Estimate the geometric changes of coal then calculate permeability and porosity of cleats with a self-programmed code.

(6) Prepare the data including new porosity and permeability in the format used by GEM© for the following time step with a self-programmed code.

5.7 APPLICATION OF COUPLED SIMULATION

The pressure depletion CBM production with vertical wells is studied here. The presented coupling models and simulation procedure are also applicable for horizontal wells and ECBM recovery process.

5.7.1 Well Models and Basic Data

The well models for simulations are illustrated in Figures 5.4 and 5.5. The well pattern and reservoir simulation model are shown in Figure 5.4. Due to the symmetry the simulation is made on a quarter of the well drainage area thus the rates and cumulative gas production simulated are one fourth of real values of the well. The boundaries for the reservoir simulation area are closed. The well model and the corresponding constraints for the geomechanical simulation are indicated in Figure 5.5. The simulation body is constrained by rollers at the bottom and sides. Thus it cannot move in the directions against the constraints. For example, at the bottom it can move horizontally but cannot move downward.

The basic data for the coupled simulation are listed in Tables 5.1, 5.2 and 5.3 and Figure 5.6. However, before the simulation the initial cleat porosity needs to be corrected in order to keep the consistency of calculations. From the known permeability the initial hydraulic apertures of cleats, $(b_h)_x$ and $(b_h)_y$, are calculated with Equation (5.2) then the corresponding mechanical apertures, $(b_m)_x$ and $(b_m)_y$, are estimated with Equation (5.1). Finally initial cleat porosity (ϕ) is obtained with Equation (5.3).

5.7.2 Grid System

In both deformation and fluid flow simulations, the grids in directions x and y are exactly the same but variable, i.e. smaller near the wellbore and larger near the

boundary with a size ratio of 1.1:1 for adjacent grids. The simulation grids and blocks are shown in Figure 5.7. The grids for the fluid flow simulation are 15(x)×15(y)×1(z) and for the geomechanical simulation are 15(x)×15(y)×16(z), of which one grid is located in the coalbed in direction z. The grid sizes in the overburden are also variable, i.e. smaller near the coalbed and larger near the upper boundary with a size ratio of 1.1:1 for adjacent grids.

5.7.3 Simulation Results

The simulated gas and water rates and cumulative gas and water production are plotted in Figures 5.8 to 5.11. For comparison the results of three simulation modes including the simulation with permeability and porosity coupled, the simulation with permeability coupled only and the simulation with constant permeability and porosity are presented in these figures. The comparison indicates that the results of the coupled simulations are significantly different from that of the simulation with constant porosity and permeability, especially in gas rates and cumulative gas production. However the results from the coupled simulations with and without porosity coupled are close. Thus the influence of porosity coupling may be not considered in coupled simulations, as made by Gu and Chalaturnyk (2005a and 2005b).

The changes in permeability and porosity from the permeability and porosity coupled simulation during production are shown in Figure 5.12 to 5.19. The corresponding grids and blocks are referred to Figure 5.7. These figures illustrate that the most drastic changes of permeability and porosity occur in the areas around the wellbore where permeability and porosity decreased significantly at the beginning of production then recovered gradually and later increased evidently. However in the areas far from the wellbore, permeability and porosity decreased just a little bit at the beginning of production then increased continuously. The results also indicate that in the areas near the wellbore the changes of permeability are anisotropic. As a result, during production permeability is anisotropic even though initial permeability is isotropic. The greatest anisotropy of permeability appeared in Block (3,1) (also in Block (1,3) due to symmetry) where the anisotropy ratio (ky/kx) reached as much as 3.04.

5.8 DISCUSSION

Here the discussion is focused on some important issues of coupled simulations and CBM production, and the limitations of presented models.

5.8.1 Length of Time Step

One importance for explicitly sequential coupled simulation is the length of time step. For simulation, smaller time steps usually need longer calculation time or higher simulation cost but results are generally more accurate. A trade-off between simulation cost and accuracy usually needs to make, especially for large-scale simulations.

For the investigated case, the step number of the coupled calculation, which is controlled by the maximum length of time steps set in GEM©, is proportional to the calculation time or cost. The relationship between the step number of coupled calculations and the maximum length of time steps is shown in Figure 5.20. It shows that when the maximum length of time steps decreases from 400 days to 150 days, the coupling simulation steps or cost increase smoothly. When it decreases from 150 days to 50 days, the coupling calculation steps increase steeply and when it decreases from 50 days to smaller days, the coupling calculation steps increase very quickly.

The influence of the maximum length of time steps on the accuracy of simulation results is illustrated in Figures 5.21 and 5.22. The results of Figure 5.21 show that with the decrease of the maximum length of time steps the calculated gas production increases but the rates of increases decline continuously and the convergence occurs when the maximum length of time step is smaller than 30 days. If the results estimated with the maximum length of time steps of 20 days are the "true" values, when the maximum length of time steps increases from 20 days to 30 days the relative error of the calculated gas rates is less than 1%. If it increases from 20 days to 100 days the relative error is less than 5.3% and to 150 days is less than 8.1%. The results of Figure 5.22 indicate that if the results estimated with the maximum length of time steps of 20 days are the "true" values, when production time is smaller than 1000 days and the maximum length of time steps increases from 20 days to 400 days the relative error of the calculated cumulative gas is less than 4.1%. When the production time is greater than 1000 days but if the maximum length of time step is smaller than 150 days the relative error of the calculated cumulative gas is still less than 4.8%. Therefore if the

maximum length of time steps is smaller than 150 days, the accuracies of simulated gas rates and cumulative gas are all acceptable and reliable for engineering projects.

Based on the above analysis a trade-off is made, i.e. the maximum length of time steps ranging from 150 days to 50 days is efficient and accurate enough for the studied case. Then the maximum length of time steps of 100 days is selected for all simulation results in this study. For other coalbeds a similar study is also needed to make in order to determine a proper length of time steps.

5.8.2 Relation between Permeability and Stresses

The changes of permeability and porosity are complicated due to the changes of in situ conditions such as pore pressures and absorbed gas volumes. For example, for pressure depletion CBM production, in situ stresses will increase due to pressure decreases during production thus cleats are compressed resulting in the decrease of cleat permeability and porosity. On the other hand, with the desorption of methane coal matrix will shrink causing cleat apertures to increase thus permeability and porosity increase. However, the shrinkage of coal matrix will also cause in situ stresses to decrease. Therefore the increase or decrease of permeability and porosity during production depends on the factor that dominates the cleat deformation.

For the investigated case, the changes of porosity and permeability during production in Block (3,1) (referring to Figure 5.7) are compared with the changes of pore pressures and in situ stresses in Figure 5.23. The results indicate that the change of permeability has no monotonic relation with the changes of pore pressures, mean stresses and horizontal (directions x and y) effective stresses. During the whole production time the pore pressure continuously decreases but permeability does not continuously increase or decrease. During a short period of time at the beginning of production (less than 150 days) permeability is reversely related to mean and horizontal stresses, i.e. permeability decreases while mean and horizontal stresses increase. During 600 days to 3000 days permeability and effective stresses in direction x have a reverse relation, i.e. permeability slowly increases while effective stresses slowly decreases, and permeability and effective stresses in direction y all decrease, but mean stresses smoothly increase. During 4000 days to 7300 days permeability increases rapidly but horizontal and mean effective stresses do not change evidently.

The above results conflict with the relation between permeability and effective stresses presented by McKee et al (1988) and Seidle et al (1992):

$$\frac{k}{k_0} = e^{-3c_p \cdot \Delta\sigma'} \quad \text{.....(5.42)}$$

where the change of effective stresses, $\Delta\sigma$', in McKee et al's (1988) model is the change of mean effective stresses while in Seidle et al's (1992) model is the change of the horizontal effective stress. However, no matter which (mean or horizontal) effective stresses are used in Equation (5.42), the relation between the change of effective stresses and permeability is monotonic, i.e. an increase of effective stresses will result in a decrease of permeability and vice versa.

However, the results in Figure 5.23 show that although in situ stresses including mean and horizontal stresses keep relatively stable during 4000 days to 7300 days the permeability still quickly increases. The conflict of this result with Equation (5.42) comes from that in the formulation of Equation (5.42) the change of stresses was considered as the only cause to the change of permeability. However, during CBM production due to desorption of methane coal matrix shrinks. Then a part of shrinkage strains will convert to the relaxation or decrease of in situ stresses that may cancel out the increase of in situ stresses due to pore pressure decline. Thus the in situ stresses do not change. But the other part of shrinkage strains will result in an increase of cleat apertures thus an increase of permeability.

Owing to the complicated relation between permeability and pore pressures (and in situ stresses), as shown in Figure 5.23, the analytical CBM permeability models applied Equation (5.42) in the formulation, such as the models presented by Shi and Durucan (2003) and Gilman and Bechie (2000), remain questionable.

5.8.3 Relation between Permeability and Porosity

The relation between permeability and cleat apertures is fundamental for predicting the change of permeability during production. The most common used and widely accepted relation in petroleum industry is the one in which the ratio of permeability to one-third power, $(k/k_0)^{1/3}$, is equal to the porosity ratio (related with apertures), ϕ/ϕ_0, i.e.

$$\left(\frac{k}{k_0}\right)^{1/3} = \frac{\phi}{\phi_0} \quad \text{.....(5.43)}$$

This relation was supported by the experimental results measured by Jones, Jr. (1975). Using fractured rocks (Portland cement, Carthage marble, Smackover limestone, and Ellenburger dolomite) Jones, Jr. (1975) found that the relation between ϕ/ϕ_0 (estimated from hydraulic apertures) and $(k/k_0)^{1/3}$ was a straight line.

However one should note that Equation (5.43) is based on the assumption that fractures are isotropic and the anisotropy in apertures or permeability is ignored. This assumption is generally not creditable for most coalbeds where the anisotropy ratio of permeability may be as high as 17:1 according to the results of field well tests (Koenig and Stubbs, 1986). In addition this relation is only suitable to hydraulic apertures since fractures were considered as smooth plate channels and the difference between hydraulic and mechanical apertures was not considered in the formulization. The results of Jones, Jr. (1975) were also based on hydraulic apertures. Therefore the reliability of the analytical CBM permeability models, such as the models of Seidle and Huitt (1995), Palmer and Mansoori (1998), and Chkatamarla et al (2004), is also questionable because they all directly applied Equation (5.43) in the formulation without considering cleat anisotropy and the difference between mechanical apertures and hydraulic apertures.

The experimental results of Somerton et al (1975) are the few who studied the relation between permeability and porosity for coalbeds and their results show that Equation (5.43) is not applicable for coalbeds. With the Virginia Pocahontas coal Somerton et al (1975) found that $(k/k_0)^{1/3}$ plotted against the log of stresses was not the same straight line as ϕ/ϕ_0 and departed far from ϕ/ϕ_0. In their study the ratio of porosity was based on mechanical apertures estimated from the compressibility test data. However, if we assume the cleats are homogenous and isotropic before and after cleats deformed, from Equation (5.1) one can obtain that the relation between $(k/k_0)^{1/6}$ and ϕ/ϕ_0 (based on mechanical apertures) should be a straight line. Using the Somerton et al's (1975) data one can find that the lines of $(k/k_0)^{1/6}$ and ϕ/ϕ_0 against the logarithm of stresses are much closer comparing with the lines of $(k/k_0)^{1/3}$ and ϕ/ϕ_0. This indicates that for coalbeds the power of 1/6 is more applicable than the power of 1/3. The remaining errors are probably caused by the sample diversities (since different samples were used for porosity and permeability measurements) and the anisotropies in cleats and deformations.

Due to the limitations in quantity and accuracy of experimental results, it is not clear at this moment that k/k_0 to which power (1/6, 1/3 or other) is the best to describe the correlation of $(k/k_0) \sim \phi/\phi_0$ for coalbeds. But this does not affect the

generality of the presented models since the power, n, in Equations (5.34a) and (5.34b) can be treated as a variable. The value of n is equal to two if the mechanical aperture is greater than the hydraulic aperture otherwise equal to one according to Barton et al (1985). If a more accurate or reliable value is obtained from further studies for coalbeds it should be applied to Equations (5.34a) and (5.34b).

5.8.4 Influence of Mechanic and Hydraulic Apertures

The comparison of the influence of distinguishing mechanical apertures with hydraulic apertures on simulated results is difficult because for the same initial permeability the two calculation modes (distinguishing aperture difference or not) have different initial porosity. Although porosity is estimated from Equation (5.3), the aperture used in the case of identical apertures is actually equal to the hydraulic aperture in the case of different apertures where the mechanical apertures are calculated from the hydraulic apertures with Equation (5.1). Thus the initial hydraulic apertures in both modes are the same but the initial mechanical apertures and porosity in both cases are different.

For the studied coalbed initial isotropic permeability is 4 mD thus the initial porosity estimated for the "identical apertures" case is 0.986% while for the "different apertures" case is 0.2348%. The results for these two calculation modes are compared in Figure 5.24 and 5.25. The figures indicate that the results from different calculation modes are significantly different. However, due to the difference of initial porosity it is difficult to estimate how much is attributed to the calculation mode and how much is owing to the difference in initial porosity.

5.8.5 Influence of Initial Water Saturation

Whether a well produces water or not and how much water it produces are important for CBM developments. With the same data set listed in Tables 5.1-5.3 except initial water saturation, coupled simulations are made with initial water saturation of 0.1%, 50% and 100% in cleats and the results are compared in Figure 5.26 to 5.29. The results show that with the decrease of initial water saturation gas rates increase significantly in the early production stage while decrease in the late production stage. The cumulative gas production increases with the decrease of initial water saturation during the whole production time of 20 years. The water rates and cumulative water production decrease with the decrease of initial water saturation. The results indicate that initial water

saturation not only influences the cost to handle the produced water but also the cumulative gas production and final recovery. Thus the development of coalbeds with lower initial water saturation would produce a better economic result even not considering the saving on the cost of dealing with produced water.

5.8.6 Limitations

The limitations of the proposed permeability and porosity coupling models are related to the assumptions in the formulation. One limitation is due to the assumption that face cleats are orthogonal to butt cleats. This is generally valid for most coalbeds. But in some cases cleats may be modified by tectonic deformations thus cleat sets may be not normal to each other. Another limitation is from the assumption of elastic deformation of cleats. Although this assumption is made in all available models for CBM production, if cleats are not strong enough the asperity degradation and permanent damages may occur in loading due to pressure drops, such as in drilling and completion. Then the aperture of cleats (corresponding to porosity and permeability) will not be recovered after the load is removed.

Other limitations are related to the used simulators. One limitation is in the deformation simulator, FLAC3D©. For the deformation simulation of orthogonal anisotropic elastic continuum media, FLAC3D© only has Terzaghi's (1943) effective stresses mode and Biot's effective stress mode is not available at this moment. Another limitation is in the fluid flow simulator, GEM©. The coupling (permeability updating) steps of simulations are limited to 255 steps because when preparing outputs GEM© needs to simultaneously open all data files that are saved in each coupling step but the maximum number of data files that GEM© can operate is 255. These limitations will be removed with the improvements of these simulators.

5.9 SUMMARY

From the study of this chapter we summarize as following:

(1) New porosity and permeability coupling models used in coupled simulations have been established for CBM and ECBM recovery. The models consider the influences of the discontinuity and anisotropy of coal. With these models the anisotropies in permeability, the matrix shrinkage/swelling due to gas desorption/adsorption, mechanics

parameters and the thermal expansion/contraction due to temperature changes can be simulated in coupled simulations.

(2) Due to considering the changes of permeability and porosity during CBM production the results using the proposed coupled simulation procedure and models are significantly different from the simulation results using constant permeability and porosity. The gas rates and cumulative gas production of the former are usually larger than those of the later.

(3) Permeability and porosity change drastically in the areas near to wellbores during CBM production. Although initial permeability is assumed to be isotropic the deformation of coal can result in the anisotropy of permeability. The anisotropic ratio of permeability reached as much as 3.04 in the investigated case.

(4) The explicitly sequential coupled simulation for CBM production is reliable and affordable if a proper trade-off is made between the simulation cost and simulation accuracy.

(5) Permeability and porosity have no monotonic relation with pore pressures and mean and horizontal effective stresses for CBM production. The application of Equation (5.42) to formulate CBM analytical permeability models is questionable and not reliable.

(6) Due to neglecting the cleat anisotropy and the difference between mechanical apertures and hydraulic apertures, the relation of Equation (5.43) and the analytical permeability models based on this relation in the formulation are questionable. The power of 1/6 in the relation between permeability ratio and porosity ratio shows more applicable than the power of 1/3 for coalbeds.

(7) Initial water saturation influences not only the cost to handle produced water but also the cumulative gas production and final gas recovery. The development of coalbeds with lower initial water saturation would produce a better economic result even not considering the saving on the cost of dealing with produced water.

Table 5.1: Basic Well Parameters

Top depth of coalbed (m)	900
Seam thickness (m)	10
Drainage area of well (m^2)	850×850
Well radius (m)	0.1
Seam pressure (kPa)	8754.3
Seam temperature (^oC)	30.5
Cleat spacing (m)	0.02
Cleat porosity (decimal)	0.001
Cleat permeability (mD)	4
Matrix porosity (decimal)	0.005
Matrix permeability (mD)	0.001
Water density (kg/m^3)	990
Water viscosity (cp)	0.644
Water saturation in cleats (decimal)	1
Compressibility of coal matrix (1/kPa)	1.45E-07
Compressibility of water (1/kPa)	5.80E-07
Reference pressure of compressibility (kPa)	8500
Langmuir volume (m^3/ton)	22.653
Reciprocal of Langmuir pressure (1/kPa)	2.417×10^{-4}
Methane sorption time (day)	100
Coefficient of matrix shrinkage (g/ml)	4.6×10^{-4}

Table 5.2: Mechanics Parameters

Parameters	Overburden	Coal Matrix
Density (kg/m^3)	2300	1542
Young's modulus (MPa)	1000	3399.2
Poisson's ratio	0.3	0.32
Compressive strength (MPa)		60
Material constant A defined by Equation (5.5a)		2
	Cleats	
	Intersecting x	**Intersecting y**
Initial normal stiffness (MPa/m)	101976	101976
Maximum shear stiffness of cleat (MPa/m)	25494	25494
Shear dilation angle (°)	10	10
Peak shear displacement (mm)	0.1	0.1
Original JRC	5	5
Type of cleat	matched cleat	matched cleat
Maximum cleat closure/Initial mechanical cleat width	0.6	0.6

Table 5.3: Production Constraints

Water production constraint	
Time (day)	0~17
Minimum BHP (kPa)	101.325
Maximum water rate (m^3/day)	10
Gas production constraint	
Time (day)	18~7300
Minimum BHP (kPa)	275

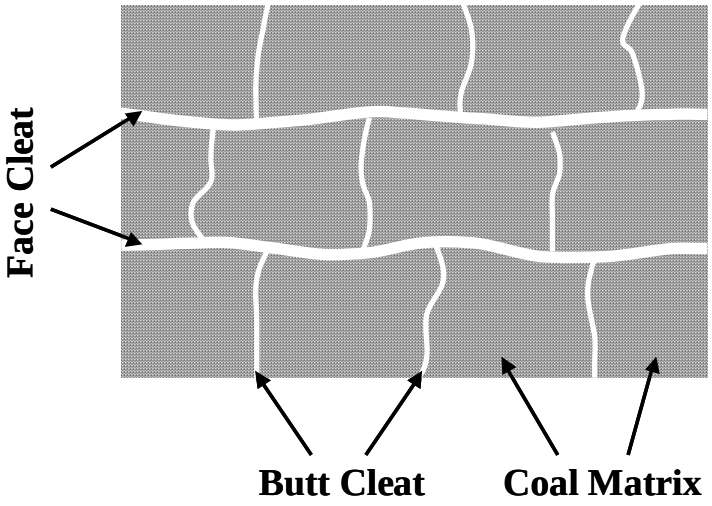

Figure 5.1: Ideal Pore Structure of Coalbed
(modified from Davidson et al, 1995)

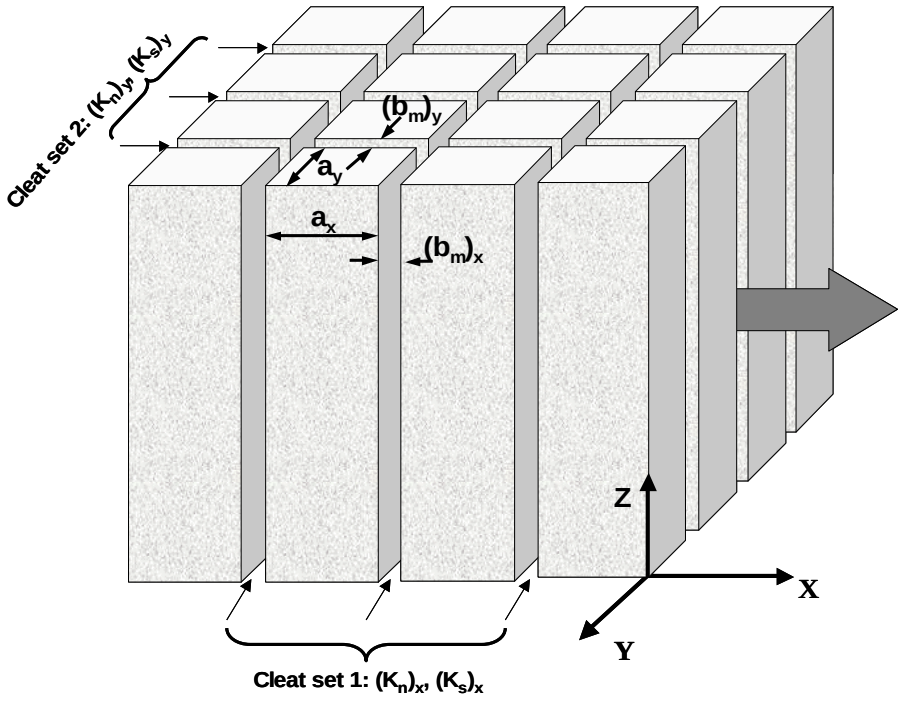

Figure 5.2: Fracture System with Matchstick Matrix Blocks
(modified from Seidle et al, 1992)

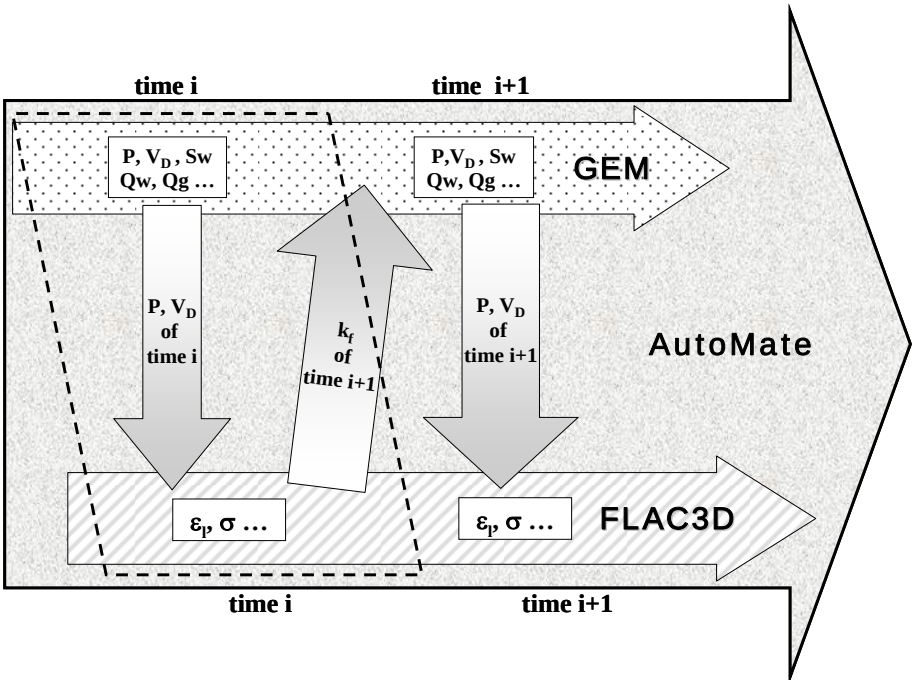

Figure 5.3: Procedure of Reservoir and Geomechanical Coupled Simulation

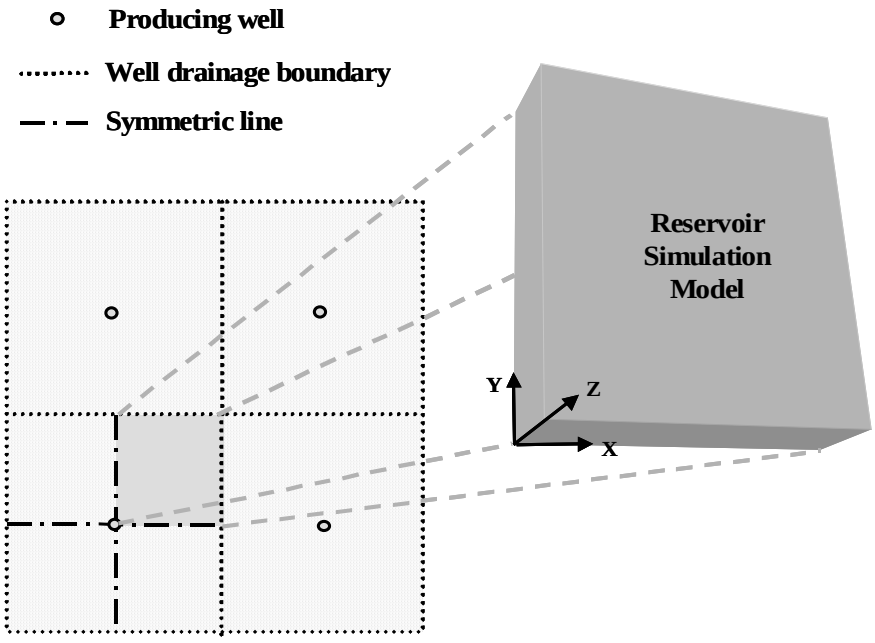

Figure 5.4: Model of Reservoir Simulation

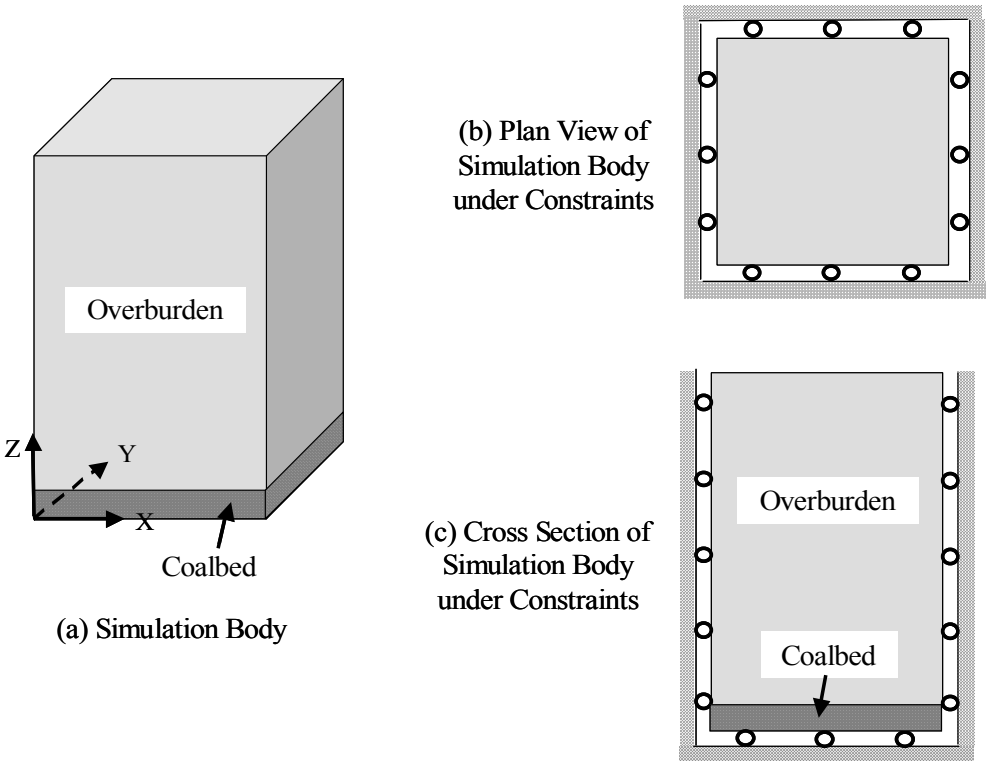

Figure 5.5: Model of Geomechanical Simulation

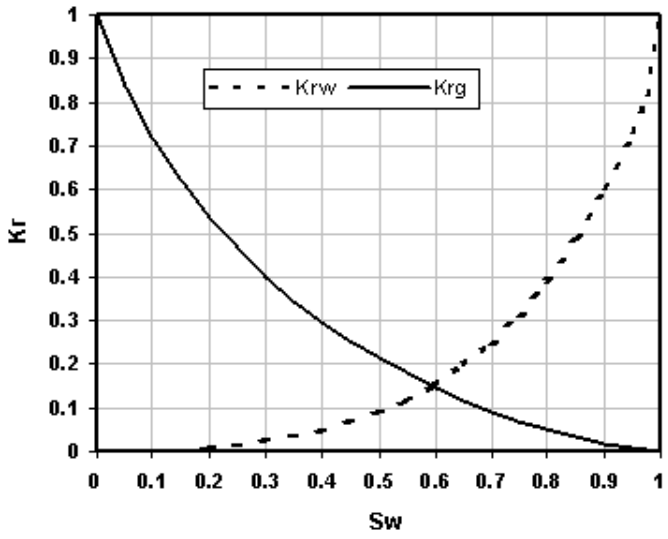

Figure 5.6: Gas and Water Relative Permeability (Gash et al, 1993)

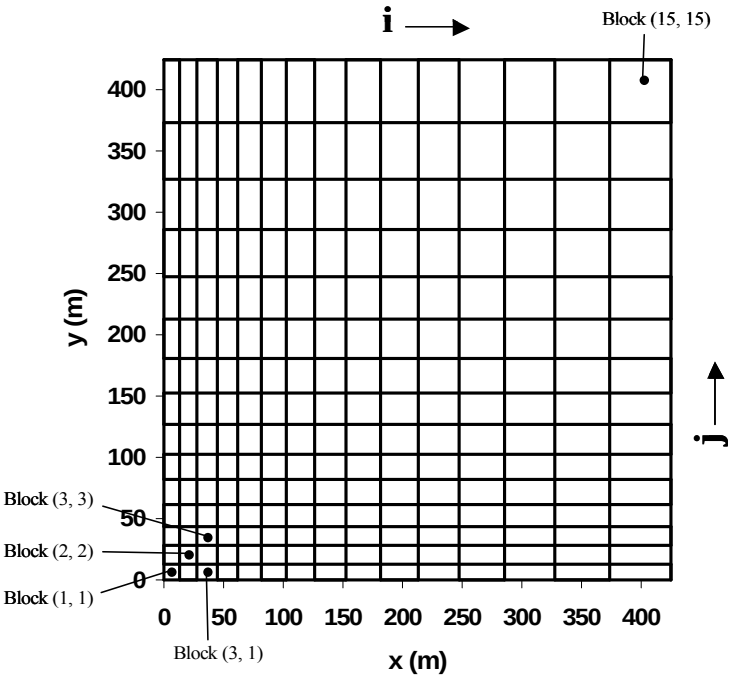

Figure 5.7: Grids and Blocks in Coalbed

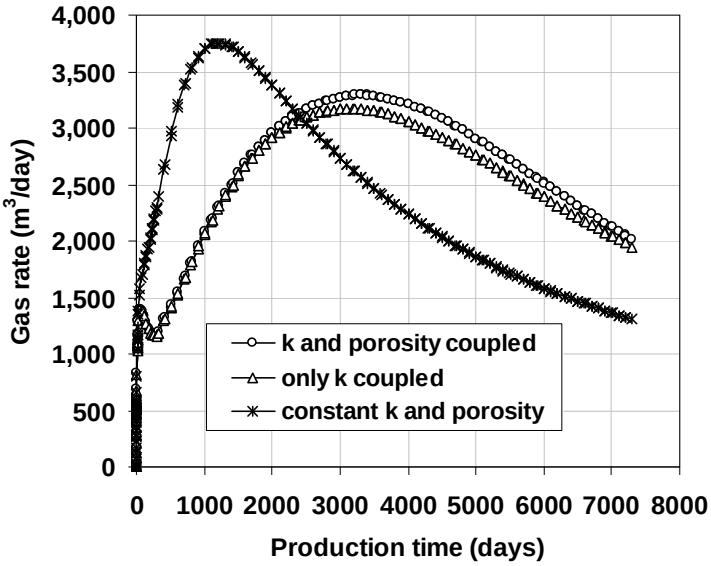

Figure 5.8: Comparison of Gas Rates from Different Simulation Modes

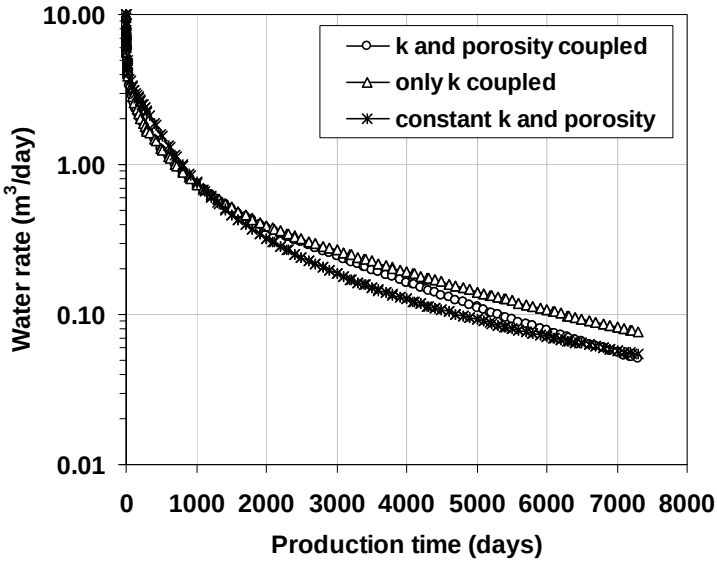

Figure 5.9: Comparison of Water Rates from Different Simulation Modes

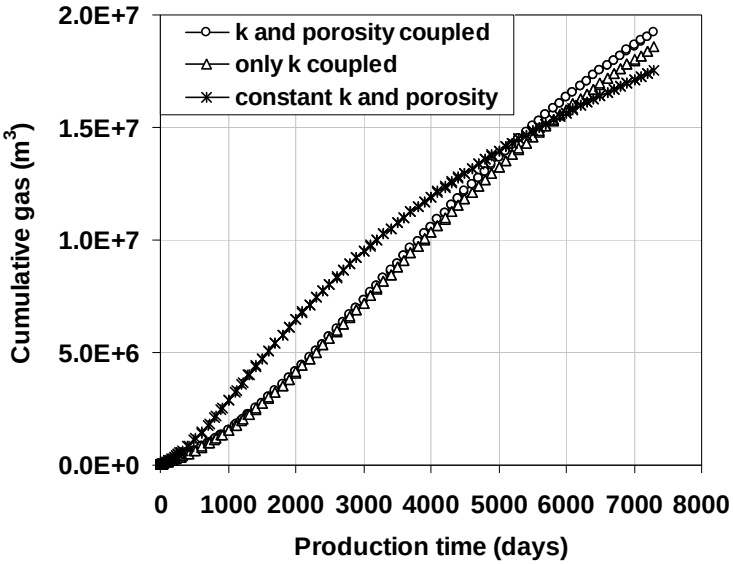

Figure 5.10: Comparison of Cumulative Gas Production from Different Simulation Modes

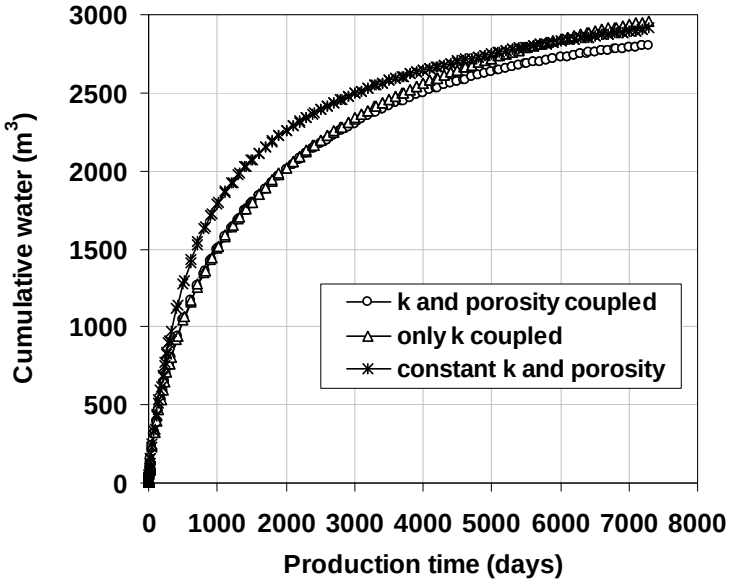

Figure 5.11: Comparison of Cumulative Water Production from Different Simulation Modes

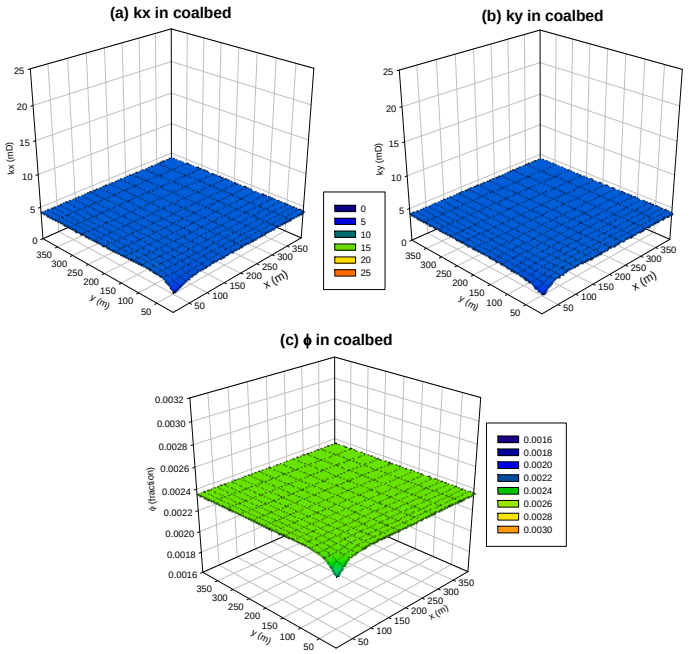

Figure 5.12: Permeability and Porosity in Coalbed at 18 Production Days

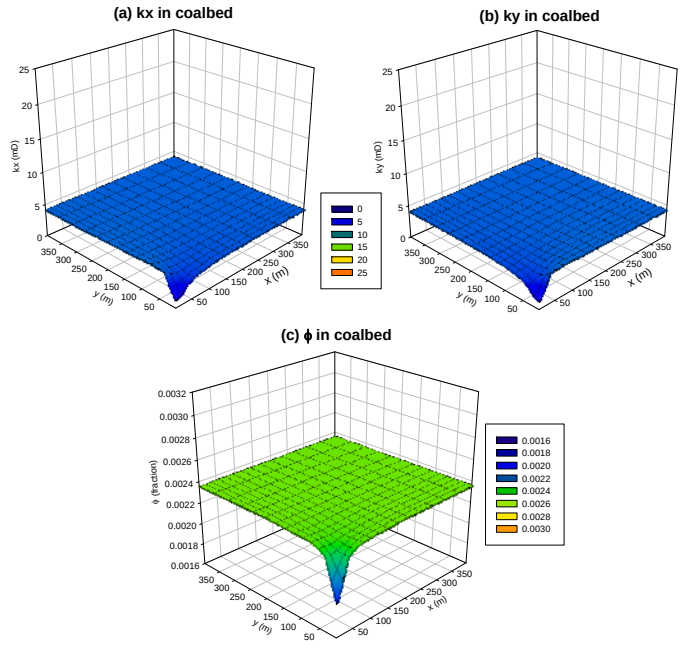

Figure 5.13: Permeability and Porosity in Coalbed at 112 Production Days

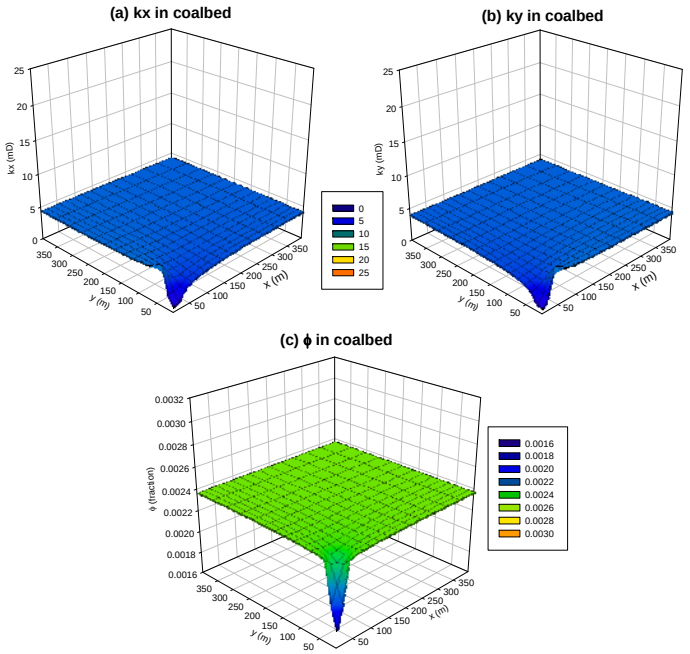

Figure 5.14: Permeability and Porosity in Coalbed at 300 Production Days

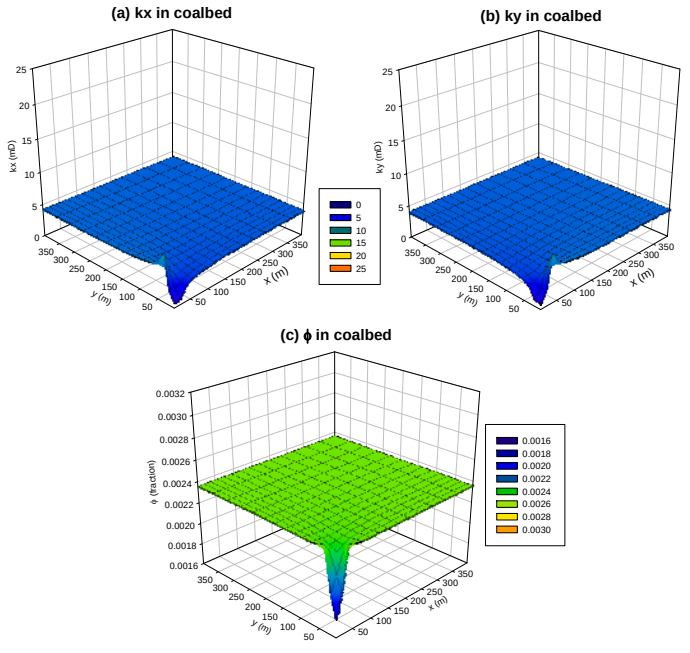

Figure 5.15: Permeability and Porosity in Coalbed at 1020 Production Days

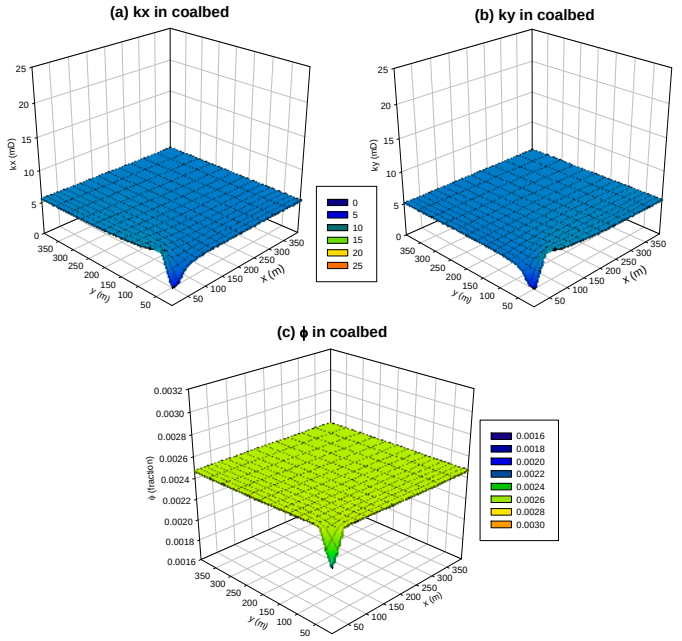

Figure 5.16: Permeability and Porosity in Coalbed at 3000 Production Days

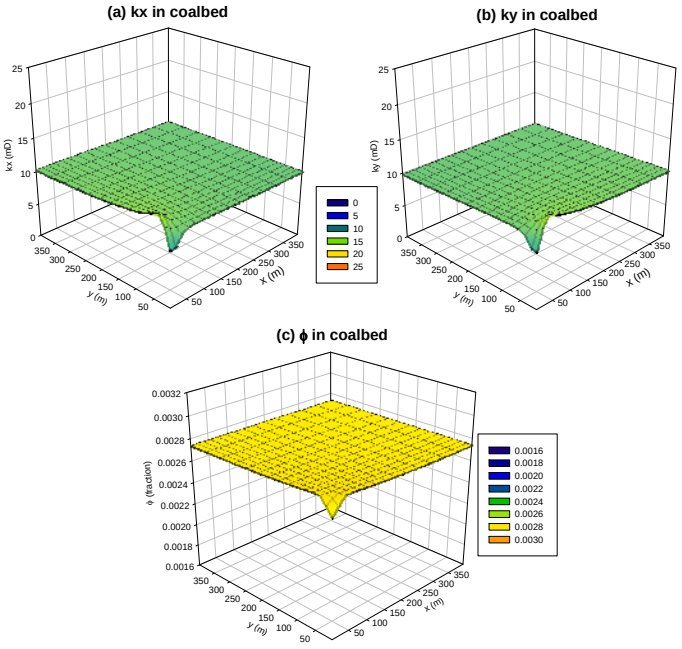

Figure 5.17: Permeability and Porosity in Coalbed at 5000 Production Days

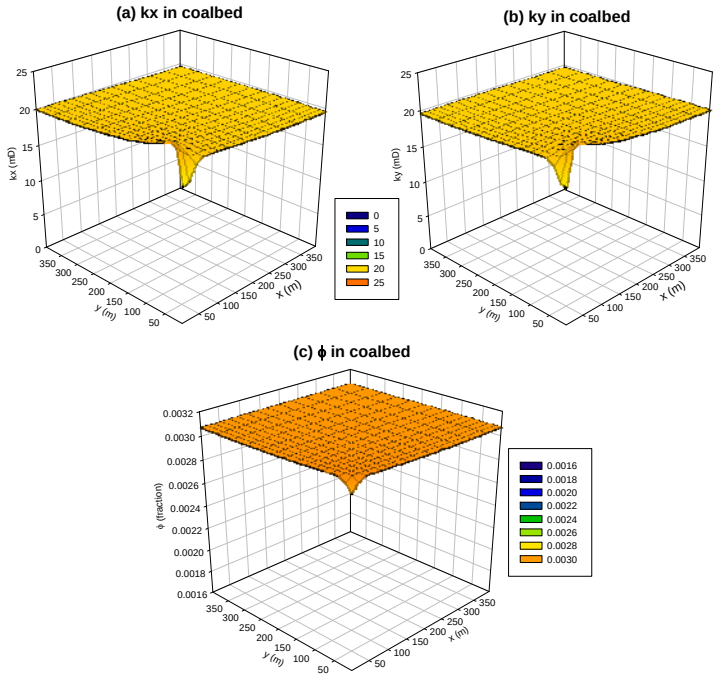

Figure 5.18: Permeability and Porosity in Coalbed at 7300 Production Days

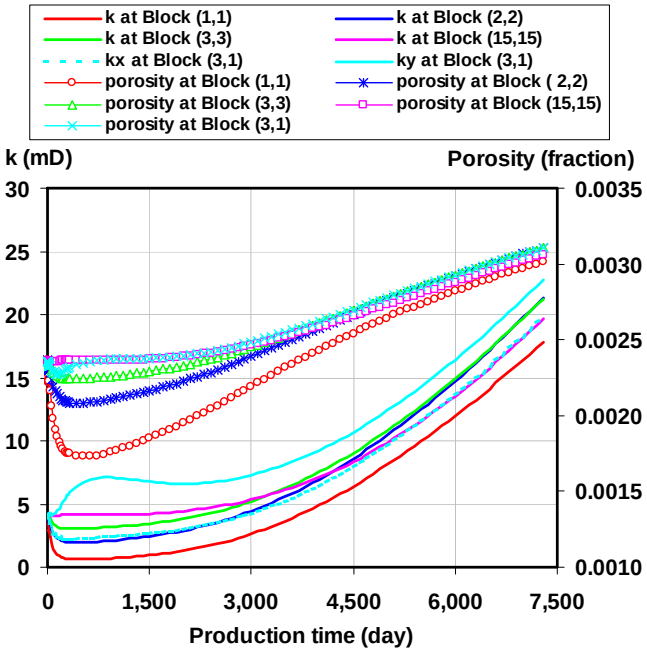

Figure 5.19: Permeability and Porosity Changes during Production

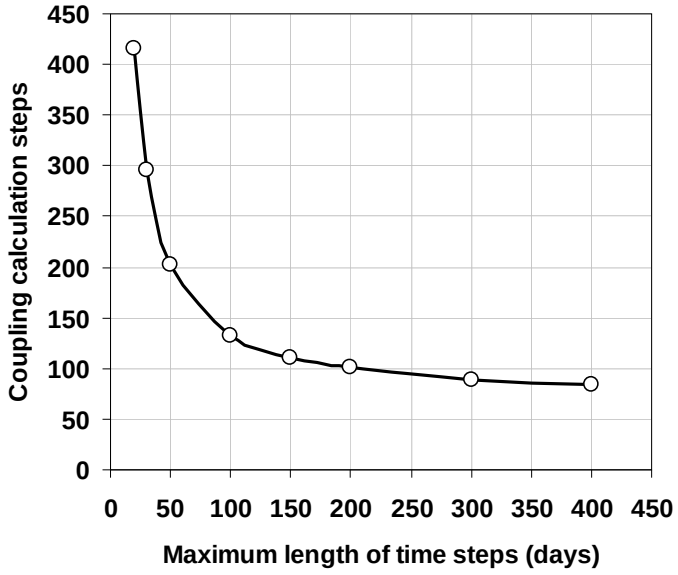

Figure 5.20: Change of Coupling Calculation Steps with Maximum Length of Time Steps

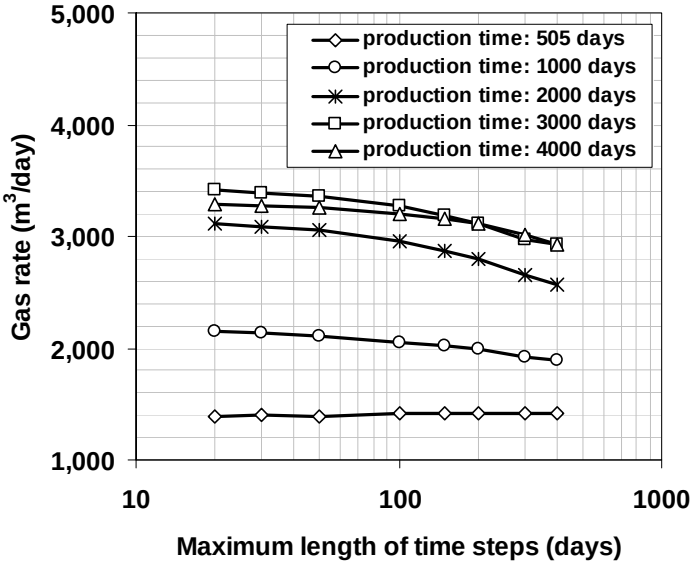

Figure 5.21: Influence of Maximum Length of Time Steps on Calculated Gas Rates

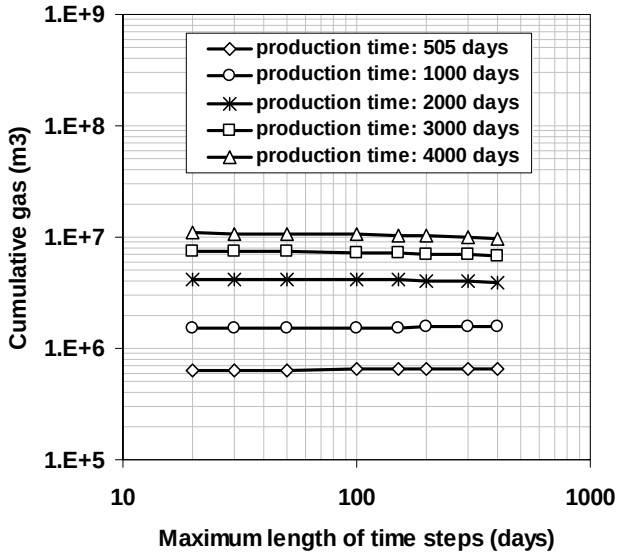

Figure 5.22: Influences of Maximum Length of Time Steps on Calculated Cumulative Gas Production

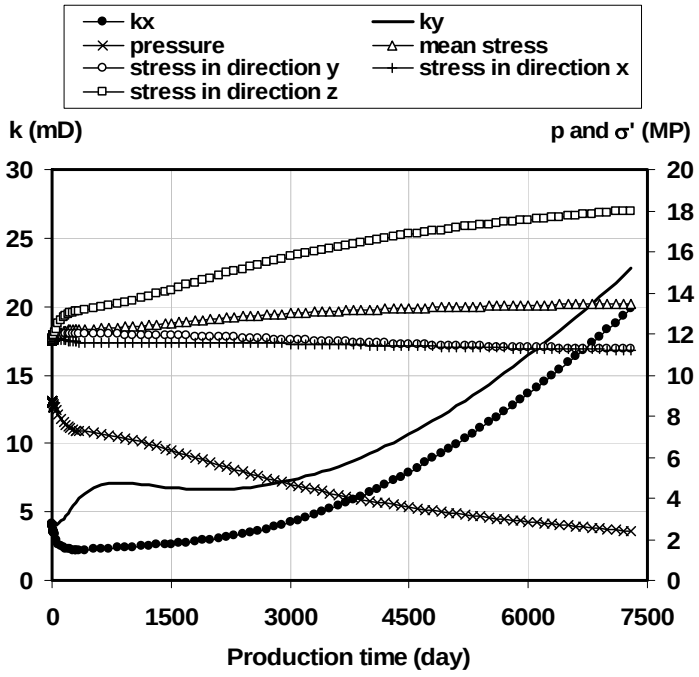

Figure 5.23: Comparison of Changes in Permeability, Porosity, Pressures and Stresses in Block (3,1)

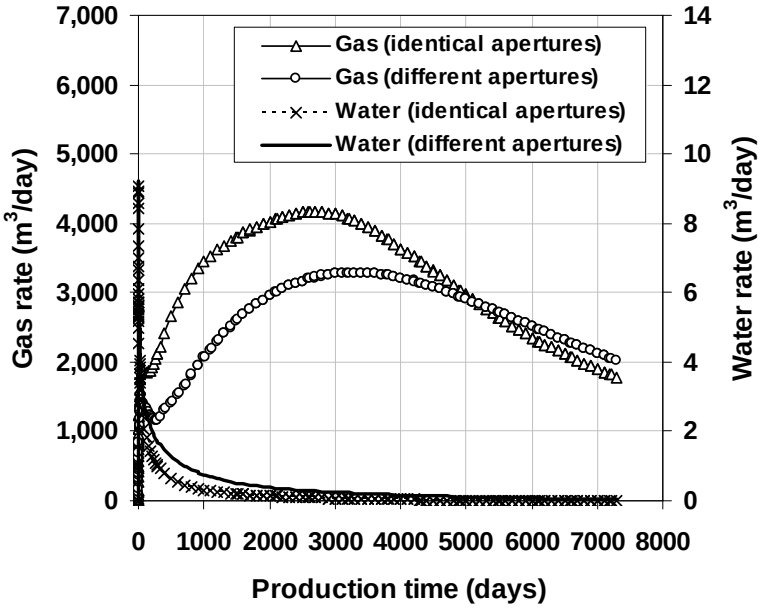

Figure 5.24: Comparison of Gas and Water Rates from Modes of Different and Identical Apertures

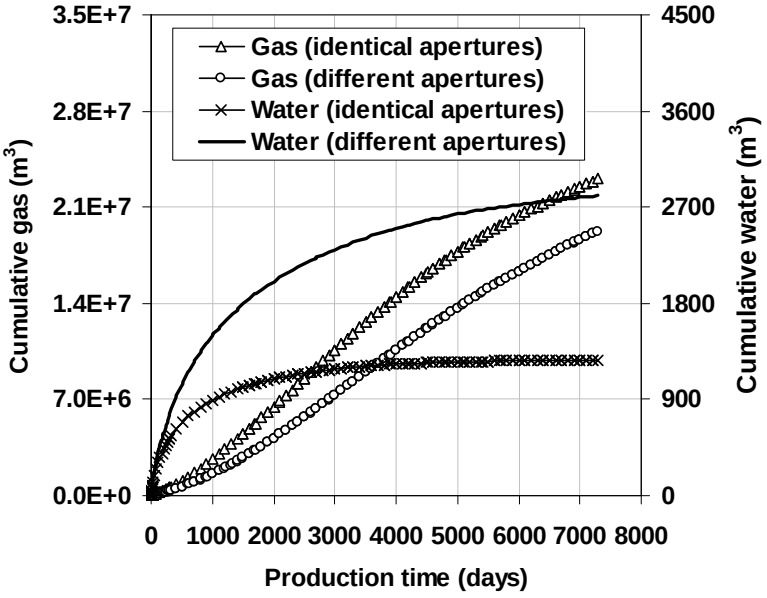

Figure 5.25: Comparison of Cumulative Gas Production from Modes of Different and Identical Apertures

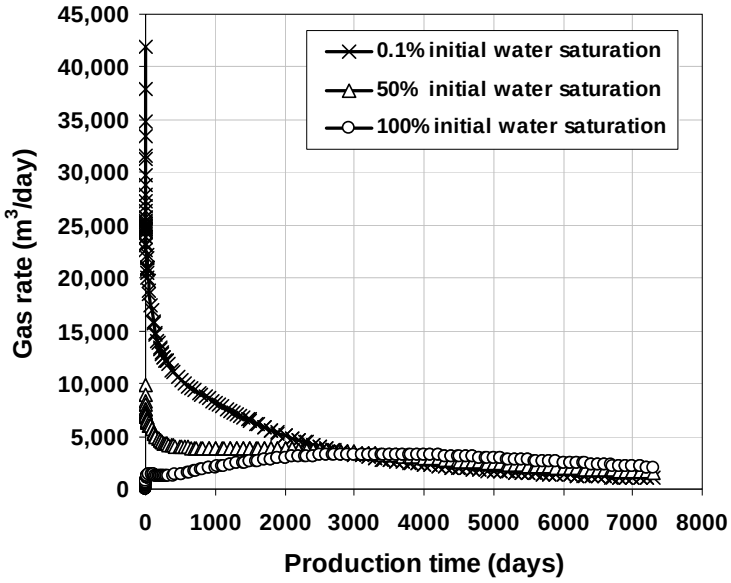

Figure 5.26: Influence of Initial Water Saturation on Gas Production Rates

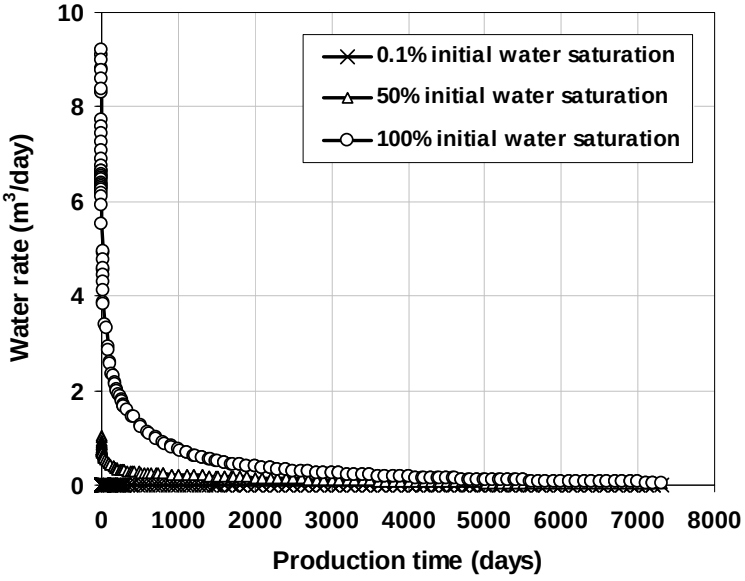

Figure 5.27: Influences of Initial Water Saturation on Water Production Rates

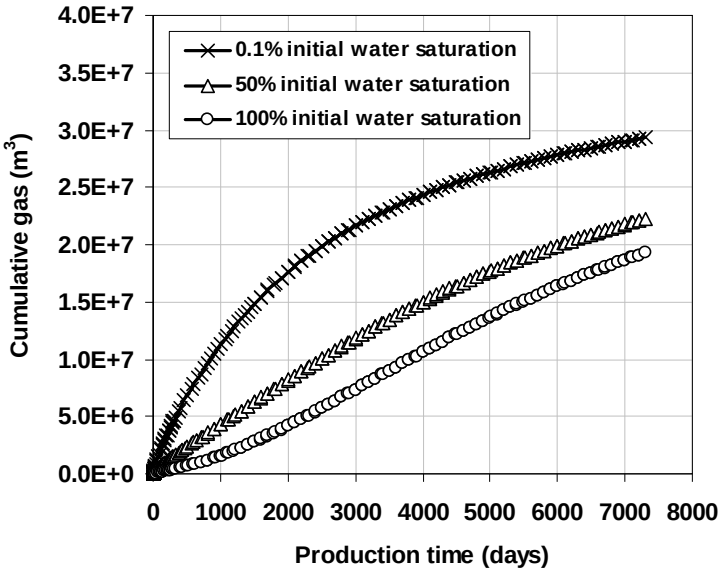

Figure 5.28: Influences of Initial Water Saturation on Cumulative Gas Production

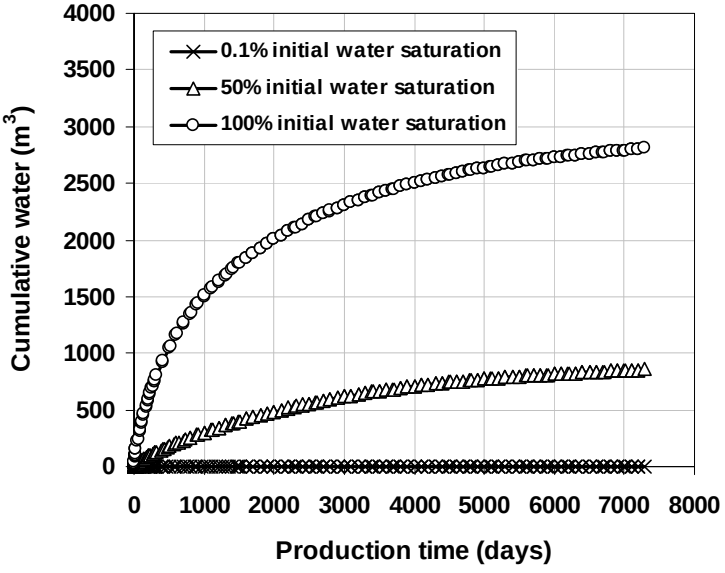

Figure 5.29: Influences of Initial Water Saturation on Cumulative Water Production

6 SIMULATION OF LAB COAL DEFORMATION TESTS

6.1 INTRODUCTION

A comprehensive review made by Gu and Chalaturnyk (2005a) indicated that the permeability of coalbeds (i.e. the permeability of cleats or fractures since matrix is almost impermeable) is the most important parameter for pressure depletion coalbed methane (CBM) production and enhanced coalbed methane (ECBM) recovery. However, the permeability of a coalbed is not constant but varies drastically during production due to the changes of stresses and/or strains that result from the alternations of in situ conditions such as pressures, gas desorption or adsorption, and temperature. In general, a decrease of pressures causes an increase of effective stresses and cleat compression or closure thus a decrease of permeability. Concurrently, the decrease of pressures initiates gas desorption from coal resulting in the shrinkage of coal matrix and the widening or expansion of cleat apertures thus an increase of permeability. Field results have shown that the permeability of coalbeds decreases with the increase of minimum effective stress, corresponding to the increase of coalbed depths (Enever et al, 1999). Mavor and Vaughn (1998) illustrated that the permeability of three wells increased 2.7 to 7 times after produced for 3 to 4 years from field well tests. The results of van der Meer and Fokker (2003) indicated that the permeability of a coalbed decreased from 3.65 mD to 0.985 mD due to the injection of CO_2. Due to its significant influences on production, the dynamic change of permeability should be considered in the prediction and evaluation simulations of CBM and ECBM processes.

There are two types of permeability models that can be used to consider the influence of permeability changes during production in simulations, i.e. analytical permeability models and permeability coupling models. In this chapter, a comprehensive review of analytical permeability models will be made and their limitations discussed. Then a model of coal deformation (i.e. the equivalent elastic medium model) is validated by means of numerically simulating the deformation of a coal specimen under uniaxial compression in a vacuum and under the axial constraint condition during CO_2 adsorption. The simulation results predicted with

---

A version of this chapter has been published. Gu, F. and Chalaturnyk, R.J., 2006. Journal of Canadian Petroleum Technology, 45(10):52-62.

two representative analytical permeability models and the discontinuum medium permeability coupling model are also compared.

6.2 ANALYTICAL PERMEABILITY AND POROSITY MODELS

Analytic models can be classed into empirical models and theoretical models. The former includes the models of Somerton et al (1975), Harpalani and McPherson (1985), Gray (1987), Puri and Seidle (1991), and Durucan et al (1993). They were obtained by analyzing experimental results using the regression analysis method, and represented specific coal specimens and corresponding in situ stress ranges. The empirical nature restricts the general applicability in other coalbeds, thus we will not discuss them here. Our further discussions will focus on theoretical models.

6.2.1 Basic Permeability and Porosity Relations

As a background for subsequent discussions, the basic permeability and porosity relations used in the formulations of analytical permeability and porosity models are provided below.

According to Mckee and Hanson (1975), the permeability and porosity of media containing a homogenous fracture (cleat) set have a relationship of:

$$k \propto \frac{\phi^3}{(1-\phi^2)} \quad \text{.....(6.1a)}$$

If porosity is of an order of 1%, from Equation (6.1a) the following equation can be derived:

$$\frac{k}{k_0} = \left(\frac{\phi}{\phi_0}\right)^3 \quad \text{.....(6.1b)}$$

Assuming coalbeds or coal seams as a matchstick fracture system (illustrated in Figure 6.1) and cleats or fractures as homogeneous and smooth plate channels, porosity and permeability can be expressed as (Van Golf-Racht, 1982d):

$$\phi = \frac{2b}{a} \quad \text{.....(6.2a)}$$

$$k = \frac{1}{24} b^2 \phi = \frac{b^3}{12a} \quad \text{..... (6.2b)}$$

6.2.2 Models Considering Pressure Change

Based on Equation (6.1a), Mckee et al (1988) formulated porosity and permeability models of coalbeds as:

$$\frac{\phi}{\phi_0} = \frac{e^{-\bar{c}_p \cdot \Delta\sigma'}}{1-\phi_0(1-e^{-\bar{c}_p \cdot \Delta\sigma'})} \quad \text{.....(6.3a)}$$

$$\frac{k}{k_0} = \frac{e^{-3\bar{c}_p \cdot \Delta\sigma'}}{1-\phi_0(1-e^{-\bar{c}_p \cdot \Delta\sigma'})} \quad \text{.....(6.3b)}$$

If porosity is of an order of 1%, Equation (6.3b) can be simplified to:

$$\frac{k}{k_0} = e^{-3\bar{c}_p \cdot \Delta\sigma'} \quad \text{.....(6.3c)}$$

Based on the matchstick fracture (cleat) system, Seidle et al (1992) presented a similar model of permeability as Equation (6.3b) for the experimental hydrostatic stress condition. In the model, the change of effective stress was replaced by the change of hydrostatic stress.

6.2.3 Models Considering Shrinkage/Swelling

On the basis of the matchstick fracture (cleat) system, Seidle and Huitt (1995) presented an equation to predict the change of porosity due to shrinkage/swelling:

$$\frac{\phi}{\phi_0} = 1 + (1 + \frac{2}{\phi_0})\beta_D V_m (\frac{b' p_0}{1+b' p_0} - \frac{b' p}{1+b' p}) \quad \text{.....(6.4)}$$

The change of permeability is computed with Equation (6.1b).

From Equations (6.2a) and (6.2b), Harpalani and Chen (1995) formulated permeability and porosity models due to methane desorption based on the matchstick fracture (cleat) system as:

$$\frac{\phi}{\phi_0} = \frac{1+2 \cdot l_m^* \cdot \Delta p / \phi_0}{1-l_m^* \cdot \Delta p} \quad \text{.....(6.5a)}$$

$$\frac{k}{k_0} = \frac{(1+2 \cdot l_m^* \cdot \Delta p / \phi_0)^3}{1-l_m^* \cdot \Delta p} \quad \text{.....(6.5b)}$$

6.2.4 Models Considering Both Pressure Change and Shrinkage/Swelling

In formulating this type of analytical models, the principle of superposition was applied to strains or stresses in order to consider the influences of pressure changes and the shrinkage/swelling of coal matrix due to gas desorption/adsorption. The interaction between stresses and strains was neglected. Models of this type could be divided into two groups: the models of superposing strains and the models of superposing stresses.

6.2.4.1 Models of Superposing Strain

Sawyer et al (1990) presented a model to calculate the change of porosity as:

$$\phi = \phi_0[1 + c_p \Delta p] - c_m^{'}(1-\phi_0)(\tfrac{\Delta p_m}{\Delta C_m}) \cdot \Delta C \quad \text{……..……(6.6)}$$

The change of permeability is calculated with Equation (6.1b).

Levine (1996) calculated the width of a deformed fracture by:

$$b = b_0 + \Delta\varepsilon_{LP} \cdot s + \Delta\varepsilon_{LD} \cdot s \quad \text{…….(6.7)}$$

The new permeability is calculated with Equation (6.2b).

Palmer and Mansoori (1998) derived a model to calculate the change of porosity as a function of pore pressures:

$$\tfrac{\phi}{\phi_0} = 1 + \tfrac{c_m^{''}}{\phi_0}\Delta p + \tfrac{\varepsilon_V}{\phi_0}(\tfrac{K}{M} - 1)(\tfrac{\beta p}{1+\beta p} - \tfrac{\beta p_0}{1+\beta p_0}) \quad \text{……...(6.8a)}$$

where c_m" was defined as: c_m"=1/M + [K/M+f-1]·c_s. Ignoring matrix compressibility, Mavor and Vaughn (1998) simplified Equation (6.8a) to:

$$\tfrac{\phi}{\phi_0} = 1 + c_f \Delta p + \tfrac{\varepsilon_V}{\phi_0}(1 - \tfrac{K}{M})(\tfrac{p_0}{p_0 + p_\varepsilon} - \tfrac{p}{p + p_\varepsilon}) \quad \text{…….……...(6.8b)}$$

where c_f is defined as:

$$c_f = \tfrac{1}{\phi_0 \cdot M} \quad \text{……..…….…….(6.9)}$$

The change of permeability is also calculated by Equation (6.1b).

Considering the influence of multiple absorptive gases Chikatamarla et al (2004) presented the following model to predict porosity change of cleats:

$$\phi - \phi_0 = \tfrac{1}{M}\Delta p + (\tfrac{K}{M} - 1)\left\{\sum_{i=1}^{i=n}(\beta_D)_i[(V_D)_i - (V_{D0})_i]\right\} \quad \text{……...…...(6.10)}$$

The change of permeability is calculated with Equation (6.1b) as well.

6.2.4.2 Models of Superposing Stress

In formulating this kind of models, it is assumed that coalbeds are subject to a constant overburden and undergo uniaxial (vertical) deformation, i.e. horizontal strains are assumed to be zero.

Similar to the procedure of Seidle et al (1992), Gilman and Bechie (2000) proposed a permeability model similar to Equation (6.3c):

$$\frac{k}{k_0} = e^{-3\Delta\sigma_x / E_F} \quad \text{……..…(6.11a)}$$

Using Terzaghi's effective stress formula (Terzaghi, 1943), the change of horizontal effective stresses due to the changes of pressures and the absorbed gas volume is estimated with:

$$\Delta\sigma_x = -\frac{\upsilon}{1-\upsilon}\Delta p + \frac{E}{1-\upsilon} c_m \cdot \Delta m \quad \text{.....(6.11b)}$$

Shi and Durucan (2003) formulated a model to predict the change of horizontal effective stresses during production as:

$$\Delta\sigma_x = -\frac{\upsilon}{1-\upsilon}\Delta p + \frac{E}{1-\upsilon}\frac{\varepsilon_V}{3}\left(\frac{p}{p-p_\varepsilon} - \frac{p_0}{p_0-p_\varepsilon}\right) \quad \text{.....(6.12)}$$

The change of permeability is calculated by Equation (6.3c).

6.2.5 Comments to Analytical Models

The main advantage of analytical models is their easy application in present reservoir simulators with minor code changes. However, these models have some limitations due to the assumptions and simplifications made in the formulations, as discussed below.

(1) The permeability of coalbeds was assumed to be isotropic throughout the production life.

This assumption implies initial permeability and the change of permeability are all isotropic. Nevertheless, due to the significant difference between butt cleats and face cleats, initial permeability is usually not isotropic in coalbeds. Based on the results of field well tests, Koenig and Stubbs (1986) reported the anisotropy ratio of permeability in the bedding plane was as high as 17:1 in the Rock Creek coalbeds of the Warrior Basin in the USA. In addition, it is shown in Chapter 5 that during production the change of in situ stresses is not isotropic in most areas of a coalbed even if initial permeability is assumed to be isotropic, illustrating that the change of permeability is not isotropic as well.

To consider the influence of permeability anisotropy in analytical models, one may use the average permeability:

$$k_{average} = \sqrt{k_{butt} \cdot k_{face}} \quad \text{.....(6.13)}$$

However, to what extent the permeability anisotropy of coalbeds can be included with this method is not known and further investigation is needed.

(2) Coal mass is assumed as a continuum isotropic medium undergoing a linear elastic deformation due to the changes of stresses and/or strains.

Coal is actually a discontinuum medium containing cleats and matrix. The results of triaxial tests by Hobbs (1964) and uniaxial tests by Czaplinski and Gustkiewicz (1990) indicate that a typical curve of strain versus stress consist of a concave part under lower stresses and a linear part under higher stresses, as shown in Figure 6.2. The concave part is due to the decrease of cleat apertures with the increase of stresses while the linear part is mainly from the compression of coal matrix. The analytical models applied the theory of linear elasticity to continuum isotropic media, i.e. used a constant Young's modulus and a constant Poisson's ratio, to simulate the deformation of coal mass. It will be shown later that with the theory of linear elasticity, it is easy to mimic the linear part of coal deformation (the deformation of coal matrix) but difficult to simulate the concave part (the deformation of cleats).

Allowing the moduli of coal mass to vary with stresses may partly overcome this limitation. However, multiple tests under different stress conditions are required. For coal mass with anisotropic matrix or cleats, the moduli would be anisotropic and its changes would depend not only on the quantity of stresses but also on the stress directions. Thus the application of this method would be costly and inefficient.

(3) The application of the principle of superposition is problematic.

In the formulation of analytical models, the changes of either stresses or strains were superposed in order to obtain the total change of stress or strain. To do so, it was assumed that the change of stress or strain caused by the alternation of fluid pressures was independent of the change of stress or strain by the shrinkage/swelling strain due to gas desorption/absorption. In estimating the change due to gas desorption/absorption, the shrinkage/swelling strains measured under no constraint condition were applied in analytical models. In reality, the changes of stress or strain from these two sources are interdependent. The shrinkage/swelling strains under in situ stress conditions are much smaller than that under no constraint condition. This means that the change of stress or strain due to gas desorption/absorption was overestimated in analytical models. The application of shrinkage/swelling strains measured under in situ stresses can improve the estimation. Nevertheless, in situ stresses are not static but dynamic during production. Experimental measurements of shrinkage/swelling strains under dynamic in situ conditions would be very challenging and costly. A similar problem also happened in estimating the change of stress or strain due to the alternation of fluid pressures.

In addition, for the models of superposing stresses, uniaxial or vertical deformation was assumed throughout coalbeds, i.e. horizontal strains were assumed to be zero. However this assumption does not really hold. Because the change of fluid pressures and the change of shrinkage/swelling strains are not uniform throughout coalbeds during production, horizontal strains would not keep being zero but change non-uniformly. For the models of superposing strains, the volumetric strains due to gas desorption/absorption and due to pressure changes were all converted to the change of cleat porosity. Actually, the change of strain in the direction normal to the bedding plane (usually vertical direction) would mainly cause the displacement of overburdens rather than contribute the change of cleat porosity and permeability since few cleats develop along the bedding plane.

(4) Cleats were assumed as smooth plate channels.

This assumption ignored the influences of tortuosity, surface roughness, and contact areas of cleats on fluid flow. In other word the mechanical aperture of a cleat was assumed to be identical to the hydraulic aperture of that cleat. However, the results of Barton et al (1985) indicated that a mechanical aperture and a hydraulic aperture are not equivalent. Their relationship can be described by an empirical equation:

$$b_h = \min\left\{ b_m, \frac{{b_m}^2}{JRC^{2.5}} \right\} \quad \text{.....(6.14)}$$

Based on Equation (6.14), the change of permeability ratio (k/k_0) with the closure of two apertures are calculated and shown in Figure 6.3. The calculation is based on initial permeability of 4 mD, fracture spacing of 0.02 m and a joint roughness coefficient of 5. These values represent average values of many coalbeds. The results show that for the same degree of fracture closure, the decrease of permeability of a mechanical (physical) aperture is severer than thee decrease of a hydraulic aperture. Thus, ignoring the difference between mechanical (physical) apertures and hydraulic (fluid flow) apertures would likely result in significant errors in predicting permeability changes.

To the author's knowledge, there is no published study available on the relation between mechanical apertures and hydraulic apertures for coal cleats. The applicability of Equation (6.14) to coal cleats needs to be validated with laboratory measurements.

6.3 PERMEABILITY AND POROSITY COUPLING MODELS

Another type of permeability and porosity models is coupling models that are used to couple the deformation of coalbeds into fluid flow in reservoir and geomechanical coupled simulation. For the coupling models introduced below, extensional stresses and stains are defined as positive. This convention differs from that used in geomechanics where compressional stresses and strains are defined as positive.

6.3.1 Continuum Medium Coupling Models

In the continuum medium permeability and porosity coupling models, coal mass in deformation simulation is considered as a homogeneous medium undergoing linear elastic deformation and discontinuity is ignored. The difference between the mechanical apertures and corresponding hydraulic apertures of cleats or fractures is also neglected. Coal mass in fluid flow simulation is abstracted as a matchstick fracture system, as shown in Figure 3.7. The anisotropy of cleats is not considered. The dimension of a unit containing one coal matrix block and one cleat is assumed unchanged in deformation. In other words, the change of the coal matrix block is offset by the change of the cleat. From Equation (6.2a) and (6.2b) the permeability and porosity models, i.e. Equations (3.3) and (3.5) developed in Chapter 3, are repeated in following:

$$\phi = \frac{\phi_o - 2\Delta\varepsilon_L}{1 + \Delta\varepsilon_L} \quad \text{.....(6.15a)}$$

$$\frac{k}{k_o} = \frac{(1 - \frac{a}{b}\Delta\varepsilon_L)^3}{(1 + \Delta\varepsilon_L)} \quad \text{.....(6.15b)}$$

where $\Delta\varepsilon_L = \Delta a/a$. The change of linear strain is obtained from the simulation of coal deformation with a geomechanics simulator, such as FLAC© (Itasca, 2002a) or FLAC3D© (Itasca, 2002b).

6.3.2 Discontinuum Medium Coupling Models

In the discontinuum medium permeability and porosity coupling models, coal mass is treated as a discontinuum medium containing matrix and cleats. This system is described with a matchstick fracture system shown in Figure 6.1. Matrix is represented by matchsticks and may have anisotropic properties of shrinkage/swelling and thermal expansion. Cleats are the two distinct and

orthogonal fracture sets and have different apertures, normal stiffnesses, and shear stiffnesses.

According to Amadei and Goodman (1981) the mechanics properties of an orthogonal discontinuous medium can be represented with the properties of an "equivalent" continuum medium and the deformation can be estimated based on this equivalent continuum medium. Coal mass is a typical orthotropic fractured medium thus can be represented with an "equivalent" continuum medium. Based on the equivalent continuum medium, the porosity and permeability models, i.e. Equations (5.34) and (5.36) established in Chapter 5, are as following:

For $u_s/u_s^p<0.3$

$$\frac{k_i}{(k_i)_0}=\frac{[1+\frac{a_j}{(b_m)_j}\Delta\varepsilon_{f\,j}]^{3n_j}}{1+(\Delta\varepsilon^t_{L\,j}-\Delta\varepsilon_{f\,j})+\frac{(b_m)_j}{a_j}\Delta\varepsilon^t_{L\,j}} \quad \text{.....(6.16a)}$$

$$\phi=\sum_{i=x,y}\frac{(b_m)_i}{a_i}\cdot\frac{1+\frac{a_i}{(b_m)_i}\Delta\varepsilon_{f\,i}}{1+(\Delta\varepsilon^t_{Li}-\Delta\varepsilon_{f\,i})+\frac{(b_m)_i}{a_i}\Delta\varepsilon^t_{Li}} \quad \text{.....(6.16b)}$$

For $u_s/u_s^p\geq 0.3$

$$\frac{k_i}{(k_i)_0}=\frac{\{1+\frac{a_j}{(b_m)_j}[\Delta\varepsilon_{f\,j}+\Delta\gamma_{f\,j}\tan(\psi^m)_j]\}^{3n_j}}{1+[\Delta\varepsilon^t_{L\,j}-\Delta\varepsilon_{f\,j}-\Delta\gamma_{f\,j}\tan(\psi^m)_j]+\frac{(b_m)_j}{a_j}\Delta\varepsilon^t_{L\,j}} \quad \text{.....(6.16c)}$$

$$\phi=\sum_{i=x,y}\frac{(b_m)_i}{a_i}\cdot\frac{1+\frac{a_i}{(b_m)_i}[\Delta\varepsilon_{f\,i}+\Delta\gamma_{f\,i}\tan(\psi^m)_i]}{1+[\Delta\varepsilon^t_{Li}-\Delta\varepsilon_{f\,i}-\Delta\gamma_{f\,i}\tan(\psi^m)_i]+\frac{(b_m)_i}{a_i}\Delta\varepsilon^t_{Li}} \quad \text{.....(6.16d)}$$

In these models, the mechanical and hydraulic apertures are distinguished by the parameter n. According to Bandis et al (1983) if a mechanical aperture is greater than its hydraulic aperture, n is equal to 2. Otherwise, it is equal to 1. The changes of "normal and shear strains" of cleats are defined as:

$$\Delta\varepsilon_f=\frac{(\Delta b_m)_n}{a} \quad \text{.....(6.17a)}$$

$$\Delta\gamma_f=\frac{\Delta u_s}{a} \quad \text{.....(6.17b)}$$

If the influence of shear dilation of cleats is ignored, i.e. the change of shear strains, $\Delta\gamma_f$, or shear dilation angle, ψ^m, is set to be zero, (6.16c) and (6.16d) become (6.16a) and (6.16b), respectively. If we further ignore the change of a unit containing one matrix block and one cleat (i.e. $\Delta\varepsilon_L^t=0$) and the difference between the mechanical apertures and hydraulic apertures of cleats (i.e. n=1), (6.16a) and

(6.16b) can be simplified to (6.15a) and (6.15b), respectively, since $-\Delta\varepsilon_f=\Delta\varepsilon_L$ ($-\Delta b_m=\Delta a$). Therefore, the continuum medium permeability and porosity coupling models are a special case of the discontinuum medium permeability and porosity coupling models.

6.4 SIMULATION OF COAL MASS DEFORMATION

In order to show the applicability of the "equivalent" continuum medium model to coal mass, the experimental results of Czaplinski and Gustkiewicz (1990) are numerically simulated. The experiments included a uniaxial compression test in vacuum, a CO_2 swelling test without external loads, and several CO_2 swelling tests under axial constraint in the longitudinal (vertical) direction. The data set is very rare and unique since all the tests were completed on the same coal specimen. This eliminated errors due to the discrepancy of different specimens.

The coal sample was obtained from the 317 seam in the Brzeszcze mine of Upper Silesia, Poland. The specimen was cut perpendicular to the bedding and had a height of 2 cm and a square base of 1×1 cm^2. Two pairs of resistance gauges were mounted on the sample to measure the longitudinal (vertical) and transverse (horizontal) strains, respectively. The applied force was measured with a dynamometer connected with the piston. All the tests began and ended in a high vacuum of 0.013 Pa. The experiments were conducted under an isothermal condition of 298 K. The mean uniaxial compressive strengths of the coal in the directions perpendicular to and parallel to the bedding were 21 MPa (in the vertical direction) and 20 MPa (in the horizontal direction) respectively, under a degasified vacuum of 0.13 Pa. The strengths decreased to 15 MPa (in the vertical direction) and 8 MPa (in the horizontal direction), respectively, under CO_2 saturation at a pressure of 3.92 MPa (Czaplinski and Gustkiewicz, 1990).

6.4.1 Uniaxial Compression

Prior to the swelling during the sorption of CO_2, the sample underwent a uniaxial compression test. The load was added in the longitudinal (vertical) direction with a screw piston. The loading-unloading cycle completed in a vacuum. The changes of strains during the loading process are reproduced from Czaplinski and Gustkiewicz's results (1990) and shown in Figure 6.2. From the

linear part of the measured strains, Czaplinski and Gustkiewicz (1990) estimated the Young's modulus and Poisson's ratio were 1800 MPa and 0.18, respectively.

Using these measured mechanics parameters (listed in Table 6.1) and an isotropic linear elastic continuum model, the uniaxial compression of the specimen is simulated with FLAC 3D© (Itasca, 2002b) and the results are also illustrated in Figure 6.2. The results show that the isotropic linear elastic continuum model can match the horizontal strains very well, but is unable to simulate the deformation in the vertical direction. As mentioned by Czaplinski and Gustkiewicz (1990), the nonlinear deformation under lower stresses (less than 2 MPa) was due to the closure of cracks inside the specimen. Under stresses higher than 2 MPa, the cracks approached residual apertures, thus the change of strains was mainly due to the deformation of matrix in the range of linear elasticity and linearly related to the change of stresses.

Further simulations were made based on an "equivalent" continuum medium model to consider the influence of cracks in the specimen. It is assumed the 2 cm high specimen contained one horizontal crack or cleat (fracture) since no measurements about the cracks were made. The simulation models are shown in Figure 6.4. The mechanics parameters of the matrix are the same as those listed in Table 6.1. The equivalent model and moduli for the specimen are established based on the results of Amadei and Goodman (1981). The moduli are explicitly renewed after each calculation step of 0.1 MPa. The changes of normal stiffnesses are estimated with the empirical model presented by Bandis et al (1983) and the changes of shear stiffnesses with the empirical model presented by Jing et al (1993).

Because no information about the cleat aperture and stiffnesses is available, the stiffnesses are chosen from the general ranges and the cleat aperture is assumed based on the average values of coal. According to Pusch and Borgesson (1998), normal stiffnesses of rocks varied in a range of 2×10^5 to 2×10^7 MPa/m. Rosso (1976) measured the samples of siltstone, sandstone, clay fractures, and carbonaceous crossbeds in which fractures were created by direct shear and obtained a range of shear stiffness of 1×10^4 to 10×10^4 MPa/m. Chappell (1987) tested the stiffnesses for one type of coal and obtained a range of normal stiffnesses of 2000 to 6680 MPa/m and a range of shear stiffnesses of 500 to 1800 MPa/m. In order to find the best match to the measured strains, sensitivity studies on input data, especially on the normal stiffness and the initial aperture of the cleat are made. The best match is shown in Figure 6.5 and the corresponding data

set is tabulated in Table 6.2. The results indicate that using the equivalent continuum model, the deformation of the specimen can be successfully simulated.

6.4.2 Deformation during CO_2 Adsorption under Constraint

6.4.2.1 Swelling Strains under No Constraint

Czaplinski and Gustkiewicz (1990) also measured the swelling process of the specimen under different sorption pressures under no external load condition and the results are shown in Figure 6.6. The measured stains need to be corrected to obtain the swelling strains because the measured strains include the compression strains of "grain" under sorption pressures. The compression strains of "grain" are estimated with:

$$\Delta\varepsilon = \frac{1-2\upsilon}{E}\Delta p \quad \text{.....(6.18)}$$

By adding the compression strains of "grain" to the measured strains, the real swelling strains due to CO_2 adsorption are obtained. They are also plotted in Figure 6.6 and marked as "corrected".

According to the results of Seidle and Huitt (1995) and Harpalani and Chen (1995), the volumetric strain of coal matrix has an approximately linear correlation with the adsorbed methane. The volumetric strain of this coal might have a similar correlation with adsorbed methane. However, since the CO_2 adsorption isotherm for this coal is not available, the real swelling strains are fitted as a function of swelling pressures and applied in the numerical simulations. The selection of mathematical function types for regression analysis is purely for higher correlation coefficients. With correlation coefficients of about 99%, the fitted equations are:

$$\varepsilon_L^v = 0.4507 \cdot (p_s)^{0.5356} \quad \text{.....(6.19a)}$$

$$\varepsilon_L^h = 0.3698 \cdot (p_s)^{0.5235} \quad \text{.....(6.19b)}$$

6.4.2.2 Simulation of Sorption Stresses and Strains

To measure the sorption (swelling) stresses, the specimen was enclosed in a test cell and one of initial vertical stresses of 0.6, 1.2, 3.5, and 4.8 MPa was applied on the specimen in a vacuum. The sample was then subjected to a cycle of sorption (72 hours) then desorption (72 hours) of CO_2 under sorption pressures of 0.5, 1, 2, and 3 MPa. Each cycle began and ended in a high vacuum. The

longitudinal (vertical) stresses and strains and transverse (horizontal) strains were recorded during the cycles.

In this investigation the sorption process corresponding to the initial stress of 4.8 MPa is simulated using the equivalent continuum medium model and the same mechanics properties established previously from the simulation of the uniaxial compression (see Tables 6.1 and 6.2). The measured vertical swelling strains under the initial vertical stress of 4.8 MPa are shown in Figure 6.7 and the measured vertical stresses and horizontal strains in Figure 6.8. For convenience of simulation, the measured vertical strains are fitted with the following equation and also shown in Figure 6.7:

$$\varepsilon_L^{vc} = 0.08162 \cdot (p_s)^{0.3396} \quad \text{.....(6.20)}$$

In simulation, the vertical strains calculated with Equation (6.20) are converted to vertical displacements and input to the simulation model. The changes of swelling strains are estimated with Equations (6.19a) and (6.19b). Then the changes of total stresses induced by the changes of swelling strains are calculated using a code programmed with FISH language inside FLAC3D® (Itasca, 2002b) with relevant constitutive equations and input into the simulation model. The simulated vertical stresses and horizontal strains are matched with the measured data and plotted in Figure 6.8. The results indicate that when the sorption pressures are smaller than 1 MPa the simulation stresses and strains match the experimental data well. However, when the sorption pressures are larger than 1 MPa, the simulated stresses and strains are higher than experimental results and the discrepancies continue to increase with increasing sorption pressures.

The primary reason for the mismatches is due to the change of deformation behaviour of coal, which was probably caused by shear failure of the specimen. Because the shearing strength of the coal sample is not available, the ranges of shearing strengths are estimated through simulating the stress states at peak compressive strengths with the Mohr-Coulomb criterion. According to Czaplinski and Gustkiewicz (1990), the mean uniaxial compressive strengths perpendicular and parallel to the bedding are 21 MPa and 20 MPa, respectively, under the degasified vacuum of 0.13 Pa, and are 15 MPa and 8 MPa, respectively, under the CO_2 adsorption pressure of 3.92 MPa. The results imply the strength of coal deceased with increasing sorption pressures. The friction angle is also not available thus selected from published data. Morgenstern and Noonan (1974)

measured the friction angle of a Canadian coal in a range of 40.5 to 67.8 degrees. Das and Sheorey (1986) obtained the friction angle of several Indian coals in a range of 35 to 51 degrees. Vaziri et al (1997) reported the friction angles of a coal in a range of 30 to 50 degrees. From these data, a lower bound friction angle of 30 degrees and an upper bound friction angle of 67.8 degrees are used for this analysis. The Mohr-Coulomb failure envelopes simulated from the compression strengths under the adsorption pressures of 0 and 3.92 MPa are presented in Figure 6.9.

An assessment of shear failure for the stress states during CO_2 sorption against the failure envelopes is shown in Figure 6.10. It shows that the stress state circle under the sorption pressure of 0.4 MPa has touched all the failure envelopes with a friction angle of 67.8 degrees. The circle also touches the lower bound of the failure envelopes with a friction angle of 30 degrees. With the increase of sorption pressures, the diameter of the stress state circles increases but they keep tangent to the vertical axial. If sorption pressures are greater than about 3.0 MPa, the stress state circles would touch all the failure envelopes. Based on this analysis, the shear failure in the measured specimen might begin at the sorption pressure of 0.4 MPa if the friction angle is closed to the upper bound. With the increase of sorption pressures, shear failure develops. Therefore our assumption that the shear failure of this specimen occurred under the sorption pressure of around 1 MPa is reasonable.

The analysis concludes that before shear failure the simulation of the deformation of the specimen under the axial constraint during CO_2 sorption is successful and that the equivalent continuum medium model is suitable to simulate the deformation of coal mass.

6.5 Simulation of CBM Recovery with Different Permeability Models

In this section, we will compare the results of CBM production simulated with different permeability models, i.e. two analytical permeability models and the discontinuum medium permeability coupling model. The selected analytical models are the simplified version of the Palmer and Mansoori's model (Mavor and Vaughn, 1998) and the Shi and Durucan's model (Shi and Durucan, 2003). The one reason to choose these two models is they represent two types of models formulated by superposing strains and stresses respectively. Another reason is

they express the matrix shrinkage with the same Langmuir-type model thus it is easy to compare the simulation results based on the same input data.

The basic data utilized for the simulations are listed in Tables 6.3, 6.4 and 6.5. In order to let the analytical models have the same shrinkage strain as the discontinuum medium permeability coupling model under any sorption pressure, the maximum volumetric strain (ε_V) of the analytical models at infinite pressure is set equal to the product of Langmuir volume and the volumetric coefficient of matrix shrinkage, and the pressure at half of ε_V equal to the Langmuir pressure. To avoid the discrepancy due to importing additional data, the pore compressibility in the simplified Palmer and Mansoori's model (Mavor and Vaughn, 1998) and the cleat compressibility in the Shi and Durucan's model (Shi and Durucan, 2003) are all calculated with Equation (6.9). In the coupled simulation, coal deformation is simulated with FLAC3D© (Itasca, 2002b). To generate consistent simulation results, fluid flows are all simulated with GEM© (CMG, 2003a). The grid sizes and the length of time steps are all the same for the different simulations. The grid sizes are increased from the wellbore to the boundary with a ratio of 1.1 in adjacent grid blocks. Permeability in each block is explicitly renewed after each time step. The simulation grids and blocks are shown in Figure 6.11.

6.5.1 Change of Permeability

The changes of permeability with the changes of pore pressures are shown in Figure 6.12. The results indicate that different models have different relations between pore pressures and permeability. The analytical models have unique relations between pore pressures and permeability, but the coupling model does not. The permeability estimated with the discontinuum medium permeability coupling model is dependent not only on pore pressures, but also on the location in the coalbed (i.e. in situ conditions). In the locations closer to the wellbore, e.g. in Block (1,1), with pore pressures decreasing permeability decreases continuously (i.e. dominated by the compression induced by pressure drops) then drastically increases (i.e. dominated by the shrinkage of coal matrix due to methane desorption). In locations near to the boundary, e.g. in Block (15,15), with pore pressures decreasing permeability experiences a continuous increase (i.e. dominated by the shrinkage of coal matrix due to methane desorption).

The comparison of the changes of permeability with the changes of stresses is illustrated in Figures 6.13 and 6.14. The results show that the permeability from

the coupling model and Shi and Durucan's model (Shi and Durucan, 2003) changes inversely to the change of horizontal effective stresses, and that the permeability from the simplified Palmer and Mansoori's model (Palmer and Mansoori, 1998) changes inversely with the mean effective stresses.

The changes of in situ effective stresses simulated from coupled simulation are also shown in Figure 6.13 for Block (1,1) and in Figure 6.14 for Block (15,15). The results show that the changes of in situ stresses depend not only on pore pressures but also on locations in the coalbed (i.e. local in situ stresses). For the locations close to the wellbore, e.g. in Block (1,1), the vertical stress, horizontal stress, and mean stress all drastically increase at the beginning of production. Then, the vertical stress continues to increase while the horizontal stress decreases with flat decreasing slopes resulting in a relative stable mean stress. For the locations near to the boundary, e.g. in Block (15,15), the vertical stress increases with higher slopes comparing with the locations near the wellbore while the horizontal stress decreases very slowly, resulting in steady increasing mean stresses. The results in Figures 6.13 and 6.14 also imply there is no monotonic relation between pore pressures and horizontal stresses. Closer to the wellbore, e.g. in Block (1,1), after about 330 days the pore pressure decreases smoothly but the horizontal stress continuously decreases. However, near to the boundary, e.g. in Block (15,15), the pore pressure experiences a large drop but the horizontal stress only reduces a small amount.

6.5.2 Comparison of Productivity

The comparison of productivity from different models is illustrated in Figures 6.15 to 6.17. For comparison, the results simulated with constant permeability are also plotted in the figures. The results indicate that the gas production rates, cumulative gas production, and cumulative water production with the coupling model have different trends. The time to reach the peak production rate with the coupling model is much later than that with other models for this case. The gas rate and the cumulative gas and water production with the coupling model are lower than that with other models in the early production stage then continuously increase. The gas rate with the coupling model in the later production stage is higher than the gas rates with other models. All these imply that geomechanics plays a very important role in predicting production and would influence decision making for coalbed development.

6.6 SUMMARY

We summarize the study of this chapter as following:

(1) Analytical permeability models considering the influences of pressure drops and the shrinkage/swelling of coal matrix due to gas desorption/adsorption can be easily applied in current reservoir simulators. However, they have such limitations as assuming permeability is isotropic, applying the linear elastic continuum model for coal mass (a discontinuum medium), neglecting the interaction between stresses and strains when applying the principle of superposition, and ignoring the difference between mechanical and hydraulic apertures.

(2) The swelling strains of coal under constraint conditions are much smaller compared with those under unconfined or no constraint conditions. Analytical permeability models were developed with application of the principle of superimposition to the changes of strains or stresses under in situ stress conditions. Thus, the swelling strains used in these models should be measured under in situ stress conditions rather than under no constraint conditions, even though the latter is common practices in the application of analytical models.

(3) The linear elastic deformation model, suitable to isotropic continuum media but generally assumed in analytical permeability models, cannot adequately simulate the deformation behaviour of coal mass due to its nonlinear deformation characteristic. The equivalent continuum medium model considering the influence of discontinuity and anisotropy of coal matrix and cleats can properly simulate the nonlinear deformation behaviour of coal mass.

(4) Unlike analytical permeability models, the change of permeability predicted with the discontinuum medium coupling permeability model has no unique relation with the change of pore pressures. It relates to the locations in a coalbed (i.e. local in situ conditions). The permeability coupling model provides better estimates of permeability and production because it includes the influences of many factors, such as the in situ deformation, discontinuities and anisotropies of coal mass.

Table 6.1: Mechanics Parameters of Specimen Matrix

Young's modulus (MPa)	1800
Poisson ratio	0.18
Uniaxial compressive strength (MPa)	21

Table 6.2: Data Set of Best Matching

Matrix	Material constant A in Equation (5.5a)	2
Cleat	Space (m)	0.02
	Aperture (micron)	30
	Initial normal stiffness (MPa/m)	28800
	Maximum shear stiffness (MPa/m)	3600
	Maximum closure/initial aperture	0.75
	Peak shear displacement (mm)	0.1
	Original (peak) joint roughness	5
	Shear dilation angle	10

Table 6.3: Basic Well Parameters

Top depth of coalbed (m)	900
Seam thickness (m)	10
Drainage area of well (m^2)	850×850
Well radius (m)	0.1
Seam pressure (kPa)	8754.3
Seam temperature (^oC)	30.5
Cleat space (m)	0.02
Cleat porosity (decimal)	0.000986
Cleat permeability (mD)	4
Matrix porosity (decimal)	0.005
Matrix permeability (mD)	0.001
Water density (kg/m^3)	990
Water viscosity (cp)	0.644
Water saturation in fracture (decimal)	1
Compressibility of coal matrix (1/kPa)	1.45E-07
Compressibility of water (1/kPa)	5.80E-07
Reference pressure of compressibility (kPa)	8500
Langmuir volume (m^3/ton)	22.653
Reciprocal of Langmuir pressure (1/kPa)	2.417×10^{-4}
Methane sorption time (day)	100
Coefficient of volumetric matrix shrinkage (g/ml)	4.6×10^{-4}

Table 6.4: Mechanics Parameters

Parameters	**Overburden**	**Coal Matrix**
Density (kg/m^3)	2300	1542
Young's modulus (MPa)	1000	3399.2
Poisson's ratio	0.3	0.32
Compressive strength (MPa)		60
Material constant A in Equation (5.5a)		2
	Cleats	
	Intersecting x	**Intersecting y**
Initial normal stiffness (MPa/m)	101976	101976
Maximum shear stiffness of cleat (MPa/m)	25494	25494
Shear dilation angle (°)	10	10
Peak shear displacement (mm)	0.1	0.1
Original JRC	5	5
Type of cleat	matched cleat	matched cleat
Maximum cleat closure/Initial mechanical cleat width	0.6	0.6

Table 6.5: Production Constraints

Water production constraint	
Time (day)	0 to 17
Minimum BHP (kPa)	101.325
Maximum water rate (m^3/day)	10
Gas production constraint	
Time (day)	18 to 7300
Minimum BHP (kPa)	275

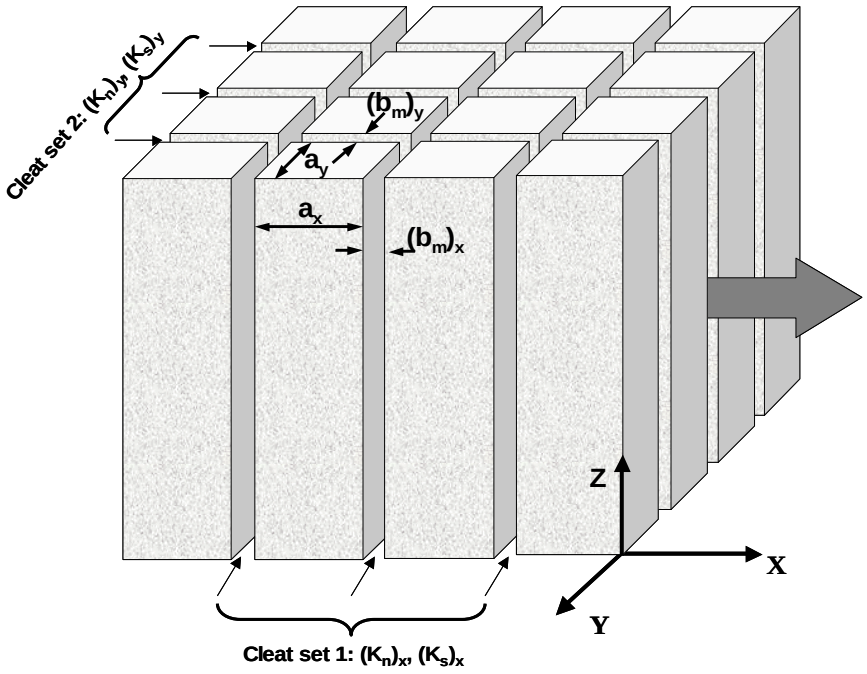

Figure 6.1: Fracture System with Matchstick Matrix Blocks (modified from Seidle et al, 1992)

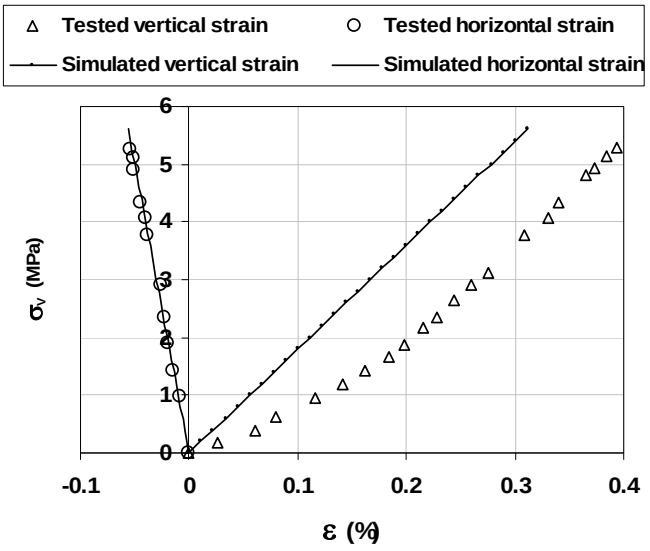

Figure 6.2: Simulation of Uniaxial Compression with Isotropic Continuum Elastic Model

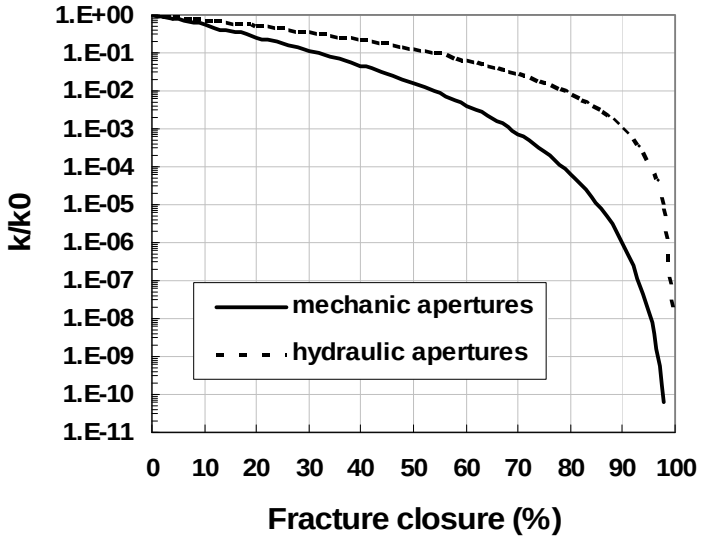

Figure 6.3: Influences of Mechanical and Hydraulic Fracture Closures on Permeability

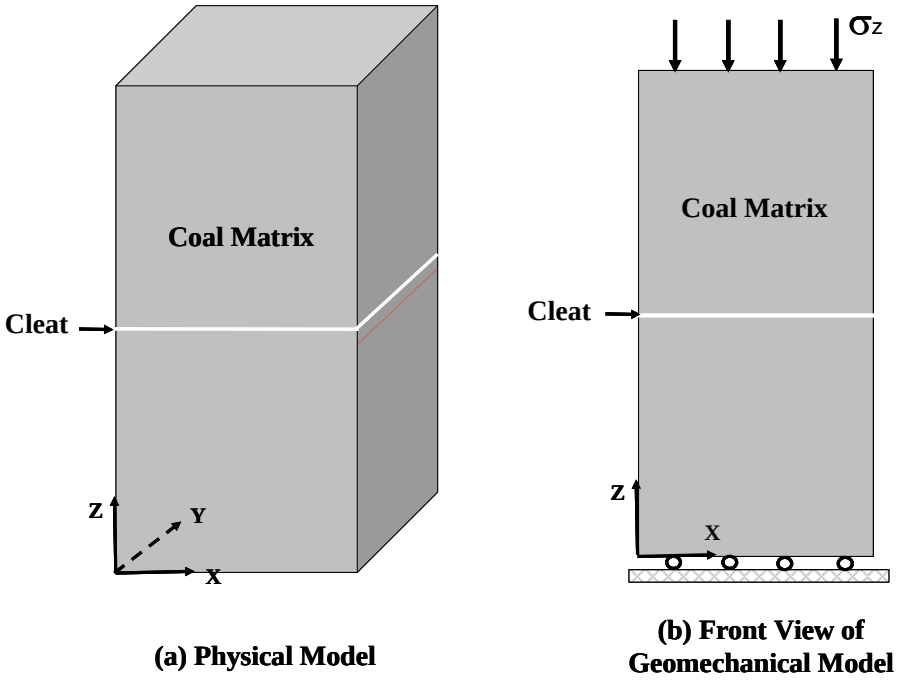

Figure 6.4: Simulation Model of Tested Specimen

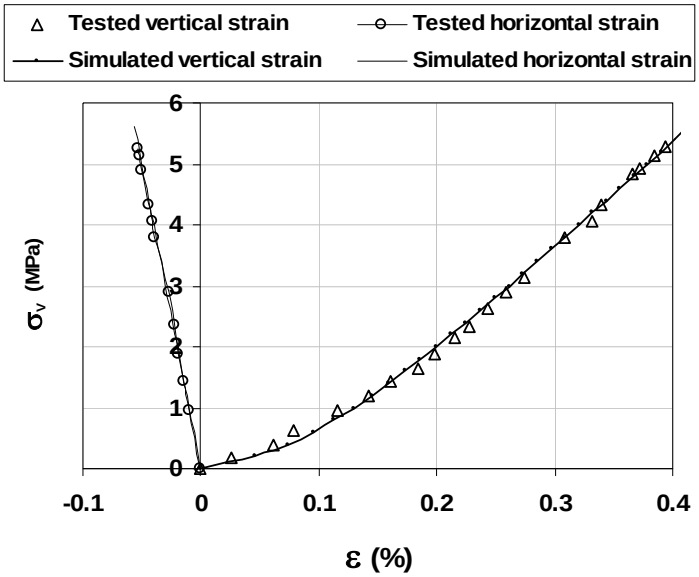

Figure 6.5: Simulation of Uniaxial Compression with Equivalent Continuum Model

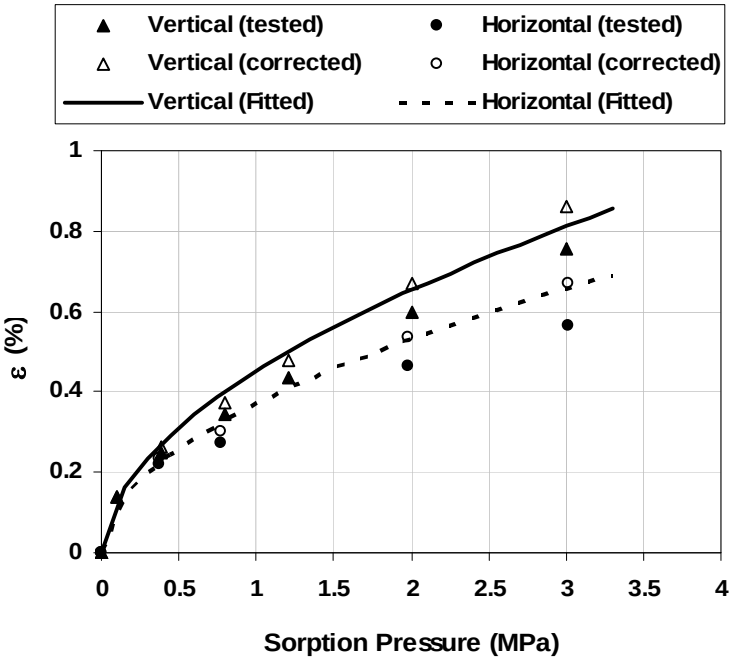

Figure 6.6: Swelling Strains due to CO_2 Adsorption

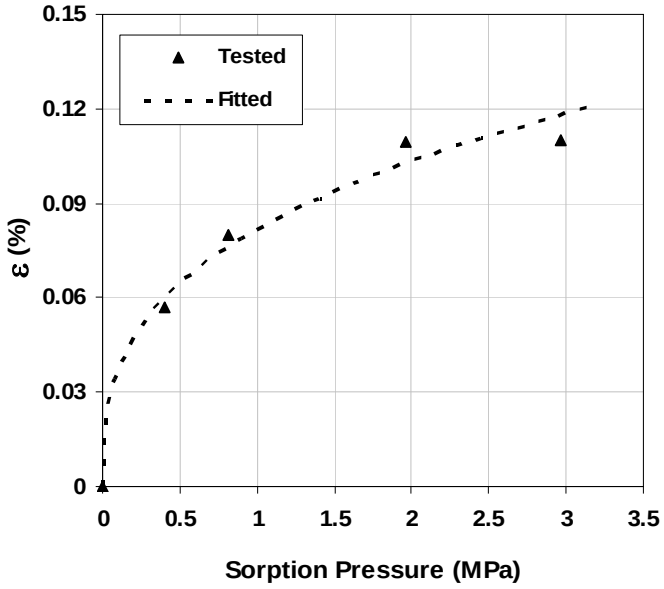

Figure 6.7: Swelling Strains due to CO_2 Adsorption under Initial Vertical Stress of 4.8 MPa

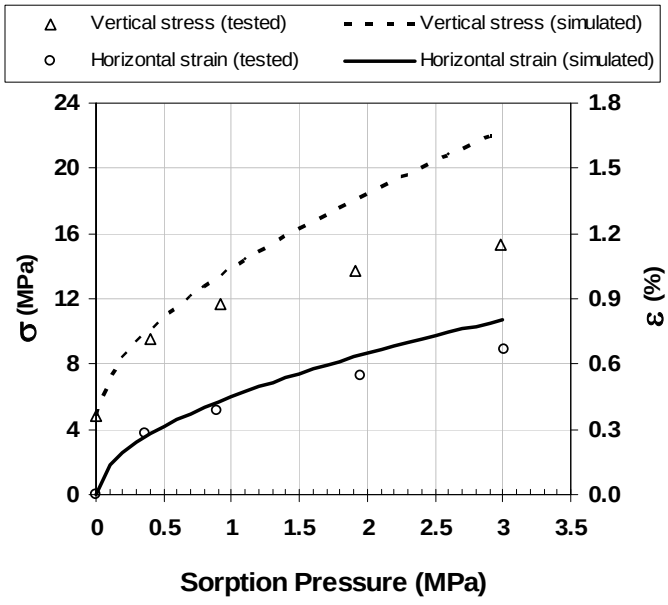

Figure 6.8: Simulation of Coal Swelling due to CO_2 Sorption under Initial Vertical Stress of 4.8 MPa

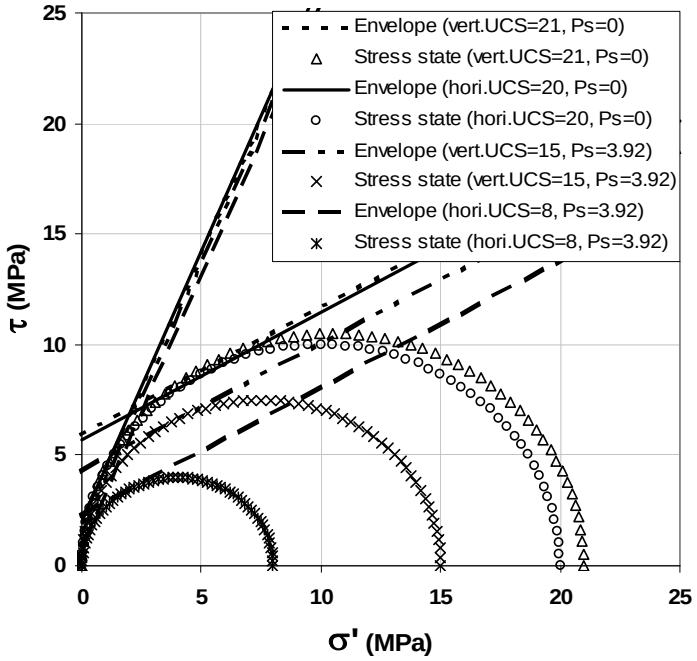

Figure 6.9: Simulation of Shear Strength

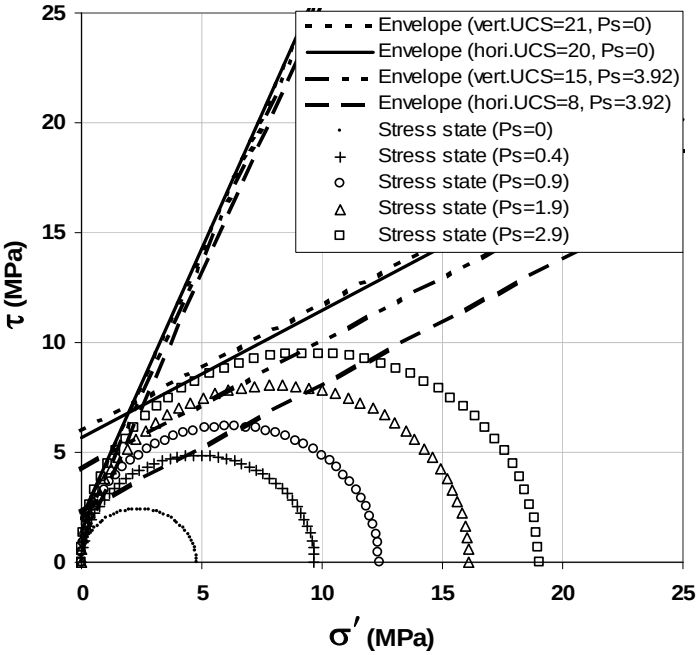

Figure 6.10: Stress States during CO_2 Sorption

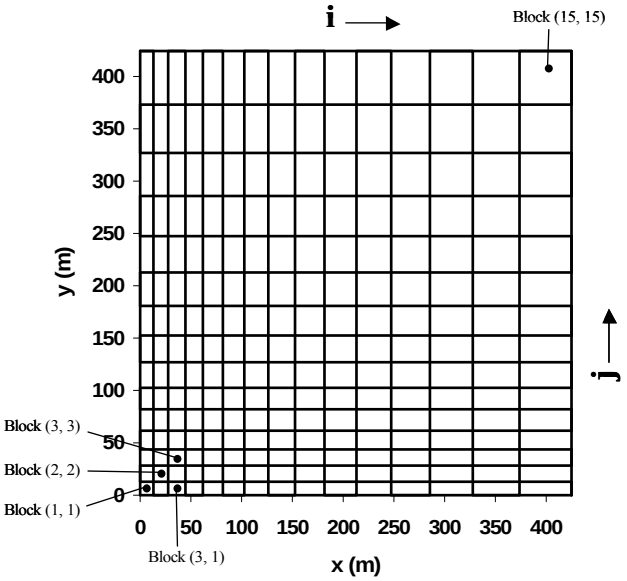

Figure 6.11: Grids and Blocks in Coalbed

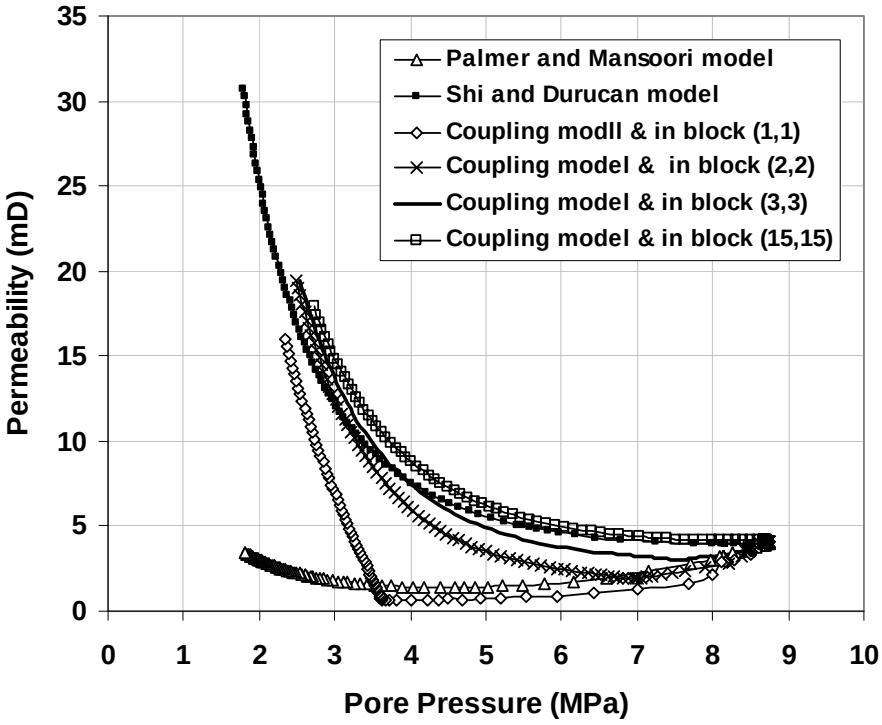

Figure 6.12: Permeability Changes with Pore Pressure

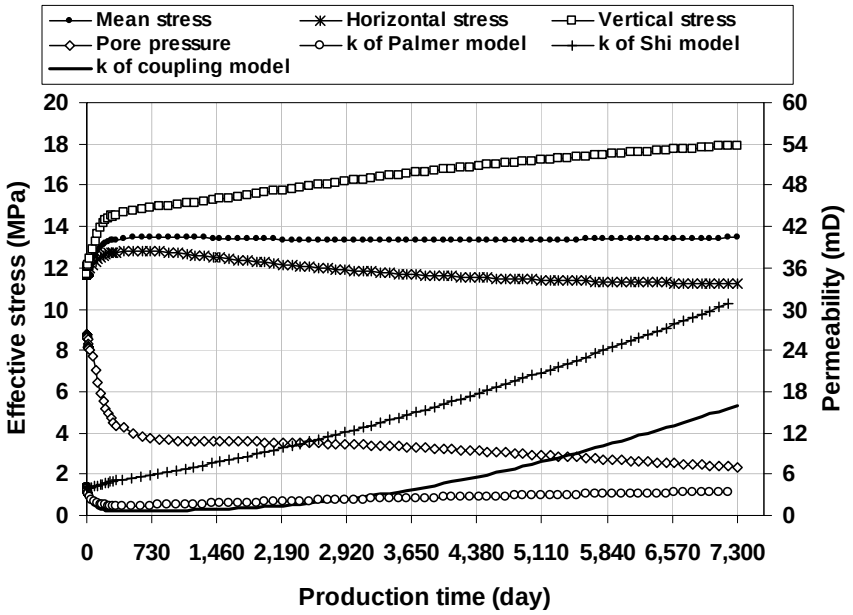

Figure 6.13: Changes of Stresses and Permeability with Production Time in Block (1,1)

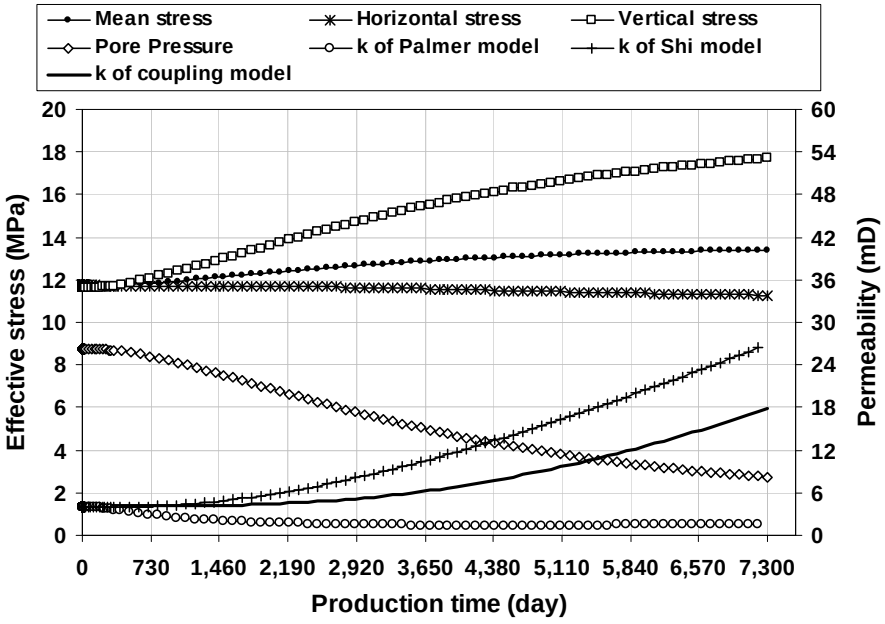

Figure 6.14: Changes of Stresses and Permeability with Production Time in Block (15,15)

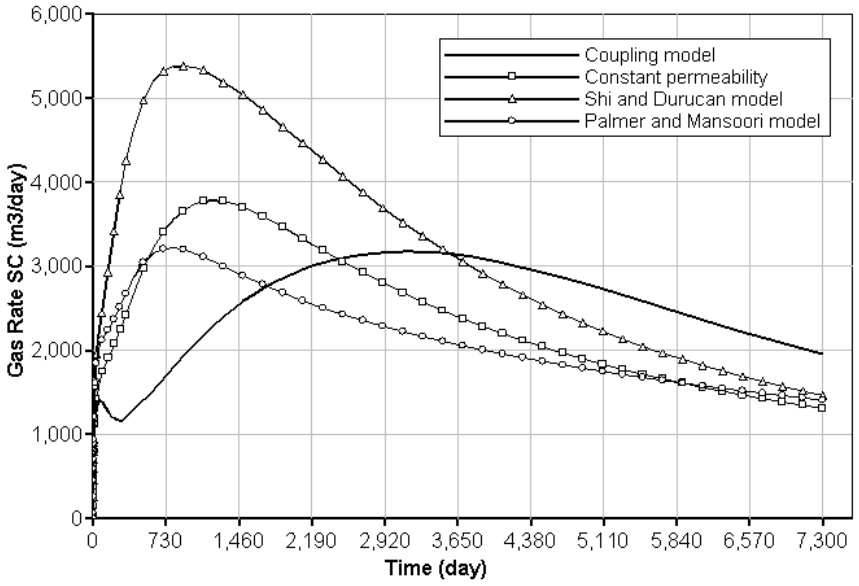

Figure 6.15: Comparison of Gas Production Rates from Different Permeability Models

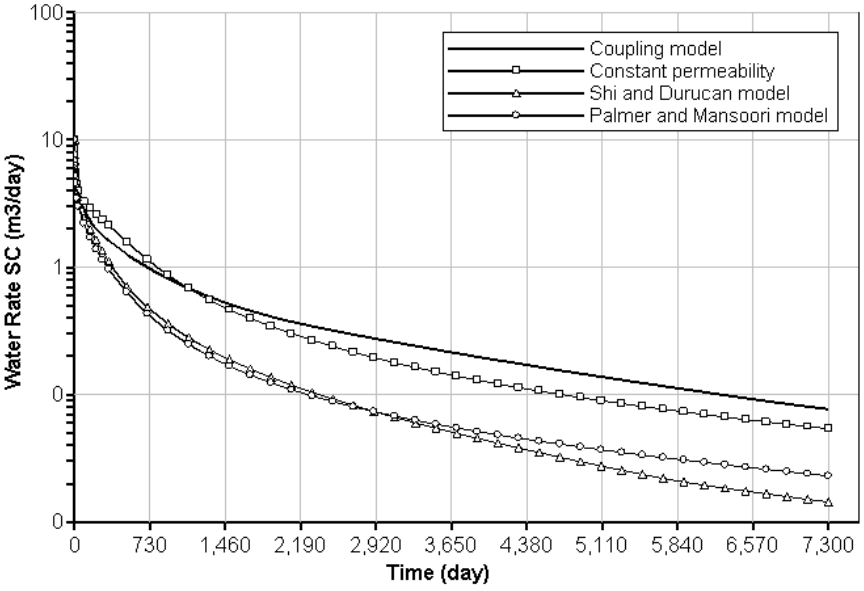

Figure 6.16: Comparison of Water Production Rates from Different Permeability Models

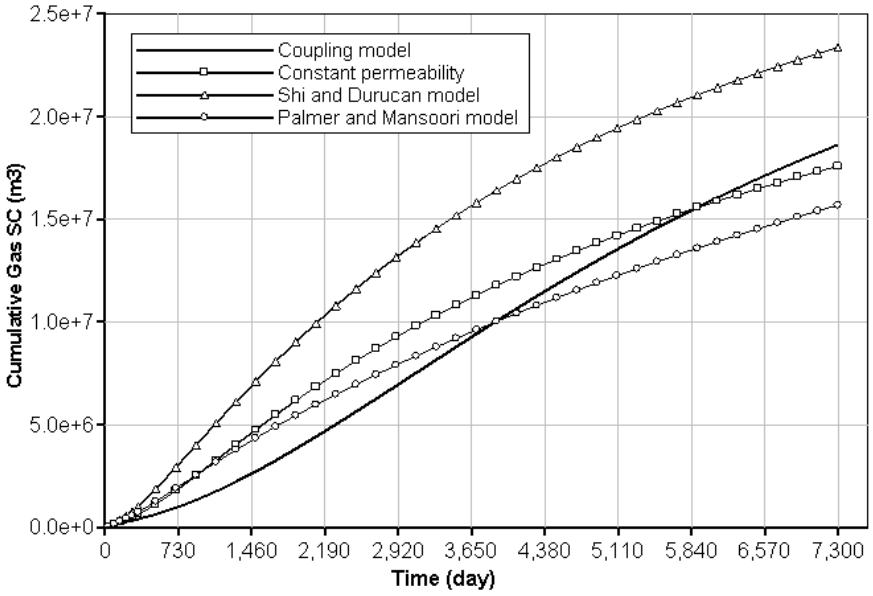

Figure 6.17: Comparison of Cumulative Gas Production from Different Permeability Models

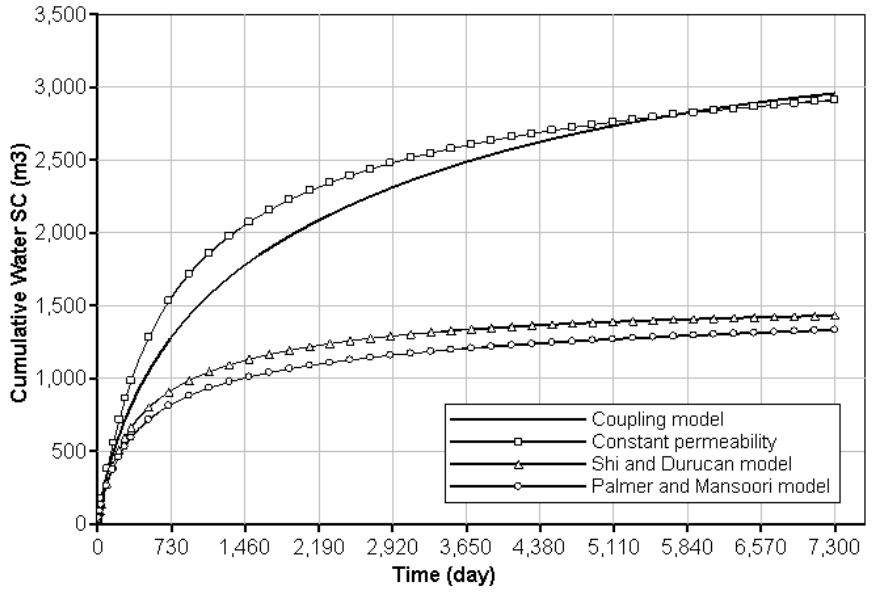

Figure 6.18: Comparison of Cumulative Water Production from Different Permeability Models

7 SIMULATION OF FIELD ECBM PILOT TESTS

7.1 INTRODUCTION

It has been scientifically proven that carbon dioxide (CO_2) is a major component of greenhouse gases (GHG) and the reduction of CO_2 emissions into the atmosphere can significantly mitigate the GHG effect. Most emitted CO_2 comes from the combustion of fossil fuels for energy, such as electricity generation, transportation, house warming, oil refinery and gas process. Given their inherent advantages such as availability, competitive cost, easy transportation and storage, and large resources, fossil fuels will remain a dominant component of the world's energy supply for at least this century (Bachu and Shaw, 2003). Therefore the emissions of CO_2 from human activities are not expected to decrease pronouncedly.

Nevertheless there are some approaches that can be used to reduce CO_2 emissions into the atmosphere. The methods include: improving the efficiency of energy utilization and conversion systems, switching to the fuels that are less carbon-intensive, expanding nuclear and renewable power generation capacity, and capturing and storing CO_2 into geological formations, also called geological sequestration, (White et al, 2003). Among these solutions, geological sequestration is increasingly seen as a cost-effective strategy for achieving deep reduction of CO_2 emissions (Beecy et al, 2001). Geological sinks used for CO_2 sequestration include depleted oil and gas reservoirs, deep unminable coal seams and deep saline reservoirs. The first and second types are the most attractive geological formations for CO_2 sequestration due to their "value-added" merit.

The advantages of deep unminable coal seams for CO_2 sequestration include the huge coal resources around the world and the fact that the sorption capacity of coal to CO_2 is 1.8 to 10 times of that to methane (Mavor et al, 2002). CO_2 injection into coal seams would not only be a sequestration process but also an enhanced coalbed methane (ECBM) recovery process. As a result CO_2 sequestration may be operated at a low cost or even net profit depending on the revenue of produced methane. In addition since coalbed methane is a clean-burning fuel, considered more environmentally friendly than coal, oil even

---

A version of this chapter was presented at an international conference. Gu, F. and Chalaturnyk, R.J., 2006. The 2006 International Coalbed Methane Symposium. The University of Alabama, Tuscaloosa, USA.

conventional natural gas, using captured coalbed methane to replace coal or oil for electricity generation, vehicle burning and house heating etc. can further reduce tremendous greenhouse gas emissions.

Numerical simulators are necessary tools for the design and evaluation of ECBM and CO_2 sequestration process. In the past decades a lot of efforts have been invested in the development of simulation models, especially the models for pressure depletion coalbed methane (CBM) process, and great achievements have been made (King and Ertekin, 1991; King and Ertekin, 1995). However, due to the complexities of mechanisms simulations with these models still meet many challenges (Law et al, 2002). Among the challenges, the estimation of permeability changes during the processes is probably the most important one because permeability is a key parameter influencing their success. The change of permeability is very difficult to predict since it depends on the changes of in situ stresses and strains, which are relevant to rock properties and the changes of pore pressures, adsorbed gas volumes and temperatures. Conventional reservoir simulators usually have no capacity to simulate the changes of stresses and strains thus permeability variations are computed by means of analytical models, which directly relate the change of permeability to the change of pore pressures (CMG, 2005). However, the assumptions and simplifications made in the formulation of analytical models degrade their ability to capture some important characteristics of coalbeds, such as the discontinuity of coal mass and the anisotropies in permeability and other properties. In order to fully consider the influences of the alterations of in situ conditions on the change of permeability (and porosity) in simulations, permeability and porosity coupling models and an explicit-sequential coupled simulation method have been established and demonstrated in Chapter 3, 4, 5 and 6 (Gu and Chalaturnyk, 2005a; Gu and Chalaturnyk, 2005b; Gu and Chalaturnyk, 2006b). With the models and simulation method, the influence of the changes of pore pressures, adsorbed gas volumes and temperatures on permeability and porosity can be simulated. In addition, such characteristics as the discontinuity of coal mass and the anisotropies in permeability, the coefficients of shrinkage/swelling, rock mechanics moduli and the coefficients of thermal expansion, can all be taken into account in simulations.

This chapter will mainly present the application of the reservoir and geomechanical coupled simulation method along with the discontinuum medium permeability and porosity coupling models to the history match of the ECBM and CO_2 sequestration pilot tests in Alberta, Canada.

7.2 BACKGROUND OF SIMULATION WELL

Alberta Research Council (ARC) led a consortium of research institutes, universities and companies to make a series of micro-pilot tests of ECBM and CO_2 sequestration in Fenn Big Valley of Alberta, Canada, during March 1998 to June 2000. The tests were implemented in two Medicine River (upper Mannville) coal intervals of wells FBV 4A and FBV 5. The well histories and tests were detailed by Mavor et al (2004). The history matching of this study will focus on the tests in FBV 4A and the tests in FBV 5 will not be introduced here.

7.2.1 Well History and Field Tests

One important history of FBV 4A that needs to address is the well was hydraulically fractured twice since the existence of hydraulic fractures would change the resistance and path of fluid flow. In August 1992, the first fracturing treatment used 200 m^3 of liquid CO_2 (40 m^3 for pre-pad and 160 m^3 for slurry). The injecting rate was 8 m^3/min at 20 MPa. The fracture gradient was 14.1 kPa/m or 17.78 MPa at the middle depth of the coal seam. In January 1993, the well was fractured again and 14 m^3 of CO_2 was injected followed by 1,600 m^3 of N_2. Both liquids were pumped at 1 m^3/min at a surface pressure of 13 MPa (g).

The well production history before the tests is not known since there is no access to the data. The tests began in March 1998 and the whole test process can chronologically be divided into four major parts. The first part includes an initial production and shut-in test to acquire the initial produced gas components and coalbed properties before CO_2 injection. The second part contains initial injection of two CO_2 segments and a following production period. The third part includes the extended injection test of 12 separate CO_2 segments over 31 days and a following production test. The last part is a flue gas injection test and a following shut-in test.

7.2.2 Previous Simulations and Limitations

Other investigators have simulated some parts of these pilot tests. Pokker and van der Meer (2004) simulated the third part of the pilot tests, i.e. the extended CO_2 injection and following production tests. In their simulation, in order to match the injection pressures a hydraulic fracture was assumed to open if the pressure was higher than fracturing pressure and close if lower than fracturing pressure. The fracture was assumed to extend from about 7 meters in the first

cycle to about 12 meters in the last cycle. In addition, the formation permeability was also assumed to decrease steadily, e.g. assuming the permeability in the last cycle was 4.6 times smaller than that in the first cycle.

Shi and Durucan (2005) simulated the flue gas injection test of the last part of the pilot tests using their analytical permeability model. In their simulation, a radial drainage model was used and the history of hydraulic fracturing was ignored. In order to match the field data, initial gas distributions and matrix shrinkage coefficients of gases were adjusted in an acceptable range.

7.2.3 Selection of Simulation Parts

In this study the coupled simulation will be made to a part of the pilot tests of well FBV 4A due to the limitations of available data and the total restart times in GEM (CMG, 2005), the multiphase and multicomponent fluid flow simulator used in this study. In order to minimize the uncertainties of input data, the second part of the pilot tests, which includes the initial injection of two CO_2 segments and a production period, is selected to simulate. The initial conditions of this simulation are estimated from the first part of pilot tests and well history.

7.3 INPUT DATA FOR COUPLED SIMULATION

The input data include reservoir and fluid properties, the mechanics properties of reservoir and overburdens, and gas rates in injection and production tests. The output and matching data are bottom hole pressures (BHP), water production rates and produced gas compositions.

7.3.1 Basic Data

The input reservoir and fluid data are from several sources, but mainly from Mavor et al (2004) and Shi and Durucan (2005). The drainage area is 30 acres (1.21406×10^5 m^3), representing the designed unit of a five-spot well pattern, and its boundaries are closed. Due to the symmetry, the simulation is made only for one quarter of the well drainage area. The basic well data are listed in Table 7.1 and the Langmuir and sorption parameters of the reservoir coal under in situ conditions (containing moist and ash) are shown in Table 7.2. Because measured relative permeability data were not available, in order to keep consistent the same relative permeability, i.e. the data that were used by Mavor et al (2004) in interpreting the well test before CO_2 injection are applied in this simulation and

shown in Figure 7.1. The data were measured by Gash et al (1993) with one coal sample from the San Juan Basin.

The mechanics properties of the reservoir and overburdens are estimated based on the above mentioned references and our experiences, and are tabulated in Table 7.3. The density of overburdens is equivalent to a stress gradient of 22.62 kPa/m (or 1.0 psi/ft). It is closed to the typical stress gradient in the Western Canadian Sedimentary Basin (WCSB), i.e. 24 kPa/m for the depths greater than 1200 meters (Bell et al, 1994). The minimum effective stress (fracture closure stress) estimated is about 14.5 MPa. Due to no shrinkage/swelling data available, the shrinkage/swelling coefficients of coal matrix are assumed to be 5.0×10^{-4} g/ml for CH_4, 9.0×10^{-4} g/ml for CO_2 and 3.0×10^{-4} g/ml for N_2. They are closed to the values of Canadian coals measured by Chikatamarla et al (2004).

7.3.2 Hydraulic Fracture and Initial Gas Compositions

One challenge of this history matching is to define the existing hydraulic fracture and gas compositions around the hydraulic fracture before the pilot tests. Generally artificial fractures in reservoirs would significantly influence the flow resistance and flow path even when their conductivities are low thus history matches should consider their influences. Before the pilot tests, well FBV 4A was hydraulically fractured twice. To our knowledge, however, creating two fractures is very unlikely since the injection pressures of the second fracturing were not very high. Thus it is assumed there is one two-wing hydraulic fracture in the reservoir. Besides, since CO_2 and N_2 were applied in previous two fracturing treatments and did not completely flow back, the in situ gas compositions around the fracture were disturbed and not the same as the initial coalbed condition. The best way to estimate the length and conductivity of the hydraulic fracture and gas compositions is to make continuous coupled simulations including all the historical events from the initial disturbance of the coalbed. Nevertheless, because there is no access to such history data as drilling, production and operations history, and hydraulic fracturing treatments, no attempt on a complete coupled simulation is made in this study.

A simple estimation is made to the geometry of the hydraulic fracture in this study. According to Mavor et al (2004), the apparent fracture lengths interpreted from the falloffs of the cyclic CO_2 injections (the third part of pilot tests), varied from 6.0 m to 36.4 m. According to our knowledge and considering the history of two hydraulic fracturing treatments, the apparent (effective) fracture is more

likely due to re-activating the existing fracture rather opening a new fracture. A propped fracture of 54.9 m is assumed since the fracture length analyzed from well test interpretations is usually smaller than that from other analysis methods, such as the post-fracturing simulation, the analysis of production history, and pressure decline analysis after the shut-in of fracturing treatments (Gu et al, 1998). This length of the propped fracture may be still conservative for the scales of two hydraulic fracture treatments. The conductivities of the propped fracture will be discussed in detail in Section 7.4.

The gas compositions around the hydraulic fracture are also estimated. According to the production data collected before the pilot tests, the averaged compositions of produced gas were 91.2% of CH_4, 1.8% of C_2H_6, 0.3% of C_3H_8, 1.6% of CO_2, and 5.1% of N_2. The CO_2 and N_2 were from the two hydraulic fracturing treatments in which CO_2 and N_2 were used. Thus it is reasonable to assume that there is a region around the hydraulic fracture where CO_2 and N_2 invaded into the formation during the fracturing treatments and a part of them were absorbed in coal matrix. In the simulations the depth of the invasion zone, which is not an insensible parameter to the simulations, is assumed to be 10.0 m. The gas components are assumed to be homogenous and the same as the compositions of the produced gas before the pilot tests. The gas compositions in other areas are determined by subtracting the fractions of CO_2 and N_2 from the produced gases thus they are 97.75% of CH_4, 2.25% of C_2H_6 and C_3H_8. In simulation C_3H_8 is treated as C_2H_6 and its fraction is added to that of C_2H_6 since there is no detailed information about C_3H_8.

7.3.3 Field data

Field measured data are the rates of injection and production, produced gas compositions and bottom hole pressures during the tests. For confidential reason the data are scaled. The injection rates and bottom hole pressures during injection and falloff tests are shown in Figure 7.2 and the production rates and bottom hole pressures during production and build-up tests in Figure 7.3. The gas compositions during production are indicted in Figure 7.4.

7.4 SIMULATION SCENARIOS

In order to match the well history many scenarios are simulated, including:

1. The propped fracture completely lost its function, i.e. its conductivity is zero. This might happen due to such factors as high fluid damage, proppand embedment into the formation and proppand crushing.

2. The length and dimensionless conductivity, CD_f, of the propped fracture are fixed in each simulation but vary from one simulation to another.

3. The length of the propped fracture is fixed but the fracture conductivity changes with time and locations. In simulation initial fracture conductivity is assumed for the stress condition before the pilot tests then the change of conductivity is calculated based on in situ stresses with the Walsh's model (Walsh, 1981). In addition, because the pressures in the hydraulic fracture would be different from that in the reservoir during injection and production and the simulation would be complicated, for simplification the pressures in the fracture are assumed to decrease linearly from the BHP at the wellbore to the reservoir pressure at the fracture tip.

4. The length of the propped fracture is fixed but the fracture width and conductivity are calculated with the mechanism of hydraulic fracturing (Ji et al, 2005) if the BHP is greater than the fracture closure stress otherwise they are assumed to be zero.

5. The simulations here are different from Scenario 3 in that the base fracture conductivity is a variable rather than a fixed value. During injection and falloffs the base conductivity is fixed and given a higher value. But during the early time of production (i.e. during 12.0 ~ 12.18 days in Figure 7.3) the base conductivity is assumed to decline linearly from the higher value to a lower value with the drops of BHP until BHP reaches the lowest value (i.e. at about 12.18 days in Figure 7.3). Then in the following production and build-up tests the base conductivity is fixed at that lower value.

Each scenario includes tens of simulations. In all scenarios the hydraulic fracture is simulated in the reservoir simulations with the method of permeability enhancement (Carlson, 2003).

7.5 SIMULATION RESULTS

It is unnecessary and impossible to present all lengthy simulation results in this limited space. We will focus on the representative scenarios or those having difficult to understand and give some summaries and comments to the others. In general, the injection and production gas rates, the BHP in the build-up test after the production, and the produced gas compositions are relatively easy to match while the BHP during injection and production is difficult to match. However, the

matches to the BHP of falloff tests and to production water rates are very poor in all simulations.

7.5.1 Scenario 1

Scenario 1 is an ultimate case of a hydraulic fracture. The simulation results show that the injection pressures continuously increased and reached very high levels during injection of two CO_2 segments. The matches to the injection pressures are very poor and unacceptable.

7.5.2 Scenario 2

Scenario 2 might happen if proppand used in hydraulic fracture treatments are rigid. The simulation results indicate that the injection pressures and production pressures can be separately matched through adjusting the dimensionless conductivity of the hydraulic fracture but they cannot be simultaneously matched with a single conductivity value. As shown in Figures 7.5 and 7.6, the injection pressures can be reasonably matched with CD_f=0.12 while the production pressures are well matched with CD_f =0.025 if ignoring the first injection segment where the wellbore storage effect and the mechanism of hydraulic fracturing might play important roles. The results also imply the existing hydraulic fracture might have quite different conductivities during injection and production.

7.5.3 Scenario 3

Scenario 3 may be closer to field realities comparing with Scenario 2 since a hydraulic fracture also deforms and its conductivity varies with the changes of in situ stresses, which can result from the changes of pore pressures during production and injection. The simulation results show that the history match to the BHP has been improved. Nevertheless, the overall match is similar to those shown in Figure 7.5 and 7.6 of Scenario 2.

7.5.4 Scenario 4

Scenario 4 may be a case because (a) the BHP of the first CO_2 injection segment looks like the early time period of a typical pressure curve of hydraulic fracturing, i.e. BHP continuously increases and reaches a peak (fracturing) pressure then decreases; (b) the BHP was ever greater than the fracture closure pressure (about 0.76 scaled BHP in Figure 7.2) for a while thus there was a

possibility of reopening the existing hydraulic fracture. However, the results show that the matches to the field data are still poor.

7.5.5 Scenario 5

Scenario 5 is proposed after carefully examined the simulation results of Scenarios 2, 3 and 4 and the field BHP data. As mentioned in the analysis of Scenario 2, the conductivity of the existing hydraulic fracture might be significantly different during injection and production (see Figure 7.5 and 7.6). The field BHP data also support this inference and are analyzed as the following:

(1) As indicated in Figure 7.2, for a period of time during the injection of the first gas segment, the BHP was greater than the fracture closure pressure (about 0.76 scaled BHP). However, since the BHP was not very high and the duration was not long, more likely the existing hydraulic fracture was re-opened or re-activated rather than a new fracture was formed during this time. When the hydraulic fracture became wider, the used proppand and rock debris produced in the past hydraulic fracturing treatments might be free to move and support the widened fracture. As a result, the fracture would have a high conductivity. During the following injection and falloffs the conductivity might retain high since the proppand and rock debris might be able to stand the in situ stresses.

(2) At the beginning of production, nevertheless, the BHP dropped so drastically (see Figure 7.3) that the in situ stresses at the lowest BHP (about 21 MPa) would be more than twice of the in situ stresses during the gas injection (about 10 MPa on average). The high in situ stresses might excess the strength of the proppand and rock debris and crash them. In addition, the support points of the proppand and rock debris might also be sparse thus stress concentrations would form at the support points. The stresses at these support points might also be greater than the strength of the proppand and rock debris and the possibility of crashing the proppand and rock debris increase. Therefore, the fracture conductivity might decrease significantly with the in situ stress increasing during this period.

(3) After the proppand and rock debris might be crashed and compacted (at about 12.15 days), the fracture conductivity remained low since the pressures in the fracture was continuously increasing but always smaller than the fracture closure pressure during the following production and build-up tests.

The simulation results of Scenario 5 are showed in Figures 7.7 to 7.12. The simulations of the injection and production rates are illustrated in Figures 7.7 and 7.8. The results indicate that the overall simulations of the injection and

production rates are very good but some production rates at the beginning of production have to be decreased since the BHP drops to zero.

The matches of the BHP are indicated in Figure 7.9 and 7.10. The results show that the match of the BHP in the production and build-up tests is very good (Figure 7.10). The match of the second gas injection segment is accepted but the match of the first gas injection segment and the falloffs is very poor (Figure 7.9). The wellbore storage effect is probably the major reason of the poor match. Although it is not simulated, the wellbore storage effect is expected to be significant since the injection fluid was gas. The re-opening process of the existing hydraulic fracture may also play an important role. However, because the mechanism of re-opening is complicated and the study is beyond the scope of this study, it is also not simulated and a base conductivity is given at the beginning of the injection.

The match of production water is illustrated in Figure 7.11 and the match is obviously poor. There are several reasons that possibly cause the poor match. At the first, coal is extremely heterogeneous and the relative permeability curves are variable. Meaney and Paterson (1996) showed that the relative permeability curves varied significantly even they were measured with the samples from the same basin. Therefore the relative permeability curves that we borrowed from the results of one test of one sample from San Juan Basin in the USA may not represent the reality of the upper Mannville coal in Alberta. Further it may not represent the coal in the vicinity of well FBV 4A. The attempt to improve the match using other relative permeability curves is not made because the analysis of absolute reservoir permeability was based on this set of relative permeability curves (Mavor et al, 2004). Using other relative permeability curves would destroy the consistency of analysis. Secondly, the poor match of water rates may relate to the drainage and imbibition processes. Both processes were involved in the injection and production tests but the relative permeability curves used in our simulation were measured based on the drainage process. The results of Reznik et al (1974) showed that the gas relative permeability in drainage process was significantly higher than that in imbibition process. If the studied coal has the similar characteristic, more water would stay in the vicinity of the wellbore during injection and would be easier produced in production. This would improve the match of water rates. The third reason of the poor match may be due to the changes of relative permeability with the changes of in situ stresses. The Reznik et al's studies (Reznik et al, 1974) indicated that the relative permeability of

drainage and imbibition processes changed significantly with the overburden stresses applied. Since the in situ stresses changed drastically in the injection and production of the pilot tests, the relative permeability might also change greatly for the studied coal.

The match of produced gas components is shown in Figure 7.12. The results indicate that the match is good except the beginning period of the production.

Overall, the matches are acceptable given the limitations of the simulators to the wellbore storage effect and re-opening process of a existing hydraulic fracture, the lack of relative permeability curves, and the uncertainties in other input data (such as initial gas distributions around the existing hydraulic fracture, the length of the hydraulic fracture, and field measurements).

7.6 SUMMARY

We summarize the results and learning of the history match as following:

(1) The early part of the injection and production pilot tests of ECBM and CO_2 sequestration in well FBV 4A at Fenn Big Valley of Alberta, Canada, has been successfully simulated and matched with the discontinuum medium porosity and permeability coupling models and the explicit-sequential coupled simulation.

(2) According to the simulation experiences, it is very difficult to simulate the change of conductivity of an existing hydraulic fracture during injection and production. Further studies are needed on understanding its dynamics during injection and production and on the method to incorporate the fracture dynamics in reservoir (and geomechanical coupled) simulations since usually coalbeds are hydraulically fractured due to low permeability.

(3) Relative permeability curves are important for the history match and prediction simulation of CBM and ECBM processes. The measurements should consider the influences of heterogeneity, drainage and imbibition processes, and in situ stresses.

(4) The wellbore storage effect has significant influence to BHP in gas injection and production. More studies are needed on minimizing the influence in field measurements and on the method to include the influence in reservoir (and geomechanical coupled) simulations.

Table 7.1: Basic Formation Parameters

Items	Value
Coal top depth, m	1253.6
Drainage Area, m^2	1.21406×10^5
Coal thickness, m	3.97
Formation temperature, °C	45
Initial average pressure, kPa	7651
Absolute permeability, mD	3.65
Natural fracture porosity, %	0.1
Initial water saturation, %	59.2

Table 7.2: Langmuir and Sorption Parameters

Langmuir pressure, kPa	CH_4	7129
	C_2H_6	1496.9
	CO_2	3030
	N_2	10618
Langmuir volume, ml/g (In situ condition)	CH_4	12.035
	C_2H_6	9.304
	CO_2	27.180
	N_2	5.068
Sorption time of coal, hours		4.93

Table 7.3: Mechanics Properties

Parameters	Overburden	Coal Matrix
Density, kg/m^3	2305.87	1460
Young's modulus, MPa	1000	2900
Poisson's ratio	0.3	0.35
Effective stress ratio (horizontal to vertical)	0.7	0.7
Compressive strength, MPa/m		60
Cleats		
	Intersecting x	**Intersecting y**
Initial normal stiffness, MPa/m	29000	29000
Maximum shear stiffness of cleat, MPa/m	7250	7250
Shear dilation angle, °	10	10
Peak shear displacement, mm	0.1	0.1
Original JRC	5	5
Type of cleat	Matched cleat	Matched cleat
Maximum cleat closure/Initial mechanical cleat width	0.6	0.6

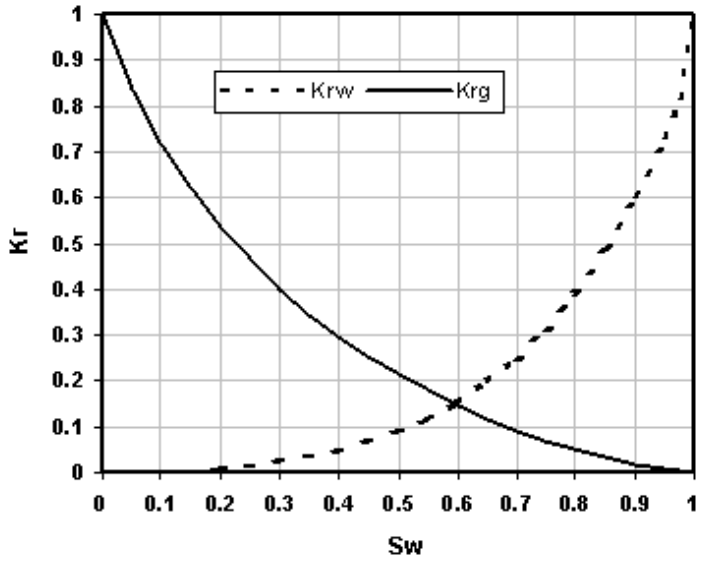

Figure 7.1: Curve of Relative Permeability of Coalbed (Gash et al, 1993)

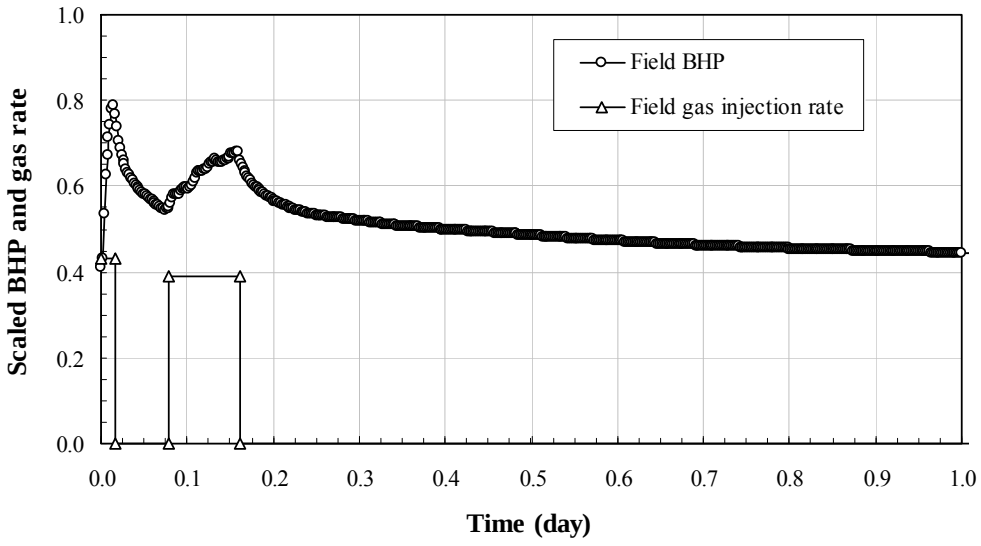

Figure 7.2: Field Rates and BHP during Injection and Falloff Tests

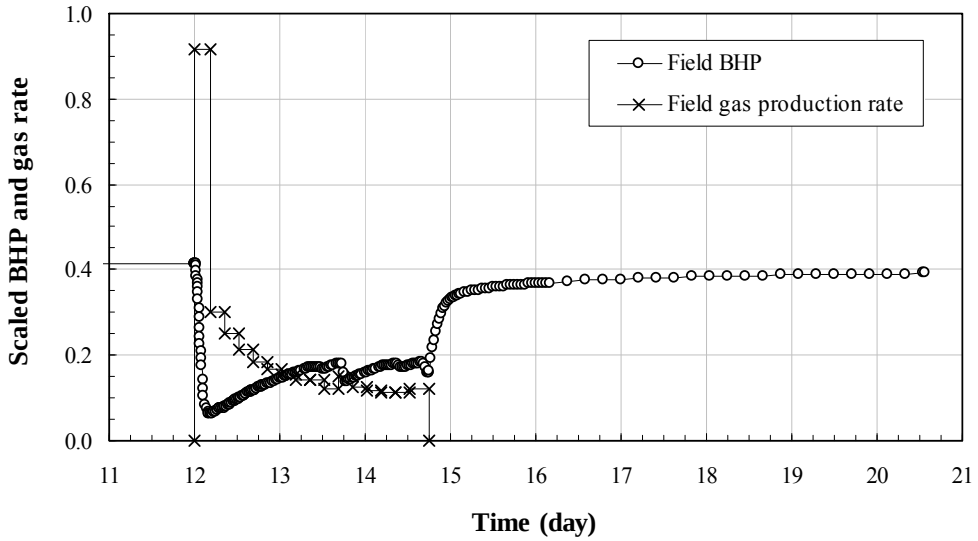

Figure 7.3: Field Rates and BHP during Production and Build-up Tests

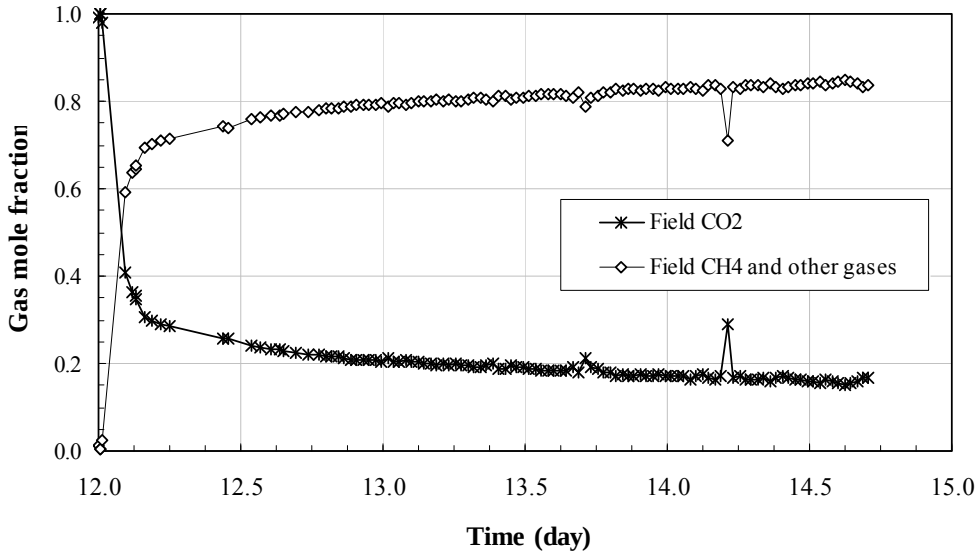

Figure 7.4: Field Gas Compositions during Production

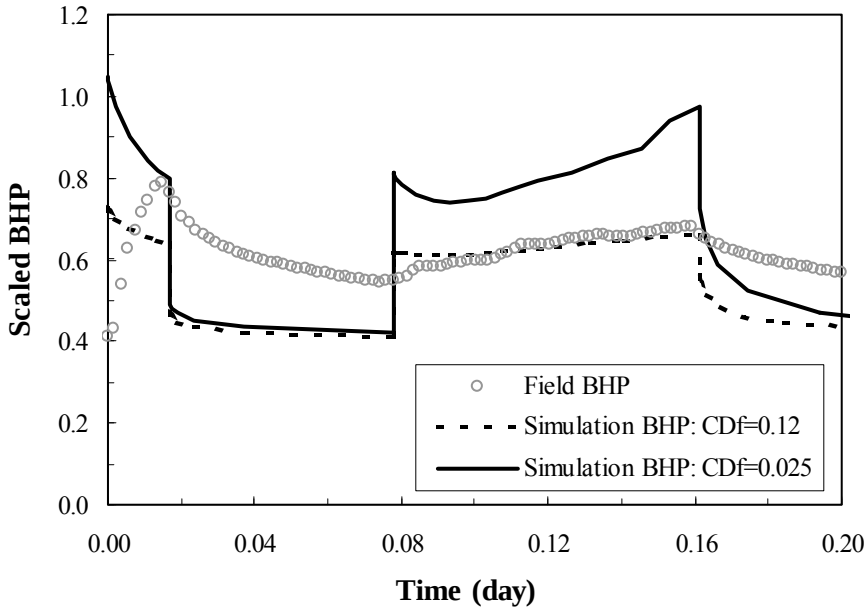

Figure 7.5: Comparison of Simulation BHP during Injection and Falloffs

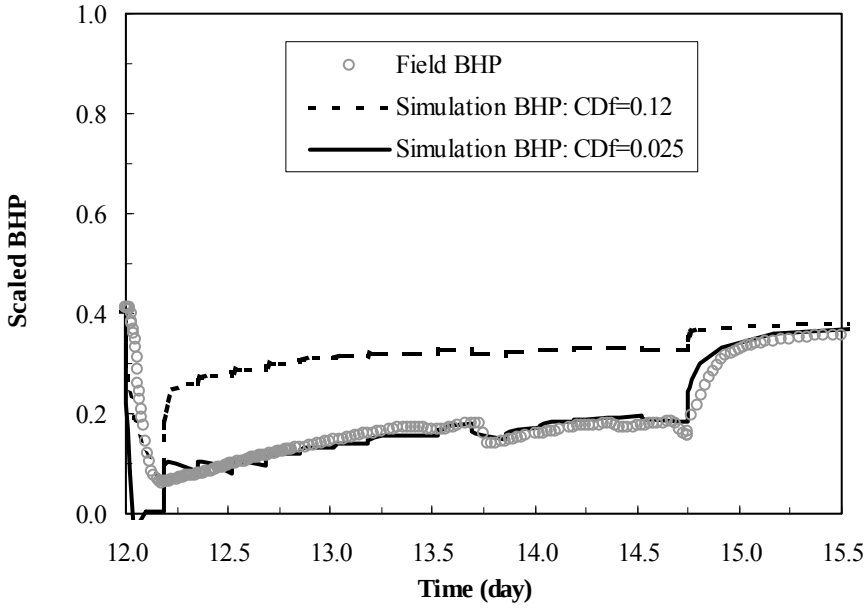

Figure 7.6: Comparison of Simulation BHP during Production and Build-up

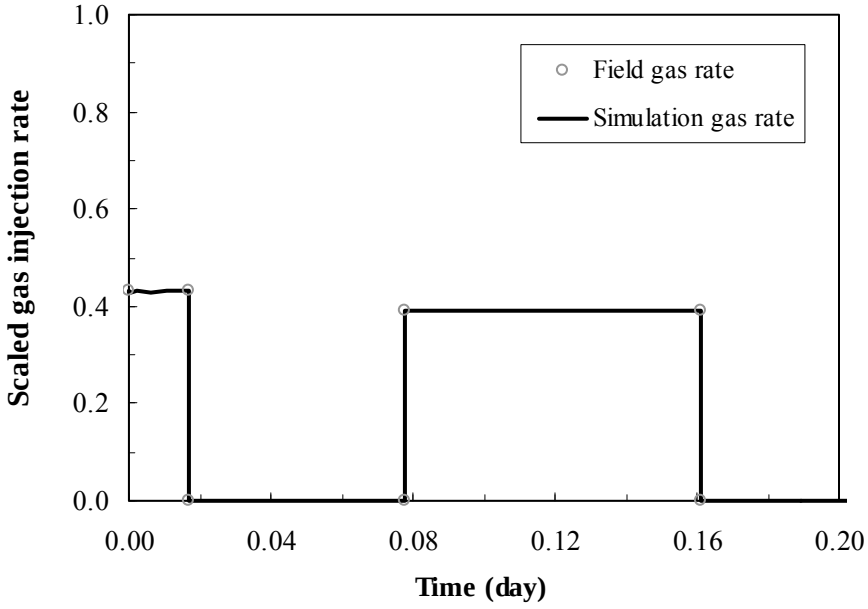

Figure 7.7: Simulation of CO_2 Injection Rates

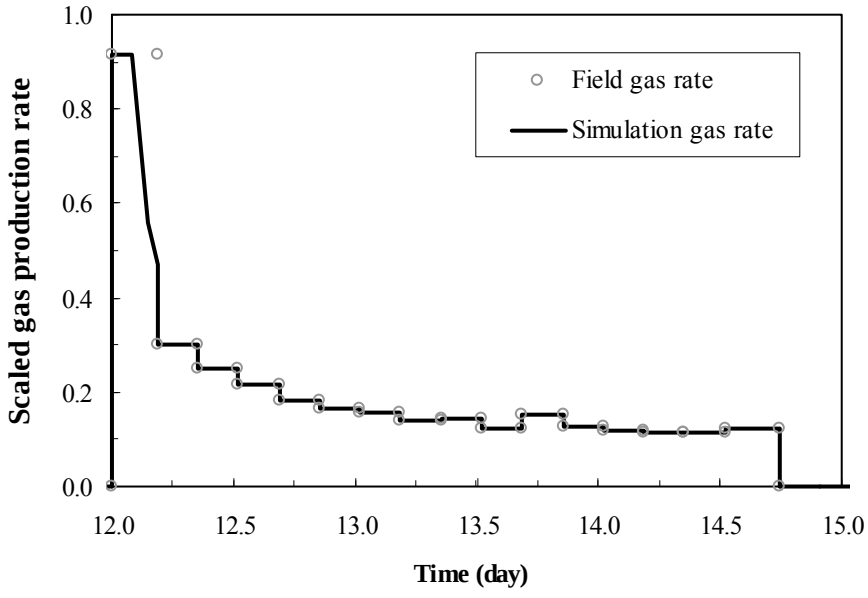

Figure 7.8: Simulation of Gas Production Rates

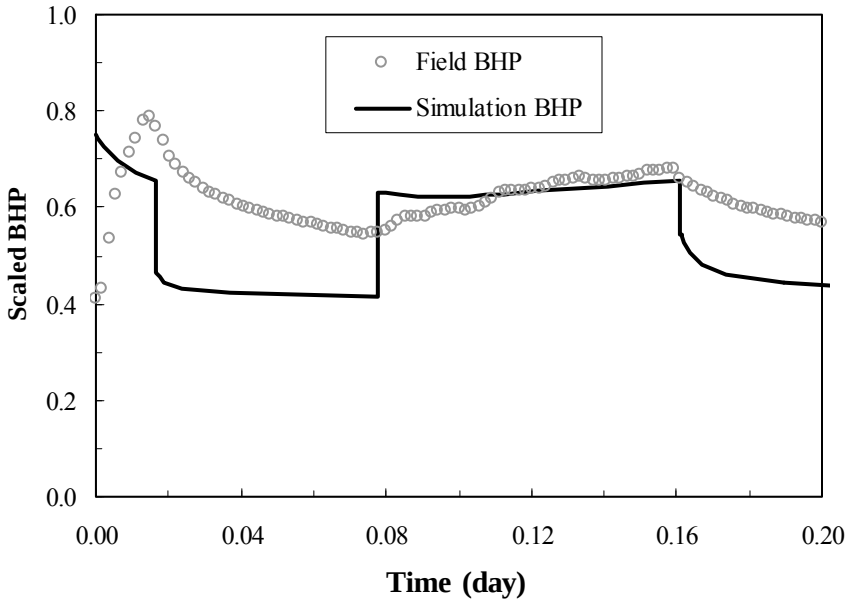

Figure 7.9: Match of BHP during Injection and Falloffs

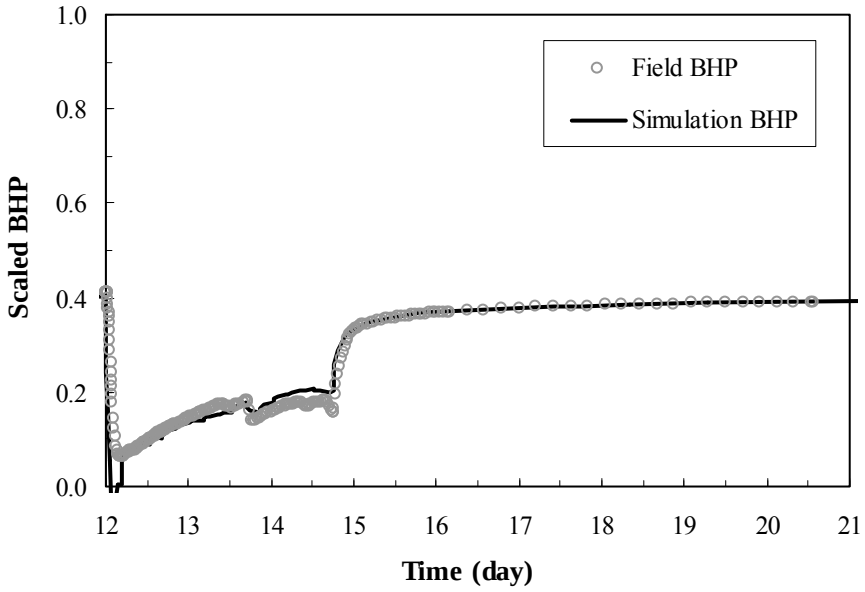

Figure 7.10: Match of BHP during Production and Build-up

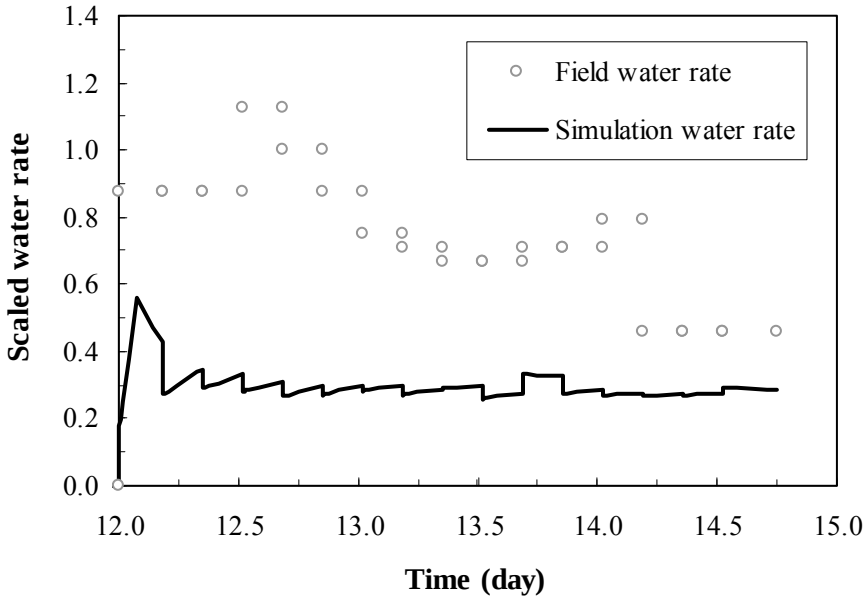

Figure 7.11: Match of Water Production Rates

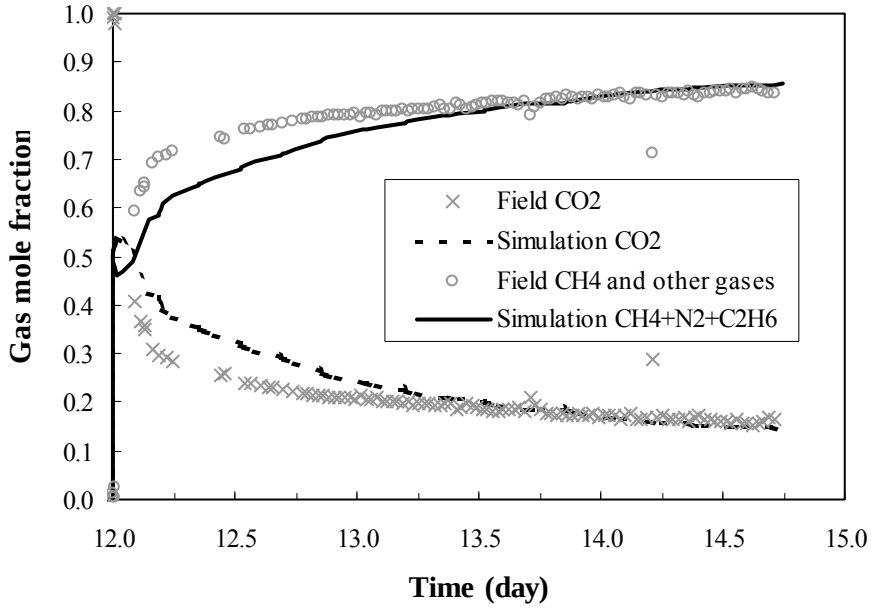

Figure 7.12: Match of Produced Gas Components

8 CONCLUSIONS AND RECOMMENDATIONS

8.1 GENERAL

Coalbeds are extremely complicated porous media due to their characteristics of heterogeneity, dual porosity and stress sensibility. It is very difficult to simulate CBM recovery process and CO_2 sequestration and ECBM recovery process. In the past decades a lot of efforts have been devoted to developing simulation models and great achievements have been made. Nevertheless, many improvements need to make in order to correctly simulate the performances of these processes since some important mechanisms are still not or not properly taken into account in simulations. Of those mechanisms, the influence of geomechanics is probably the paramount one because geomechanics has significant influences to the permeability of coalbeds, the key parameter for the success of CBM recovery process and CO_2 sequestration and ECBM recovery process. However, the permeability of coalbeds is not a constant during these processes but changes drastically due to the alterations of in situ conditions, e.g. the changes of in situ stresses, gas desorption/absorption and temperatures. In present reservoir simulators, the influence of geomechanics to coalbed permeability is considered by using analytical models. Due to the assumptions and over simplifications made in their formulations analytical models have limitations or problems.

The objective of this research is to develop comprehensive permeability and porosity models and corresponding simulation procedures to properly estimate the changes of permeability and porosity in the simulations of CO_2 sequestration and ECBM recovery process based on coalbed characteristics, geomechanics fundamentals, industrial needs and the status of simulation techniques. A set of continuum medium porosity and permeability coupling models is established and the explicitly sequential coupled simulation method to apply these models in reservoir and geomechanical coupled simulations is proposed. Using these models and the simulation method a sensibility study, especially for the parameters related to in situ stresses and matrix shrinkage, has been made to CBM recovery process. Based on the understanding, a set of discontinuum medium porosity and permeability coupling models is developed. The new models are more comprehensive and adaptable to different coalbeds comparing with the early models, including treating coal mass as a discontinuum medium, distinguishing hydraulic apertures and mechanical apertures and considering the anisotropies in

permeability, the coefficients of shrinkage/swelling due to gas desorption/adsorption, mechanics parameters (such matrix moduli and cleat stiffnesses), and the coefficients of thermal expansion. The method to apply these models in reservoir and geomechanical coupled simulations is also presented. Then the proposed deformation model of coal mass is successfully used to simulate a set of lab tests including a uniaxial compression test in vacuum and a CO_2 swelling test under axial constraints in the longitudinal (vertical) direction. At last the discontinuum medium porosity and permeability coupling models and corresponding simulation method are successfully applied to simulate a part of a series of micro-pilot tests of ECBM and CO_2 sequestration at Fenn Big Valley of Alberta, Canada.

8.2 LITERATURE REVIEW

- Coalbeds are dual porosity media containing micropores which exist in coal matrix and macropores called cleats or fractures. Micropores provide the main site of gas storage. Gas absorbs on the walls of micropores and the gas absorption capacity of coal is described with adsorption isotherms. Coal matrix swells due to gas adsorption and shrinks due to gas desorption. Cleats are the major conduit of fluid flow in coalbeds and have permeability with the characteristics of anisotropy, stress dependency, gas adsorption/desorption dependency, and stress history dependency.

- The methods of coalbed methane recovery include pressure depletion coalbed methane (CBM) recovery and enhanced coalbed methane recovery (ECBM). The ultimate methane recovery with CBM method is generally not greater than 50% of the gas-in-place. CO2, N2 even flue gas can be applied in ECBM process. However the techniques of ECBM are under development and field experiences are limited.

- The available analytical models used to predict the change of permeability and porosity can be classed into empirical and theoretical models. The former was established based on experiment results made with the specimens of specific coalbeds and cannot be extended to other coalbeds. The later includes the models considering the influences of pressure changes only, the influences of shrinkage/swelling of matrix only, and the

influences of both. According to the application, the models can also be divided into the models applied in CBM or ECBM.

- For fractured rock, the tortuosity, roughness and contact area of fractures would influence fracture permeability. Many analytical models have been developed to predict the change of permeability or conductivity of a single fracture due to the changes of in situ stresses. They include the models of Barton et al, Walsh, Bai and Elsworth, and Willis-Richards et al, etc. There are several constitutive models available to describe the deformation of fractures, such as the Goodman's empirical model, Barton et al's empirical model and Jing et al's theoretical model. For fractured rocks with massive fractures, equivalent continuum models are the best to simulate their deformations since constitutive models need too high computing resources to be affordable or available.

- Based on the degree of coupling, the coupled simulations can be classed into full coupled, sequential coupled and decoupled simulations. There are few models developed to simulate coalbed methane production in a small scale with full coupled simulation method. The coupled simulations of fractured rocks have been studied for almost 20 years and applications can be found in single phase situation such as hydrogeology, geotechnical engineering and radiation waste storage. For multiphase, multicomponent and large scale fractured reservoirs in petroleum industry, sequential coupled simulation with equivalent continuum approach for fractured rock mass is a practical solution at present.

8.3 CONTINUUM MEDIUM POROSITY AND PERMEABILITY COUPLING MODELS

- The influences of geomechanics are important for CBM recovery and ignoring the influences may lead to errors in the evaluation of coalbed methane production.

- On the basis of geomechanics and considering the changes of in situ total stresses, pore pressures, adsorbed gas and heat expansion, the models to predict the changes of cleat permeability and porosity have been developed for reservoir and geomechanical coupled simulation.

Permeability anisotropy of coal seams can also be considered using the developed model.

- The explicitly sequential coupled simulation method and simulation procedure have been established to simulate CBM recovery using recognized, developed and well-supported industrial simulators.

- The simulation results of the study case show that the matrix shrinkage due to methane desorption will result in the increase of cleat permeability in most seam areas close to a producer even though the mean effective stresses increase during CBM recovery. The methane production rates and cumulative production from explicitly sequential coupled simulations using the permeability coupling model (developed in this chapter) are higher than that from conventional simulation (constant permeability).

8.4 SENSITIVITY STUDY OF CBM RECOVERY

- Caution should be exercised in estimating the change of permeability from the change of strains in coupled simulations. If the anisotropic deformation of coal is not treated properly and linear strains are simply computed as one third of the volumetric strain, the simulated CBM production rates and cumulative gas production would be overly optimistic.

- Permeability, well control area, seam depth (corresponding to in situ stresses), the Langmuir volume (corresponding to initial gas content) and the Langmuir pressure are the most sensitive parameters that influence CBM production in coupled simulations.

- Cleat spacing, coefficient of matrix shrinkage and pressure gradient (related to initial gas content and initial stresses) are the second sensitive parameters that influence CBM production in coupled simulations.

- Young's modulus and Poisson's ratio are insensitive parameters influencing CBM production in coupled simulations.

- Due to the consideration of matrix shrinkage of coal, the maximum gas rate and final cumulative gas production from coupled simulations are

higher than those from conventional simulations (constant permeability) when matrix shrinkage dominates the deformation of the coal, i.e. when pressures decrease matrix shrinkage will result in the increase of permeability although in situ stresses would increase and as a results the compression of cleats would increase.

8.5 DISCONTINUUM MEDIUM POROSITY AND PERMEABILITY COUPLING MODELS

- New porosity and permeability coupling models used in coupled simulations have been established for CBM and ECBM recovery. The models consider the influences of the discontinuity and anisotropy of coal. With these models the anisotropies in permeability, the matrix shrinkage/swelling due to gas desorption/adsorption, mechanics parameters and the thermal expansion/contraction due to temperature changes can be simulated in coupled simulations.

- Due to considering the changes of permeability and porosity during CBM production the results using the proposed coupled simulation procedure and models are significantly different from the simulation results using constant permeability and porosity. The gas rates and cumulative gas production of the former are usually larger than those of the later.

- Permeability and porosity change drastically in the areas near to wellbores during CBM production. Although initial permeability is assumed to be isotropic the deformation of coal can result in the anisotropy of permeability. The anisotropic ratio of permeability reached as much as 3.04 in the investigated case.

- The explicitly sequential coupled simulation for CBM production is reliable and affordable if a proper trade-off is made between the simulation cost and simulation accuracy.

- Permeability and porosity have no monotonic relation with pore pressures and mean and horizontal effective stresses for CBM production. The application of Equation (5.42) to formulate CBM analytical permeability models is questionable and not reliable.

- Due to neglecting the cleat anisotropy and the difference between mechanical apertures and hydraulic apertures, the relation of Equation (5.43) and the analytical permeability models based on this relation in the formulation are questionable. The power of 1/6 in the relation between permeability ratio and porosity ratio shows more applicable than the power of 1/3 for coalbeds.

- Initial water saturation influences not only the cost to handle produced water but also the cumulative gas production and final gas recovery. The development of coalbeds with lower initial water saturation would produce a better economic result even not considering the saving on the cost of dealing with produced water.

8.6 APPLICATION TO LAB COAL DEFORMATION TESTS

- Analytical permeability models considering the influences of pressure drops and the shrinkage/swelling of coal matrix due to gas desorption/adsorption can be easily applied in current reservoir simulators. However, they have such limitations as assuming permeability is isotropic, applying the linear elastic continuum model for coal mass (a discontinuum medium), neglecting the interaction between stresses and strains when applying the principle of superposition, and ignoring the difference between mechanical and hydraulic apertures.

- The swelling strains of coal under constraint conditions are much smaller compared with those under unconfined or no constraint conditions. Analytical permeability models were developed with application of the principle of superimposition to the changes of strains or stresses under in situ stress conditions. Thus, the swelling strains used in these models should be measured under in situ stress conditions rather than under no constraint conditions, even though the latter is common practices in the application of analytical models.

- The linear elastic deformation model, suitable to isotropic continuum media but generally assumed in analytical permeability models, cannot adequately simulate the deformation behaviour of coal mass due to its

nonlinear deformation characteristic. The equivalent continuum medium model considering the influence of discontinuity and anisotropy of coal matrix and cleats can properly simulate the nonlinear deformation behaviour of coal mass.

- Unlike analytical permeability models, the change of permeability predicted with the discontinuum medium coupling permeability model has no unique relation with the change of pore pressures. It relates to the locations in a coalbed (i.e. local in situ conditions). The permeability coupling model provides better estimates of permeability and production because it includes the influences of many factors, such as the in situ deformation, discontinuities and anisotropies of coal mass.

8.7 APPLICATION TO FIELD ECBM PILOT TESTS

- The early part of the injection and production pilot tests of ECBM and CO2 sequestration in well FBV 4A at Fenn Big Valley of Alberta, Canada, has been successfully simulated and matched with the discontinuum medium porosity and permeability coupling models and the explicit-sequential coupled simulation.

- According to the simulation experiences, it is very difficult to simulate the change of conductivity of an existing hydraulic fracture during injection and production. Further studies are needed on understanding its dynamics during injection and production and on the method to incorporate the fracture dynamics in reservoir (and geomechanical coupled) simulations since usually coalbeds are hydraulically fractured due to low permeability.

- Relative permeability curves are important for the history match and prediction simulation of CBM and ECBM processes. The measurements should consider the influences of heterogeneity, drainage and imbibition processes, and in situ stresses.

- The wellbore storage effect has significant influence to BHP in gas injection and production. More studies are needed on minimizing the

influence in field measurements and on the method to include the influence in reservoir (and geomechanical coupled) simulations.

8.8 RECOMMENDATIONS

CBM and ECBM processes involve many complicated mechanisms including multiphase flow in stress dependent low permeability media, matrix shrinkage/swelling due to gas desorption/adsorption, adsorption/desorption of multicomponent gases and non-linear deformation of discontinuous media etc. However, due to the limitation of time, understanding, experimental results and simulation tools etc., this research only tackled some of these difficulties. Through many years of research, I think the following areas are important and still need further research efforts.

- Coal matrix shrinkage/swelling and gas desorption/adsorption under conditions of multiple gases and constraints

Many past studies on coal matrix shrinkage/swelling and gas desorption/adsorption were about single gas component rather than multiple gases. How multiple gases absorb on coal matrix and how gas components influence the deformation are not fully understood, especially under in situ constraint conditions.

- Change of relative permeability with alteration of in situ stresses

Relative permeability curves are necessary data for the simulations of CBM and ECBM processes. In most coalbeds cleats are initially filled by water (brine) thus multiphase flow usually occurs. The studies of Reznik et al (1974) and Gash et al (1993) indicated the relative permeability of coalbeds changed with overburden or confining stress applied. However, the studies in this area are very few. Further research needs to focus on how relative permeability changes with in situ stresses and how to simulate this in coupled simulation.

- Influence of hydraulic fractures

Due to the nature of low permeability, coalbeds usually need to be hydraulically fractured before a CBM or ECBM recovery process begins. The conductivity of hydraulic fractures is not constant but changes with in situ conditions during production. As shown in this research, it is a challenge to properly include and simulation the property change of hydraulic fractures in the reservoir and geomechanical simulation.

- Relationship between hydraulic aperture and mechanical aperture

Studies indicate that fractures cannot be simplified as a smooth plate channels. Hydraulic apertures are different from mechanical apertures. The former is used to describe fluid flow in fractures but the latter represents the physical size of fractures. For coalbeds, the relationship between them is not clear. In addition, the accurate measurement of mechanical apertures is also difficult since the apertures of cleats are very small, in a scale of microns.

- Effective stresses in coalbeds

In our study, effective stresses are estimated with Terzaghi's (1943) logic due to the limitation of simulation tools. The study of Zhao et al (2003) illustrated that the Biot's effective stress law was valid for several coals from Chinese mines but the Biot's coefficient was not a constant but a bilinear function of volumetric stress and pore pressure. Besides, for orthotropic media Cheng (1997) showed that directional Biot's coefficients were required. Effective stress law of coals (an orthotropic medium) is not truly understood and needs more investigations.

BIBLIOGRAPHY

Amadei, B., and Goodman, R.E., 1981. A 3-D constitutive relation for fractured rock masses. Selvadurai, A.P.S.(Editor), Mechanics of Stuctured Media (Part B). Elsevier Scientific Publishing Company, New York, USA, pp. 249–268.

Al-hawaree Mohamad, 1999. Geomechanics of CO2 Sequestration in Coalbed Methane Reservoir. Thesis of Master Degree. Department of Civil and Environmrntal Engineering, University of Alberta, Edmonton, Alberta, Canada.

Arri, A.E., Yee, D., Morgan, W.D. and Jeansonne, M.W., 1992. Modeling Coalbed Methane Production With Binary Gas Sorption. The SPE Rocky Mountain Regional Meeting. The Society of Petroleum Engineers, Richardson, Texas, USA, paper SPE 24363.

Bachu, S. and Shaw, J., 2003. Evaluation of the CO_2 Sequestration Capacity in Alberta's Oil and Gas Reservoirs at Depletion and the Effect of Underlying Aquifers. Journal of Canadian Petroleum Technology, 42(9): 51-61.

Bagheri, M.A. and Settari, A., 2006. Effects of fractures on reservoir deformation and flow modeling. Can. Geotech. J. , 43: 574-586.

Bagheri, M.A. and Settari, A., 2008. Modeling of Geomechanics in Naturally Fractured Reserovirs. SPE Reservoir Evaluation & Engineering, February Issue: 108-118.

Bandis, S.C., Lumsden, A.C. and Barton, N.R., 1983. Fundamentals of Rock Joint Deformation. Int. J. Rock Mech. Min. Sci. & Geomech. Abstr., 20(6):249-268.

Barton, N., Bandis, S. and Bakhtar, K., 1985. Strength, Deformation and Conductivity Coupling of Rock Joints. Int. J. Rock Mech. Min. Sci. & Geomech. Abstr., 22(3): 121-140.

Barton, N. and Choubey, V., 1977. The Shear Strength of Rock Joints in theory and Practice. Rock Mechanics, 10: 1-54.

Bai, M., Elsworth, D. and Roegiers, J.-C. 1993. Modeling of Naturally Fractured Reservoirs Using Deformation Dependent Flow Mechanism. Int. J. Rock Mech. Min. Sci. & Geomech. Abstr., 30: 1185-1191.

Bai, M. and Elsworth, D., 1994. Modeling of Subsidence and Stress-Dependant Hydraulic Conductivity for Intact and Fractured Porous Media. Rock Mechanics and Rock Engineering, 27(4): 209-234.

Bai, M. and Roegiers, J.-C., 1994. Fluid Flow and Heat Flow in Deformable Fracutred Porous Media. Int. J. Engng Sci., 32(10): 1615-1633.

Bai, M., Roegiers, J.-C. and Elsworth, D., 1995. Poromechanical response of fractured-porous rock masses. Journal of Petroleum Science and Engineering, 13: 155-168.

Bart, M., Shao, J.F., Lydzba, D. and Haji-Sotoudeh, M., 2004. Coupled hydromechanical modeling of rock fractures under normal stress. Can. Geotech. J., 41: 686–697.

Beecy, D.A., Kuuskraa, V.A. and Schmidt, C., 2001. A Perspective on the Potential Role of Geologic Options in A National Carbon Management Strategy. First National Conference on Carbon Sequestration. Washington, DC, USA.

Bell, J.S., Price, P.R. and McLellan, P.J., 1994. In-situ Stress in Western Canada Sedimentary Basin. Chapter 29 in the Geological Atlas of the Western Canada Sedimentary Basin, ISPG/ARC/CSPG.

Bogdanov, I.I., Mourzenko, V.V., Thovert, J.-F. and Adler, P.M., 2003. Effective permeability of fractured porous media in steady state flow. Water Resources Research, 39(1): paper 1023.

Brown, S.R., 1987. Fluid Flow Through Joints: The Effect of Surface Roughness. Journal of Geophysical Research, 92(B2): 13337-1347.

Brown, S.R., 1995. Simple mathematical model of a rough fracture. Journal of Geophysical Research, 100(B4): 5941-5952.

Brown, S.R., 1998. Fluid permeability of deformable fracture network. Journal of Geophysical Research, 103(B2): 2489-2500.

Carlson, M.R., 2003. Practical Reservoir Simulation. PennWell Corporation, Tulsa, U.S.A.

Ceglarska-Stefanska, G., 1994. Effect of gas pressure in methane inclued swelling on the porous structure of coals. Studies in Surface and Catalysis, 87: 671-677.

Ceglarska-Stefanska, G. and Brzoska, K., 1998. The effect of coal metomorphism on methane desorption. Fuel, 77(6): 645-648.

Ceglarska-Stefanska, G. and Czaplinski, A., 1993. Correlation between sorption and dilatometric processes in hard coals. Fuel, 72(3): 413-417.

Ceglarska-Stefanska, G. and Zarebska, K., 2002a. Expansion and Contraction of Variable Rank Coals During the Exchange Sorption of CO2 and CH4. Adsorption Science & Technology, 20(1):49-62.

Ceglarska-Stefanska, G. and Zarebska, K., 2002b. The competitive sorption of CO2 and CH4 with regard to the release of methane from coal. Fuel Processing Technology, 77-78:423-429.

Charlier, R., Fourmaintraux, D., Samier, P., Radu, J.-P. and Guiducci, C., 2002. Numerical Simulation of the Coupling Behavoir of Faults during the Depletion of a High-Pressure/High-Temperature Reservoir. The SPE/ISRM Rock Mechanics Conference. The Society of Petroleum Engineers, Richardson, Texas, USA, paper SPE 78199.

Chappell, B.A., 1987. Predicted and Measured Rock Mass Moduli. Journal of Mining Science and Technology, 6(1):89-104.

Chaback, J.J., Morgan, D. and Yee, D., 1996. Sorption Irreversibilities and Mixture Compositional Behavior During Enhanced Coal Bed Methane Recovery Processes. The Gas Technology Conference. The Society of Petroleum Engineers, Richardson, Texas, USA, paper SPE 35622.

Chen, M. and Bai, M., 1998. Modeling Stress-dependent Permeability for Anisotropic Fractured Porous Rocks. International Journal of Rock Mechanics & Mining Sciences, 35(8):1113-1119.

Chen, E.P., 1986. Two-Dimensional Continuum Model for Jointed Media. The 27th U.S. Symposium on Rock Mechanics. Society of Mining Engineers Inc., Littletown, CO, USA, pp.862-867.

Chen, E.P., 1989. A constitutive model for jointed rock mass with orthogonal sets of joints. Journal of Applied Mechanics (Trans ASME), 56:25-32.

Chen, H.Y. and Teufel, L.W., 1997. Coupling Fluid-Flow and Geomechanics in Dual-Porosity of Naturally Fractured Reservoirs. The 1997 SPE Annual Technical Conderences and Exibition. The Society of Petroleum Engineers, Richardson, Texas, USA, paper SPE 78199.

Cheng, A. H.-D., 1997. Material Coefficients of Anisotropic Poroelasticity. International Journal of Rock Mechanics & Mining Sciences, 34(2): 199-205.

Chikatamarla L., Cui, X. and Bustin, R.M., 2004. Impactions of Volumetric Swelling/Shrinkage of Coal in Sequestration of Acid Gases. The 2004 International Coalbed Methane Symposium. The University of Alabama, Tuscaloosa, Alabama, USA, paper 0435.

CMG, 2003a. User's Guide GEM. Computer Modelling Group Ltd., Calgary, Canada.

CMG, 2003b. User's Guide STARS. Computer Modelling Group Ltd., Calgary, Canada.

CMG, 2005. User's Guide GEM. Computer Modelling Group Ltd., Calgary, Canada.

Crosdale, P.J., 1999. Mixed methane/carbon dioxide sorption by coal: New evidence in support of pore-filling models. The 1999 International Coalbed Methane Symposium. The University of Alabama, Tuscaloosa, Alabama, USA, paper 9927.

Czaplinski, A., Gustkiewicz, J. and Holda, S., 1986. An Apparatus for investigation of Changes of Stresses and Strains of Rock Samples under Sorption. Archiwum Gornictwa (Archives of Mining Sciences, Warsaw, Poland), 31(4):703-716.

Czaplinski, A. and Gustkiewicz, J., 1990. Sorption Stresses and Deformations in Coal. Strata as Multiphase Medium (in Polish, an English version was provided by the second author), 2:455-468.

Dabbous, M.K., Reznik, A.A., Taber, J.J. and Fulton, P.F., 1974. The Permeability of Coal to Gas and Water. SPE J., December Isssue:563-572.

Das, M.N. and Sheorey, P.R., 1986. Triaxial strength behavior of some Indian coals. Journal of Mines, Metals & Fuels, 34:118-122.

Davidson, R. M., Sloss, L. L. and Clarke L. B., 1995. Coalbed methane extraction. IEA Coal Research, London.

Durucan, S., Daltaban, T.S., Shi, J.Q. and Foley, L., 1993. Permeability Characterisation for Modelling Methane Flow in Coal Seams. The 1993 International Coalbed Methane Symposium, The University of Alabama, Tuscaloosa, Alabama, USA, paper 9315.

Durucan, S., Daltaban, T.S., Shi, J.Q. and Wang, J.M., 1995. Numerical Modelling and Verification of Stress and Pore Pressure Dependent Dynamic Permeability Behaviour of Coal Seams around Wellbores. The 1995 International Unconventional Gas Symposium. The University of Alabama, Tuscaloosa, Alabama, USA, paper 9528.

EIA (Energy Information Administration, U.S. DOE), 2004. U.S. Crude Oil, Natural Gas, and Natural Gas Liquids Reserves: 2003 Annual Report. Washington DC, USA.

Elsworth, D., 1989. Thermal Permeability Enhancement of Blocky Rocks: One-Dimensional Flows. Int. J. Rock Mech. Min. Sci. & Geomech. Abstr., 26(3/4):329-339.

Elsworth, D. and Bai, M., 1992. Flow-Deformation Response of Dual-Porosity Media. Journal of Geotechnical Engineering, 118(1):17-124.

Elsworth, D. and Xiang, J., 1989. A reduced degree of freedom model for thermal permeability enhancement in blocky rock. Geothermics, 18(5/6):697-709.

Enever, J.R.E and Hening A., 1997. The relationship between permeability and effective stress for Australian Coals and its implications with respect to coalbed methane exploration and reservoir modelling. The 1997 International Coalbed Methane Symposium. The University of Alabama, Tuscaloosa, Alabama, USA, paper 9722.

Enever, J., Casey, D., and Bocking, M., 1999. The Role of In-situ Stress in Coalbed Methane Exploitation. In: M. Mastalerz, M. Glikson and S.D. Golding (Editors), Coalbed Methane: Scientific, Environmental and Economic Evaluation. Kluwer Academic Publishers, Dordrecht, Netherlands, pp.297-303.

Fossum, A.F., 1985. Effective elastic properties for a randomly jointed rock mass. Int. J. Rock Mech. Min. Sci. & Geomech. Abstr., 22:467-470.

Gash B.W., Volz, R.F., Potter, G., and Corgan, J.M., 1993. The effects of cleat orientation and confining pressure on cleat porosity, permeability and relative permeability in coal. The 1993 International Coalbed Methane Symposium. The University of Alabama, Tuscaloosa, Alabama, USA, paper 9321.

Gangi, A.F., 1978. Variation of whole and fractured porous rock permeability with confining pressure. Int. J. Rock Mech. Min. Sci. & Geomech. Abstr., 15: 249-257.

Gavrilenko, P. and Gueguen, Y., 1989. Pressure dependence of permeability: a model for cracked rocks. Geophysical Journal International, 98:159-172.

Gerrard, C.M., 1982. Elastic models of rock masses having one, two and three sets of joints. Int. J. Rock Mech. Min. Sci. & Geomech. Abstr.,19:15-23.

George, J.D. St. and Barakat, M.A., 2001. The change in effective stress associated with shrinkage from gas desorption in coal. International Journal of Coal Geology, 45:105–113.

Ghafouri, H.R and Lewis, R.W., 1996. A Finite Element Double Porosity Model For Heterogeneous Deformable Porous Media. International Journal for Numerical and Analytical Methods in Geomechanics, 20: 831-844.

Gilman, A. and Bechie, R., 2000. Flow of Coal-Bed Methane to a Gallery. Transport in Porous Media, 41:1-16.

Goodman, Richard E., 1989. Rock Mechanics (2nd ed.). John Wiley & Sons, New York. pp.182-183.

Goodman, R.E., 1976. Methods of Geological Engingeering in Discontinous Rocks. West Publishing Company, New York, USA.

Gong, J., 2002. Steam-Assisted Gravity Drainage Process Enhancement. Thesis of Master Degree. Department of Civil and Environmrntal Engineering, University of Alberta, Edmonton, Alberta, Canada.

Gray, I., 1987. Reservoir Engineering in Coal Seams: Part 1--- The Physical Process of Gas Storage and Movement in Coal Seams. SPE Reservoir Engineering, February Issue:28-34.

Gu, F., Duan, Y., Yang, H., Yuan, Z. and Zhang, W., 1998. Evaluating Hydraulic Fractures by Integrated Techniques. The 49th Annual Technical Meeting, Petroleum Society, Calgary, Canada, paper CIM 98-86.

Gu, F. and Chalaturnyk, R.J., 2005a. Analysis of Coalbed Methane Production by Reservoir and Geomechanical Coupled simulation, Journal of Canadian Petroleum Technology, 44(10): 33-42.

Gu, F. and Chalaturnyk, R.J., 2005b. Sensitivity Study of Coalbed Methane Production with Reservoir and Geomechanic Coupled simulation. Journal of Canadian Petroleum Technology, 44(10): 23-32.

Gu, F. and Chalaturnyk, R.J., 2006a. History Matching on Micro-Pilot Tests for ECBM and CO_2 Sequestration with Geomechanical and Reservoir Coupled Simulation. The 2006 International Coalbed Methane Symposium. The University of Alabama, Tuscaloosa, Alabama, USA, paper 0618.

Gu, F. and Chalaturnyk, R.J., 2006b. Numerical Simulation of Stress and Strain due to Gas Sorption/Desorption and Their Effects on In situ Permeability of Coalbeds. Journal of Canadian Petroleum Technology, 45(10): 52-62.

Gustkiewicz, J. and Orengo, Y., 1998. Behavior of coal caused by water or carbon dioxide. In: Lin, Yunmei(Editor), Advances in Rock Mechanics. World Scientific Publishing Co. Pte. Ltd., Singapore, pp.18-27.

Gutierrez, M., Lewis, R.W. and Masters, I., 2001. Petroleum Reservoir Simulation Coupling Fluid Flow and Geomechanics. SPE Reservoir Eveluation & Engineering, June issue:164-172.

Hall, F.E., Zhou, C., Gasem, K.A.M. and Robinson Jr., R.L., 1994. Adsorption of Pure Methane, Nitrogen, and Carbon Dioxide and Their Binary Mixtures on Wet Fruitland Coal. The 1994 Eastern Regional Conference & Exhibition. The Society of Petroleum Engineers, Richardson, Texas, USA, paper SPE 29194.

Harpani S. and Chen, G., 1993. Gas Slippage and Matrix Shrinkage Effect on Coal Permeability. The 1993 International Coalbed Methane Symposium. The University of Alabama, Tuscaloosa, Alabama, USA, paper 9325.

Harpalani, S. and Chen, G., 1995. Estimation of changes in fracture porosity of coal with gas emission. Fuel, 74(10):1491-1498.

Harpalani, S. and Chen, G., 1997. Influence of gas production induced volumetric strain on permeability of coal. Geotech.Geol. Eng., 15: 303–325.

Harpalani, S. and McPherson, M. J., 1985. Effect of Stress on Permeability of Coal. The 26th U.S. Symposium on Rock Mechanics. A.A. Balkema Publishers, Rotterdam, Boston, USA, pp.831-839.

Harpalani, S. and Schraufnagel, R.A., 1990a. Shrinkage of coal matrix with release of gas and its impact on permeability of coal. Fuel, 69: 551-556.

Harpalani, S. and Schraufnagel, R.A., 1990b. Influence of Matrix Shrinkage and Compressibility on Gas Production From Coalbed Methane Reservoirs. The 65th Annual Technical Conference and Exhibition. The Society of Petroleum Engineers, Richardson, Texas, USA, paper SPE 20729.

Harpalani S. and Zhao, X., 1989. An Investigation of the Effect of Gas Desorption on Coal Permeability. The 1989 Coalbed Methane Symposium. The University of Alabama, Tuscaloosa, Alabama, USA, paper 8923.

Hettema, M.H.H., Schutjens, P.M.T., Verboom, B.J.M., and Gussinklo, H.J., 2000. Production-Induced Compaction of a Sandstone Reservoir: The Strong Influence of Stress Path. SPE Reservoir Evaluation and Engineering, 3(4): 342-347.

Hobbs, D.W., 1964. The strength and the stress-strain characteristics of coal in triaxial compression. Journal of Geology, 72(2):214-231.

Hu, K.X. and Huang, Y., 1993. Estimation of the Elastic Properties of Fractured Rock Masses. Int. J. Rock Mech. Min. Sci. & Geomech. Abstr., 30(4):381-394.

Huang, T.H., Chang, C.S. and Yang, Z.Y., 1995. Elastic Moduli for Fractured Rock Mass. Rock Mech. Rock Engng., 28(3): 135-144.

Huddleston, J.C., Marshall, J.S. and Pilcher, R.C., 1995. Analysis of Sorption and Thermodynamic Data and a Discussion of an Empirical Model for Sorbed Gases in Coal. The 1995 International Unconventional Gas Symposium. The University of Alabama, Tuscaloosa, Alabama, USA, paper 9523.

Indraratna, B., Ranjith, P.G. and Gale, W., 1999. Single phase water flow through rock fractures. Geotechnical and Geological Engineering, 17: 211-240.

Itasca, 2000. UDEC (Universal Distinct Element Code) User's Guide. Itasca Consulting Group, Inc., Minneapolis, USA.

Itasca, 2002a. FLAC (Fast Lagrangian Analysis of Continua) User's Guide. Itasca Consulting Group, Inc., Minneapolis, USA.

Itasca, 2002b. FLAC3D (Fast Lagrangian Analysis of Continua in 3 Dimensions) User's Guide. Itasca Consulting Group, Inc., Minneapolis, USA.

Ji, L., Settari, A., Sullivan, R.B. and Orr, D., 2005. Methods for Modelling Dynamic Fractures in Coupled Reservoir and Geomechanics Simulation. The Society of Petroleum Engineers, Richardson, Texas, USA, paper SPE 90874.

Jing, L. and Hudson, J.A., 2002. Numerical Methods in Rock Mechanics (CivilZone review paper). International Journal of Rock Mechanics & Mining Science, 39:409-427.

Jing, L., Stephansson, O. and Nordlund, E., 1993. Study of Rock Joints Under Cylic Loading Conditions. Rock Mech. Rock Engng., 26(3):215-232.

King, G.R. and Ertekin, T., 1991. State-of-the-Art Modelling for Unconventional Gas Recovery; SPE Formation Evaluation, March issue: 63-71,.

King, G.R. and Ertekin, T.,1995. State-of-the-Art Modelling for Unconventional Gas Recovery, Part II: Recent Developments (1989-1994). The SPE Rocky Mountain Regional/Low-Permeability Reservoirs Symposium. The Society of Petroleum Engineers, Richardson, Texas, USA, paper SPE 29575.

Koenig, R.A. and Stubbs, P.B., 1986. Interference Testing of a Coalbed Methane Reservoir. The SPE Unconventional Gas Technology Symposium. The Society of Petroleum Engineers, Richardson, Texas, USA, paper SPE 15225.

Krishnan, G.R., Zaman, M.M. and Roegiers, J.-C., 1996. Permeability Measurements Under Different Stress Paths for a Weakly Cemented Sandstone. The 2nd North American Rock Mechanics Symposium, Montreal, Canada.

Krooss, B.M., Gensterblum, Y. and Siemons, N., 2001. High-pressure Methane and Carbon Dixide Adsorption on Dry and Moisture-equilibrated Carboniferours Coals. The 2001 International Coalbed Methane Symposium. The University of Alabama, Tuscaloosa, Alabama, USA, paper 0119.

Laubach, S.E., Marrett, R.A., Olson, J.E. and Scott, A.R., 1998. Characteristics and origins of coal cleat: A review. International Journal of Coal Geology, 35: 175-207.

Law, D. H-S., van der Meer, L.G.H. and Gunter, W.D., 2002. Numerical Simulation Comparison Study for Enhanced Coalbed Methane Recovery

Processes, Part 1: Pure Carbon Dioxide Injection. The SPE Gas Technology Symposium. The Society of Petroleum Engineers, Richardson, Texas, USA, paper SPE 75669.

Lekhnitskii, S.G., 1963. Theory of Elasticity of An Anisotropic Elastic Body. Holden-Day Inc., San Francisco. pp.19-21.

Levine, J. R., 1996. Model study of the influence of Matrix shrinkage on absolute permeability of coal bed reservoirs. Gayer, R. and Harris, I.(Editors), Coalbed Methane and Coal Geology. The Geological Society, London, UK, pp 197-212.

Lin, W., Tang, G.-Q. and Kovscek, A.R., 2008. Sorption-Induced Permeability Change of Coal during Gas-Injection Processes. SPE Reservoir Evaluation & Engineering, August Issue: 792-802.

Liu, J., Elsworth, D. and Brady, B.H., 1999. Linking stress-dependent effective porosity and hydraulic conductivity fields to RMR. International Journal of Rock Mechanics & Mining Sciences, 36: 581-596.

Longuemare, P., Mainguy, M., Lemonnier, P., Onaisi, A., Gerard, Ch., Koutsabeloulis, N., 2002. Geomechanics in Reservoir Simulation: Overview of Coupling Methods and Field Case Study. Oil & Gas Science and Technology-Rev. IFP, 57(5): 471-183.

Manik, J., Ertekin, T. and Kohler, T.E., 2002. Development and Validation of a Compositional Coalbed Simulator. Journal of Canadian Petroleum Technology, 42(4): 39-45.

Masters, I., Pao, W.K.S. and Lewis, R.W., 2000. Coupling temperature to a double-porosity model of deformable porous media. International Journal For Numerical Methods In Engineering, 49: 421-438.

Matsuki, K., Wang, E.Q., Sakaguchi, K. and Okumura, K., 2001. Time-dependent closure of a fracture with rough surfaces under constant normal stress. International Journal of Rock Mechanics & Mining Sciences, 38: 607-619.

Mavor, M.J., Owen, L.B. and Pratt, T.J., 1990. Measurement and Evaluation of Coal Isotherm Data. The 65th Annual Technical Conference and Exhibition. The Society of Petroleum Engineers, Richardson, Texas, USA, paper SPE 20728.

Mavor, M. J. and Vaughn, J. E., 1997. Increasing Absolute Permeability in the San Juan Basin Fruitland Formation. The 1997 International Coalbed Methane Symposium. The University of Alabama, Tuscaloosa, Alabama, USA, paper 9738.

Mavor, M. J. and Vaughn, J. E., 1998. Increasing Coal Absolute Permeability in the San Juan Basin Fruitland Formation. SPE Evaluation & Engineering, June Issue, pp.201-206.

Mavor, M.J., Gunter, W.D., Robinson, J.R., Law, D.H.S. and Gale, J., 2002. Testing for CO2 Sequestration and Enhanced Methane Production From Coal. The SPE Gas Technology Symposium. The Society of Petroleum Engineers, Richardson, Texas, USA, paper 75683.

Mavor, M. J. and Gunter, W.D., 2004. Secondary Porosity and Permeability of Coal vs. Gas Composition and Pressure. The Society of Petroleum Engineers, Richardson, Texas, USA, paper 90255.

Mavor, M.J., Gunter, W.D., and Robinson, J.R., 2004. Alberta Multiwell Micro-Pilot Testing for CBM Properties, Enhanced Recovery. The Society of Petroleum Engineers, Richardson, Texas, USA, paper 90256.

McKee, C. R., Bumb, A. C. and Koenig, R. A., 1987. Stress-Dependent Permeability and Porosity of Coal. The 1987 Coalbed Methane Symposium The University of Alabama, Tuscaloosa, Alabama, USA, paper 8742.

McKee, C. R., Bumb, A. C. and Koenig, R. A., 1988. Stress-Dependent Permeability and Porosity of Coal and Other Geologic Formations. SPE Formation Evaluation, March Issue: 81-91.

Meaney, K. and Paterson, L., 1996. Relative Permeability in Coal. The 1996 SPE Asia Pacific Oil & Gas Conference. The Society of Petroleum Engineers, Richardson, Texas, USA, paper SPE 36986.

McKee, C.R. and Hanson, M.E., 1975. Explosively Created Permeability from Single Charges. SPE Journal, December Issue: 495-501.

Min, K.-B. and Jing, L., 2003. Numerical determination of the equivalent elastic compliance tensor for fractured rock masses using the distinct element method. International Journal of Rock Mechanics & Mining Science, 40: 795-816.

Min, K.-B., Rutqvist, J., Tsang, C.-F., and Jing, L., 2004. Numerical determination of the equivalent elastic compliance tensor for fractured rock masses using the distinct element method. International Journal of Rock Mechanics & Mining Science, 40: 795-816.

Minkoff, S.E., Stone, C.M., Arguello, J. G., Bryant, S., Eaton, J., Peszynska, M., Wheeler, M., 1999. Staggered In Time Coupling of Reservoir Flow Simulation and Geomechanical Deformation: Step 1 — One-Way Coupling. The 1999 SPE Reservoir Simulation Symposium. The Society of Petroleum Engineers, Richardson, Texas, USA, paper SPE 51920.

Minkoff, S.E., Stone, C.M., Bryant, S., Eaton, J., Peszynska, M., Wheeler, M. F., 2003. Coupled fluid flow and geomechanical deformation modeling. Journal of Petroleum Science and Engineering, 38: 37– 56.

Moffat, D.H. and Weale, K.E., 1955. Sorption by Coal of Methane at High Pressure. Fuel, 34: 449-462.

Morgenstern, N.R. and Noonan, D.K.J., 1974. Fractured Coal Subjected to Direct Shear. In: Advances in Rock Mechanics (Proceedings of the Third Congress of the International Society for Rock Mechanics). National Academy of Sciences, Washington, DC, USA, pp.282-288,.

Nguyen, T.S., 1996. Description of the computer code FRACON. In: Stephansson, O., Jing, L. and Tsang, C.F.(editors), Coulped Thermo-Hydro-Mechanical Process of Fractures Media. Elsevier, pp.539-544.

Noorishad, J. and Tsang, C.F., 1996. ROCMAS simulator: A Thermohydromechanical Computer Code. In: Stephansson, O., Jing, L. and

Tsang, C.F.(editors), Coulped Thermo-Hydro-Mechanical Process of Fractures Media. Elsevier, pp. 551-558.

Ohnishi, Y., Chan, T. and Jing, L., 1996. Constitutive Models for Rock Joints. In: Stephansson, O., Jing, L. and Tsang, C.F.(editors), Coulped Thermo-Hydro-Mechanical Process of Fractures Media. Elsevier, pp. 57-92.

Ohnishi, Y., and Kobayashi, A., 1996. THAMES. In: Stephansson, O., Jing, L. and Tsang, C.F.(editors), Coulped Thermo-Hydro-Mechanical Process of Fractures Media. Elsevier, pp. 545-549.

Olsson, R. and Barton, N., 2001. An improved model for hydromechanical coupling shearing of rock joints. International Journal of Rock Mechanics & Mining Science, 38(3): 317-329.

Palmer, I. and Mansoori, J., 1996. How Permeability Depends on Stress and Pore Pressure in Coalbeds: A New Model. The 1996 SPE Annual Technical Conference and Exhibition. The Society of Petroleum Engineers, Richardson, Texas, USA, paper SPE 36737.

Palmer, I. and Mansoori, J., 1998. How Permeability Depends on Stress and Pore Pressure in Coalbeds: A New Model. SPE Evaluation & Engineering, December Issue: 539-544.

Pariti, U.M. and Harpalani, S., 1993. Study of Coal Sorption Isotherms Using A Multicomponent Gas Mixture. The 1993 International Coalbed Methane Symposium . Tuscaloosa, Alabama, USA, paper 9356.

Patching, T.H., 1965. Variations in Permeability of Coal. Rock Mechanics Symposium, Department of Mines and Technicial Surveys (Mines Branch), Ottawa, Canada, pp.185-199.

Patching, T.H. and Mikhail, M.W., 1986. Studies of gas sorption and emission on Canadian coals. CIM bulletin, 79(No. 887):104-109.

Pokker, P.A. and van der Meer, L.G.H., 2004. The injectivity of coalbed CO_2 injection wells. Energy, 29:1423-1429.

Promeroy, C. D. and Robinson, D. J., 1967. The Effect of Applied Stresses on the Permeability of A Middle Rank Coal to Water. Int. J. Rock Mech. Min. Sci., 4: 329-343.

Puri, R. and Seidle, J., 1991. Measurement of Stress Depletion Permeability in Coals and Its Influence on Coalbed Methane Production. The 1991 Coalbed Methane Symposium. The University of Alabama, Tuscaloosa, Alabama, USA, paper 9142.

Puri, R. and Yee, D., 1990. Enhanced Coalbed Methane Recovery. The 65th Annual Technical Conference and Exhibition. The Society of Petroleum Engineers, Richardson, Texas, USA, paper SPE 20732.

Pusch, R. and Borgesson, L., 1998. Strain parameters of discontinuities in rock for finite element calculation. Engineering Geology, 49(3): 201-206.

Reid, G.W., Towler, B.F. and Harris, H.G., 1992. Simulation and Economics of Coalbed Methane Production in Power River Basin. The SPE Rocky Mountain Regional Meeting. The Society of Petroleum Engineers, Richardson, Texas, USA, paper SPE 24360.

Reeves, S. R., 2001. Geological Sequestration of CO2 in Deep, Unmineable Coalbeds: An Integrated Research and Commercial-Scale Field Demonstration Project. The 2001 SPE Annual Technical Conference and Exhibition. The Society of Petroleum Engineers, Richardson, Texas, USA, paper SPE 71749.

Renshaw, C.E., 1995. On the relationship between mechanical and hydraulic apertures in rough-walled fracture. Journal of Geophysical Reserch, 100(B12):24629-24636.

Reznik, A.A., Dabbous, M.K., Fulton, P.F. and Taber, J.J., 1974. Air-Water Relative Permeability Studies of Pittsburgh and Pocahontas Coals. Socieyt of Petroleum Engineer Journal, December Issue:556-562.

Reznik, A.A., Lien, C.L. and Fulton, P.F., 1978. Permeability Characteristics of Coal. The 4th Underground Coal Conversion Symposium. Sandia National Laboratories, Albuquerque, New Mexico, USA, pp.435-451.

Reucroft P.J. and Patal H., 1986. Gas-induced swelling in coal. Fuel, 65(June issue): 816~820.

Reucroft P.J. and Sethuraman A.R., 1987. Effect of Pressure on Carbon Dioxide Induced Coal Swelling. Energy & Fuels, 1(1): 72~75.

Roadifer, R.D., Moore, T.R., Raterman, K.T., Farnan, R.A. and Crabtree, B.J., 2003. Coalbed Methane Parametric Study: What's Really Important to Production and When?. The 2003 SPE Annual Technical Conference and Exhibition. The Society of Petroleum Engineers, Richardson, Texas, USA, paper SPE 84425.

Robertson, E.P. and Christiansen, R.L., 2005. Measurement of Sorption-Induced Strain. The 2005 International Coalbed Methane Symposium. The University of Alabama, Tuscaloosa, Alabama, USA, paper 0532.

Rose, R.E. and Foh, S.E., 1984. Liquid Permeability of Coal as a Function of Net Stress. SPE/DOE/GRI Unconventional Gas Recovery Symposium. The Society of Petroleum Engineers, Richardson, Texas, USA, paper SPE 12856.

Rosso, R.S., 1976. A Comparison of Joint Stiffness Measurements in Direct Shear, Triaxial Compression, and In Situ. International Journal of Rock Mechanics and Mining Sciences & Geomechanics Abstracts, 13:167-172.

Ruistuen, H., Teufel, L.W. and Rhett, D., 1999. Influence of Reservoir Stress Path on Deformation and Permeability of Weakly Cemented Sandstone Reservoirs. SPE Reservoir Evaluation and Engineering, 2(3): 266-272.

Rutqvist, J., Tsang, C.F. and Tsang, Y., 2003. Analysis of stress- and moisture induced changes in fractured rock permeability at the Yucca mountain drift scale test. In: Stephansson, O., Hudson, J.A. and Jing, L.(editors). International Conference on Coupled T-H-M-C Processes in Geosystems(GeoProc 2003). Stockholm, Sweden. pp.147-152.

Rutqvist, J., Wu, Y.-S., Tsang, C.-F. and Bodvarsson, G., 2002. A modeling approach for analysis of coupled multiphase fluid flow, heat transfer, and deformation in fractured porous rock. Int. J. Rock Mech. Min. Sci., 39: 429-442.

Sawyer, W.K. and Paul, G.W., 1990. Development and Application of A 3D Coalbed Simulator. The Canadian International Technical Meeting. The Petroleum Society, Calgary, Canada, paper 90-119.

Sawyer, W.K., Zuber, M.D., Kuuskraa V.A., Horner, D.M., 1987. Using Reservoir Simulation and Field Data to Define Mechanisms Controlling Coalbed Methane Production. The 1987 Coalbed Methane Symposium. The University of Alabama, Tuscaloosa, Alabama, USA, paper 8763.

Schwerer, F.C. and Pavone, A.M., 1984. Effect of Pressure-Dependent Permeability on Well-Test Analyses and Long Term Production of Methane from Coal Seams. The SPE/DOE/GRI Unconventional Gas Recovery Symposium. The Society of Petroleum Engineers, Richardson, Texas, USA, paper SPE 12857.

Seidle, J.P., Jeansonne, M.W. and Erickson, D.J., 1992. Application of Matchstick Geometry to Stress Dependent Permeability in Coals. The SPE Rocky Mountain Regional Meeting. The Society of Petroleum Engineers, Richardson, Texas, USA, paper SPE 24361.

Seidle, J.P. and Huitt, L.G., 1995. Experimental Measurement of Coal Matrix Shrinkage Due to Gas Desorption and Implications for Cleat Permeability Increases. The International Meeting on Petroleum Engineering. The Society of Petroleum Engineers, Richardson, Texas, USA, paper 30010.

Settari, A. and Walters, D.A., 2001. Advances in Coupled Geomechanical and Reservoir Modeling With Applications to Reservoir Compaction. SPE Journal, September Issue:334-342.

Shi, J.Q. and Durucan, S., 2003. Changes in permeability of coalbeds during primary recovery-Part 1: model formulation and analysis. The 2003 International Coalbed Methane Symposium. The University of Alabama, Tuscaloosa, Alabama, USA, paper 0341.

Shi, J.Q. and Durucan, S., 2005. A Model for Changes in Coalbed Permeability During Primary and Enhanced Methane Recovery. SPE Evaluation & Engineering, August Issue:291-299.

Singh B., 1973a. Continuum characterization of jointed rock masses Part I-the constitutive equations. Int. J. Rock Mech. Min. Sci. & Geomech. Abstr., 10: 311-335.

Singh B., 1973b. Continuum characterization of jointed rock masses Part II-significance of low shear modulus. Int. J. Rock Mech. Min. Sci. & Geomech. Abstr., 10: 337-349.

Sitharam, T.G., Sridevi, J. and Shimizu, N., 2001. Practical equivalent continuum characterization of jointed rock masses. International Journal of Rock Mechanics & Mining Science, 38: 437-448.

Sitharam, T.G., and Latha, G.M., 2002. Simulation of excavations in jointed rock masses using a equivalent continuum approach. International Journal of Rock Mechanics & Mining Science, 39: 517-525.

Snow, D.T., 1969. Anisotropic permeability of fractured media. Water Resource Reseasch, 5(6): 1273-1289.

Somerton, W.H., Soylemzoglu, I.M. and Dudley, R.C., 1975. Effect of Stress on Permeability of Coal. Int. J. Rock Mech. Min. Sci & Geomech. Abstr., 12:129-145.

Stevenson, M.D., Pinczewski, W.V., Somers, M.L. and Bagio, S.E., 1991. Adsorption/Desorption of Multicomponent Gas Mixtures at In-Seam Condition. The SPE Asia-Pacific Conference. The Society of Petroleum Engineers, Richardson, Texas, USA, paper SPE 23026.

Swan, G., 1980. Stiffness and associated joint properties of rock. Conference on Applications of Rock Mechanics to Cut-and-Fill Mining. Institute of Mining and Metallurgy, London, pp.169-178.

Swan, G., 1983. Determination of stiffness and other joint properties from roughness measurements. Rock Mech. Rock Eng., 16:19-38.

Szwilski, A.B., 1984. Determination of the Anisotropic Elastic Moduli of Coal. Int. J. Rock Mech. Min. Sci & Geomech. Abstr., 21(1): 3-12.

Terzaghi, K., 1943. Theoretical Soil Mechanics, John Wiley and Sons, New York.

Tran, D., Settari, A. and Nghiem, L., 2002. New Iterative Coupling between A Reservoir Simulator and A Geomechanics Module. The SPE/ISRM Rock Mechanics Conference. The Society of Petroleum Engineers, Richardson, Texas, USA, paper 78192.

Tsang, Y.W., 1984. The Effect of Tortuosity on Fluid Flow Through a Single Fracture. Water Resources Research, 20(9): 1209-1215.

Tsang, C.F., 1987. Coupling processes associated with nuclear waste repositories. Academic Press, UAS.

Tse, R. and Cruden, D. M., 1979. Estimating Joint Roughness Coefficients. Int. J. Rock Mech. Min. Sci. & Geomech. Abstr., 16: 303-307.

Tuncay, K. and Corapcioglu, M.Y., 1995. Effective stress principle for saturated fractured porous media. Water Resources Research, 31(12): 3103-3106.

Van Golf-Racht, T.D., 1982a. Fundamentals of fractured reservoir engineering. Elsevier Scientific Publishing Company, New York, USA, pp.162-163 and p.434.

Van Golf-Racht, T.D., 1982b. Fundamentals of fractured reservoir engineering. Elsevier Scientific Publishing Company, New York, USA, pp.311-313.

Van Golf-Racht, T.D., 1982c. Fundamentals of fractured reservoir engineering. Elsevier Scientific Publishing Company, New York, USA, pp.179-180.

Van Golf-Racht, T.D., 1982d. Fundamentals of fractured reservoir engineering. Elsevier Scientific Publishing Company, New York, USA, p.710.

Van Der Meer, L.H.H. and Fokker, P.A., 2003. The Injectivity of Coalbed CO_2 Injection Wells. The 2003 International Coalbed Methane Symposium. The University of Alabama, Tuscaloosa, Alabama, USA, paper 031.

Vaziri, H.H., Wang, X., and Palmer, I.D., 1997. Well-bore completion technique and geotechnical parameters influencing gas production. Canadian Geotechnical Journal, 34:87-101.

V.I.P.S., 2004. Introduction of Products. Vector International Processing Systems Limited, Berkshire, United Kingdom.

Walker, P.L.,Verma, Jr, S.K, Rivera-Utrilla, J. and Khan, M.R., 1988. A direct measurement of expansion in coals and macerals induced by carbon dioxide and methanol. Fuel, 67:719-726.

Walsh, J.B., 1981. The effect of pore pressure and confining pressure on fracture permeability. Int. J. Rock Mech., 18:429-435.

Wang, H. F., 2000. Theory of Linear Poroelasticity with Application to Geomechanics and Hydrogeology. Princeton University Press, USA.

Walsh, J.B. and Grosenbaugh, M.A., 1979. A New Model for Analysing the Effect of Fracture on Compressibility. J. of Geophysical Research, 84(B7):3532-3536.

Wei, Z.Q. and Hudson, J.A., 1986. Moduli of jointed rock masses. The International Symposium on Large Rock Caverns, Pergamon Press, New York, USA, pp.1073-1086.

White, C.M., Strazisar, B.R., Granite, E.J., Hoffman, J.S. and Pennline, H.W., 2003. Separation and Capture of CO_2 from Large Stationary Sources and Sequestration in Geological Formations---Coalbeds and Deep Saline Aquifers. Journal of the Air & Waste Management Association, 53:645-715.

Willis-Richards, J., Watanabe, K. and Takahashi, H., 1996. Progress toward a stochastic rock mechanics model of engineered geothermal systems. Journal of Geophysical Reserch, 101(B8):17481-17496.

Yang, R. T. and Saunders, J. T., 1985. Adsorption of gasses on coals and heat-treated coals at elevated temperature and pressure: 1.Adsorption from hydrogen and methane as single gases. Fuel, 64:616-620.

Yang, Z.Y., Lo, S.C. and Di, C.C., 2001. Reassessing the Joint Roughness Coefficient (JRC) Estimation Using Z2. Rock Mech. Rock Engng., 34(3):243-251.

Yoshida, H. and Horii, H., 2004. Micromechanics–based continuum model for a jointed rock mass and excavation analysis of a large scale cavern. International Journal of Rock Mechanics & Mining Science, 41: 119-145.

Young, G.B.C., Paul, G.W., McElhiney, J.E., McBane, R.A., 1992. A Parametric Analysis of Fruitland Coal Methane Reservoir Productivity. The SPE Annual Technical Conference and Exhibition. The Society of Petroleum Engineers, Richardson, Texas, USA, paper SPE 24903.

Zahner, R., 1997. Application of material balance to determine ultimate recovery of a San Juan Fruitland coal well. SPE Annual Technical Conference and Exhibition. The Society of Petroleum Engineers, Richardson, Texas, USA, paper 38858.

Zhao, Y., Hu, Y., Zhao, B. and Yang, D., 2004. Nonlinear Coupled Mathematical Model for Solid Deformation and Gas Seepage in Fractured Media. Transport in Porous Media, 55: 119-136.

Zhao, Y., Hu, Y., Wei, J. and Yang, D., 2003. The Experimantal Approach to Effictive Stress Law of Coal Mass by Effect of Mechane. Transport in Porous Media, 53: 235-244.

Zimmerman, R.W., Chen, D.W. and Cook, N.G.W., 1992. The Effect of Contact Area on the Permeability of Fractures. Journal of Hydrology, 139: 79-96.

Zutshi, A. and Harpalani, S., 2004. Matrix Swelling with CO_2 Injection in A CBM Reservoir and Its Impact on permeability of Coal. The 2004 International Coalbed Methane Symposium. The University of Alabama, Tuscaloosa, Alabama, USA, paper 0425.